Bulletin 55
(Part 1 of 3 Parts)

THE SHOCK AND VIBRATION BULLETIN

Part 1
Welcome, Keynote Address
Invited Papers, Isolation and
Damping and Damping Practices

JUNE 1985

A Publication of
THE SHOCK AND VIBRATION
INFORMATION CENTER
Naval Research Laboratory, Washington, D.C.

Office of
The Under Secretary of Defense
for Research and Engineering

SYMPOSIUM MANAGEMENT

THE SHOCK AND VIBRATION INFORMATION CENTER

J. Gordan Showalter, Acting Director

Rudolph H. Volin

Jessica Hileman

Elizabeth A. McLaughlin

Mary K. Gobbett

Bulletin Production

Publications Branch, Technical Information Division,
Naval Research Laboratory

Bulletin 55
(Part 1 of 3 Parts)

THE SHOCK AND VIBRATION BULLETIN

JUNE 1985

A Publication of
THE SHOCK AND VIBRATION
INFORMATION CENTER
Naval Research Laboratory, Washington, D.C.

The 55th Symposium on Shock and Vibration was held in Dayton, Ohio, October 22-24, 1984. The Aeronautical Systems Division, Wright-Patterson Air Force Base, Ohio, was the host.

Office of
The Under Secretary of Defense
for Research and Engineering

CONTENTS

PAPERS APPEARING IN PART 1

SESSION CHAIRMEN AND COCHAIRMEN

Date	Session Title	Chairmen	CoChairmen
Tuesday, 23 October, A.M.	Opening Session	Mr. Jerome Pearson, Air Force Wright Aeronautical Laboratories, Wright-Patterson Air Force Base, OH	Dr. J. Gordan Showalter, The Shock & Vibration Information Center, Naval Research Laboratory, Washington, DC
Tuesday, 23 October, P.M.	Dynamic Testing	Mr. Edwin M. Rzepka, Naval Surface Weapons Center, Silver Spring, MD	Mr. Frederick Anderson, U.S. Army Missile Command, Redstone Arsenal, AL
Tuesday, 23 October, P.M.	Fluid-Structure Interaction	Mr. Arthur D. Carlson, Naval Underwater Systems Center, New London, CT	Dr. Y. S. Shin, Naval Post Graduate School, Monterey, CA
Wednesday, 24 October, A.M.	Plenary A	Mr. Henry Caruso, Westinghouse Electric Corporation, Baltimore, MD	
Wednesday, 24 October, A.M.	Flight Vehicle Dynamics	Mr. Joseph J. Popolo, Grumman Aerospace Corporation, Bethpage, NY	Mrs. Phyllis Bolds Air Force Wright Aeronautical Laboratories, Wright-Patterson Air Force Base, OH
Wednesday, 24 October, A.M.	Damping and Isolation	Dr. John P. Henderson, Air Force Wright Aeronautical Laboratories, Wright-Patterson Air Force Base, OH	Dr. David I. G. Jones, Air Force Wright Aeronautical Laboratories, Wright-Patterson Air Force Base, OH
Wednesday, 24 October, P.M.	Seismic Loads	Mr. James P. Ballard, U.S. Army Engineer Waterways Experiment Station, Vicksburg, MS	Mr. Donald Bettge, Federal Emergency Management Agency, Washington, DC
Wednesday, 24 October, P.M.	Damping Practices	Dr. Lynn C. Rogers, Air Force Wright Aeronautical Laboratories, Wright-Patterson Air Force Base, OH	Mr. Michael Parin, Anatrol Corporation, Cincinnati, OH
Thursday, 25 October, A.M.	Plenary B	Dr. Ronald L. Eshleman, Vibration Institute, Clarendon Hills, IL	

Thursday, 25 October, A.M.	Machinery Dynamics	Dr. Ronald L. Eshleman, Vibration Institute Clarendon Hills, IL	Mr. Robert Leon, Liberty Technology Center, Inc. Conshohocken, PA
Thursday, 25 October, A.M.	System Identification	Dr. H. Joseph Weaver, Lawrence Livermore Laboratory, Livermore, CA	Dr. David Brown University of Cincinnati, Cincinnati, OH
Thursday, 25 October, P.M.	Structural Analysis	Mr. Tommy L. Dobson, 6585 Test Group, Holloman, Air Force Base, NM	
Thursday, 25 October, P.M.	Short Discussion Topics	Mr. James Bair, Aeronautical Systems Division, Wright-Patterson Air Force Base, OH	

WELCOME

Mr. Keith Collier
Deputy Director
Air Force Wright Aeronautical Laboratories
Wright-Patterson Air Force Base, OH

On behalf of the Air Force Wright Aeronautical Laboratories, I welcome you to the 55th Shock and Vibration Symposium, and to Dayton, Ohio, the birthplace of aviation. I am told that this is the gathering of folks who worry about being unbalanced, often have or cause the shakes, and sometimes undergo shock treatment. Are you sure you are in the right place?

It was in Dayton that two brothers named Wilbur and Orville, authentic American geniuses, brought aviation to the world. At our Carillon Park, on the banks of the Great Miami River, you can see a replica of the Wright Brothers bicycle shop where they built the first successful airplane. They flew gliders at Huffman Prairie, near Area B of Wright-Patterson Air Force Base, before going to Kitty Hawk, and before going into history.

The Wright Brothers faced unprecedented problems in aerodynamics, structures, propulsion and materials. On their first airplane the large propellers were unbalanced, and caused the light shafts to vibrate, threatening to tear the props off their mounts. They solved this problem, but characteristically, it came back to haunt the local section of the AIAA recently when they built a replica of the Wright Model B Flyer. It had the same prop vibration problem, and it had to be solved again.

You know that story. Any time a new vehicle flies faster, has more power and is lighter, it has vibration problems. These problems have been the object of continuing new technology efforts by the four AFWAL laboratories since they were founded in the 1960's. The Avionics Laboratory has qualified new electronics for vibration effects in older airplanes. The Flight Dynamics Laboratory has developed new Military Standards for dynamics environments. The Materials Laboratory has developed new turbine-blade coatings to damp vibration, and the Propulsion Laboratory has developed more powerful engines with less vibration.

In the 1970's these four independent laboratories were combined under the Air Force Wright Aeronautical Laboratories, or as the Air Force has want to do, we turned that into the word AFWAL. AFWAL is now involved in a new series of aerospace vehicles, such as the Advanced Tactical Fighter, the Transatmospheric Vehicle, the space-based laser and the space-based radar. In each of these vehicles a new military capability and a new technical challenge is represented.

You met last in Dayton 10 years ago and discussed avionics reliability. When you meet here again in another 10 years, you will be heavily involved in these planned new vehicles. I can promise you that they, too, will challenge you with even more vibration problems than the last generation did.

Again, welcome to Dayton, the birthplace of aviation. I encourage you to return again next July to see the biggest military airplane show in the nation, the Dayton Air Fair. While you are here, visit the Carillon Park, the Wright Brothers Memorial and the Air Force Museum. We are proud of these institutions that carry the history of aviation and aviation technology.

I suggest that you take a moment, while you are here, to contemplate how far aviation has come, and how far we have to go. I wish you continued success in your technical endeavors to help speed us on the path of high technology systems. Again, welcome.

KEYNOTE ADDRESS

Colonel Craig O. Schaum
Deputy for Engineering
Aeronautical Systems Division
Wright-Patterson Air Force Base, OH

Welcome to Dayton. Welcome to Wright-Patterson Air Force Base, and welcome to Aeronautical Systems Division. I will start with a film on the Aeronautical Systems Division since many of you may not be familiar with what we do. We are very proud of what we do, and the film shows some of the systems we are working on and some of the things we do here at Wright-Patterson Air Force Base.

While you are viewing the movie though, think, if you will, with me a little bit about the progress we have made in this area. In avionics, for example, back in 1912 we made our first air to ground radio transmission. It took five years more to have a two-way conversation. In 1932 we had our first instrument flight, and it was not until 1937 that we had our first automatic landing. We have come a long way from those days to the F-15"s, the F-16's and the digital airplanes we are thinking about flying and working on today. But let's take a look at the movie, and then we'll talk about some things that have happened in recent history. (Colonel Schaum showed a movie on the current development and acquisition activities of the Aeronautical Systems Division.)

That movie will give you an idea of some of the activity that goes on around here. Incidentally, the B-1 that you saw in the movie was the B-1A model; the first B-1B flew on October 18, 1984, and we are looking forward to the B-1B having a successful test program from here on out. But it gives you an idea of some of the multitude of activities that go on around you here in Dayton, the home of the airplane.

This meeting was last held here in 1974. At that time the then ASD Commander, General James T. Stewart, welcomed the group and discussed the challenges facing ASD and the Shock and Vibration community. These challenges included, of course, rising costs, increased complexity, and the more and more field failures of equipment. He pointed out that the role of the Shock and Vibration community was to improve and to develop new technology, but more importantly to help the Research and Development community avoid some serious pitfalls which had contributed to the basic problems of high cost, poor quality and low performance.

General Stewart identified two pitfalls; first, the tendency of technical specialists, integraters and managers to operate with tunnel vision resulting in poorly integrated development efforts with little or no consideration of synergistic effects. Second, the tendency to introduce the environmental disciplines into the development cycle too late to result in well defined and properly qualified equipment.

A review of the record of these last 10 years shows progress in these directions. Recognition has dawned on the R&D world that the dynamic environments are important in the successful operational deployment of systems; that equipment must be designed to operate in and withstand the environment; that realism is necessary in effective testing; that environmental stress screens are effective production quality tools, and that enviromental factors must be included in the developmental process from the beginning.

Here at ASD we are restructuring our avionics development and reliability under the heading of AVIP, or Avionics Integrity Program. We hope AVIP will provide an overall road map for a truly integrated approach to avionics development. Somehow we have accepted as a given that our high technology weapon systems will be unreliable, much as the American people have accepted the inherent unreliability of the American automobile. It is not that we don't know what causes the unreliability. In fact, we do know what causes it! We know what causes parts to break and when failures will occur. We also have the technology today to design and build our weapon systems so they will not break, or at least they will fail much less often. Dr. John Halpin, our Director of Product Assurance, will develop this AVIP concept more fully later this morning.

As General McMullen, the ASD Commander, said at this year's NACOM, "Our ability to fight

in the future will involve more than how high, how fast and how far. It must also address how often. How often are America's fighting machines ready to fight rather than out for maintenance or lack of spare parts?" I think that is right on target. We have to reorder our thinking, to abolish the mentality of "If it's high tech, it's going to break." We must all recognize that the continuing electronics revolution must bring increased reliability with it.

Readiness and sustainability demand a big part of our defense dollars. In terms of wartime tasking, system reliability is the single most significant limiting factor. With today's system reliability we would send, not one aircraft, but more likely three to net the necessary probability of success. We are looking for, and we must have, reliable systems right from the drawing board. They must operate, they must be maintainable, and they must be supportable in the field where they fight. Actually, the Air Force Systems Command has changed the concept of supportability to "supported weapon systems", which places emphasis squarely on keeping acquisition and logistics tied together during weapon system production.

As air pioneer, Julio DuHe said, "Victory smiles on those who anticipate the changes in the character of war, not upon those who wait to adapt after the changes occur." Well, folks, we have done almost that very thing. That is why we are in a race today, not an arms race necessarily, but a race of technology. As we all know, Soviet capabilities have almost caught up to ours in many areas. Our proverbial storehouse full of technology is almost empty. We are very busy here trying to restock our technology shelves. For example, in such key areas as materials development we are studying advance composites and metallics for application to nearly an entire aircraft, including engine and electronics. The all-composite aircraft may be just around the corner. This advanced composite technology, of course, relies heavily on detailed studies of the important shock and vibration technologies you will discuss during this symposium this week; these include structural analysis, vibration and shock prediction, dynamic measurements and data analysis, and laboratory simulation. While you have made significant progress in these areas in the past 10 years, the problems have also continued to grow. I will leave further discussion of these areas to the experts, such as Dr. Jim Olsen, the Assistant for Research and Technology in our Structures and Dynamics Division.

I would like to remind you that whenever you think your current achievements are so magnificent as to stand for all time, you should remember a story about the Wright brothers. Remember that after Wilbur and Orville made their history-making flight at Kitty Hawk, on December 17, 1903, they wrote home about it and added that they would be home in a few days. The Dayton newspapers wrote about it and headlined the story, "Prominent local bicycle merchants to be home by Christmas." Well, ASD might have the nickname, "Bicycle Shop", but we don't intend to be known only for our past work, but also for our current and future successes. Perhaps the single most critical element in our business today is product assurance. By product assurance, I mean basic reliability, the ability to field a system that is readily maintainable. The systems we buy today must work in the field, not just in lab tests. They must work well in the hands of our air crews and maintenance folks, not just in the hands of contract engineers with doctoral degrees. Here again, we have made progress. We work under the new guidelines that this group helped develop for environmental and reliability testing. It places emphasis on stress effects. We have combined reliability tests with environmental tests to insure that the equipment is going to operate and continue to operate in the field. We realize that some of our initiatives are new, untried game plans, but as Will Rogers once said, "Even if you are on the right track, you'll get run over if you just sit there." So, we are moving ahead. We will simplify some plans and expand others. We need new, less expensive test equipment and perhaps, different environmental tests. We need your help in those initiatives. There is no blank check so we have to work together to get the most for our money and to insure we take advantage of the right technology at the right time. Charles Kettering said, "You never stub your toe by standing still. In fact, the faster you go, the more chance you have of stubbing your toe, but also, the more chance you have of getting somewhere." I agree with that 100%. I hope that it hasn't been lost on you, the fact that the Deputy for Engineering at Aeronautical Systems Division, a former SPO director of two or three SPO's, spent most of his speech talking about supportability, reliability, maintainability and product assurance. I think that is the focus and the direction we have to take in our work in the next few years.

I have enjoyed speaking with you. I thank you for your attention, and I wish you a productive week.

INVITED PAPERS

AVIP AIR FORCE THRUST FOR RELIABILITY

Dr. John C. Halpin
Assistant for Product Assurance
Deputy for Engineering
Aeronautical Systems Division
Wright-Patterson Air Force Base, OH

Good morning. It has been a while since I attended a Shock and Vibration Symposium. When I was a student at Catholic University in Washington, DC, I remember going to some of these meetings, and it is my pleasure to be visiting with you again.

My topic is product assurance, and that is a word which has been coined out of national concern for quality and quality assurance. However, it addresses a broader set of issues which basically has to do with the question, "Does the product perform the job that is intended and desired in terms of the quality and the dependability of its performance characteristics?".

In the Aeronautical Systems Division we have had a long history of that. We have been managing aircraft since the 1920's. As the airplane evolved, people managing airframe structure were concerned with the strength, the resonance, the stability and the flutter conditions for that airframe. That eventually formulated itself into what was called an Aircraft Structural Integrity Program. That evolved into World War II where sustaining the worst loads in flight were the basic concerns of the design.

As we evolved past that, we began to accept the fact that the life of the vehicle could be attributed to factors other than operational issues and battle damage. This generated the concept of structural fatigue at the end of the 1940's, and in the 1950's, a reformulation of the Aircraft Structural Integrity Program (ASIP). This reformulation of ASIP introduced the concept of the ground fatigue test to stimulate failure processes into the airframe acquisition process. At that time it was felt fatigue-induced failure and static strength were two discrete, independent physical phenomena, despite the academic research that had gone on on the presumption of pre-existing flaws in structures.

As we moved through the 1950's and into the 1960's, inflight failures began to occur in airframes, that had been fully qualified with the agreed-upon procedures. When the sources of those failures were traced back, the origins were found to be pre-existing flaws that existed in the airframe at the time of manufacturing. These flaws were stimulated by the in-service stresses and grew to a size sufficient to cause a catastrophic failure. This led to the formal recognition of the manufacturing defect as the genesis of the observed structural failure. The life of the vehicle was then dictated by the dynamic operational loads, the material characteristics, and the temperature environments that it saw. One had to control those directly to control the life of the vehicle itself.

When we lost an F-111, when we had problems on the C-5, T-36, F-5A, KC-135 and F-4C/D aircraft, the Seaman Commission was formed to reexamine our structural development policies. At that time a debate took place as to whether we wanted to emphasize formal fracture control, or whether we wanted to emphasize a concept called Structural Reliability. Two philosophical issues were debated at that time. One, the Structural Reliability format, sought to describe the statistical expectation of flaws in a product, the occurrences of loads and the distribution of failure times that would be expected to occur in service. The Fracture Mechanics format sought to describe the distribution of flaws and to locate the tail of the flaw distribution; then use the statistical distributions of loads to project the time to first failure if you could truncate the distribution of flaws in the product.

The decision was made to implement a fracture control methodology because the desired result of the engineering management process for the vehicle was to achieve a predictable failure-free lifetime for the vehicle. We did not want a description of a low tolerable failure rate in the field. We wanted a description of a process which prevented failure from occurring in the field.

At that time we reformulated our Aircraft Structural Integrity Program in its existing form. It is in the MIL-STD-1530 document in the Air Force. It eventually grew into the revision of the FAR's for the FAA regulation in the

middle of the 1970's; it was extended to the engine structure. The Engine Structural Integrity Program started in 1975 and is a formal Military Standard today, Figure 1.

That change in thinking was then brought forward, and we were asked to examine our avionics systems from that same perspective. So, we started an activity in the 1980 time frame. Within this activity we have been debating among ourselves as to what type of a management philosophy we want for avionic systems.

Modern aircraft electronics, or Avionics, grew out of an electron tube technology which was manifested in products such as radios and navigation gear. These were desirable functions to have, but they were functions you could tolerate doing without if you had a failure in the air. How often have you heard the expression, "After all, it is only electronics."

Life has changed. Electronics is a technology that has come of age. As we have moved into the transistor and the integrated circuit era, we have evolved to applications in radar, fire control, flight control and engine control. For example, the F-16 is a completely "fly by wire" system. The F100 engine in it is controlled by a digital computer. The next engine will have a completely electronic engine control system in it. We are going into coupled fire-flight and engine control modes. We have moved from an optional technology to a technology which has captured the heart of the airplane. It is mission critical, and it is critical to safety of flight.

Now we must accept the fact that the time has come for avionics. Avionics is a serious engineering discipline, and you can't tolerate the kind of practices we have indulged in the past. That is the basic theme of our concern. Our thrust in avionics recognizes that it has been a success; also, the people have done a good job, and we are completing a transition from an all-mechanical, to a hydro-mechanical device, and into a basically electro-mechanical device with the next fighter airplane and that we need to evolve improved practices.

It is synonymous with the transition that occurred in Dayton, Ohio at National Cash Register. Twenty years ago a cash register was an all mechanical (computational) device with over 40,000 moving parts. As you know, today, cash registers are basically digital computers. The airplane in the 1990's will be the same.

With that technology growth, we have had a history in our high technology systems which is symbolized in Figure 2. For simple radios and navigation gear, we took technology growth to improved life and improved support functions. In complex systems, in this case radars, you can see the evolution from vacuum tube technology, through transistor technology, into the micro-circuit technology. Figure 3 shows the correlation between the average flight hours between maintenance demand, and the number of piece part components that make up those systems.

Technology has provided us an advantage. For example, if you look at the piece parts and the corresponding mean time to a maintenance action in the late 1950's and early 1960's, they are below about 10 hours. As the technology grew, these numbers have slowly crept up. We have been able to tolerate many more parts in the system; that means growing performance. The lesson is we have improved the performance of the radar system without penalizing the life and the reliability of the system. In fact, we experienced a modest improvement in the life characteristics. Technology has helped us absorb the complexity penalties.

One measure of complexity is the number of components in a system. There is a theorem that adds up the components as if they were weak links in a chain. "Sum of the failure rates" is the classical reliability estimation technique. That means as you put more links in that chain, the chain gets longer, and the probability of system failure becomes larger; the effective life decreases.

This is amplified by our attitudes on how we maintain systems. Contrary to a primary airframe or an engine structure, where we practice preventive maintenance, we fly an avionic system until it fails on the vehicle. We call this corrective maintenance. That means our maintenance concept, "fly-to-failure", dictates that we must have the lowest serial reliability in the system. The "sum of the failure rates" cited above for logistics reliability is a direct consequence of the renewal process in statistical reliability. That is the case here, and that is why we have something on the order, typically, of about 20 hours to failure on a complex system itself. So, our field characteristics today represent two things; the degree of complexity we build-in, and an attitude which says we will fly to failure and tolerate that failure on the vehicle itself.

The origin of corrective maintenance concepts for electronics resides in decisions made in management of the early tube technology. In the 1940's and 1950's it was not uncommon to replace tubes at scheduled intervals, generally before they failed. An argument developed which stated that when an operating tube (or item) is removed before it failed, the maximum operating life of that tube is not being achieved. Useful life is being thrown away. Replenishment spares cost is increased as a consequence. It was then argued that the community was more concerned with replacement spares cost than a high operating systems reliability, and a decision was made to

replace upon failure. From today's perspective, it is not clear that decision results in the desired or optimum life cycle cost or operational characteristics. A policy to "fly to failure" and to "replace on failure" is by necessity a policy which dictates that failures must occur on equipment generally when that equipment is operating. Because there is by policy on equipment failures, there is an attendant requirement for on-equipment diagnostics. On-equipment diagnostics mean automatic procedures called built in test as well as manual troubleshooting procedures. Trouble is the governing word. As yu know, these diagnostic procedures are technically difficult, very expensive, and often times reduce the hardware reliability through the attendant increase in systems complexity. Because the on-equipment diagnostics does not always work in a consistent manner, an additional set of equipment is utilized to verify the diagnosis and sometimes fault isolate to a lower level. The second set of equipment in the Air Force world is called the Avionics Intermediate shop. It is big, about the size of a fighter aircraft; it is expensive, about the cost of a fighter aircraft; it is difficult to move; and it is vulnerable to attack. Clearly, our corrective maintenance policy is expensive and cumbersome. It is not peculiarly a USAF or a military policy. It is a technical cultural issue; almost all electronic equipment, military or civilian, is maintained with corrective maintenance policies. We need to create alternative options. The development of a preventive maintenance option has its reigns in our ability to understand the failure processes in electronic systems.

I will give you a very simplistic view of flaws and how they relate to strength. The classical concept of fracture in any material part involves the assumption that any part that comes out of a manufacturing process will have a flaw; it will also have a strength. The strength and the flaw sizes are related to, what is called, fracture toughness which is symbolized by a curve with hash marks in the left side of Figure 4. If there are different sizes of flaws, there will be different strengths. The strength distribution is a reflection of the flaw size distribution within the part.

Consider the bi-material strip, composed of material strips with different expansion coefficients. As we subject this bi-material strip to a fluctuating temperature, or to vibration, we will stress it. Those stresses will cause the flaw to grow in size. As the flaw changes from one size to a larger size, we have a degradation in the strength or the ability of the bi-material strip to resist the induced stresses imposed by the environment. As the product degrades in strength, in time, it will see an operating stress level of similar magnitude to the degrading strength. When that stress level matches that residual strength, we produce a failure which becomes a fatigue failure.

If I change the operating stress, I can change the time to failure. The relation between the operating stress and the time to failure can be depicted by an S-N curve; a plot of delta temperature or stress versus life in Figure 4. If I have a different initial flaw size, that S-N curve will get shifted in time. This situation is pertinent, not only to an airframe and engine, but to piece parts and printed wiring assembly boards.

If we look at what we did on the airframe, and what we expect to do on the avionics system, we can make the same point I made in my opening comments. As the product comes out of the factory, it has a distribution of imperfections, Figure 5. We seek to understand the distribution of these manufacturing imperfections. In fact, when we had the F-111 incident in the late 1960's, we did a great deal of non-destructive testing to characterize the nature of the flaws in the product from the different manufacturing processes. Then we looked at the thermal and inertial loads (In the case of electronic systems, it would be the vibration spectra.), and we studied the relationship between flaw size and the time it takes to fail.

We put in some process controls. We found we could not control the flaw size to the desired level. They led to an unacceptable early time-to-failure. So, we implemented another process which is Structural Proof Testing. In that case we mechanically loaded the object to fail at a strength level which would be associated with a certain flaw size. Any article which passed that test had a flaw size not greater than that flaw size. One could then predict it had a failure-free life not shorter than that quantity.

This represented a truncation of the flaw distribution. We operated on that truncation to guarantee a failure-free interval. We implemented that on the F-111 carry-through box. We actually broke three of those boxes in the ground test facility. We have done this three times on a recurring basis as the flaw size increases to extend the failure-free life. The objective is to control the largest flaw. In fact, two additional F-111 carry-through boxes in Australia failed the cold-proof test this year. Each of those failures saved an airplane, and they also saved the crew.

Environmental stress screening of electronic assemblies is similar. It represents an integration of design usage, manufacturing quality and the ability to inspect or control the worst flaw sizes in the product. The difference in perspective is to consider the truncation of the flaw distribution as being distinct from the magnitude of the flaw

distribution and the expected frequency failure occurrence in service.

If we want to use that same concept for avionics, we have to ask ourselves a series of questions. First, we must challenge the assumption that failures in electronic systems are random. We do not believe they are random. We have a large dispersion in life because of the large dispersion in the flaws that are inherent in the manufacturing process. However, when solder joints at different locations fail, they fail for the same physical causes. What we are seeing is the variability in the location of the flaw and the flaw size. The fact that there are many locations in an assembly is not a justification for the attitude that flaws are uncorrectable. If you look at a modern airframe, we have almost a million holes in the primary airframe for the fasteners and the like, but yet we manage those to a worst case flaw size. A legitimate question to ask for electronic assemblies: "Do we know them, and can we describe the failure processes? Can we get a predictable and a useful failure-free life out of the assembly?".

Is our current maintenance policy, corrective maintenance, the only solution? If not, is it the best solution? As I said, our policy is to fly the equipment until it fails. When it fails, we are forced to do on-equipment diagnostics, which is very difficult for electronic systems, and then take corrective action. We would prefer a policy which provides us with an option for preventive maintenance as distinct from corrective maintenance.

A series of studies associated with the advanced radar systems in the early 1970's was conducted which eventually evolved a concept for multi-layered printed wiring board assemblies. Figure 6 shows the construction of a typical printed circuit board. It has fiberglass epoxy as the primary carrier. It has layers of copper conductors printed on the surface, laminated together, to provide conducting paths for the parts to talk to each other. It has holes that have been drilled through the boards at these locations. Those holes are plated with copper so you can send a signal down through the board and so that it can talk back and forth. We also have discrete parts, wires which provide strain relief for flexure and thermal expansion differences, and some flat packs which have been soldered directly to the board and through the board. The current technology is solder-pad mounting with no strain relief at all; the solder must accommodate the shear from the induced-vibration deflection and the thermal expansion.

The printed circuit board assembly is a series of thermal mismatches as well as stiffness mismatches in a layered or a laminated concept. Temperature cycling is shown as a simple illustration of the laminated concept; if you go through a series of thermal cycles, you generate that bi-material strip example where you induce tension and compression depending upon those relative expansion mismatches. That temperature cycle, in turn, drives failure processes into different locations. In fact, you generate a fatigue-life curve which relates the board deflection to the number of cycles to failure.

Figure 7 also illustrates the board deflection problem. In an acoustic environment, as the boards deflect, we induce a series of bending loads into the leads which are the source of failure; either the solder is sheared out, or the case is ruptured which then allows moisture and other environments to enter. We generally see that reported as a corrosion failure in the chip itself.

In the 1970-1971 time frame, a series of companies started some in-house test programs on some electronic assemblies, like we showed. One of them was General Electric Aircraft Lab at their Utica facility. They removed the active chips from the flat packs and the "dips", and they left some wires running through the flat pack. They mounted them on the circuit boards, and they went through the complete processing cycle, including the conformal coating; and then they went through a series of experiments with different types of simplistic thermal histories with a basic background of .02 g^2 per Hz vibration on a continuous level.

Interestingly enough, they found an induction time of 570 cycles on well developed boards that were carefully controlled in the manufacturing process. After that, the barrel of one of those plated-though holes ruptured. As they continued the test, the second hole ruptured and so on, and a fatigue-failure distribution was developed as a result of this stimulus, Figure 8.

They reduced the magnitude of the temperature cycle, and instead of the barrel of the hole failing, the failures occurred in the leads of the flat pack where they were soldered directly onto the board. Sequential failures in those soldered joints started to build up. Figure 8 shows the time to first-failure, and the time to first-failure has become much longer because of the decreased stress.

As the analysis went on, they and several others were able to construct a series of plots. Figure 9 shows a typical plot. It shows the 570 thermal cycles with the hole failure. It shows the number of cycles to failure of the soldered joint at the foot underneath the soldered flat pack. It also shows a low cycle fatigue life prediction for the copper plated through-holes using the Manson-Coffin fatigue analysis (the open circles). The analysis took the measured out-of-plane expansion strain of the wiring board, computed the difference between that and the copper, and they performed an elastic-plastic strain calculation, the

Manson-Coffin fatigue analysis, to produce an estimate of the fatigue life.

They are continuing this program at General Electric in Utica, and they have collected additional data on other assemblies. Interestingly, similar data showed up in a symposium of the Institute for Printed Circuits ten years later. A company that makes commercial printed wiring boards on the West Coast had some Japanese customers. Their Japanese customers look at durability in terms of the number of thermal cycles their product can survive. They asked the company to build a 12-layer fiberglass board with 400 plated-through holes, and to go through the same process. When they did that, they got the same time to first-failure data in the worst of the 400 holes, the filled squares in Figure 9.

It is interesting to observe that companies in different parts of the country, and at different times, have performed an analogous experiment which describes the same type of a phenomenon in quantitative terms. In effect, Figure 8 shows a very simplistic but classical fatigue diagram which suggests that the failures were not random; they were fatigue failures and are a discernible and a measurable quantity.

The change in perspective provides manufacturing quality with two options. The first option, the classical concept, is to run a "burn-in"; we do it at lower levels of assembly today and call that Environmental Stress Screening. An alternative option is to use Environmental Stress Screening as if we were running a proof test on a structure. That philosophy is to provide a level of vibration and temperature which will induce a somewhat larger stress in the product than it would see in service. A series of 20 thermal cycles of a certain order of magnitude can be run. Figure 9 shows a point where they would intercept a fatigue curve, (Remember, the assumption is these fatigue curves represent equivalent manufacturing quality.). At the point of interruption of the dashed fatigue curve, we will have failed parts which have large flaws or infant mortality types of failures. Anything that survives that magnitude is assumed to have a fatigue curve that is no worse than the dashed fatigue curve shown in Figure 9. When the product is put into service, if the operating stresses are less than those on that dashed fatigue curve, then the length of time to expected failure will be longer. That is in a fatigue format, basically the same thing one does in a crack growth format for the management of a proof test certification for an aircraft structure, a pressure vessel, a gas pipeline, or a pressure accumulator and hydraulic system.

In summary, we have two philosophical ways of looking at it. In our traditional burn-in philosophy, we tend to consider stress screening as screening at nearly the same level as the equipment experiences in service, and we hope to reduce the total concentration of flaws in the population. An alternative is to try to screen out the worst flaws in the population, then provide a reduced stress to operate for a period without failures in service. We are looking at both of those examples as the baseline for achieving avionics integrity/reliability.

If the service life extends beyond the expected time to failure, the boards will start to experience the typical fatigue failure population. If one does this calculation, one will project something like a growth of two and a half, or three and a half in the mean time between failure. If the proof test process is repeated at the completion of the failure-free period: rescreening, repair and reinsertion into service, then you can reduce the failure rates to about three per cent of the typical failure rates of today. These failures represent induced failures from other parts of the equipment you can't control.

From this perspective let us survey the causes of field failures, Figure 10. First note that 25 to 45% of all "unscheduled" maintenance actions for a modern aircraft are associated with electronic functions. Why? Because our maintenance policy is one of corrective maintenance. Figure 10 also shows that nearly 50% of the equipment taken off the airplane had physical failures in either the boards or in the parts. Another 45% to 50% had failures induced by corrosion which created thin but high resistance films on the surfaces of the connectors and eventually resulted in an open circuit in the system. This film is similar to what you see in your household on silverware. We found very few parts failed because of electrical overstress in the system itself. That says the electrical engineers are doing a very good job in designing the product from an electronic design viewpoint. The causes of the field failures are those things we do not directly address in our design methodology today; and in electronic systems, they are basically the mechanical and chemical nature of the environment in which the system operates. We then see that the electrical parts and components in the system will essentially function until a mechanical or a chemical failure process creates an open circuit due to the failure of the system itself. We are orienting ourselves to addressing and controlling these processes.

We must control the chemical and the mechanical failure process at different levels of assemblies; this includes the piece parts, the interconnections between the parts and the boards, the intermittent failure mechanisms inside the boards and the cables and connectors. This also includes the hybrids which are simulated parts on small boards inside cans, and which are mounted on a larger board. We believe those failure processes are predominantly mechanical and chemical, and there

is a time-dependent dielectric breakdown process which is a problem in power supply design.

Design criteria will be in terms of mechanical and thermal criteria. Derating by limiting temperature has been practiced, is useful, and it controls many problems in the design. However, one needs to directly address the thermal mismatch problems that are created in terms of allowable induced strains. A surface-mounted part on a board is a typical failure you will encounter. They have a spacer under that, and they also have copper leads running through it. The leads run into the board, and they are soldered to the board. That spacer material expands by an order of magnitude greater than the copper leads; it puts tension on the leads, and shears out the solder joint typically in 100 hours or so. You would be surprised how many field failures are as simple as that.

We are considering a series of allowable strains between the parts and the board in terms of the strain limits on the solders within the conductors to the boards, Figure 11. We are also considering the induced stresses in the leads, the fatigue life of the leads themselves, a dielectric margin and an allowable board deflection. We have had to come to grips with the acoustic environment. We have a great deal of very good work that has occurred in MIL-STD-810 in describing the environments in the avionics equipment bays. But, the vibration that is induced in the board itself causes the failure. We will have a process which says the parts and the board assembly can tolerate a certain deflection before a fatigue failure occurs. That deflection will then become an allowable deflection, and that will drive the design for the tuning and for the transmissibility coefficients for the environment that MIL-STD-810D describes as the exposure environment in the equipment bay itself. So, we will force criteria down to the level where we directly address the failure process itself.

The change in attitude has created some concerns. The ability to design is a strong function of how well you understand the design use of the product. We attempted to develop generic environmental profiles for broad classes of equipment. We found when we did a detailed environmental analysis on many of our systems, in most cases those generic profiles were unconservative for specific phases of the mission flights; they have caused some of our field failure problems.

Figure 12 shows some of the environmental use profiles which were the sources of our problems, and of course, the inflight vibration is one of the major sources. A major source of the thermally induced problems starts at the bottom, the desolder and resolder in the depot. Ground maintenance check-out, without any ground cooling, provides many thermal surges through the system, and often, the environmental control system in the airplane fails. We do not address any of these sources of stress. We do not address the concept of a thermal spectrum in terms of the temperature differentials in the electronic assemblies. We do that in engines where we have thermal fatigue problems. We are also considering the vibration in the mission-leg-by-mission-leg vibration profile to match that against the thermal exceedance profile in the restructuring of the CERT profile.

We have had a history as we have evolved in our airframe area, and we have put together packages called integrity programs. We call this program the Avionics Integrity Program, and our acquisition strategy is indicated in Figure 13. We must tell the builder what we want the system to do. Just as importantly, we must describe how we will use the system; that is our unique responsibility as the customer. We have not done as good a job as we should. We must describe some options we are interested in in maintenance, and we intend to buy a process. When we sign a contract with a vendor to build an airplane, we are buying a product, but first, we are also buying a process to generate that product. After all, in any given system, all of the materials you use, or the parts you use, are basically the same. They come from the same suppliers. They have the same defects in them, and they have the same failure processes in them. So, we are contracting for a development process which is oriented, in terms of the functional capability we will acquire with the system, and in terms of managing those failure processes to get a desired field characteristic. So, we will contract for a series of tasks in a time sequence, and we will contract for a series of design-like criteria which the assemblies have to meet. We will state that you need criteria for certain types of quantities. We will give you some advice as to what are reasonable orders of magnitude. This will go out to the contractors. They will do their trade-off studies and they will respond with that. They will tell us they will perform those tasks, and they will offer a set of quantitative design criteria to implement those. They can either use ours or their own. This will eventually go through a series of discussions, and a contract will be signed. As a part of that contract, the task structure will be put in the basic statement of work and funded, and the design criteria will also be put in the same statement of work. The requirement will then be, in effect, to do an analytical CERT to develop the design. At CDR provide an analysis which says, "The design on the drawings that goes down on the prototype development, in principle, can satisfy the function and the life requirements of the product." At the time the production decision is made, the functional and life requirements, as well as the active manufacturing control process, the Environmental Stress Screening procedures, etc., will be formally qualified through laboratory testing. These processes will be applied in the

manufacturing phase. Understand now the life of the product in the field varies as a function of the vibration and the number of thermal cycles the product sees. It must be realized that a product is rarely used the way we contract it. We generally alter our usage as we begin to understand the vehicle. So, we will institute a task for ourselves to track the vehicle design usage and to readjust our life expectations based on that. When we implement repair actions, we must implement the same level of quality control in our repair depots as we required industry to implement to maintain the integrity of the product.

We will end up funding the same magnitude of a development program that we did for the primary airframes and the engines, Figure 14. On an airframe we have a full static airframe article that we use to assess the design limits for static strength as well as for dynamic characteristics. We do the same thing on the engine. We have been doing this with MIL-STD-810. We will merge the functional qualification test and the environmental qualification test into one test. I have written it here as an environmental test. I don't mean to say that; but, we will use the MIL-STD-810 document as the equivalent of a static strength article to verify function in the worst cases, and that there is a static margin for the capability of the electronic assembly.

We consider durability as the ability of the product to endure the stresses it exceeds for its design life. We have a durability article in the airframe specification, and a durability test on a typical airframe is a multimillion dollar investment. We have a very difficult time funding the reliability test for the electronic assembly, and that is one of the reasons that we have had problems on some programs. We will consider funding two to three development test articles, and we will use them to demonstrate both design sufficiency and readiness for production. Readiness for production means the quality assurance process to control the flaw size distribution in the product will be ready, and it will be a part of the reliability qualification test that is conducted at that time.

When you have a failure in the test, how do you differentiate between an overstress, in terms of induced stresses in the parts, or a slightly larger flaw size in the manufacturing process? The two are intrinsically coupled together. When we have separated them because of the way we are organized in our bureaucracies, we have denied that interaction, and that is a fundamental cause of the problems in the transition from design to production.

CERT - we will probably consider simulated flight for flight as a function of a series of design missions; we do this when we consider several discrete design missions, and when we consider simulating our expected vibration spectrum and the number of thermal cycles as a function of the mission legs in the CERT profile. So, the structure of the CERT process will start to look like the durability test on the airframe in terms of the rationale of how that is put together. We will look at a damage tolerance with flaw insertion predominantly for assessing redundancy in built-in test functions in the electronic assembly; this is very similar to what we do for safety problems.

This represents a change in emphasis in reliability management. When we started using electron tubes back in the 1940's, we did not have much of a formal reliability management scheme. Most of our efforts were in manufacturing and quality control. We started to learn that tubes had vibration and thermal fatigue problems. Just after World War II, we started introducing significant mechanical engineering disciplines into the design of the system. However, the problems in tubes became so large, in terms of the high failure rate, that a great deal of work was developed in the statistical area to describe and characterize the nature of those problems for management of the product in the field.

Since the beginning of the 1960's we have had MIL-STD-781, MIL-STD-785 and MIL-STD-810; MIL-STD-810 is not a description of statistical reliability. It describes the usage and the implementation of parts programs. Since then, we have seen an emphasis on gaining management visibility in terms of describing as a function of a series of design missions; we do this when we consider several discrete design missions, and when we consider simulating our expected vibration spectrum and the number of thermal cycles as a function of the mission legs in the CERT profile. So the structure of the CERT process will start to look like the durability test on the airframe in terms of the rationale of how that is put together. We will look at a damage tolerance with flaw insertion predominantly for assessing redundancy in built-in test functions in the electronic assembly; this is very similar to what we do for safety problems.

Today a process is taking place where we are becoming oriented toward the cause of failure; this involves describing the nature of the flaws, the nature of the stresses that drive the flaws and the fundamental laws that link those two together. We are also beginning to see a reemergence of a design methodology which is oriented toward the stress function and toward some concept of fatigue or fracture control. We will then see a reemergence in the mechanical, thermal and environmental design in terms of flaw control in failure prevention types of methodology. We will retain the benefits of the statistical reliability. Instead of emphasizing the reliability visibility function, we will try to make designing to prevent field failures more visible.

To summarize, we are in the process of restructuring our electronics activities to follow the paths that worked for us in safety of flight structure. We believe the physics and chemistry are there to support that, and the advanced analytical techniques will allow us to do the type of calculations and experiments we need. We will address the causes of electronic systems failure directly. A very unfortunate by-product of statistical reliability was the impression that failures were inevitable, and there was a fatalistic acceptance of it. That was not the intent of the community that gave us that as a technical foundation, but that by-product has affected our thought and our cultural process.

We are considering making that a deterministic process; it will be deterministic in the sense of addressing where the tails of the flaw distributions are and controlling to that. We believe fault-tolerant design recognizes that products come out of manufacturing with defects. They are imperfect, and they will fail. You must control that process by controlling the flaw size distribution, and you must control the stress levels. Our products are stressed very highly when you think about it. The typical stress and strain in electronic assemblies is two to three times the allowable stress and strain in an aircraft wing, in a turbine disk or in a primary structure.

So, conservative design is the basis for fault tolerance; that means getting low stress levels. Support that for critical safety flight with redundancy because you pay penalties with redundancy. Think about that for a moment on that airplane that you fly home or on all military airplanes; we have not certified a redundant airplane in the United States Air Force in 20 years. Critical locations on the airplanes you saw flying are all series-connected. If a worst case flaw, or what we call a rogue flaw, is allowed to grow in one of those assemblies, it will take down the airplane, and in most cases, it will take the crew with it. We manage those without redundancy because we control flaw sizes, and we control stress levels. In the case of control systems we put in redundancy as an additional set of suspenders. We have had an unfortunate situation in the electronics area where we have used redundancy as a substitute for understanding and addressing directly the causes of failure.

Finally, we want to create an option where we can do some kind of a preventive maintenance. We think that is the best way to grow the system's reliability, and we think ultimately that will end up in a cheaper life cycle cost. We appreciate your interest. We are looking forward to your support. There will be many challenges in your area. We are willing to work with you, and we need your capabilities.

Suggested Figures

Figure 1	Showing Aircraft Structural Integrity Program of 1970, the Engine Structural Integrity Program of 1975, and the Avionics Integrity Program (AVIP) of 1980.
Figure 2	Depicting a transition from the electron tube technology, through transistors, to integrated circuits.
Figure 3	Depicts the flight hours between failures and number of components.
Figure 4	Relation between flaws and structural strength.
Figure 5	Discussion of distribution of imperfections in a product and flaw size.
Figure 6	Construction of a typical printed wiring board. Loads and deflections of a printed circuit board.
Figure 7	Fatigue life governed by board deflections and defects.
Figure 8	Fatigue failures in printed wire board assemblies.
Figure 9	Fatigue failures in printed wiring board assemblies and the concept of using Environmental Stress Screening as a proof test.
Figure 10	Distribution of causes of aircraft electronic equipment failures.
Figure 11	Failure processes/criteria.
Figure 12	Design to usage environmental profiles and sources of environmentally induced problems.
Figure 13	AVIP - Acquisition approach.
Figure 14	Comparative ground test.

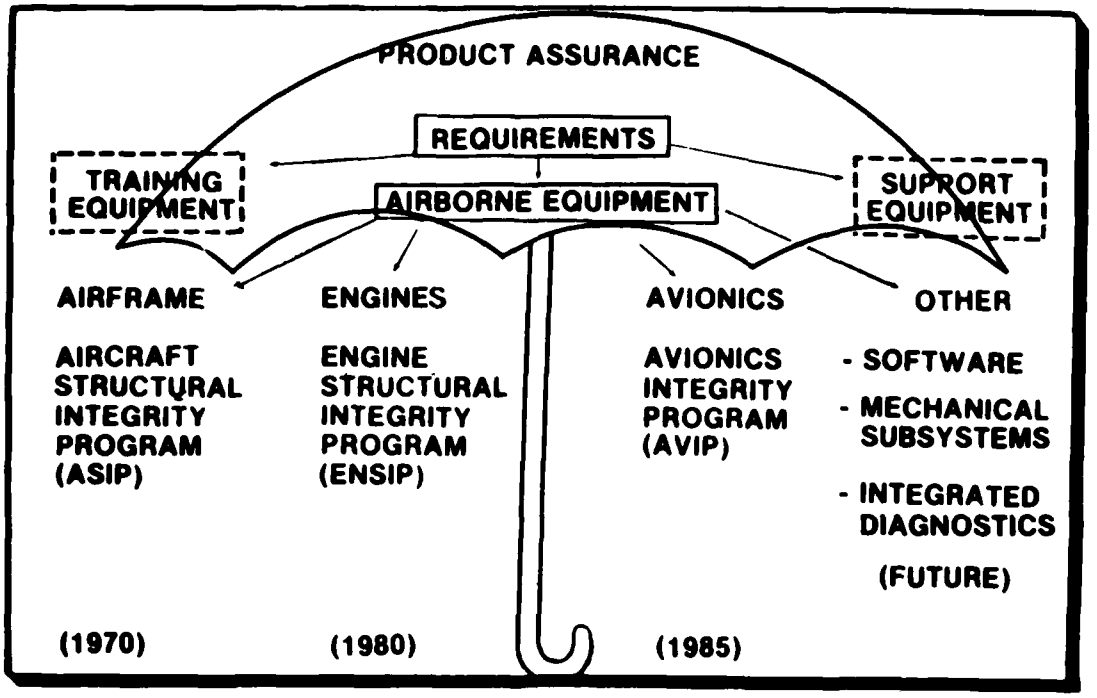

Fig. 1 — Showing Aircraft Structural Integrity Program of 1970, the Engine Structural Integrity Program of 1975, and the Avionics Integrity Program (AVIP) of 1980

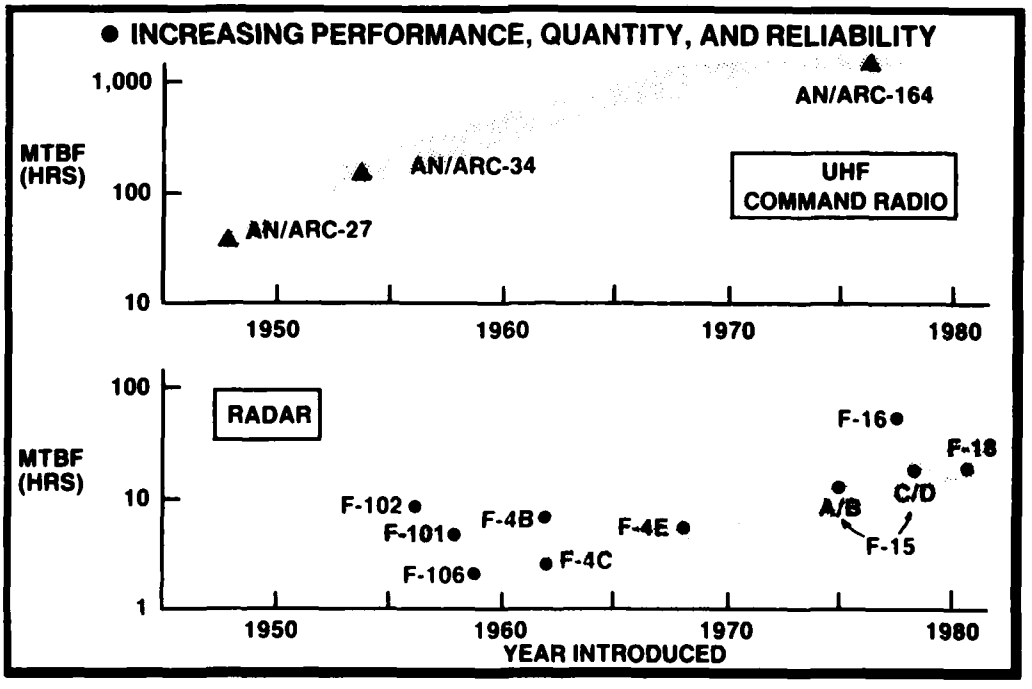

Fig. 2 — Depicting a transition from the electron tube technology, through transistors, to integrated circuits

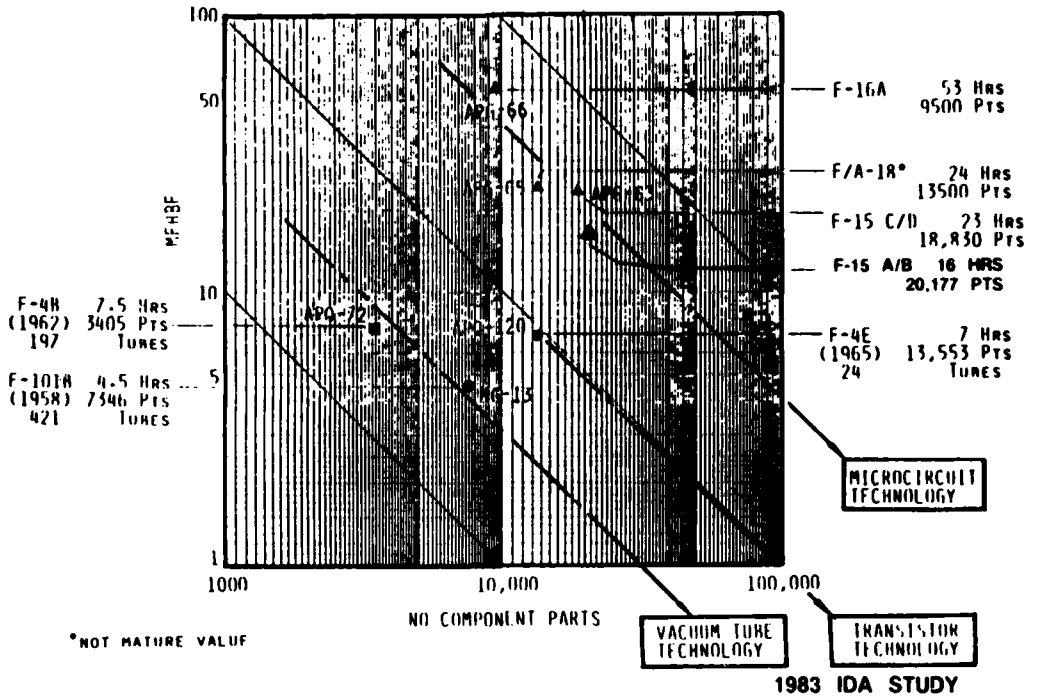

Fig. 3 — Depicts the flight hours between failures and number of components

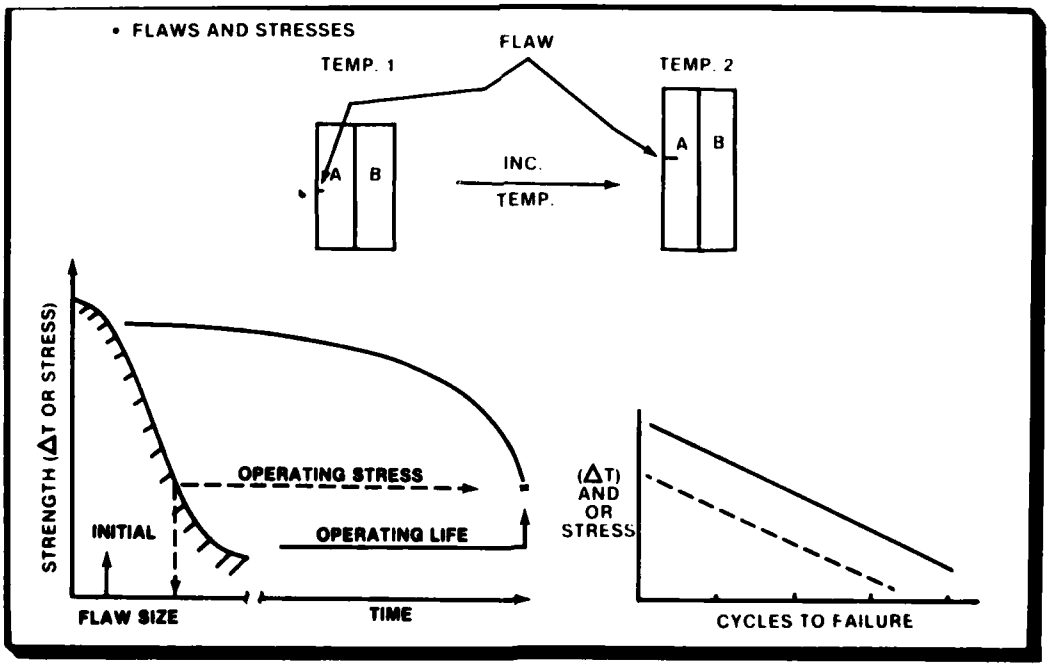

Fig. 4 — Relation between flaws and structural strength

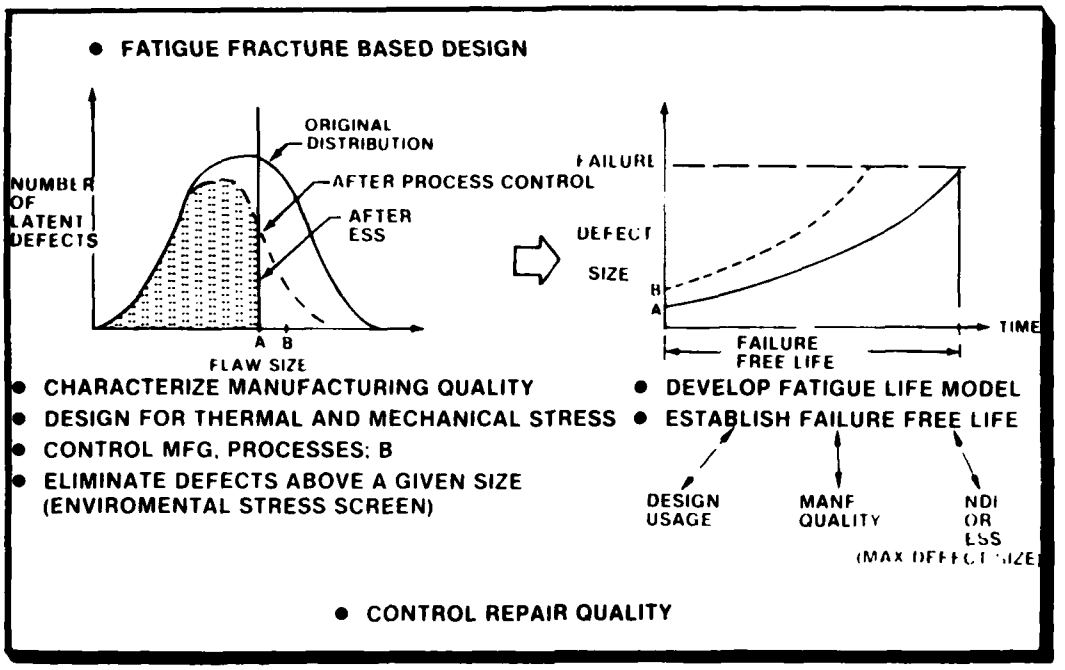

Fig. 5 — Discussion of distribution of imperfections in a product and flaw size

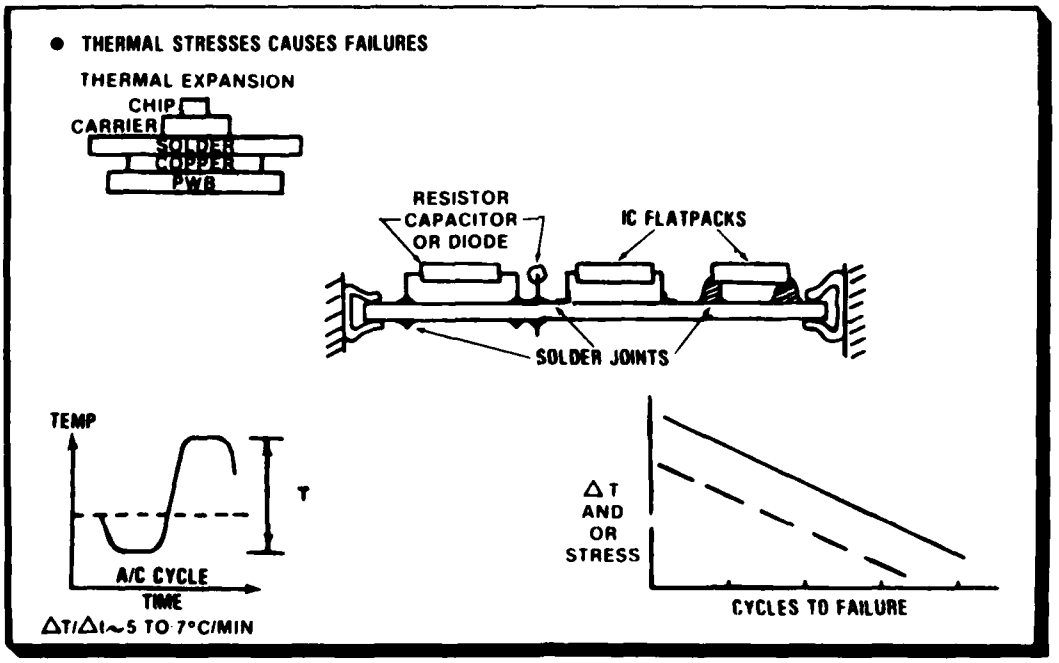

Fig. 6 — Construction of a typical printed wiring board. Loads and deflections of a printed circuit board.

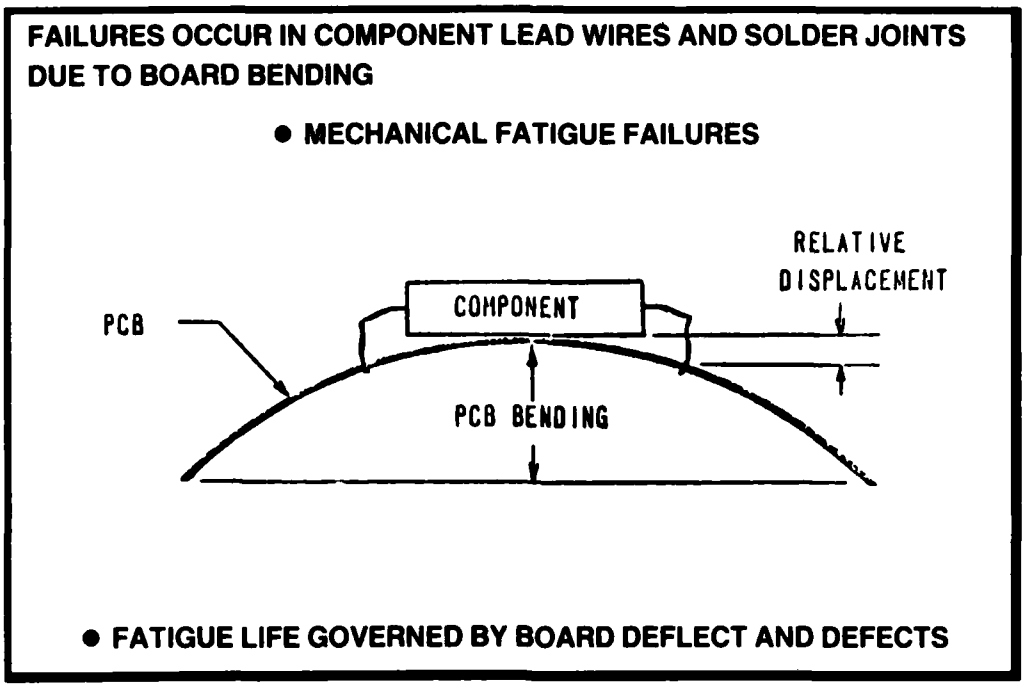

Fig. 7 — Fatigue life governed by board deflections and defects

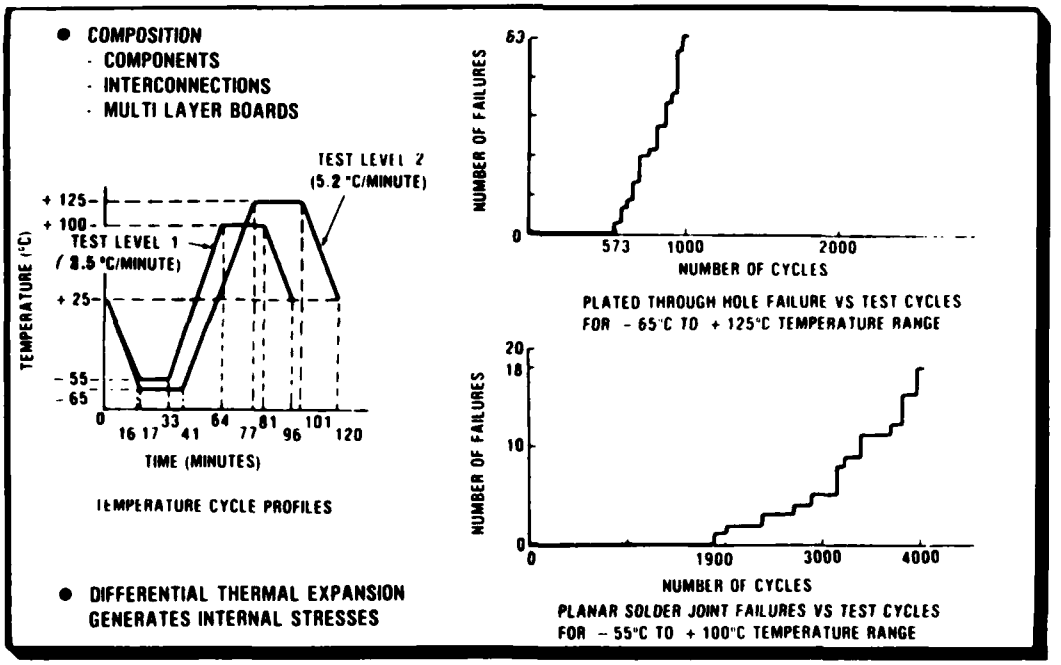

Fig. 8 — Fatigue failures in printed wire board assemblies

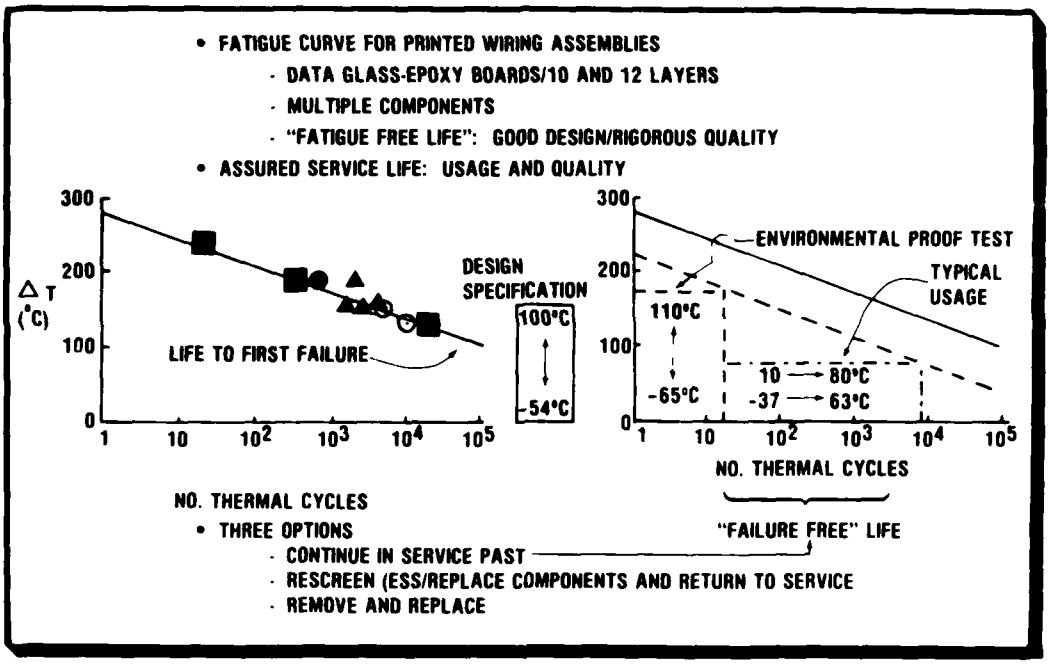

Fig. 9 — Fatigue failures in printed wiring board assemblies and the concept of using Environmental Stress Screening as a proof test

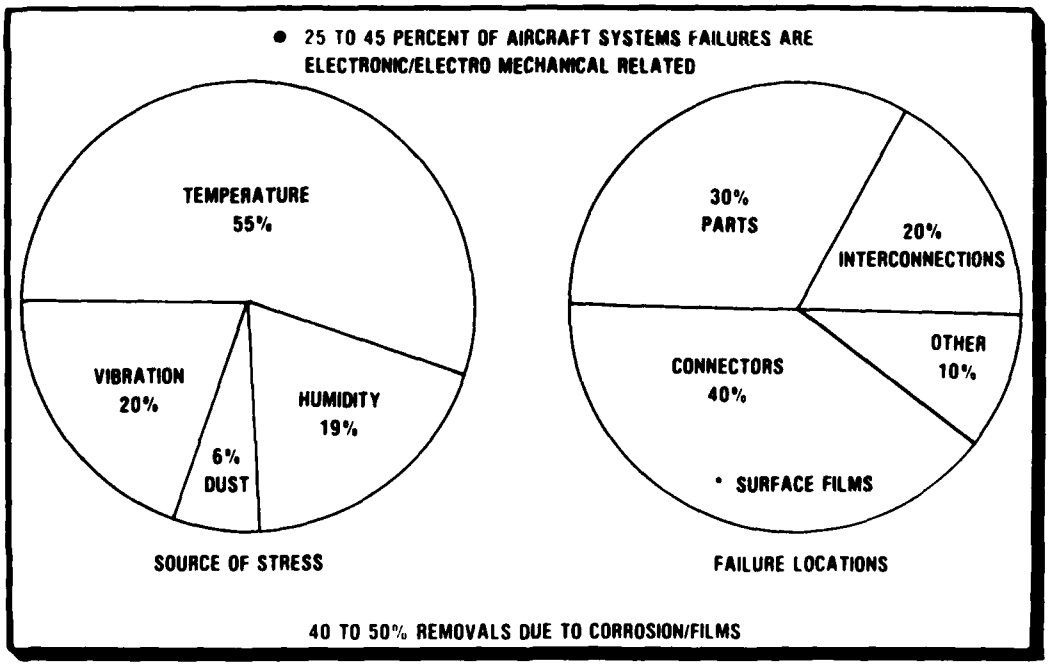

Fig. 10 — Distribution of causes of aircraft electronic equipment failures

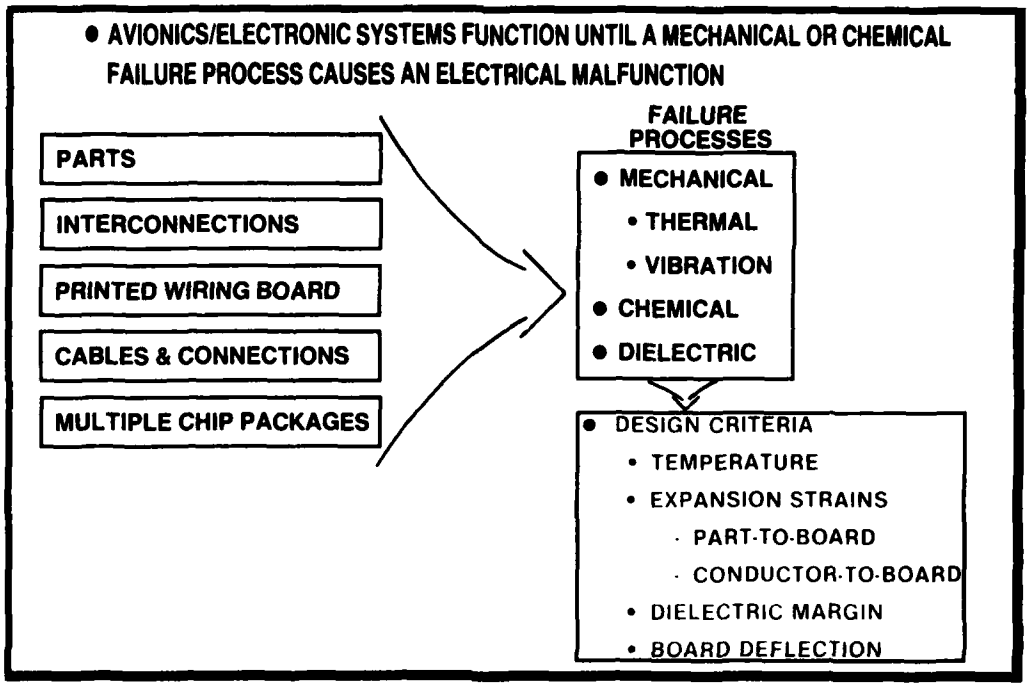

Fig. 11 — Failure processes/criteria

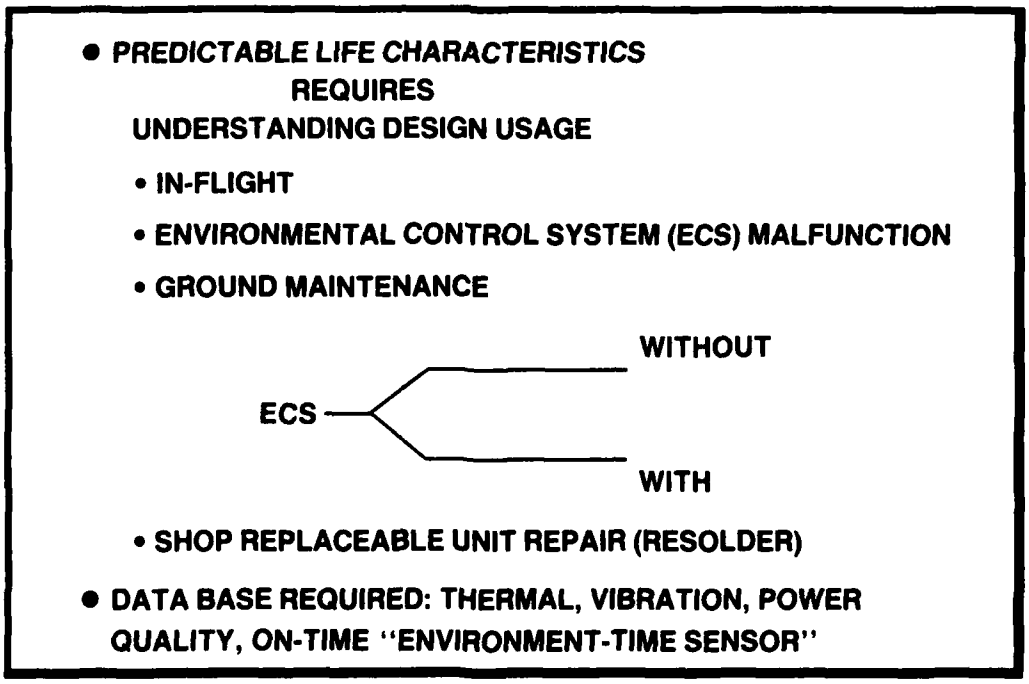

Fig. 12 — Design to usage environmental profiles and sources of environmentally induced problems

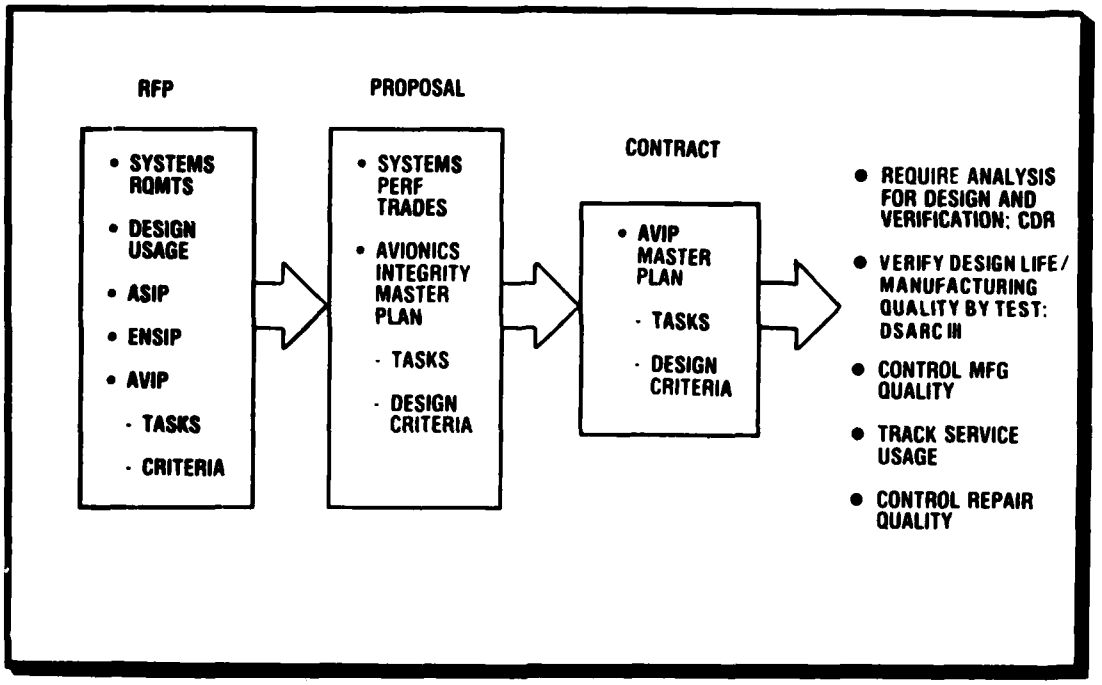

Fig. 13 — AVIP — Acquisition approach

PRODUCT ASSURANCE REQUIREMENT	QUALIFICATION TESTS		
	AIRFRAME	ENGINE	ELECTRONICS
• STATIC TEST	• STATIC ARTICLE (STRENGTH)	• STATIC ARTICLE (STRENGTH)	• ENVIRONMENTAL QUAL TEST (DESIGN LIMITS)
• DURABILITY • RELIABILITY	• DURABILITY ARTICLE - DURABILITY FLAW SIZES - FATIGUE TEST - REQ. LIFE (2 X DL)	• DURABILITY ARTICLES (2) - DURABILITY FLAW SIZES - AMT - REQ. LIFE	• REL. DEMO ARTICLES (> 2) - ESS FLAW SIZES/QUALITY - CERT - TEST TIME TO DEMO MTBF AND REQ. LIFE (NEW)
• DAMAGE TOLERANCE • FAULT TOLERANCE	• DAMAGE TOL. ARTICLE - INTRODUCE DAMAGE TOLERANCE FLAWS - TEST FOR REQUIRED UNREPAIRED SERVICE TIME USAGE - DEMO. MIN. REQ RESIDUAL STRENGTH	• DAMAGE TOL. ARTICLE	• FLAW INSERTION BUILT IN TEST • VERIFICATION OF REDUNDANCY

Fig. 14 — Comparative ground test

DYNAMICS R&D IN THE AFWAL STRUCTURES AND DYNAMICS DIVISION

Dr. James J. Olsen
Assistant for Research and Technology
AFWAL/FIB
Wright-Patterson AFB, OH 45433

ABSTRACT

This paper gives a brief overview of the recent accomplishments, current activities and plans for in-house R&D, contractual R&D and systems support in structural dynamics by the Structures and Dynamics Division, Flight Dynamics Laboratory, Air Force Wright Aeronautical Laboratories.

INTRODUCTION AND GENERAL OBJECTIVES

The activities and plans of the AFWAL Structures and Dynamics Division (Table 1) are guided by the AFWAL Major Thrusts and the Division Planning Areas (Table 2). The Division Planning Areas are intended to maintain a continued approach to providing structures and dynamics technology to the Air Force and to solving problems of weapon systems in the field, independent of the year-to-year fluctuations of budget levels.

In terms of general objectives (including dynamics) for Planning Area 1, Survivable Structures, we estimate that research and development in Structures and Dynamics could achieve a 50% reduction in the time necessary to repair battle-damaged aircraft structure for 75% of repairs. With respect to aircraft operations in combat, we believe our new AGILE dynamic test facility will allow dramatic improvements in aircraft capability to operate on rough/soft/short airfields. Ski-jump takeoffs, if feasible for USAF aircraft, could reduce takeoff distances up to 50%. For fighter aircraft with external stores, with flutter suppression we could double the speed for flutter onset for certain critical store combinations and allow safe carriage in high speed, low level flight.

In Planning Area 2, Advanced Aeronautical Structural Concepts, we could achieve a 10% reduction in the weight of today's aluminum structures through new low density alloys. Using graphite/epoxy composites on 50% of an advanced fighter structure could result in 20% weight reduction from today's baselines. High temperature and high strain organic composites are on the horizon which will allow their use at Mach numbers above 2, with even more weight reduction over graphite/epoxy.

In Planning Area 3, Aircraft Structural Integrity, we could obtain 50% reduction in structural inspection costs for advanced fighters by allowing (at least) doubled inspection intervals for laminated metallic and organic composite structures. Development of a fatigue and fracture data base for metal-matrix composites can allow their use to achieve a 20% reduction in structural weight for fighters and 30% for manned, maneuverable reentry vehicles. Fuel tank sealing is still a problem for some combat aircraft, but 30% to 50% improvement in maintenance manhours per flight hour is surely achievable.

In Planning Area 4, Spacecraft Structures, structural weight fractions as low as 10% may be necessary for manned, maneuverable transatmospheric vehicles. For large surveillance satellites vibration levels can be reduced to sub-micron levels by the late 1980's, and lifetimes can be tripled to 15 years with integrated active and passive vibration control. Development of active and passive control of the structural shape of laser mirrors and the dynamic response of supporting structures will allow substantial increases in time-on-target and an increase of laser brightness on target by a factor of 100.

In the Structures and Dynamics Technology Base, we believe it is essential to maintain a cadre of structural experts in the Air Force, with the facilities necessary to lay the foundation for future weapon systems and solve problems of today. We expect (more than one) order of magnitude improvement in the Air Force's capability to analyze, understand and improve the structural performance of its aircraft fleet. Flight-induced loads are changing drastically as aircraft enter new maneuver regimes, and the future's burgeoning computer capabilities must be employed to design

future weapon systems to withstand those loads. Increased engine power and supersonic weapon-delivery will cause substantially higher levels of turbulence, noise, buffet and resulting vibrations. At the same time aircraft wings may become even more flexible to achieve the required combat maneuverability. All of these factors point to new flight regimes, new loading conditions, new kinds of aircraft, new kinds of analyses and tests and the need for a technology base of experts who can move from a solid foundation to react to new conditions. To achieve these goals, tools must be available for rapid preliminary design studies involving new materials, structural concepts and unusual configurations. Integrated analysis and optimization programs developed for supercomputers can eliminate the piecemeal or compartmentalized approach to design, and these programs must be supported by effective pre and post processors (Computer Aided Design Systems).

CURRENT PROGRAMS AND PLANS IN DYNAMICS

Survivable Structures

Ballistic Vulnerability and Hardening

Combined in-house/contract programs under the direction of Mr. J. D. Oetting of FIBC are determining the relative susceptibility of metal and composite fuel tanks to ballistic damage, particularly hydrodynamic ram (Figure 1). In another program on composite compression structures, a series of composite plates will be ballistically impacted while loaded in compression and then loaded to failure. Analysis methods are to be verified and/or modified, and a representative fighter-wing box beam will be constructed (using the most promising design concepts) and tested. The long term goal is to develop guidelines for the design of composite integral fuel tanks which will survive ballistic impacts by 1986 and develop structural concepts with increased ballistic survivability by 1988.

Short/Rough/Damaged Runways

The AGILE facility (Figure 2) is now operational in FIBT, and the AGILE Project Director is Bill Johnson of FIBE. The idea is to replace much of expensive, time-consuming and sparsely-instrumented flight (taxi) tests with precisely controlled laboratory dynamic tests. AGILE can simulate the dynamic response of aircraft with weights up to 100,000 lbs. for sinusoidal, random or transient runway inputs. Bumps/dips can be as much as 10 inches high/deep, and the "shakers" are fully responsive up to frequencies of 30Hz. Of particular current interest are the "NATO/AGARD Standard Bumps" (Figure 3). They will be used throughout NATO in the search for methods to classify the "NATO interoperability" of all of NATO's airforces. Typical response plots are shown in Figures 4, 5, and 6.

Figure 4 is an AGILE simulation of the YF-16 main gear traversing a three-inch (+)"ramp" at 60 knots, the response decaying, and then a following three-inch (-)"ramp". Even though only the main gear shakers were active, note the significant response in the nose gear. Figure 5 is an AGILE simulation of the nose gear, then the main gear, traversing a three-inch high "repair mat" at 45 knots. Note the amplification of the acceleration at the main gear axle and at the outboard wing when the aircraft "drops off" the trailing ramp of the repair mat. Figure 6 is an AGILE simulation of the YF-16 traversing a three-inch high repair mat with "sag" at 20 knots. Note the slight asymmetry of the left/right responses (due to the differing maintenance state of each landing gear).

Our immediate goals are to exploit the AGILE facility to evaluate and improve the rough field capabilities of the F-4, A-7, F-15, F-16, ATF, their successive modifications and competitive aircraft. We also intend to develop improved methods to predict airframe loads due to taxi, towing, turning, braking, jacking and rough airfields by 1986.

In related studies, Tony Gerardi and Lige Turner of FIBE initiated the analysis of applications of SKI-JUMPS to the runway denial problem in Europe. The SKI-JUMP concept has the potential of reducing the takeoff roll requirements for combat loaded aircraft by 50%. (Figure 7) In the present situation a small number of bombing passes could effectively close NATO airfields. Runways that are in the range of 10,000-15,000 feet need only to be damaged at two places in order to limit operational segments to 5,000 feet or less. An effective means of launching combat loaded aircraft in as little as 1,500 feet may be within the capability of SKI-JUMP, and the possibility of enemy action to close NATO airbases would be significantly reduced. The cost of implementing SKI-JUMP at NATO airbases may be inexpensive when compared with other solutions.

In other aspects of the "Short Runways" problem, Leonard Shaw and Howard Wolfe of FIBE are developing plans to improve analytical prediction methods for defining the aeroacoustic environments due to STOL operations. Experiments will be conducted to validate and/or modify those prediction models. The goal is to develop methods to predict STOL propulsion noise by 1990 for configurations like Figure 8 for the prevention of sonic fatigue in secondary structures.

Flutter Suppression

Terry Harris and Dale Cooley of FIBR are directing the rapid development of the technology from merely active control to fully adaptive methods to sense impending flutter, initiate the proper control algorithms and

perform the required control surface motions to suppress flutter - all within milliseconds. Figure 9 shows data traces taken during the 1982 adaptive flutter suppression wind tunnel demonstrations. In the test represented by this figure, the ejection of the tip store instantaneously caused flutter on the model. The adaptive system identified the flutter condition and initiated flutter suppression in .2 seconds. Without the flutter suppression system, this flutter mode would have quickly destroyed the model. These tests provided the first validation of the Northrop/Honeywell techniques of adaptive flutter suppression. Over the two year period since those initial demonstrations, Northrop and Honeywell have improved their original adaptive flutter suppression methods. When combined with the weighting and selection of sensors in real time, those methods have resulted in a realistic suppression of flutter over wide ranges of Mach numbers and store configurations. General Dynamics has successfully applied improved parameter identification techniques (Block Recursive Least Squares and Modified Extended Least Squares) to previously recorded wind tunnel data to show that a stabilizing signal could be produced in a fraction of a second. Recently we have awarded contracts to both Northrop and General Dynamics to design adaptive flutter suppression systems for wind tunnel demonstrations. After design reviews in the summer of 1985, we will choose one contractor to test his design in the wind tunnel. Two entries are scheduled for the NASA Langley Transonic Dynamics Tunnel - one for the fall of 1985 and one for winter 1986.

In related activities, Terry Harris and Dan Schumacher of FIBR performed flutter analyses for an F-16 fighter aircraft carrying mixtures of guided bombs, external fuel tanks, AIM-9's and AMRAAM's. Some configurations were calculated to flutter at high speeds, but they found that simple, single sensor control laws could substantially increase the flight dynamic pressure of flutter onset. At the time of the design study, General Dynamics had independently found several flutter-critical configurations during wind tunnel testing. Subsequent flight testing verified flutter for these configurations. (Flutter occurrences found in flight generally have been mild, limit-cycle flutter, rather than the violent, quickly destructive flutter observed in the wind tunnel.) The work accomplished by FIB provided a very timely indication of potential to prevent flutter for the F-16 through active flutter suppression.

The overall goal of the flutter suppression work is to demonstrate (in the wind tunnel) the active/adaptive algorithms to suppress wing flutter with a multitude of configurations of external stores and fuel loads (1987); initiate mods for the flight test demonstration in 1986; and complete the demonstration in 1990.

Advanced Aeronautical Structural Concepts

New Alloys and Fabrication Processes

The skins and substructure of military aircraft are exposed to damaging environments that can reduce structural fatigue life and adversely affect electronic equipment. Structural surfaces that are exposed to intense sound pressure levels (such as in regions adjacent to and aft of engine exhaust) are especially vulnerable. The application of integral passive damping has shown the capability to increase the sonic fatigue life of aircraft structures and to extend the time-between-failures of sensitive electronic gear in equipment bays. Incorporating various damping concepts, such as those shown in Figure 10, into fuselage structure could result in greater structural integrity and durability, increased equipment reliability, and reduced life cycle costs during the projected service-life of the aircraft.

Carl Rupert of FIBE will direct a contract program to achieve these goals in a combined analytical and experimental effort. We have selected a baseline aircraft structure that would benefit from the application of passive damping. A contractor will design and build a replacement component using integral damping. Dynamic and structural integrity tests on both the baseline and advanced designs will provide the basis for a before-and-after comparison to demonstrate and evaluate the program's payoff. In a following program, composite coupons and test panels of candidate structural designs and damping treatments will be designed, fabricated and tested.

The long term goal is to demonstrate the ability of passive structural damping technology to substantially reduce noise and vibration in structures and in equipment bays like the B-1B by 1988.

Lt. Col. Wayne Bassett of FIBA is directing a current program to reduce high maintenance costs associated with sonic fatigue on operational aircraft. The approach is to identify component parts that require repair or replacement, that have typical, service-wide problems, and that could realize reduced costs of ownership through a redesign effort using advanced metallic technologies, such as laminated structures. Several candidates that offer excellent opportunities for life cycle cost reductions have been selected for redesign. The components will be monitored in the service environment to determine actual improvements in durability and reductions in life cycle costs.

The A-7 center section leading edge flap, is of skin-stringer construction and is being recycled through the depot every four years for a complete rebuild, Figure 11. In-service damage includes cracked rib caps, cracked skins

and broken lugs. Preliminary investigations suggested that sonic fatigue has been the primary cause of failure. A baseline production flap was tested in an intense sonic fatigue environment in the laboratory and (after the equivalent of 1,400 service hours) exhibited the same types of failures we are finding in service. A redesigned flap using laminated skins with visco-elastic adhesives to dampen the aero-acoustic excitations was also tested, Figure 12. The new design withstood the equivalent of 80,000 service hours without signs of failure. It was then intentionally damaged to simulate battlefield damage, repaired and withstood the equivalent of an additional 40,000 hours of service life with only minor damage.

The F-111 outboard spoiler, Figure 13, represents typical aluminum honeycomb structures and is operating in an intense acoustic environment. As a result, the skins are cracking and delaminating from the honeycomb core. In some cases, whole sections of the spoiler have ripped off in flight. We are still involved in the detailed design of an improved spoiler that will also incorporate visco-elastic damping, Figure 14. On the basis of preliminary sonic fatigue tests, we expect to realize an 8-fold increase in durability of the new spoiler over the existing spoiler with only minimal increases in weight and fabrication cost.

Aircraft Structural Integrity

Conventional mechanically fastened metals continue to present high maintenance costs associated with sonic fatigue. Ralph Shimovetz and Howard Wolfe of FIBE are directing the development of an acoustic prediction handbook for use with micro, mini, and large scale computers. The programs will be designed to be compatible with CAD systems as they evolve. The basic version will be distributable on floppy disk for the AF standard Zenith computer. An existing acoustic finite element program will be modified to include structural-acoustic interaction and graphics pre and post-processing capability.

Fuel Tank Dynamics

Marty Richardson of FIBT is investigating the dynamic aspects of fuel tank leakage. Fuel tank leakage has been a dangerous and costly problem plaguing the aircraft industry and the government with extensive maintenance efforts and lengthy tie-up of aircraft. A newly recognized phenomenon involving the altering of the high frequency dynamics of fuel tank panels, as a result of a fluid-structure interaction, has shown to cause cracking and reductions in fatigue life. The increase in strain response of dry versus wet panels is illustrated in Figure 15.

This new process is a relatively high frequency mechanism and has been overlooked in the past. This effort will develop analytical methods to predict the combined effects of high frequency vibration and low frequency maneuvers on the fatigue life of fuel tanks. The work will be verified experimentally using various tank configurations to provide a basis for improved design techniques. The long term goal is to determine if there is an unexpectedly strong coupling between fluid and structural vibrations at frequencies up to 30 Hz and to modify fuel tank design practices, if necessary.

Spacecraft Structures

Under Surveillance Satellites, Dr. Vipperla Venkayya of FIBR is directing the development of dynamic analysis and optimization methods for satellite structures in the presence of active controls (Figure 16). Both continuum and discrete methods will be used in the development of analytical models for large space structures. Among the discrete methods, finite element and finite difference analysis procedures will play the primary role. The nonlinear dynamic analysis will be based on parameter identification techniques applied to small scale linear models in an iterative scheme. Figure 17 is an illustration of some of the stringent requirements on static structural deformation and dynamic response. Figure 18 reflects our assessment of the current state-of-the-art and the broad outlines of our approach to precision pointing, shape-control, vibration-control and thermal-control.

Laboratory examples of potential sensors and actuators will be constructed and integrated into a simplified spacecraft structure in the VCOSS program directed by Major Hugh (Clark) Briggs of FIBG. The interaction of the sensors, actuators, and structure with the control system will be explored. These studies will include the structural dynamics of actual hardware, including nonlinearities such as friction and saturation. The applicability of a particular constellation of sensors, actuators, and control system will be assessed for use in the NASA-Marshall laboratory experiment. The VCOSS test article is a 45-foot Astromast with an offset reflector hung from a five degree-of-freedom suspension system, Figure 19.

Dr. Lynn Rogers of FIBA is directing the exploitation of passive damping in the RELSAT programs. The approach is to establish integrally designed concepts which are fully integrated with the requirements of systems hardware. Structural assemblies will be fabricated and tested in a vibroacoustic environment. Selection of viscoelastic materials will be made on the basis of adhesive and mechanical hysteresis properties with due regard for outgassing and creep. Equipment support structures and components will be identified to reduce vibration and shock response and to improve reliability, Figure 20.

An extension of the damping ideas to the PACOSS program is also directed by Dr. Rogers.

Under PACOSS passive damping concepts are being established for various types of structure. Trade studies are being made to determine attainable performance levels with various combinations of passive damping and active control. Once the proper balance has been predicted, a dynamic test article will be fabricated and subjected to dynamic experiments, Figures 21 and 22. These experiments will include modal parameter identification and tests of settling time and jitter.

The overall goals of the spacecraft structures and dynamics program are to develop methods to reduce enormous mathematical models of satellite structures to manageable numbers of equations (1986); perform small-scale analytical and experimental evaluations of sensors, algorithms and actuators for active control of the vibrations of large, flexible, antennas (1987); develop design methods to optimize spacecraft structures in the presence of those active control systems and structural buckling; develop structural concepts for efficient load-carrying, zero-slop joints for deployable antennas (1988); demonstrate full-scale application of the use of passive damping in equipment bays to improve the vibration environment and the reliability of satellite (RELSAT) electronic components; develop analysis and design methods to minimize thermal distortions and fatigue in large satellites; perform a full-scale integration of passive and active controls (PACOSS) of the dynamic response of satellites to vibration environments, slewing maneuvers and pointing corrections (1989); and conduct shuttle-based flight tests for vibration control (VCOSS) by 1991.

The goals of related efforts in Weapon Satellites are: Improve conventional cooling techniques which impose unacceptable vibrational excitations to control thermal deformations; (Figure 23) develop a computer to model High Energy Laser (HEL) mirrors to design better mirrors and maximize beam quality in future systems; develop active/passive methods to control the thermal distortion of high energy laser mirrors and their vibratory response to cooling fluid turbulence; develop and validate full-scale, intrinsically hardened structures for future maneuverable satellites (1990); and conduct full-scale demonstrations of active/passive control of structural, thermal and dynamic response in AFWAL/FIB's structural and dynamic test facilities (1990).

Technology Base

In the Ground Loads area one major contract program with Northrop, directed by Roger Aschenbrenner of FIBE, is developing a master computer program for use in predicting the ground-induced loads on any USAF aircraft from any anticipated source. The objective is to develop a generic procedure to quickly assess the structural capability of any military aircraft regardless of its geometric or structural arrangements or the surfaces on which it operates. The program's modules will contain the geometric, structural and aerodynamic characteristics of all aircraft presently in the AF fleet, and also contain models for the various operating surfaces. Figure 24 shows the landing gear types and types of operating surfaces which are represented in the program modules. The modular structure will enable the updating of environmental and aircraft parameters as they become available. This program will be usable in varying levels of sophistication, depending on the amount of data available for the aircraft. Our long term goal is to develop and maintain the personnel, expertise, computational tools, data bases and facilities to allow the anticipation, prediction, measurement, interpretation and control of excessive dynamic ground loads on any current or future USAF or competitive aircraft.

In Flight Loads current programs are few, but Clem Schmid of FIBE expects to extend today's linearized aerodynamic and structural methods to nonlinear problems associated with abrupt and/or large incidences and rates of motion. We hope to exploit the expanding technology of computational fluid dynamics to predict steady flight loads, unsteady loads, turbulence and buffet for wings with external stores and for complex tail configurations by 1990.

In the automated design area, Dr. V. Venkayya is directing a program to develop a computerized preliminary design system based on finite element models. (Figure 25) This integrated system will have an executive system and a scientific data base supported by the engineering modules which cover the disciplines of structures and dynamics, airloads, aeroelasticity, sensitivity analysis, optimization and response to controls. (Figure 26) These modules can be exercised independently or together in developing optimum structures for aerospace vehicles. The system will have the provision for defining a variety of objective functions such as minimum mass, maximum stiffness, etc. The constraint provisions include strength, stiffness, frequency, flutter velocity, static aeroelastic requirements, etc.

Under Vibration and Acoustics, Ralph Shimovetz of the Acoustics and Vibrations Branch is directing a program to determine how an acoustic disturbance can affect the flow separation about airfoils operating at high angles of attack. The effort will characterize the influence of frequency and intensity of acoustic discrete tones on flow separation and reattachment for three airfoils and three speeds in a quiet wind tunnel. Figure 27 shows how the flow reattaches to the airfoil when the acoustic excitation is operating. Also shown is the impact of the acoustic signal on the lift coefficient with angle of attack. The dramatic change in post-stall characteristics is evident.

Long term goals in vibrations and acoustics include a program under Otto Maurer of FIBG to develop dynamic modeling which is strongly based on experiment. This requires advancements in the areas of experimental modal analysis (error estimation and assessment, identification of types, magnitude and seriousness of identified global or local nonlinearities). This will lead to determinations when linear approximations or separate nonlinear treatment should be applied. Other areas being studied include dynamic model condensation, sensitivity analysis for location and optimization of structural changes, interconnection theory or structural dynamic modification leading to dynamic component synthesis.

We will continue to update our data base under John Ach of FIBG in the ever-changing area of environmental vibration and acoustics. This involves performance of our own flight test vibration surveys and other government and industry efforts. This data base forms the backbone for empirical acoustic and vibration prediction methods which are required for the development of design criteria and vibration specifications.

In unsteady aerodynamics and aeroelasticity, contrary to our long tradition, current programs are few. However, our goals under Mike Shirk and Dale Cooley of FIBR are to rekindle our technology base, develop an agreement for a long range cooperative program with NASA and to improve the Air Force's ability to predict subsonic, supersonic and transonic steady aerodynamics, unsteady aerodynamics and aeroelastic response of complex fighter and transport wings, Figure 28; investigate the potential payoff of highly flexible, aeroelastically tailored wings to provide unprecedented maneuverability for new fighters (1987); and extend transonic unsteady aerodynamic prediction method XTRAN to control surfaces, external stores, nacelles, fuselages and multiple surfaces.

DYNAMICS FACILITIES

There are several facilities in the Structures and Dynamics Division which we use for Research and Development in Structural Dynamics.

Gene Maddux of FIBE runs the Photomechanics Facility which employs optically based metrology to measure structural response to thermal and mechanical loads. Mode shapes and resonant frequencies can be determined at frequencies from .001 Hz to 100 KHz. Displacements due to static or thermal loads can be measured from 10^{-9} to several inches. An Optical Image Analysis System is in development to reconstruct 3D video images of stereoradiographs of damaged composites. It will also be used to automate the data reduction of fringe patterns from holographs, speckle, noise, etc.

The Vibration and Acoustics Laboratory consists of two high intensity sound chambers and a large semireverberant chamber which is convertible into an anechoic room. A high bay test preparation area allows the performance of various kinds of dynamic experiments. Several electrodynamic noise generators, a random siren and electrodynamic shakers ranging in force output from a pound to 12,000 pounds compose the basic dynamic excitation system. Simultaneous data recording capabilities of up to 36 channels are available. The number of recording channels can be extended by time sharing. The resurgence of vibratory and sonic fatigue concerns at the Air Logistics Centers and operational airbases has stimulated the design and demonstration of new structural concepts to reduce maintenance and repair costs. Test and experimental support of these activities requires the upgrading of the acoustic and vibration laboratory. Improvements contemplated include an increase of sound power level in the two small acoustic chambers, extension of frequency bandwidth, simultaneous shaker and acoustic excitation, increase of the available airflow pressure and enlargement of one of the acoustic test chambers to accept test vehicles of at least the size of an ALCM. If a requirement for acoustic testing of large structural sections exists in the near future, recommissioning of the large acoustic test chamber for sonic fatigue work will be considered.

The two Mobile Field Measurement Systems, which are housed in two Diesel powered vans, are self-contained measurement laboratories. A large variety of dynamic and static data including vibration, acoustic noise, temperature acceleration, pressure, humidity, strain, etc., can be recorded and processed. The vans also contain on-board electrical generators to provide the power necessary for self-contained operation. Planned improvements include the installation of an all digital or pulse code modulated data acquisition system and the addition of a processing system which would allow on-site data analysis and evaluation of measurement results. The latter improvements particularly will enhance the capability of performing modal tests or ground vibration tests in the field.

A laboratory type ground vibration test (GVT) capability is presently available which allows modal testing of structures up to approximately fighter-size. Figure 29 shows a GVT of a F-16 aircraft which was performed with the available system. About nine shakers with different output force levels and pneumatic suspensions of various structural weights are available for this purpose. The planned addition to the field measurement and analysis capability would expand the system usage to a mobile modal test system.

AGILE consists of three 50,000-pound hydraulic shakers and their control systems to simulate the response of any aircraft (up to

100,000 pounds) to operation on damaged and repaired runways. Each shaker has a potential dynamic amplitude of 10 inches and is separately programmable to allow sinusoidal, random or transient runway profiles. The facility can be completely enclosed and is capable of testing any fighter. C-130 size aircraft could be accommodated with additional modifications. (See Figure 2.)

A Satellite Thermal and Dynamic Testing Laboratory is being considered as a potential improvement in the static and dynamic test facilities to allow thermal, vibration and transient testing of very flexible antenna and slewing-weapon structures. Reviews will be made of existing and planned Industrial and Government facilities to see if there is a need for an AFWAL in-house facility. Major Hugh Briggs of FIBG and AFIT is constructing an experimental facility to evaluate the hardware and algorithms for active control of structural response.

The Structures Integration Military Construction Program (MCP) is scheduled in 1988. The MCP will result in the integration of nearly all structures and dynamics analytical, experimental and administrative functions in one location. The current dispersed locations require that we interrupt dynamic tests in FIBG/B24C to conduct vibration of AGILE tests in FIBT/B65. The integrated laboratory will allow the development of the satellite test facility and will allow FIBG to improve their support of AGILE tests.

ACKNOWLEDGEMENTS

Thanks are due to the following scientists and engineers in the Structures and Dynamics Division who helped put this review together: Leonard Shaw, Dave Oetting, Bill Johnson, Tony Gerardi, Lige Turner, Howard Wolfe, Terry Harris, Dan Schumacher, Carl Rupert, Wayne Bassett, Marty Richardson, Vipperla Venkayya, Hugh (Clark) Briggs, Lynn Rogers, Don Paul, Roger Aschenbrenner, Clem Schmid, Ralph Shimovetz, Otto Maurer, John Ach, Dale Cooley and Gene Maddux. Special thanks to Ms. Sharon Templeton who assembled the inputs and typed the manuscript most expertly and rapidly.

A DECADE OF RELIABILITY TESTING PROGRESS

Robert N. Hancock
LTV Aerospace and Defense Company
Vought Missiles and Advanced Programs Division
Dallas, TX

INTRODUCTION

At the 45th Shock and Vibration Symposium, which was held at the Dayton Convention Center in 1974, the S&V community was alerted to problems that existed in Avionics Reliability by an Air Force Systems Command Colonel named Ben Swett. Colonel Swett had just completed a two-year study directed by General Marsh at the Air Force Systems Command (AFSC) headquarters[1], and he described problems and some proposed fixes. At the same meeting Mr. Jack Short told how problems were being corrected in a program called Rivet Gyro[2] at the Wright-Patterson Air Force Base under the direction of the Air Force Systems Command. The Air Force Systems Command programs instigated many actions which are still in progress. The intention in this paper is to review the progress that has been made toward the solutions that were proffered at the 1974 meeting and to list some of the tasks that still need development. The problems that were disclosed in 1974 fell into both the technical and the administrative arenas. The latter will be mentioned where lack of action interferes with technical progress, the primary topic.

BACKGROUND

The fundamental problem described by Colonel Swett which caused the Air Force Systems Command study was that great numbers of design and workmanship defects were still present in equipment after it had been placed in field service. The thesis at the time was that the reliability testing (or laboratory testing in general) had been inadequate to disclose the defects. This, of course, subsequently proved to be true. Figure 1, which was taken from Colonel Swett's 1974 presentation, typifies the problem that he described. In this figure we see the measured vibration on an A-7D, at the Forward Looking Radar attach points, both during gunfire and at other flight conditions. The ordinate in this case is vibration amplitude in G-peak. Compared against these two measured vibration traces is the MIL-STD-781 "2.2G sinusoid at a non-resonant frequency between 20 and 60 Hz" which was used to do the vibration demonstration and acceptance testing on the "government furnished" equipment. It is quite obvious from this figure that the test would be inadequate to evaluate performance of the equipment during the vibrations that would be expected in flight. The study disclosed that there apparently existed a disparity ratio of approximately 10 between laboratory and field measurements of reliability. That is, the laboratory tests indicated the equipment was ten times more reliable than later proved to be the case once the equipment was put into field service.

Four causes were proposed for the existence of the disparity.

1. The ten-to-one ratio was caused by MIL-STD-781, 6.5 to 1 from test conditions and about 2 to 1 from test plans. Of course, we can recognize now, based on the comparison and the Figures shown, there is no reason for the test and field results to be correlated at all.

2. It was pointed out that only avionics were required to comply with 781; other electronic products lines used MIL-STD-756 predictions with some feedback and/or MIL-STD-810 testing which might be expanded to provide reliability data output.

3. The third reason given was that MIL-STD-781B testing would not be effective even if it were fully complied with because of built-in disparities, statistical discrimination, impact of cost, test times and manipulation of variables definitions.

4. It was further stated that confusion on this subject within the Air Force Systems Command was not merely due to semantics but that the problem was basically institutional.

Figure 2 is a copy of the slide used to describe the institutional problem in 1974. Since 1974 the reliability and environmental communities have met each other and are largely working toward some redefined common purposes,

even though there are still areas in which the two communities agree to disagree. These are probably driven by the differences in backgrounds for the two communities, environments largely coming from the hardware or physics orientation and reliability from a statistical orientation. Since the differences in MIL-STD-781 and MIL-STD-810 were pointed out by Colonel Swett, most of the technology members of the reliability and environmental communities have accepted the basic concepts described by him, and they have proceeded with corrections and modifications. Major changes in these areas are briefly reviewed later.

The Swett test prescription is largely presented in Figure 3 which was taken from his 1974 paper. These three bullets prescribed the combined environment reliability test of which much was to be made later.

In 1975 the joint logistics commanders convened a Workshop on Electronic Systems Reliability at Airlie House, Virginia, which was chaired by Commander Neil Mandel (Neil is now in charge of the Environmental Stress Screening project for the IES). The recommendations which emanated from that 1975 meeting are summarized in Figure 4. These were somewhat broader in scope yet accomplished many of the recommendations made in the Air Force Systems Command study, and indeed the Air Force Systems Command study report was incorporated as part of this workshop. To the best of my knowledge all the recommendations that were made at this workshop and enumerated here have been carried out to a certain degree.

TEST PURPOSES

In the discussions and studies that followed the 1974 meeting it was obvious that gross misunderstandings existed about the purposes and the benefits to be derived from various tests which were being specified in various places. In general, the reliability community assumed that the environmental qualification test (also assumed to be conducted in accordance with MIL-STD-810) had removed all environmental design defects, so only workmanship defects, or the so-called random defects, would be present in a piece of hardware. Hence, many of their actions and tests were predicated on the basis that reliability was a function of parts count, since out of so many parts a certain number of random failures could always be expected. That thought still exists in some quarters, and it has not yet been totally accepted that quantum leaps in reliability can be made by removing design defects from the hardware through the use of properly defined and conducted test procedures followed by corrective action.

In an attempt to clear up some of the misconceptions about purposes of test, the environmental community (which includes many of the S&V community), working through the IES, defined a set of seven tests which are displayed in Figure 5[4]. There are seven tests because there are seven purposes and functions to be satisfied, as shown in Table I. Table I describes the purpose; it gives a title with an alternate short title in some cases. It also points out the primary beneficiary and further describes the tests in a few more details so that it will be possible to refer to these unambiguously. Line seven of the Table attempts to describe whether or not each individual test would be better conducted with combined environments or with separate environments. These obviously should require trade-off, depending on the type hardware involved and the hardware assembly level. Figure 5 is reproduced from the Atlanta CERT Proceedings, except it has been modified to include low rate initial production (LRIP) with the RDT&E phase since it has been proposed by some that TAAF, or reliability growth testing, should not be conducted on full-scale engineering development hardware but rather that it is much more effective when conducted during initial production runs. The challenge is open to find when it is most effective in the program schedule.

Environmental stress screening (ESS) is shown in this list of seven tests even though it is defined as a process and not a test; a test has a go, no-go implication where failures are indeed bad. The thought is encouraged by the Environmental Stress Screening of Electronic Hardware (ESSEH) work group of the IES that failures are good during environmental stress screening.

Figure 6 is extracted from a paper by Marone[5], in which he has shown the effect of finding parts failures at various levels of assembly. This curve was used to describe the parts acceptance test justification, but if we view it from the other direction, then it serves just as well to describe the cost benefits of a screen when conducted by the manufacturer rather than consumer. The left part of the curve indicates that it cost $5.00 to find and replace a bad component at the part level. At the printed wiring assembly level the cost is $50.00; at the LRU level the cost is $500.00, and at the system level, the cost is $1,500.00 before it goes to the field. In his paper Marone gave a field replacement cost of approximately $15,000.00 average. So you can see on this curve that for lowest cost it is obviously better to find the problem at the lowest assembly level possible, preferably at the part level. That being generally accepted as true, the output from the ESSEH work group of the IES has shown it to be cost effective to workmanship screen with environmental stresses at every level of assembly.

A recent study sponsored by the Flight Dynamics Laboratory[6] proposed extensive application of environmental stress screening and a set of judiciously applied Test Analyze

and Fix (TAAF) tests and compared the costs of this test program to an average of a traditional development test program derived from studies of eight store systems. The cost savings shown through the use of combined environment reliability tests-reliability growth tests and life-cycle profiling of the test environments was approximately $6 million for the test program. The majority of the cost savings came from reduced flight test programs, because in most preceeding weapons store programs, both reliability growth and reliability extended demonstration tests had been done during actual flights, involving as many as several hundred flights and the expenditures of several hundred missiles. These tests combined flight test and other operational performances along with the reliability performance evaluation, so it is unlikely that the total cost of the program would ever show up against reliability program costs.

Table II summarizes the results obtained by Boeing, Wichita[7] on reliability growth testing seven offensive avionics sub-systems in the B-52 weapon system. The results on these seven sub-systems were dramatic in terms of both decreased maintenance, through increased MTBF, and decreased life-cycle-costs as shown in the last column. From having performed the corrective action shown necessary by the reliability growth tests, $224.23 million dollars is estimated as the life cycle cost savings over a te year period. Boeing reported a number of lessons learned in the reliability growth tests of these B-52 equipments. Chief among them were the following: 1) don't have the production chief engineer run the reliability growth test, 2) have at least three common meetings with the customer to promote openness, 3) don't cut reliability growth tests under six months (2,400 hours minimum tests), 4) never do reliability growth tests on Full Scale Development hardware, 6) start reliability growth testing early but not with the first unit (use #5 to #10), 7) SPO and the contractor need a reliability growth test Czar.

The concept of combined environment reliability testing has been well proved at both the Flight Dynamics Laboratory and the Pacific Missile Test Center as reported by Burkhard[8] and Meeker[9]. Burkhard showed Lab to field test MTBF ratios approaching one for several pieces of equipment, and he developed some basic criteria for the selection of the environments to be employed during combined environment reliability testing. Meeker has used combined acoustics, vibration and temperature for a number of years to conduct acceptance tests on Navy missiles. He justified his facilities, and indeed the tests themselves, on the basis that laboratory testing was much cheaper than flight testing and field problem correction. The Pacific Missile Test Center has used the tests in the process of acceptance testing, but they have also performed the functions of the reliability growth test and even production screening for primary and second source producers.

PROCUREMENT DOCUMENTS

Specifications and Standards were recognized to be a source of a problem in the 1974 AFSC study, and in the 1975 JLC study and in most subsequent studies. However, in recent years, since reliability and environmental document development plans were issued by DMSSO (Defense Material Specifications and Standards Office) for comment by industry and professional societies, much improvement has been made in the specifications and standards employed in procurement. Table III lists some of the major ones that we in this community, and in the reliability and environmental communities, are likely to encounter. Note that these have all been revised since 1977. Table IV lists those currently working under the guidance of DMSSO[10]. After Colonel Swett left the Air Force Systems Command, he was employed at the Pentagon, very productively, to produce a new Department of Defense Directive on Reliability and Maintainability, DOD 5000.40, which was issued 8 July 1980. Some common characteristics of the documents listed are as follows: 1) Most of these documents require tailoring of the test environments and procedures to suit the test purpose and the type of hardware involved. 2) Interaction between the producer and customer is required through the employment of required Data Item Descriptions (DID's). Those from MIL-STD-810 are an excellent reference on this point. They are as follows: a) Environmental Management Plan, b) Life-Cycle Enviromental Profile, c) Environmental Design Criteria and Test Plan, d) Operational Environmental Verification Plan. 3) Most standards and specifications have been reformatted to contain task descriptions which are much easier to follow than in the old specifications and standards. MIL-STD-785 is a good example, listed in Table V. 4) Lengthy documents such as MIL-STD-781 have been revised in format so that they contain a relatively compact basic section, and they have the lengthy descriptions of environments contained in a companion document called a Handbook. The Handbook format allows much easier and quicker revision of the contents, such as rapid inclusion of new environments as they become available. MIL-STD-781D is in the process of final revision prior to release; its release should be within the next three months. At some time in the near future it is suggested this community should meet along with the rest of the environmental engineers to seriously consider combining the MIL-STD-810 and the MIL-STD-781 Handbooks. While we are together, we should seriously consider adding MIL-STD-810 to the list of documents contributing to reliability engineering. It is currently omitted in MIL-STD-785. We might also include the statement in MIL-STD-810 that MIL-STD-785 exists.

TEST TECHNOLOGY

How can we measure the effectiveness of the new procedures, the specifications, the standards and the test directives which have been implemented over the past ten years? One way would be to use the initial figure of merit employed by Colonel Swett in his 1974 paper which compared the lab test measurements of MTBF to field test measurements. Figure 7 has been prepared to show the progression of that ratio. General achievement of a 2:1 lab/field ratio was discussed at the 1980 IES Annual Technical Meeting as a target for the 1990 time period. But conceivably, such is currently possible in a well managed laboratory, and by 1990 less than 2:1 will be generally expected in most laboratories and for most procurements. However, if that is to take place, we in this technical community should establish our own target for improvements in our ability to predict and define the environments at a particular location where a black box is apt to be mounted in a weapons platform. Concurrently the reliability community should establish a commn definition of failure between the laboratory and the field.

Description of a set of goals might be as displayed in Figure 8. An IES work group derived this figure about three years ago. It proposes to depict our state-of-the-art for defining an environment at a particular location, in a given weapons system platform, during the full scale development phase of a program. As can be seen, currently, we can define pyrotechnic shock inputs to a black box at a particular location with about 40% accuracy. We can probably define maximum or average random vibration inputs with about 55 to 60% accuracy. We can probably specify the climatic environments that a black box can expect at a particular location, for given flight profile, with about a 75 to 76% accuracy. If we are going to test with less than a 2 to 1 disparity ratio for MTBF in the laboratory, as compared to the field, we must do better than that. Hence, we have shown the objective over the next five to ten years of achieving a 90% accuracy for ability to define these environments within a reasonable cost and schedule.

Speaking of cost, however, if we transfer this plot to another set of ordinates that shows the spending requirements for those where we show the major deficiency (Fig. 9), we might help plan our R&D for the next few years. To improve our ability to predict pyrotechnic shock with a 90% accuracy, we would expect to spend five times as much ten years from now as we are spending now. In other words, we should expect to put some money into studying these environments so that we can do a better job on defining them for purposes of achieving field reliability.

FUTURE OUTLOOK

The past ten years have shown significant progress in test methods, acquisition document improvement, and other areas just reviewed. Most of the areas that were targeted for improvement in 1974 have been addressed with positive results. Emphasis has been moved from reliability assessment much more in the direction of achievement. Communications between technical personnel of the contractor and customer have been forced through the implementation of reporting provisions of several documents, MIL-STD-810 and 785 for example. Including the Data Item Descriptions in MIL-STD-810 did much to prevent contract managers on each side of the house from ignoring their technical staffs. Evidence is being accrued daily that these improvements in tests and acquisition practices have resulted in acquisition of military hardware with improved reliability; although, the press still includes the words "unreliable" along with "over-priced" whenever military procurement makes the news. Hopefully, when the initiatives published by Deputy Secretary of Defense Carlucci[11] are implemented, many of these complaints will disappear. It seems the initiatives are becoming a part of military procurement, since Deputy Secretary of Defense Thayer[12] reinforced several of the Carlucci initiatives while he was at the Pentagon.

In addition to continuing the improvments that have been started both within the technical community and in the field of acquisition practices, there are perhaps specific items of action that can be stated to generally encompass areas that will be receiving additional work in the future. Some of these are enumerated below with a few explanatory words to indicate action and direction.

1. Continue to improve procurement methods. The main problem with procurement methodology is the same as in any system where conpensation is not based directly on performance. It is still difficult in many military procurement packages to understand what is being bought. By the time we get through the social reforms that are purchased, it is difficult to tell, in many cases, if a piece of actual hardware is being produced. Then at the completion of many contracts, a poorly performing contractor is rewarded by receiving lucrative follow-on corrective type contracts (ECP's).

2. Contract administrators need to recognize and identify the need for, and the purposes of the different types of laboratory and field tests. Much mischief is still caused by misapplication of tests broadly called acceptance tests or qualification tests when the exact test conditions and

criteria for acceptance and qualification have not been specified.

3. Continue to improve definition methods. The often discussed data bank is needed. Also, we should add statistical probability and accuracies to amplitude and durations of the environments described in MIL-STD-810 and MIL-STD-781.

4. More combined environment facilities should be available. In 1975 the IES estimated that $400 million dollars would be required to facilitize the country adequately for mission profile CERT requirements. At the present time we think that this requirement has been approximately half filled.

5. A "top" environmental engineering document (similar to MIL-STD-785) should be published.

6. Procurement activities should contractually require and fund contractors to do environmental stress screening in all production procurements, and growth reliability tests on all new design and secondary source procurements. DOD, put your money where your mouth is. The life-cycle cost effectiveness of these procedures has been proved beyond the point of argument. Yet, contractor and system program office management personnel continue to look at the short term dollar and cut costs by eliminating tests. If benefits are to be derived from improved methods, the removal option should be deleted.

Through supplements to AFR 800-18 within the past two years, the Air Force Systems Command has required the use of combined environment reliability testing and environmental stress screening on future procurements. NAVMAT and DARCOM have also issued instructions for the use of environmental stress screening with random vibration and temperature. The use of combined environment reliability testing during development is expected to increase.

The paper by Colonel Swett in 1974 got our attention. The work that was started as a result of that and other activities at about the same time period still has our attention. The environmental engineer is receiving some needed recognition, and some quarters have recognized that neither testing nor statistics create reliability, but rather it is created by statics and dynamics, and design stress engineers, who have the ability to design for fatigue as well as stress maxima. The above discussion indicates that frustration will not end in the immediate future because contracting and procurement methodology is slow to change. So we will not be allowed to do a perfect job right away, however, the opportunities that have been opened during the past ten years have allowed us to proceed much farther than in the past with our design capabilities. The outlook is optimistic for this to continue in the foreseeable future.

REFERENCES

1. Swett, Lt. Col. Ben. H., "Avionics Reliability," Shock and Vibration Bulletin 45, Part 2, pp 29 - 42, June 1975.

2. Short, John E., "The Rivet Gyro Story," Shock and Vibration Bulletin 45, Part 2, pp 17 - 28, June 1975.

3. "Joint Logistics Commander (JLC) Electronics Systems Reliability Workshop Summary Report", 30 July 1975, Cdr. C. D. Mandel, Jr., Chairman, Hq., Navy Material Command, Washington, DC 20360.

4. Hancock, R. N., "Hardware Program Requirements for Environmental Engineering," Proceedings of the DOD Combined Environment Reliability Test (CERT) Workshop, 2 - 4 June 1981, Atlanta, GA, sponsored by ASD, WPAFB, OH 45433.

5. Marone, Victor (Westinghouse), "Incoming Electronic Parts Screening," Proceedings, Institute of Environmental Sciences, 1981.

6. Allen, H. W., Ely, R. A., and Knoble, K. L., (Vought Corp.) "Assessment of Stores Reliability Testing," AFWAL-TR-83-3025, March 1983.

7. Robinson, R. C., et al, "B-52 OAS Test Analyze and Fix Final Report," Boeing document D675-15539-2 dated 12/82. Paper presented at 1983 IES Annual Meeting entitled "B-52 TAAF, A Story That Needs Telling".

8. Burkhard, Alan H., "CERT Evaluation Program - What Was Learned," Proceedings of the DOD CERT Workshop, 2 - 4 June 1981, Atlanta, GA, pp 3.3 - 3.3.23.

9. Meeker, D. Brent, "Management Lessons Learned from CERT of Air-Launched Missiles," Proceedings of the DOD CERT Workshop, 2 - 4 June 1981, Atlanta, GA, pp 3.4 - 3.4.10

10. Greene, Kurt, Defense Material Specifications and Standards Office, OUSD "Reliability Standardization Program Management", Proceedings 1983, pp 226 - 228, Institute of Environmental Sciences, Mt. Prospect, IL 60056.

11. Carlucci, Frank DEP SEC DEF Memorandum of 32 Initiatives Codified by DOD Directive 5000.2 on 8 March 1983.

12. Thayer, Paul, DEP SEC DEF Memorandum for Secretaries of the Military Department, Subject "Improving Contract Requirements" dated 11 January 1984.

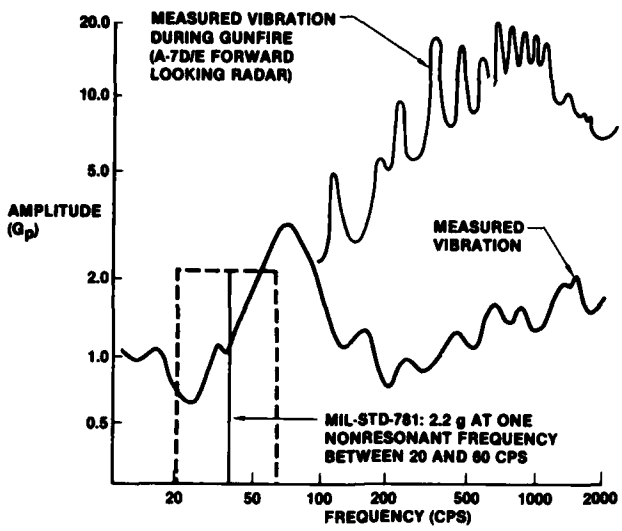

FIGURE 1: AFSC'S FIELD/LAB ENVIRONMENT COMPARISON

"RELIABILITY" (781) AND "ENVIRONMENTAL TESTING" (810) ARE TWO SEPARATE WORLDS WITHIN AFSC

THEY ARE SEPARATED BY:

- **MIL SPECS AND STANDARDS**
- **AIR FORCE REGULATIONS**
- **ORGANIZATIONAL STRUCTURE**
- **PRODUCT TYPE**
- **VIEWPOINTS, ATTITUDES AND TERMINOLOGY**

RELIABILITY (781) IS:	ENVIRONMENTAL TESTING (810) IS:
WELL ORGANIZED	LEFT TO SPO'S AND AFCMD
SIDELINE TO EQPT DEV	MAINLINE OF EQUIP DEV
STATISTICS	SPEC COMPLIANCE
UNREALISTIC TEST CONDITIONS	UNREALISTIC TEST PROCEDURES
POOR PREDICTOR OF TRUE MTBF	NO PREDICTOR OF TRUE MTBF
(OPTIMISTIC BY 10 X)	(NO RELIABILITY DATA OUTPUT)

FIGURE 2: SWETT'S PROBLEM DESCRIPTION

TEST CONDITIONS AND PROCEDURES

- COMBINE PERFORMANCE, RELIABILITY, AND ENVIRONMENTAL QUALIFICATION TESTS INSOFAR AS PRACTICAL:
  - SELECT STRESS TYPES AND LEVELS
  - DESIGN PROCEDURES TO MAXIMIZE DATA
- CANCEL TEST SUBSUMED BY COMBINATION
- EMPLOY COMBINED-STRESS TESTING FOR:
  - PARTS RATING
  - EVALUATION TEST
  - QUALIFICATION TEST — PROTOTYPE
  - SCREENING ("BURN-IN")
  - PRODUCTION SAMPLING — PRODUCTION

FIGURE 3: SWETT'S DT&E TEST PRESCRIPTION

- EXPEDITE A SERIES OF INTERIM AND LONG TERM REVISIONS OF MIL-STD-781
- EXPEDITE THE REVISION OF MIL-STD-785 TO EXPAND THE COVERAGE AND INTEGRATED TEST PLANNING AND TO REVISE THE SECTIONS DEALING WITH RELIABILITY PROGRAM PLANS
- EXPEDITE THE ORGANIZATION OF A REAL-TIME FIELD DATA COLLECTION SYSTEM WHICH INCLUDES RELIABILITY DATA
- EVALUATE MIL-STD-756 FOR REVISION OR CANCELLATION
- REVISE MIL-STD-721 TO PROVIDE FOR COMMON LANGUAGE AND DEFINITIONS
- DEVELOP JLC GUIDANCE DOCUMENT(S) FOR RELIABILITY
- EXPEDITE THE PREPARATION OF A RELIABILITY DESIGN HANDBOOK
- EXPEDITE THE PREPARATION OF A MISSION PROFILE METHODOLOGY
- EXPEDITE THE INCORPORATION OF RELIABILITY DESIGN TECHNIQUES INTO SYSTEM DESIGN
- EXPEDITE THE ESTABLISHMENT OF A RELIABILITY TRAINING PROGRAM AND SPACES FOR MILITARY PERSONNEL
- EXPEDITE THE DEVELOPMENT OF RELIABLE SOFTWARE AND THE INTEGRATION OF SOFTWARE RELIABILITY INTO TOTAL SYSTEM RELIABILITY
- JLC-SPONSORED INTERSERVICE PERIODIC FORUMS

FIGURE 4: SUMMARY OF JLC INITIAL PROGRAM

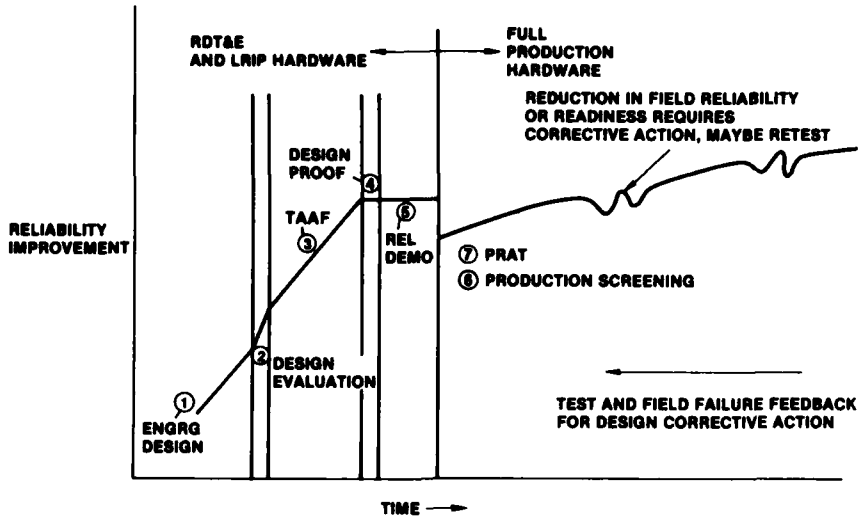

FIGURE 5: RELIABILITY IMPROVEMENT TREND WITH ENVIRONMENTAL TESTING (IES)

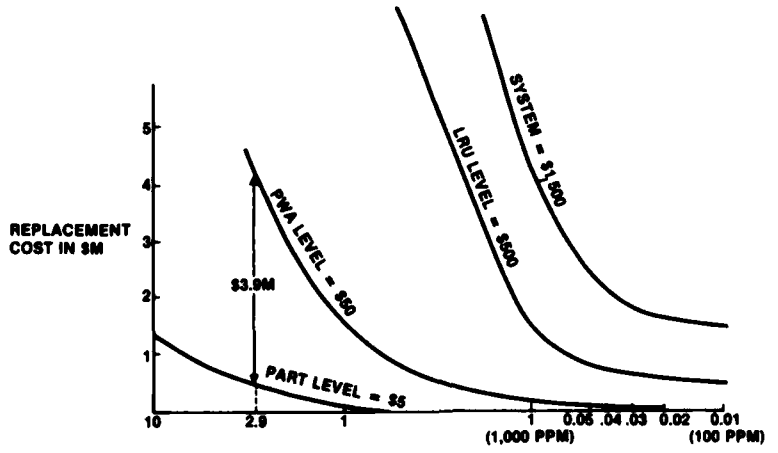

FIGURE 6: THE COST TO FIND A BAD PART BASED ON 3 MILLION IC'S PER YEAR (WESTINGHOUSE)

TABLE I: SUMMARIZED TEST CHARACTERISTICS

REF	NO. ON FIGURE 5	1	2	3	4	5	6	7
1	TITLE	ENGRG DESIGN (DESIGN-TEST-(DESIGN)	DESIGN-EVALUATION	TAAF TEST-ANAL.-FIX	DESIGN PROOF (ENV QUAL)	REL DEMO	PRODUCTION SCREENING WITH BURN-IN	PRODUCTION REL ACCEPT-TEST (PRAT)
2	MAJOR PURPOSE	ENGRG DESIGN (INFORMATION - TRADE OFF) DESIGN ALTERNA-TIVES UNDER ENV EXPOSURE	OKAYS DESIGN FOR TAAF ENTREE	RELIABILITY GROWTH	CONTRACT GATE - PROVES DESIGN OKAY TO PRODUCE	CONTRACT GATE GO-AHEAD TO PROD.	DISCLOSE WORKMAN-SHIP DEFECTS, IN-FANT MORTALITY	MAINTAIN QUALITY
3	PRIMARY BENEFICIARY	PRODUCER	PRODUCER	PRODUCER	CONSUMER	CONSUMER	PRODUCER	CONSUMER
4	LENGTH OF TEST(S)	MANY SHORT (DAYS) TEST OVER SEVERAL WEEKS	SEVERAL DAYS	MONTHS	DAYS	MONTHS	HOURS	WEEK(S)
5	LEVEL OF ENV	AS APPROPRIATE	SERVICE EXTREMES	LIFE PROFILE	SERVICE EXTREMES	LIFE PROFILE	CONSTANT SUFFI-CIENT FOR PURPOSE	VARYING
6	ENV DESC	(STIMULATION)	(SIMULATION)	LIFE-CYCLE PROFILE	SIMULATION OF EXTREMES	LIFE CYCLE PROFILE (SIMULATION)	(STIMULATION)	LIFE CYCLE PROFILE (SIMULATION)
7	SEPARATE OR COM-BINED ENVIRONMENTS	SEPARATE	COMBINED	(SIMULATION) COMBINED	COMBINED AND SOME SEPARATE	COMBINED	2 OR 3 COMBINED	3 OR 4 COMBINED
8	OPTIMUM ASSY LEVEL UTILITY	BLACK BOX	MODULES OR BLACK BOX	MODULES OR BLACK BOX	BLACK BOX OR "SET"	COMPLETE SET - e.g. ANTENNA, RECEIVER AMP DISPLAY AND CABLES	ALL	COMPLETE UNIT (SAMPLE)
9	RELATED STANDARDS AND SPECIFICATIONS	MIL-A 8870	MIL-STD-810	DARCOM P702-4	MIL-STD-810 MIL-STD-1670	MIL-STD-781	NAVMAT P 9492 IES-RP	MIL-STD-781
10	REL INFORMATION OUTPUT	PROBABLY NOT	NO	YES	NO	YES	NO	NO
11	SPECIMEN CONSUMED	YES	YES	YES	YES	YES	NO	NO
12	SCHEDULE FIX AND RETEST TIME	YES	YES	YES	NO	NO	YES	NO
13	OPTIMUM CONTRACT PHASE UTILITY	V&D	V&D	FSD/V&D	FSD	FSD END	PROD.	PROD.

TABLE II: RESULTS OF BOEING TAAF ON B-52 AVIONICS

SUBSYSTEM CONTRACTOR	NO. OF FAILURES	SUBSYSTEM MTBF (HR) DEMO	PRODUCTION	LSC SAVINGS ($M)
IBM	9	1333	1555	0.11
HONEYWELL	11	1401	3243	0.66
LEAR SIEGLER	12	1923	4830	1.68
NORDEN	50	223	284	14.76
SPERRY	90	161	275	11.10
SUNDSTRAND	159	92	289	88.06
BMAC	126	101	309	107.84
	457			
OAS SYSTEM		30	67	224.23

TABLE III: NEW AND REVISED DOD RELIABILITY TEST RELATED DOCUMENTS

NUMBER	TITLE
DOD 5000.40	RELIABILITY AND MAINTAINABILITY (8 JULY 1980)
AFR 800-18	AIR FORCE RELIABILITY AND MAINTAINABILITY PROGRAM (15 JUNE 1982)
MIL-STD-785B	RELIABILITY PROGRAM FOR SYSTEMS AND EQUIPMENT DEVELOPMENT AND PRODUCTION (15 SEPTEMBER 1980)
MIL-STD-781C	RELIABILITY DESIGN, QUALIFICATION AND PRODUCTION ACCEPTANCE TESTS: EXPONENTIAL DISTRIBUTION (21 OCTOBER 1977)
MIL-STD-721C	DEFINITIONS OF TERMS FOR RELIABILITY AND MAINTAINABILITY (12 JUNE 1982)
MIL-STD-1635	RELIABILITY GROWTH TESTING (3 FEBRUARY 1978)
MIL-STD-2068	RELIABILITY DEVELOPMENT TESTS (21 MARCH 1977)
MIL-HDBK-189	RELIABILITY GROWTH MANAGEMENT (13 FEBRUARY 1981)
MIL-STD-810D	ENVIRONMENTAL TEST METHODS AND ENGINEERING GUIDELINES (19 JULY 1983)

TABLE IV: RELIABILITY STANDARDIZATION PROJECTS

MIL-STD-781	RELIABILITY TESTING	REVISION D
MIL-STD-785	RELIABILITY PROGRAM REQUIREMENTS	REVISION C
MIL-HDBK	ENVIRONMENTAL STRESS SCREENING	NEW
MIL-STD	BAYESIAN RELIABILITY DEMONSTRATION	NEW
MIL-HDBK	RELIABILITY DESIGN HANDBOOK (ELECTRONIC)	NEW
MIL-HDBK	RELIABILITY DESIGN HANDBOOK (MECHANICAL)	NEW
MIL-HDBK	GUIDELINES FOR DERATING - ELECTRONICS	NEW
MIL-HDBK	SNEAK CIRCUIT ANALYSIS	NEW
MIL-STD	SOFTWARE RELIABILITY	NEW

TABLE V: RELIABILITY PROGRAM - MIL-STD-785

TASK 300 DEVELOPMENT AND PRODUCTION TESTING

TASK	
301	ENVIRONMENTAL STRESS SCREENING (ESS)
302	RELIABILITY DEVELOPMENT/GROWTH TEST (RDGT) PROGRAM
303	RELIABIITY QUALIFICATION TEST (RQT) PROGRAM
304	PRODUCTION RELIABILITY ACCEPTANCE TEST (PRAT) PROGRAM

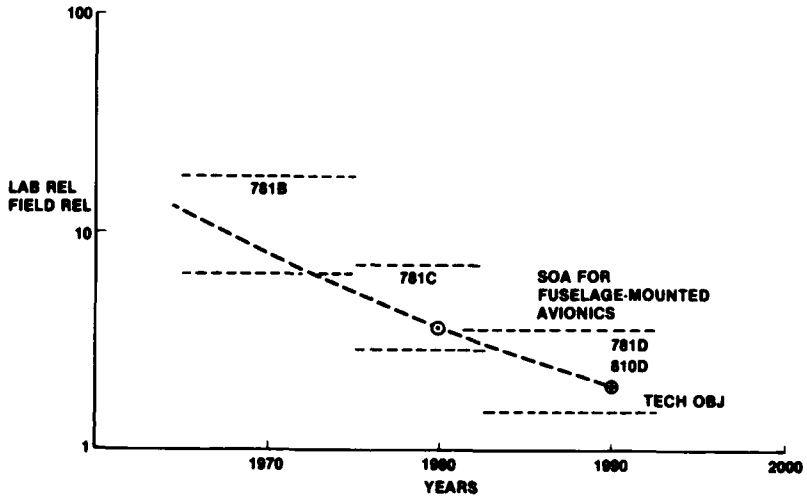

FIGURE 7: ESTIMATE OF RELIABILITY TEST EFFICIENCY

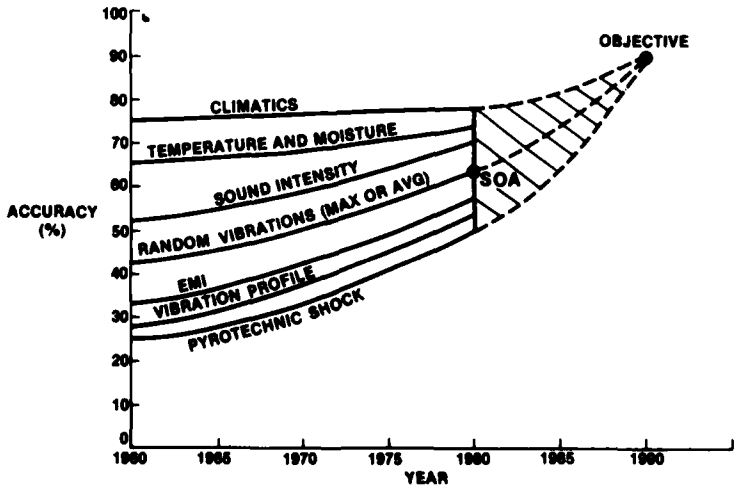

FIGURE 8: ESTIMATE OF STATE-OF-THE-ART FOR ENVIRONMENT DEFINITIONS (AT A PARTICULAR LOCATION)

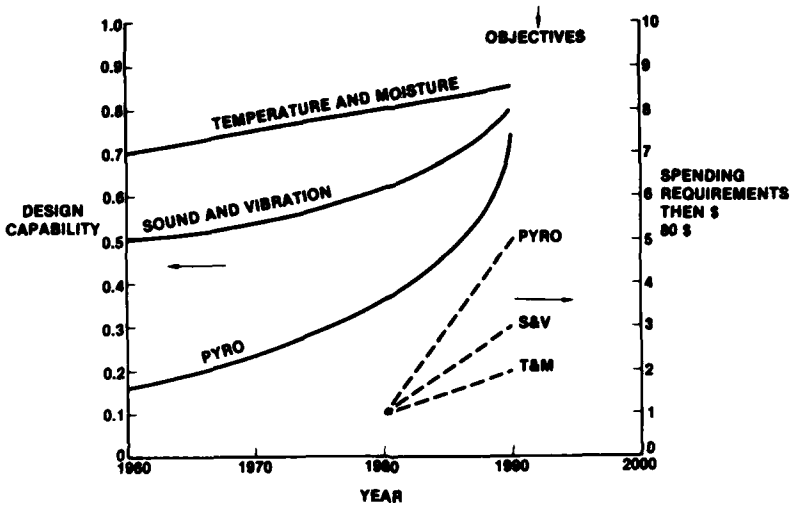

FIGURE 9: COSTS OF IMPROVING ENVIRONMENT DESIGN AND CONTROL CAPABILITIES

CERT - WHERE WE HAVE BEEN - WHERE WE ARE GOING

Dr. Alan Burkhard
Air Force Wright Aeronautical Laboratories
Wright-Patterson Air Force Base, Ohio

Since it is so early in the morning, you must either have insomnia or be interested in this topic. Either way, what we will talk about today is Combined Environment Reliability Test (CERT), where we have been and where we are going with the technology. I will try to recapture what led to the development of this technology, what has been accomplished, and then what kind of activities and ideas are underway to move beyond CERT.

Why was it necessary to develop the concept now called CERT? What is CERT? I will try to give you a thumbnail tutorial on the development of CERT, the engineering process you go through to develop a CERT profile and finally how you might go about applying CERT in a contractual situation. I also want to describe the technology and perception challenges that the development and validation of CERT uncovered. These are the areas that future development and focus of development efforts need to be undertaken.

Figure 1 is the famous pie chart that shows the contribution of different environmental stress factors to the observed field failure rate of avionics equipment (Reference 1). There is no indication that the advances in avionics technology in terms of new chips or component types would significantly change this pie chart. In fact some of the new component types may actually accentuate these problems. Figure 2 is from the same study as Figure 1, but it has not been given as much notoriety. But, it shows very graphically the low state of credibility that environmentally based testing had fallen in terms of having a real impact on equipment acquisition in a positive way (increasing equipment fielded reliability). Looking at Figure 2 you will notice that approximately 50 percent of the field failures were not observed in any of the environmental testing done on this equipment. Conversely, the other 50 percent of the field failures were observed in an environmental test, but for some reason nothing was done about these problems. This suggests that these tests were of nominal technical effectiveness - over one half of the environmentally induced field failure modes were not excited by the laboratory environmental tests. When an environmentally based test did identify an environmentally induced failure mode, often nothing was done about it except pass it on in the deployed equipment. Acquisition decision managers had gained the perspective that testing was not telling the true story.

Figures 3, 4 and 5 outline the background and give a summary of about 10 to 15 years of effort to do something about this problem. The results of these activities have become encapsulated in the concept or acronym CERT. The basic underlying thrust of this effort was to re-establish test credibility in the minds of the decision makers. It was decided that since most of the decision makers were not environmental experts or testers of equipment, the testing approach must be relatable in their frame of reference. The approach was to develop realistic test profiles that reflect in a relatable way the missions and flights that occur in actual practice. It was recognized that there are many inherent inefficiencies in real time mission profile simulation where the environmental stress conditions reflect the levels to be experienced in actual deployment. But such an approach has a strong attractive appeal since one can not easily quibble about the test results since the environmental conditions reflect real life.

This was the thinking back in the early 1970's. There was a joint program among the Aeronautical Systems Division (ASD) Deputy of Engineering, Wright Aeronautical Laboratories and the PRAM Program Office entitled "The CERT Evaluation Program" (Reference 2). This program was undertaken to evaluate the technical merit of CERT, to demonstrate that this type of testing had productivity and to identify what the level of CERT productivity was. Productivity was considered from both the technical and cost effectiveness view points. The effectiveness of CERT was examined for three levels of test realism; since no laboratory test can duplicate everything that can occur during the deployment of an equipment system. The levels of test realism were based upon practical considerations as to what can be easily simulated in a laboratory test and what has been

found by other studies as being the big swinger in terms of affecting equipment failure rate. The failure modes and rates that occurred in the tests were compared to the reported field failure rates for the item tested under CERT profiles. To maintain credibility with the decision makers, the reported field failure rates of equipment were not modified or corrected to attempt to only consider the field failures due to environmental effects. This was done since unmodified field data was being used to judge the reliability of deployed systems since it is the only available data.

The magnitude of the CERT Evaluation Program was massive. It resulted in over 24,500 test hours, involving 80 different kinds of avionics equipment items which had over 200 different types of failures. While CERT did not induce all the reported field failure modes, every failure that occurred in the CERT testing was field-relevant. Field-relevant meant that the failure which occurred in the test also occurred in significant quantities in the field. They were not the failure modes that only occur once or twice in a 12-month period. Low occurrence failure modes were assumed to be representative of mishandling; someone drops a black box, or does something that occurs spasmodically. It was found that there was nearly a four-to-one improvement in how well one could estimate field failure rates from a CERT test over previous methods of testing.

One technical issue that was floating around during the time period of the CERT Evaluation Program was do you really need to combine the environments? The often unstated but understood issue was that there exists many single environment test chambers. Why not just develop better single environment tests and not combine the environments? The CERT Evaluation Program did find that certain failure modes do require more than one environmental stress to excite them to failure. The cost effectiveness of combining the environments was a moot question because the basic driving approach behind the development of the CERT testing concept is to re-establish test credibility by having an approach that is relatable to the acquisition decision maker. The approach used to develop a CERT test profile was conceptually appealing to a typical acquisition decision manager in that: [1] the environments occur simultaneously as in service, [2] no engineering pretest judgment need to be made as to which order or sequencing of single environment tests would be appropriate for a given test item, [3] any possible synergism among environmental stresses would naturally occur, [4] test conditions can be directly related to usage in deployment environment and [5] there is a potential for a reduction in the number of test items necessary since there is a net reduction in the number of tests conducted by combining single environment tests.

Even so, as Hank Caruso alluded, some people think CERT is a "four letter word." This is because a lot of mystique has developed around the concept. Actually, CERT is a concept; it is not a specific test profile that you can find in a MIL-STD document. It is not a specific stress range nor a specific stress combination. It is not a facility at some location. It is in reality what we should have been doing all along; using engineering principles and practices to develop testing programs - not cookbooks. Environmental testing got sidetracked back in the 1960's into doing "cookbook" by the numbers testing. This was reflected in MIL-STD-781A, MIL-STD-781B, MIL-STD-810A, MIL-STD-810B and many NATO standards.

What we are talking about is an engineering approach to environmental testing which gets into the concepts of test tailoring. Tailoring should take into account the total picture. That is, [1] what your application is, [2] what your test objectives are, (3) how the equipment is made, (4) and how much money will be spent on testing. All of these factors must be taken into account when you do test tailoring. What this says to me is that the TESTER HAS TO GET OUT OF THE TEST LABORATORY AND START TALKING TO THE PEOPLE IN THE DESIGN GROUPS AND TO THE GROUPS WHO PREPARE PROPOSALS RESPONSES. The kind of test in terms of stress conditions and duration depends upon these factors which are not just technical issues. All of this is encased in the testing concept we call CERT.

Let us focus a few minutes on the technical details of CERT. As with any test you conduct in a laboratory, it has some sort of characteristics or some other way of boiling down all of the possible uses to a subset of manageable and controllable conditions you use for the test. In the CERT concept this is called a test cycle, and it has some strong characteristics. It should reflect the application; if you are talking about aircraft application, you might have an aircraft which flys training missions, low level bombing missions and high level flights. These have to be reflected in the test cycle in their proper mix and proportion. Data concerning how an aircraft is to be flown is used to design other subsystems such as the jet engines and the basic aircraft structure. But, until now it has not been used consistently for the design of aircraft avionics equipment systems. You have to know something about your deployment scenarios. If it will only be deployed in one place in the world, you do not have to design for world-wide applications, just the proper localized effects. Another characteristic of the CERT test profile is that the CERT profile maintains the proper sequencing of stress values. That is, if high temperature occurs before a specific vibration condition in actual deployment, the test reflects this.

Figure 6 is about as close to a structure as you will find for a CERT test sequence in terms of a table you can turn to; MIL-STD-810D gives the basic structure for a CERT profile. On the left hand side, it says "Test Phase Definition". You have "Ground Cold Day", then you have "Ground Hot Day", followed by "Transition to Moist Day". These cover the three major natural environmental conditions that exist world-wide. If you do not have any of these conditions in your particular application, you just delete those conditions which do not apply. The rest of the CERT profile depends upon the unique characteristic of the application.

This means that the environmental engineer needs to know information similar to what the equipment design team needs to know. They need to know how the plane will be flown, where it will be deployed, the interfaces between the aircraft and the equipment. This information is available but not commonly utilized for environmental test formulation.

Every new aircraft has projected missions which the aircraft designers use to design the airframe and the jet engines. This same data could be used by the equipment test engineer for formulating the CERT profiles. Data on how existing aircraft are being flown also exists since about 20% of the aircraft have been instrumented with on-board mission recorders to collect flight loads data for structural life considerations. This data can be used to structure CERT profiles. From the aircraft mission data, equipment mounting and placement information, the CERT profile can be structured.

There have been four general ways such information has been formulated into actual CERT test profiles. These four ways are presented in descending order of priority with the lowest priority giving the most unrealistic test conditions. These four ways are [1] use measured data from the specific application of interest, [2] use measured data from similar applications, [3] use appropriate approximations based upon the physics of the situation, and [4] use the tabular data contained in the military standard documents.

In general, if you have measured information on the aircraft in the location of interest for the selected flight mission, no further analysis is generally needed. Most often such is not the case, and engineering calculations need to be made. The thermal conditions can be determined by using the environmental control system (ECS) computer programs. These programs are used to design the aircraft cooling system but can be used to predict cooling air temperatures based on aircraft flight conditions. If the technical detail of data does not exist for such analysis, then an approximation is to assume the equipment is in a ram-air cooled bay. This approach gives results as if the on-board cooling system is not functioning. As the last resort, the tabular values of MIL-STD-781C appendix B can be used.

Vibration data exist for almost every Air Force aircraft. Such data was collected during the development of the airframe during initial flight testing. This data can be used to determine the appropriate vibration conditions and spectra for the CERT test. Commonly, this data can not be used without being corrected for Mach effects and dynamic pressure differences between those achieved in flight test and anticipated in actual deployment. Again, lacking such data, the MIL-STD-810D tables can be used realizing that these values are for high dynamic pressure at transonic flight conditions and as such need to be corrected for long term CERT testing. And as a last resort the tabular values in MIL-STD-781C appendix B could be used.

Electrical cycling is an environmental parameter that is emerging in significance as the physical size of the individual electronic components decrease. So, proper on and off cycling and operational functionality should be included in the CERT test cycle. If the equipment is left on for the entire mission or just turned on for a certain portion of a given mission, it should be done in that same way in the test.

Tailoring implies a responsibility in terms of the person who is planning the CERT test profile. He must be able to advocate the developed test profile rather than saying, "It says in Table X, Figure 2 of the MIL-STD this is what you use." This means that appropriate engineering discipline and homework has to be accomplished. Obviously, a consideration in the tailoring process outside the pure engineering process is the cost effectiveness of each environmental factor or stress state. This is one of the future challenges in environmental engineering. Today it is almost impossible to articulate the impact of including or excluding a given environmental stress state from the CERT profile from a cost effectiveness viewpoint. Even worse, it is difficult to articulate the effect of some environmental stress states on the observed field failure rate.

Even so, a tailored environmental test program is recognized as the wave of the future. This wave is reflected in acquisition documents and military standards. To help out in the tailoring process and to start to get a grip upon the tailoring process, handbooks have been published and national workshops on the subject have been held. But, these are just the initial sortie into this development of the test tailoring process.

Figure 7 shows some recent additions to the approved Data Item List that are available to program offices. Data Items are the documents that can be put on contract to obtain data or the results of an analysis. The starred Data Items are the ones that are directly applicable

to the tailoring process as outlined in the front of MIL-STD-810D and CERT.

Many benefits are available and can be accrued by using CERT in the acquisition process. One of these benefits is having realistic requirements. In the past it was common for the equipment user to ask for a higher level of equipment reliability than was actually required. This approach was based upon what has traditionally occurred. When they asked for a reliability level of X, they were provided equipment with less than X. Therefore, by asking for more than what is needed, it is hoped that the desired level of reliability might be achieved. But, this approach really does not address the basic problem since the level of reliability displayed by an equipment is directly a function of the environmental stress states it must withstand and live under. For example, an equipment will display a 1,000-hour mean time between failure (MTBF) when it is deployed in a large transport type aircraft. But, when installed in a high performance fighter type of aircraft, it may only display 250-hour MTBF. So, the reliability requirements need to be specified as desired MTBF values for a specific environmental stress profile or application. The result is that the equipment design can be standardized, but false expectations of the deployment MTBF being X in every application are removed. Furthermore, in general, what parts fail in one deployment application will be different in rate and type when the equipment is installed in another but different deployment application. This difference in equipment behavior contributes to the problem of doing initial logistic spares planning.

Rapid evaluation of new or under development equipment can be done using CERT testing. It has been used in concurrent development and production programs since the equipment items used in the CERT test can be placed in the field or vise versa. CERT is realistic in terms of environmental stresses. CERT has been used to take selected equipment and expose it to simulated operational usage at a rapid rate so that any deficiencies occur in the CERT test items long before they show up in the deployed equipment. Thus, there would be time to develop corrective actions and implement them into the deployed equipment before it starts having this same failure mode.

Many equipment acquisition programs have a flight test program which is to provide performance data. Often the equipment experiences environmentally induced failures during flight testing which results in unproductive extra flight test flights to gather the needed performance data. CERT can increase the productivity of flight testing if the equipment to be flight tested is CERT tested to the flight test environmental stresses before flight testing. Thus, environmental problems can be identified on the ground in a controlled situation for easy identification of failure mode for rapid corrective action. This results in fewer during flight test failures and more productive and cost effective flight testing. The cost of a CERT test hour is two orders of magnitude less than a wasted flight test flight.

Figure 8 shows data that was taken from an acquisition program that was done within ASD. It shows the savings accrued by combining all of the single environment tests into a single CERT test program. These are savings to the acquisition program manager who could use these savings to purchase more performance or just reduce program costs. This system is performing significantly better in the field than anticipated (Reference 3).

CERT testing can impact logistic supportability of an equipment system. CERT has been found to be very effective in identifying the true source of retest ok (ReOK) or bench checked serviceable problems. Bench checked serviceable is a fancy term for "it failed on the aircraft, was removed for maintenance and brought into the repair shop, but they were unable to find any problem with the unit." This type of problem accounts for about 40 percent of all avionics maintenance actions. Specifically, 26 percent of the bench checked serviceable removals on one of our fighter aircraft was found to be failure mode induced by a specific environmental stress state that occurs during usage on the aircraft. This type of problem is a big source of headaches for the maintenance personnel since every maintenance action requires the expenditure of resources. Maintenance personnel can develop questioning attitudes about the reliability of their checkout equipment or the item under test since the problems seem never to be corrected. CERT is gaining acceptance in supporting the correction of these types of failure modes. The advantage of CERT over other methods for this type of failure mode is you can let the test tell you what stress states are causing the problem rather than having to guess.

In my opinion what is happening in the environmental test arena is that CERT is the bow wave of a major change that is beginning to take shape in terms of how tests are formulated, how testing is perceived and how it will be used in the future. Environmental testing is moving away from cookbook testing to engineering test methods. This presents a unique and new problem in the equipment acquisition community. Specifically, if company A proposes a CERT test which is different than company B's CERT test, how does one evaluate the two in the source selection process? The acquisition engineers have to evaluate the submitted proposals and determine [1] will this approach meet contract requirements and [2] which one has the highest probability of success. What if the two companies propose different environmental conditions for test? How does the acquisition engineer resolve the differences? I keep

bringing it back to the acquisition engineer because they are the ones who have to evaluate proposals, and as the environmental test technology exists today, we do not have the tools necessary to say with credibility that one technical approach is superior to another. The approach to CERT included in MIL-STD-810D method 520.0 was the method used in the CERT Evaluation Program and is not meant to be "THE" or "ONLY" way. We must develop the means to effectively identify what is necessary for an appropriately tailored test.

You can read articles on defense spending, and many point out that the acquisition cycle is something like ten to twelve years from the time development starts until the equipment is deployed. A major part of this is testing which occurs at the end of the development cycle. As you know, more often than not, funds are short at the tail end of a program. Our challenge is in the area of reducing test duration while maintaining or improving the credibility of the testing. By reducing test costs and improving the effectiveness of the testing, there is less incentive to cut testing as funds become tight. The current approach to this is to use realistic profile testing because these are relatable to our management, the people who make contract decisions. But, such testing has a tremendous penalty in terms of the time it takes to get test results. There are many ways of reducing testing time via concepts of jacking up test levels or deleting what is judged as not productive or stressful stress states. But, these methods currently lack credibility, and it is not clear what unknown benefit we are giving up when these approaches are not used. We need to develop a means of reducing test duration while retaining the strong credibility that CERT now enjoys.

Another need that is really coming to the forefront by the growth of CERT and test tailoring is the need for the environmental persons to stop thinking of themselves as a tester or someone who waits at the end of the development cycle. They need to become involved in the whole equipment cycle. CERT is a vehicle which could be one of the nucleus around which this could start. This would be just the start of a long-term process to integrate test and design. If you look at the proceedings of the 49th symposium in 1979, both Dr. Curtis and Mr. Hager talked about this (References 4 and 5). There is an initial movement in that area which is called "growth testing," but we are talking about moving it further back into the acquisition process where testing and design become blurred. This full integration of design and test from an environmental perspective will not happen until we have a more complete understanding of how environments interact with equipment and how environmental stresses induce failures. If we know this, then we can convey to the designers the impact of a particular design and environmental stress combination. Then we can start to integrate the design and testing processes. This is opposed to the traditional practice of waiting until the hardware is built, then testing it in the lab to see what breaks. We must move away from that kind of mentality.

I am very concerned with what I see in the area of environmental test screening. I see a movement which seems to be more toward the thinking that there is a single magic profile that will solve all of your problems. This is the approach that was followed in the area of environmental qualification testing and reliability demonstration testing for too long (Reference 6). Environmental Stress Screening (ESS) needs to be a tailored process. Acquisition program managers and engineers need to know this. We have been trying to enlighten the engineers in the Air Force, who work in the acquisition process, about tailoring by running tutorials and educational programs. But much remains to be done. We need to understand that if we really want to have good equipment, we must do a good job of engineering the testing requirements in the same way as you engineer the equipment for a specific performance characteristic. We do the engineering to accomplish system performance, and so we need to do the engineering for the environmental test requirements.

CERT has done some positive things. I believe it has re-established test credibility, but at a price. That price is the duration of testing. Given the state of affairs of ten years ago, when Col. Swett was saying, "What a big problem we have," and when he asked us what we were going to do about it, CERT is a step toward improved test and evaluation. We are not saying it is the solution; it is just a movement forward. I believe it has established the groundwork for a movement to improve the process of evaluating products. Too often, I think we get enamored in running tests as opposed to being enamored with evaluating products. Meeting the test requirements becomes paramount as opposed to the real purpose of conducting the test program. The tailoring concept starts to address that, but more improvements must be made.

In conclusion, with CERT we are going away from the rigidized approach. CERT has established that we need to do real-time testing, but I believe if we came back ten years from now, we would not be talking about real-time CERT-type testing, but something different. That something different could be the concepts Dr. Halpin discussed in his presentation in the Opening Session of this symposium. The development of these concepts is currently being worked in my particular organization. Hopefully, these techniques will help us to move away from testing for testing's sake, or to pass a test as a square-filling exercise; instead, testing should be made an integral part of the acquisition process. In my opinion, to make that happen, we have to be able

to understand and to be able to express the interrelationships between a specific environmental condition and the result of tests on a particular product. We have started programs and activities moving in this direction. In ten years CERT, as we know it today, will be viewed as a stepping stone that has moved us in the direction we needed to go, but in all probability, it will not be the way we will be testing in the future.

REFERENCES

1. Allan Dantowitz, et al., "Analysis of Aeronautical Equipment Failures," AFFDL-TR-71-32, May 1971.

2. Alan Burkhard, et al., "CERT-Evaluation Program," AFWAL-TR-82-3085, December 1982.

3. Robert Hager, "Dynamic Analysis and Design-Challenges for the Future," Shock and Vibration Bulletin, No. 50, Part 1, September 1980.

4. Allen Curtis, "Dynamic Testing - How Far We've Come - How Much Further To Go," Shock and Vibration Bulletin, No. 50, Part 1, September 1980.

5. John Wagner, Capt. USAF, and Alan Burkhard, "Benefits of Mission Profile Testing," Proceedings of the 27th Annual Technical Meeting of the Institute of Environmental Sciences, Los Angeles, CA, May 5-7, 1981, pp. 11-22.

6. Alan Burkhard, "Evolution of Emerging Environmental Testing and Evaluation Techniques," 31st Annual Technical Meeting of the Institute of Environmental Sciences, Las Vegas, NV, April 29 - May 2, 1985.

DISCUSSION

Mr. Paladino (Naval Sea Systems Command): Were you really serious when you said the Navy tailors a test for every piece of equipment on a ship where we cannot use a standard test environment? For instance, you are involved in avionics, and you know pretty well where your components have to go; either on the flight deck, the navigation bay or wherever they are located. But on a ship, we have relay boxes, we have electronic components, and they can go anywhere on a ship. Take a carrier, we have airplanes on a carrier among other things. Our aim is to design for shock and vibration. If we pass these two, the chances of survivability in combat are high. How do we tailor tests for all of the Navy's equipment?

Dr. Burkhard: Remember, tailoring has four factors in it. One is application or purpose of the test. This is what you are talking about, the purpose of the test. You want to test where you don't really know where the equipment will be deployed; so you are making a conscious decision by tailoring, which says we know that this is a conservative test for any one application.

Mr. Caruso (Westinghouse): You made a statement about using the climatic approximation of assuming a piece of equipment would be in a ram-air cooled compartment. You said that would be a conservative way of setting up a test profile. Could you elaborate on this?

Dr. Burkhard: When you put a program on contract, the philosophy in the Air Force and throughout the DOD on Miltary Standards, is if you don't initially have measured information or the ability to predict something, then you should fall back to a position where you have a negotiating position. As this information becomes available, you have the ability to tailor the requirements which usually means, at least contractually, reducing the requirments. So, by going to a ram-air cooled condition, which normally means the onboard cooling system is not functioning, you now have the contractual way of going back at a later date and tailoring the program. If you do not do this, from our perspective, you still have a test that will more than adequately work over the product; and if that product passes that kind of test, and if you identify the failure rate, then you know the product is better than the tests are telling you.

Mr. Caruso: Are you implying (and I hope you are, but I am not quite sure how it would happen in a program environment) that at various stages in the development of an acquisition program, we will actually be allowed to change our environmental requirements after they have been agreed to at the front end?

Dr. Burkhard: That is the importance of the Data Items. Legally, there is nothing that prevents anyone from putting a clause into a contact to deliver an updated environmental program plan at several stages in the acquisition process. That can be done in the same way you update other plans as you gain more information in other technology areas. So, putting Data Items on contract, and then saying that you want the items delivered at several intervals, is the process that can make that happen.

Mr. Caruso: Traditionally, you tested to requirements that were developed seven years before, when you were most ignorant about the end use of your equipment. Now you say that, hopefully, this will change.

Dr. Burkhard: There were very few times (some, but they were mainly focused toward specific products in terms of Data Items) that forced you to do an environmental plan early in the program. Most contracts have an environmental item called a test report which is delivered after the program has been completed. So, I believe those new Data Items allow tremendous flexibility. But the problem is getting the acquisition people to get this on contract, and making it stay on contract. This means we have to be able to articulate the benefits of doing

that, because there is pressure to reduce the numbers of reports and documents that are bought from a contractor.

Mr. Caruso: There is a fourth Data Item that you did not have asterisked, and that was the operational environmental verification report (OEVR). That is one of the DID's that is included in MIL-STD-810D. I do not remember the specific wording, but it said in essence, this is to demonstrate the effectiveness of the environmental test program. Does that imply when you get through with an environmental test program, you still haven't sold off the system? Does that somehow mean it is to wait for the field results? Will this create some contractual entanglement?

Dr. Burkhard: No. We need to develop a different kind of philosophy. We need to develop an historical data base on what was required and how the systems behaved, so we can make judgments in future acquisitions. We do not currently have that information. We only know that this is good, and this is lousy. Then you spend millions of dollars trying to regenerate the information, and maybe you can generate it and maybe you can't generate it. There is some thought about getting contractors involved in keeping after-deployment historical information.

Dr. Silver (Westinghouse): Dr. Halpin mentioned yesterday a phenomenon which I think we should consider in our CERT thought; that is the non-standard environmental conditions which can be very excessive. One of the examples he mentioned is the ground-operation of installed avionics on a hot day without any air going through it. This could obviously swamp all the predictions of stress that might be in your standard evaluation. Do you have any comment on how we might consider handling that process?

Dr. Burkhard: Like the ground check-out with no cooling air and the like?

Dr. Silver: How do we fit that into our mission profile concerns?

Dr. Burkhard: I think a lot of that kind of information is just becoming common knowledge within the acquisition community, and it should be put into a mission profile because a mission profile covers the time the plane leaves until it returns. So, if it is being checked out on the ground with no cooling air, then you need to put some thermal spikes in the profile. Then the issue becomes how many spikes and how often. So there is that flexibility. I didn't realize that until I heard Dr. Halpin's presentation, but some of the airplane tech manuals allow you to do just that. They actually say it is permissible to run equipment without cooling air.

FACTORS AFFECTING THE FATIGUE LIFE OF TURBINE BLADES AND AN ASSESSMENT OF THEIR ACCURACY

Neville F. Rieger
Stress Technology Incorporated
Rochester, New York 14623

Factors which influence the fatigue life of turbomachine blades are identified, and the current state of knowledge in each area is discussed. Estimates are presented for the probable accuracy to which blade excitation, damping, material properties, and life history data can presently be determined for a given geometry and operating conditions. The influence of errors in these input data estimates on the resulting accuracy of predicted values for blade life is estimated using linear theory. Recent advances which lead to improved estimates of cumulative damage life are discussed.

INTRODUCTION

Estimation of blade fatigue life is an important aspect of turbomachinery design because blade life often determines the operational survivability of an engine. During design, blade life estimates provide a quantitative criterion against which the influence of different design features can be compared. Blade life estimation involves the synthesis of several existing technologies, and life estimates are influenced by the state of knowledge in each contributing technology area. Certain technologies such as blade finite element modeling are now highly developed as the result of intensive efforts in recent years [1]. Modern blade models have been shown to provide very accurate results for steady stresses and natural frequencies. Other areas such as blade excitation, damping, and certain aspects of materials properties are presently in a more formative stage, though these techniques also have experienced promising developments in recent years.

The subject of life estimation is related to both vibration and stress analysis, and to reliability analysis. Until recently blade dynamic analysis was commonly limited to the calculation of natural frequencies, and mode shapes. Blade stress analysis meant steady (and possibly thermal) loads only, and reliability referred mostly to statistical projections of survivability based on sample test data. Life estimation of turbomachinery blades currently involves the development of life estimates based on relevant contributions from the following component technologies:

a. Steady stress analysis (centrifugal, pressure, thermal)
b. Flow-induced excitations from non-steady loading on rotating blades
c. Damping mechanisms (material, interface friction, gasdynamic)
d. Dynamic stress from non-steady loading, natural frequencies, mode shapes
e. Material fatigue properties (local strain approach)
f. Cumulative damage (cycle counting, Miner's law)
g. Load history

The inter-relationship between these component technologies is shown in figure 1.

The preparation of blade life estimates which correlate meaningfully with actual service lives requires accurate data for each of the above technology areas, together with an efficient computer procedure based on the synthesis shown in figure 1. Such a procedure is currently under development in the EPRI-sponsored BLADE code (Blade Life Algorithm for Dynamic Evaluation). This paper contains summaries of the state of knowledge in each component technology contributing to blade life. The accuracy to which life predictions can be made based on current technology is estimated using the product of probable errors.

TYPES OF TURBOMACHINE BLADES

Turbomachine blades may be classified as follows:

a. Turbine blades (axial flow, radial flow)
b. Compressor blades (axial, centrifugal, shrouded/unshrouded)
c. Fan blades (centrifugal, axial)
d. Pump vanes (centrifugal, axial)

This paper refers mostly to the technology which has been developed for axial flow turbines, but much of this data is also applicable to axial flow compressors including fan stages. Recent developments in blade life estimates have resulted from continuing interest in axial flow machinery, but the principles discussed herein are general, and much of the data obtained can be applied to blades of other turbomachines. Figures 2 through 5 show certain common types of blades, and blade groups. These figures illustrate the various kinds of blade attachments (root, tiewire, cover) which are in present use for mounting the blades on the disk, and for blade to blade attachments. Root attachment configurations may be classified as:

- o Axial entry
  - straight, slanted, curved
  - single or multi-hook
  - ball, trapezoid, fir-tree
- o Tangential entry
  - straddle mount, internal mount
  - single hook, multi-hook
  - straight, slant

Tiewires may be classified as:

- o floating tiewire, inserted through several blades as a single piece or as two mating halves, to add damping.
- o Integral tiewire, formed by butt-welding forged lugs on the surface of adjacent blades. This adds rigidity and local constraint, and is used for frequency tuning.

Covers or shrouds may be classified as:

- o Integral cover, forged on end of single blade tip. May improve stage efficiency, and contributes damping under impact conditions.
- o Peened cover, rivetted on several blades to form a group. Adds damping by rubbing on tenons and blade ends, and by flexing.
- o Patented cover tips which lock up under centrifugal untwist, to form a blade group or a continuous row of blades.

Specific details of blade group constructions are dictated by the dynamic strength requirements of the stage, by anticipated excitations; by locations of natural frequencies, and by patent rights. The BLADE code contains subroutines to model the detailed geometry of a particular blade upon command, using a library of pre-programmed vane shapes, blade and disk root attachments, tiewire types, and cover designs. The assembled single blade geometry can later be replicated to form a blade group, by selecting appropriate attachment boundary conditions between blades.

FACTORS AFFECTING FATIGUE LIFE

The basic parameters which influence how long a specific blade design/construction will survive in a given environment are:

a. Steady stresses resulting from centrifugal loads, steady gas loads, thermal gradients, assembly tolerances, geometric untwist, attachment tolerances, attachment constraints, and tenon cold working.

b. Dynamic stresses caused by non-steady gas forces, nozzle wakes, thermal transients, start-stop transients, sequential arc operation, per-rev diaphragm harmonics, and flow instabilities. Such stresses may include the effects of geometric stress raisers in root attachments, in the vane-platform fillet, in the tiewire fillet or hole edge, cover or attachment discontinuities, and residual preload from rivetting, and assembly tolerances.

c. Structural stiffness and mass properties of the blade shape, resulting in blade and blade group natural frequencies, and the proximity of these frequencies to any strong exciting harmonics of rotational speed, such as nozzle-passing frequency (NPF). Also, those blade, or group natural frequencies which may be excited by flow instabilities.

d. Material properties such as fatigue strength, ultimate strength, strain-life properties, creep strength, corrosion effects, system damping properties; and the effects of erosion and process degradation on these factors.

e. Load history details resulting from centrifugal overload, start-up over-

speeds, and operational start-stop cycles; from the per-rev excitation spectrum arising from the diaphragm flow distribution, including NPF excitation, sequential arc operation, and from any gas flow instability conditions. This data includes all unit operation such as manufacture overspeed proof testing, process start-up problems, governor overspeed settings, startstop machine checkout runs, and all service operation.

The influence of parameters (a), (b), and (d) can be shown in a Goodman diagram, figure 6, and parameter (c) can be shown on a Campbell diagram, figure 7. Goodman diagrams are however, unable to show how the combined effect of several exciting frequencies influences fatigue life, such as those which would result from the flow spectrum of figure 8. Modern approaches to this problem of cumulative damage are summarized in the Accuracy of Life Prediction section of this paper.

The combined influence of structural changes, excitation changes, damping changes, material type or heat treatment changes, and load history changes on blade fatigue can be quantitatively addressed in terms of a single factor: the blade life value. The BLADE code is designed to perform such blade fatigue life assessments, which include the influence of each of these parameters.

STRESS CALCULATIONS: 'BLADE' CODE

Stress analyses conducted for blade life estimation are usually made using the finite element method to allow significant geometry details and other stress raisers such as holes, radii, etc. to be included directly into the calculations. Further geometry refinements which give precise stress details, and material properties which include plastic yielding and creep may also be assessed by repeated applications of this method, as needed. The accuracy attainable with well-designed finite element blade models is very good in the writer's experience. Where solid elements are used this accuracy is enhanced, through the use of the basic elasticity equations. In such applications the accuracy of this method can be as close as 1-3% for natural frequencies depending on the mode, and in the order of 2-10% for calculations of peak dynamic stresses. In practice, larger errors can result from many factors, depending on a) suitability of the gridwork chosen for the desired geometry, b) known values of the elastic modulus with temperature and dynamic effects, c) numerical error accumulations, d) number of Gauss points used, e) suitability of element types for local deformations, and so on. With experience, such analyses typically result in models which give frequency correlation to within 1-2% for the first mode, 2% for the second mode, etc. In the lower modes an important potential source for discrepancy with test results lies in the representation used for the attachment conditions in the disk root, and in the attachment conditions with adjacent blades. There is also evidence to suggest that blade frequencies may change slightly in service, under conditions where structural degradation occurs. Corrosion, etc., is thought to change the blade/disk attachment rigidity, thus changing the blade/group natural frequencies. This can have serious implications for blades originally tuned close to resonance. Errors in prediction of frequencies of blade modes may also result from inappropriate simplicity of the blade gridwork used, and from discrepancies in the blade dynamic modulus data.

Blade finite element models for life estimation often contain detailed representations of the root, i.e., blade/disk attachment region, because this location has been a frequent site for serious stress cracking occurrences. The inclusion of root flexibility is also needed to obtain accurate predictions of blade frequencies and mode shapes. Experience has shown that blade models developed from solid elements (8 node or 20 node hexahedra, and 6 or 15 node wedges) are easier to computer-generate than blade models composed of plates, beams, solid elements, etc. Solid element models are also easier to subdivide for refined stress calculations using superelements; see Steele and Lam [2].

Accurate steady stress computation depends on how suitably the blade model is prepared (element detail), and how well the applied loads are known. Centrifugal force is usually the major load, and this is accurately known with speed. Gas loads are often much smaller, and these depend upon stage power output. Generally speaking, steady loads can be defined to within 2-5% of actual values. Appropriately modeled blades can then achieve steady stress values to within 2-5% of true values in critical areas given adequate model details. It is noted that this is usually more accurate than strain gage values (5-10%), especially within high stressed regions.

Dynamic stress σ_D is often expressed in terms of excitation, damping, and steady gas bending stresses by an expression of the form:

$$\sigma_D = \frac{\pi}{\delta} S(\omega) D(\omega) \sigma_B(P) \qquad (1)$$

where π = 3.1415. . ., δ is the modal damping log. dec value, $S(\omega)$. is the excitation frequency spectrum, $D(\omega)$ is the modal coupling coefficient, and σ_B (P) is the steady gas bending stress at the same location. This expression contains all the major parameters influencing the dynamic stress value. Neither damping nor excitation are fully predictable at present, but estimates can be given for state-of-art values of both these quantities, for practical operating conditions. The modal coupling factor is obtained directly from dynamic stress calculations with a finite element model. In previous analyses this factor was computed by methods such as those given by Prohl [3]. In a turbomachine stage the significant exciting frequencies are usually known accurately, since they are multiples of rotational speed: see figure 7. The natural frequencies are known from calculations or testing to the accuracy mentioned above.

Accurate correlation of the first six to ten natural frequencies ensures the quality of both the stiffness and mass matrices of the blade model. Thus $D(\omega)$ is known to 2% or better: also see comments under Accuracy of Life Estimation. The quality of the blade dynamic model influences the dynamic response calculations, and the dynamic stress results. Care should be taken to validate more modes than those for which accurate stress data are required, as frequency is a square-root function of both the stiffness and mass matrices. Data published by Rieger [4] for HP blades, and by Steele and Lam [2] and by Kelen and Cave [5] for LP blades are representative of present capabilities for blade modeling and frequency computation.

EXCITATION

Typical sources of blade excitations are:

a. Diaphragm harmonics, including per-rev and NPF harmonics
b. Partial admission loading transients
c. Flow instabilities (rotating stall, acoustic waves)
d. Transmitted structural excitations (rotor torsional)

Diaphragm harmonics result from dimensional imperfections in the flow passage geometry and, in particular, from variations in the nozzle throat dimensions. Several current methods exist for assessing the effect of such variations. One method is to analyze the Fourier spectrum of the nozzle throat dimensions, to identify the principal harmonics, and to compare these with blade natural frequencies. This procedure gives warnings of possible strong excitation harmonics. It does not evaluate the magnitude of the resulting excitation harmonics, nor does it consider the influence of variations in the axial gap during rotation, nor of the effect of spacing errors in the rotating row. The influence of trailing wake effects is also omitted from this method. A more recent procedure [6] combines the influence of diaphragm spacing tolerances, and of blade row spacing, with the stage flow parameters (pressure drop, enthalpy) using a computer program. This procedure calculates the magnitude of blade excitation at the various per-rev frequencies as a forcing spectrum. It also gives the spectrum of dynamic forces which act on the rotating blades, in both the tangential and the axial directions. The above methods are both two-dimensional in nature. They could be applied in a stepwise radial manner to obtain approximate values for the 3D dynamic flow behavior within the stage. Secondary passage flow effects are not included in these methods.

Partial admission inlet gas flows around the stage circumference cause stepwise loadings to be applied to the rotating blades. The blades also experience load transients of the type shown in figure 9 as they move in and out of the admission arcs. Details of such loadings were first obtained by Kroon [7]. Substantial difficulties are involved in making actual strain measurements on rotating blades under the extreme conditions of temperature, pressure, and accessibility which exist with such inlet stages. However, useful data has been obtained from heater box tests using a rotating HP blade row at speed and, more conveniently, from model tests on a rotating air turbine inlet stage. Rotating water table simulations of this problem have also been performed employing the hydraulic analogy, by Heen and Mann [8], Rieger [4], and by Partington [9].

Theoretical predictions of non-steady blade forces were first made by Kemp and Sears [10] [11] who studied nozzle-passing excitations from an upstream cascade on an isolated airfoil in a moving row using vortex flow analysis. Subsequent developments in this procedure were contributed by Horlock [12], Nauman and Yeh [13], Osborne [14], Mani [15], Mukhopadhyay and Rao [16], Rao and Seshadri [17], and others. Actuator disk studies were employed by Whitehead [18] [19] to account for the effects of upstream flow distortions on the stability of flow, and to evaluate non-steady forces. Further developments of the actuator disk approach have been contributed by Smith [20], Holmes [21], Horlock and Henderson [22], Horlock, Henderson and Greitzer [23] and others, who developed efficient procedures to account for blade camber and low frequency

flow distortions. The vortex method and the actuator disk methods are convenient procedures for estimation of non-steady forces. Both procedures are presently limited to subsonic flows. Supersonic conditions may however be encountered in turbine impulse stages, and they are typical conditions in the LP stages of modern steam turbines. Similar comments apply for compressor stages. All of these computation methods are presently limited to 2D flows, whereas the flow fields of longer blades may involve significant secondary flows. Further analytical developments in both of these techniques may require 3D finite element flow analysis. Such procedures are currently being developed for stage gasdynamic flows.

Of the experimental methods which have been used to investigate non-steady blade forces, air turbine tests and water table studies have been the most widely reported. Air turbine studies have been made by Partington [9], wind tunnel studies have been made by Holmes [21], and fan tests by Henderson and Horlock [22]. Ongoing test programs by most turbomachine manufacturers have involved such methods. Both compressible and incompressible air turbine flow studies have been made to investigate nonsteady pressure fluctuations on the blade surface. The supersonic cascade work of Fleeter [24] and others is an example of advanced testing to examine the stability of supersonic cascade flows. Many early water table studies were qualitative investigations of flow patterns in airfoil cascades. The hydraulic analogy allows both subsonic and supersonic flows to be studied conveniently. Recently a rotating water table has been extensively developed by Rieger et al [25], and used by Rieger and Wicks [26]. Modifications of this concept have been independently used by Partington [9] and by Rao et al [17]. Quantitative water table testing simulates the flow field in a given stage geometry, and measures the non-steady forces on a rotating blade using a load cell. Both turbine and compressor stages have been considered. Measured results have been compared with results predicted by modified Kemp-Sears theory by Rieger et al [27], [28] and with more advanced theoretical developments by Rao et al [17]. In general the hydraulic analogy has been shown to effectively reproduce the gasdynamic details, but the correlation reported between test data and theoretical results for non-steady forces is not, as yet, in close agreement. Example of such correlation is shown in figure 10. Possible reasons are limitations in the theoretical approaches, such as the idealized geometry, inadequacy of the specific heat correction, or use of an unsuitable wake model. Existing data suggests that the probable accuracy with which non-steady forces can be predicted from laboratory tests is between 20-40 percent. Adequate representation of typical spacing errors for given stages represents an additional problem.

DAMPING

The magnitude and distribution of damping depends on the blade type, material, structural attachment details, and on the stage gasdynamic conditions. Damping is usually classified according to the following mechanisms:

a. Material damping. Crystal slip and distortion.
b. Interface damping. Coulomb friction effects at interfaces.
c. Gasdynamic damping. Work done on the gas stream.

Material damping is an inherent property of the material of which the blade is constructed: see Lazan [29]. It depends upon dynamic stress magnitude, on preload (steady stress), and to a lesser extent on temperature of operation, and on frequency. Material damping is described by Lazan's law:

$$D = \int_V D_o \, dV \qquad (2)$$

where

$$D_o = J \sigma_D^{\,n}$$

and D is the damping energy dissipated within volume dV, D_o is the energy loss per unit volume, J and n are material constants, and σ_D is the vibratory stress. Data on J and n has been obtained by many authors, and has been summarized by Lazan [29]. The validity of Lazan's law for turbine blades has been demonstrated experimentally by several authors, e.g., Wagner [30], Gotoda [31], Rieger [32], as shown in figures 11 and 12. The dependence of blade damping on stress amplitude is clearly established by these typical experimental results. The influence of centrifugal preload is also shown. The generality of such results has been demonstrated for different modes of vibration, for both high-pressure blades and for long, low-pressure blades. Recent research on the mechanism of material damping for turbine blade materials has been published by Wilkinson [33].

Interface damping occurs at attachments such as the blade-disk interface, tiewires, and covers. The mechanism involved is Coulomb friction, and the magnitude evidently depends on the normal load and

the local coefficient of friction. Of particular interest is the amount of interface damping associated with the blade-disk attachment region. This has been the subject of considerable recent research, e.g., Jones, Muszynska [34] [35] [36]. These authors studied aircraft compressor blades with axial entry tee-slot attachments, under relatively light centrifugal loads, and found considerable damping under slipping conditions. Rieger studied several blade types under various root attachment conditions, and found negligible interface friction under steam turbine operating centrifugal load conditions.

Specific studies of tiewire and cover damping, and of the effects of high-friction attachments do not appear to have been published in the open literature. Srinivasan [37] has discussed the frictional effects of fan-blade lock-up snubbers on the fan row structure as a whole. Where the load can be defined in advance, e.g., centrifugal untwist forces at tiewire, and the environment is well defined (such as air or dry steam), the evaluation of interface damping appears to be possible. Under such circumstances the energy dissipated can be estimated from:

$$E_i = \pi \mu F X \qquad (3)$$

where μ is the local dynamic friction coefficient, F is the normal applied force and X is the resulting amplitude of vibration. Recent studies based on this approach for blades are described by Srinivasan [38]. The same procedure can be used for cover-tenon damping, and for floating tiewire damping. Definition of the normal load is a problem for the cover-tenon interface, and definition of a suitable friction coefficient is another problem for the floating tiewire case.

Gasdynamic damping results from work done on the gas stream passing over the surface of an airfoil as the blade vibrates in a normal mode. For unstalled flows the resulting work leads to positive damping which is viscous (velocity dependent) in nature. Stalled flows lead to negative damping, i.e., to unstable vibrations, which draw energy from the gas stream. Substantial previous work exists on stalled flows of compressor stages. The mechanism of gasdynamic damping is viscous and linear. It is governed by the expression:

$$E_g = \pi C_g \omega X^2 \qquad (4)$$

in which E_g is the energy dissipated/cycle, C_g is the gasdynamic coefficient, ω is the circular frequency of vibration and X is the vibration amplitude. The value of C_g depends on the power output of the stage:

$$C_g = 9.55\ T(P)/N(r_o + \tfrac{1}{2} L)(r_o + L) \qquad (5)$$

The accuracy to which such damping data can be prescribed for a given stage depends on knowledge of blade material properties, interface contact conditions, gasdynamics and power output. Blade damping values are quite reproducible between test blades, but the consistency between nominally identical cases has been known to vary from 2:1 to 5:1, between known and unknown conditions. Interface loads may vary ±200%, even where tolerance control is good, and even more for worn or re-assembled blades. In the case of rivetted assemblies, the range of variation is not known. The influence of factors other than material damping may be minor for unstalled flows and blades of turbine stages, but may be more significant for compressor stages. Overall blade damping log. dec. values of 0.02 (long blades) to 0.04 (short blades) are typical from rap tests at room temperature for turbine blade steels. At speed and temperature, values may be less. The introduction of high damping devices (pins, overlapping tiewires) have lead to still higher damping values. Alternatively, titanium is a low-damping material, and for this reason titanium blades often have additional damping devices (snubbers, rubbing interfaces).

MATERIAL PROPERTIES

The fatigue life of turbine blades usually refers to high-cycle crack initiation life, since most blade fatigue damage results from high-frequency stress reversals of moderate amplitude, often superimposed on a contributing mean stress. Such conditions are well suited to life prediction using the Local Strain method of Morrow [39] and others [40] [41]. The number of cycles to crack initation, N_f, may be found using an equation of the type:

$$\frac{\Delta\varepsilon}{2} = \frac{\sigma'_f}{E} (2N_f)^b + \varepsilon'_f (2N_f)^c \qquad (6)$$

where $\Delta\varepsilon/2 = \ln(A_o/A)$ is the (true) strain amplitude at the crack location, σ'_f is the strength coefficient, σ_o is the (true) mean stress, E is the elastic modulus, b is the fatigue exponent, ε'_f is the ductility coefficient, and c is the ductility exponent. The relationship between these factors is shown in the strain life curve, figure 13, for AISI 403, which was obtained from smooth

specimen tests, in air. The scatter between the test points shown is representative of modern test capabilities for many materials. The strain-life curve is a best-fit line, and the parameters σ_f', ε_f', b, and c listed in table 1 were obtained from this curve. Provided that the local strain formulation chosen can be adequately represented by summing the elastic and plastic characteristics as shown, the fatigue parameters will then be accurately defined for the test specimens used, and the test environment. It is evidently of the greatest importance to ensure that representative material tests are performed under conditions of loading, temperature, and environment chemistry, similar to those under which the blades will operate in practice.

It is also important to note that the required stresses and strains are 'true' stress and 'true' strain values, and not the commonly-used 'engineering' values. The distinction between these two formulations is shown in figure 14. Also, the stress-strain data needed is strain controlled cyclic data, i.e., data obtained as the locus of hysteresis test loops with increasing load, as shown in figure 15. An approximating relationship between cyclicly obtained true stress and true strain is:

$$\frac{\Delta\varepsilon}{2} = \frac{\Delta\sigma}{2E} + \left(\frac{\Delta\sigma}{2K'}\right)^{1/n'} \qquad (7)$$

where K' is plastic modulus, and n' is the strain hardening exponent. Values of K' and n' are typically obtained from automated tests on material specimens. Dowling et al [41] have compared results using this rule with test data, and found correlation within 6% at 0.02% true strain for finite element data.

CUMULATIVE DAMAGE

Cumulative damage occurs where the load history contains more than one harmonic component. Special cycle counting procedures are needed where two or more harmonic components occur simultaneously in the response. Current damage assessment procedures are based on the hysteresis loop for the material. Figure 16 shows the manner in which a given stress history at a critical location on a blade may be converted into equivalent cycles using the experimentally determined cyclic stress-strain hysteresis loop in figure 15. For a typical case, a representative load history, figure 17, must be determined from the total operation history of the component. This history contains data from the manufacturer's start-up trials, and for a specific period of operation (e.g., one month) for which this data will repeat through the life of the unit. Unusual events can be included in the same manner as the initial start-up trials.

An indication of present capabilities for fatigue life prediction for material test specimens using well-defined inputs can be obtained from results of the SAE Cumulative Fatigue Damage Test Program [42] in which three different load-time histories were applied under laboratory conditions to determine the fatigue initiation life of two different steels. The materials used were MAN-TEN (U.S. Steel), a 0.23C, 1.57Mn, 47 ksi Yield, 80 ksi UTS hot-rolled alloy, and RQC-100, a 0.19C, 0.79Mn, 120 ksi Yield, 126 ksi UTS rolled, quenched and tempered steel. Tests were conducted at room temperature for several different load levels for each steel. High cycle fatigue crack initiation lives were predicted using the Local Strain approach. Predicted lives are compared with test results in figure 18. Perfect correlation corresponds to the 45 degree line. In general the results lie within a life range $\pm$300%, compared to predicted values.

This comprehensive program was conducted under laboratory circumstances, using known load spectra (not single frequency, constant magnitude loading), which included cyclic components of differing magnitude, and mean stress (tension, and compression) effects. The specimens cracked from 0.38 in. diameter holes of K_t = 2.62 which were drilled and reamed, but without edge preparation. Thus the loading and the manufacture quality were both typical of operating conditions, and of the machining quality of locations, e.g., root attachments, which apply in crack-sensitive regions of turbine blades.

It is also noted that this work was conducted under laboratory circumstances in air at room temperature, using three different loading spectra. Cumulative damage arising from these spectra were assessed using the Palmgren-Miner rule. No subsequent tests appear to have been made to include temperature effects, or creep, or the influence of other environments.

ACCURACY OF BLADE LIFE PREDICTION

Fatigue life is determined by the spectrum of alternating stress components, the steady (or mean) stress, the material fatigue strength in the environment, and the load history to which the blade is subjected. The blade alternating stress spectrum may contain many frequency

components, which must be included in the life evaluation using the Palmgren-Miner law [43], or some similar procedure. The material fatigue strength must account for both process and exposure-related effects, such as corrosion and erosion, which are time-dependent. This poses a problem for the evaluation of middle-term fatigue life (10^4 - 10^6 cycles), but is less of a problem for high-cycle fatigue, where these effects are established, and for low-cycle fatigue where their significance may be less. The shortcomings of life assessment using S-N curves, and of accelerated specimen test data also become apparent under such conditions. Blade load history is often difficult to specify for several reasons: first, it is still uncommon for detailed records to be kept, especially of the initial test-cycling which a rotor receives, i.e., actual number of run-up cycles required to perform balancing and overspeed operations. Similar comments apply to plant test records for overspeed and governor speed settings. Second, it is not possible to know in advance the gas force history to which a blade will be subjected in service, and past histories of such loadings can usually only be assembled in a speculative manner. An assessment of the accuracy to which those factors contributing to blade life can presently be determined is estimated in table 2. These figures show general, order-of-magnitude figures only, based on experience, personal discussions, and from work discussed previously in the current literature. Actual figures for particular cases may, for many reasons, differ from the figures listed, though particular cases should contain values of the same general order.

The influence of variations in steady stress, dynamic stress, material properties, and load history on blade fatigue life cannot be determined by any proven procedure at present. One simple procedure to estimate the accuracy of blade fatigue life estimates would be to assume that each factor contributes linearly to blade life, i.e.,

$$L_B = L\{\sigma_S, \sigma_D, G\Delta\varepsilon, \sum \frac{n_i}{N_i}, H(t)\} \qquad (8)$$

where σ_B is steady stress (centrifugal plus gas bending), σ_D is the multi-component dynamic stress arising from the excitation spectrum, $\Delta\varepsilon$ is the material environmental fatigue strain life, $\sum(n_i/N_i)$ is the cumulative effect of the multi-component loading expressed as the Miner's sum value (nominally 1.0), G is the influence of assembly tolerances, and H(t) represents variations in the loading cycle which equals 1.0 if the loading blocks are identical: see figure 17. The factors which influence the steady stress value are the centrifugal load, which is typically known to within 1%; the gas bending load, which varies with power setting but is typically known to within 2-5%, and the true geometry, which is achieved in practice to within 1-2%. Thus the steady stress at a given location is typically known to within 2-3% or less.

The dynamic stress value results from the sum of several q- exciting frequencies acting on several p- blade modes, and is governed by an expression of the form:

$$\sigma_D = \sum_{i=1}^{p} \sum_{j=1}^{q} \frac{\pi}{\delta_i} S_{ij}(\omega) A_{ij}(\omega) \sigma_B(P) \times \cos(i\omega t + \phi_i)\cos j\omega t \qquad (9)$$

where π is 3.1415..., δ is the modal log. dec. damping, $S(\omega)$ is the excitation ratio, $D(\omega)$ is the dynamic magnifier, $\sigma_B(P)$ is the gas bending stress, ω is rotational frequency, ϕ is the phase angle between the shaft modal responses, i is the blade mode, and j is the exciting spectrum harmonic. The parameters δ, $S(\omega)$ and $D(\omega)$ each exert a direct influence on blade dynamic stress, in addition to $\sigma_B(P)$.

Blade damping δ is influenced by material properties (δ_m), by joint friction (δ_f), and by gas pumping work (δ_g). Material damping typically represents about 50-80% of available blade damping, and such damping values are typically known to within (30-50%). Joint friction is known imprecisely (50-100%) and is highly dependent on structure details, and on any preloading. Gas damping is relatively small (except under stall flutter conditions) and depends on blade power output. It is fairly well understood (20-50%). Proportioning these values suggests that blade damping might be generally specified to accuracies within the range 35-60%.

The variability of excitation $S(\omega)$ may be estimated from blade loading during strain gage testing of blades and, more directly, from water table testing of blade load fluctuations. $S(\omega)$ fluctuations of 10-50% are commonly observed in frequency components during water table testing of stages even when thorough set-up procedures have been employed. The magnitude of such signal fluctuations may differ from harmonic to harmonic, and are due to the spacing errors in the stage assembly, signal averaging rate, rotor speed fluctuations, and axial gap variations between the stationary row

and the instrumented rotating blade.

The blade coupling coefficient $A_{pq}(\omega)$ is determined by the proximity of the p-th natural frequency to resonance with the q-th excitation harmonic of the $S(\omega)$ spectrum in accordance with the usual modal detuning expression:

$$A_{pq}(\omega) = \frac{2\xi_p(\omega/\omega_p)}{\sqrt{\{1-(\omega/\omega_p)^2\}^2+\{2\xi_p(\omega/\omega_p)\}^2}} \qquad (10)$$

where $\xi_p = \delta_p/2\pi$

$A(\omega)$ varies with tolerances in the root attachment, in the cover-tenon assembly, and with the tiewire assembly used. If these tolerance and contact conditions are contained within the structural assembly the factor G, then $A(\omega)$ is a function of the accuracy to which the blade natural frequencies can be calculated. Such accuracy is mode-dependent as noted earlier, but typically lies within the range 1-6% for the first six modes of a blade group, using finite element methods. The assembly tolerance factor G is more difficult to define with generality. Experience suggests that it could cause a further variation of 10-20% in the rotating natural frequencies, due to gaps and assembly differences. With good assembly practices, G usually causes less than 10% variation in blade group natural frequencies.

The fatigue strength of the material ($\Delta\varepsilon$) is obtained from fatigue tests on blade material samples, and from the blades themselves in failure studies. Usually such strain-life data follow curve fit lines quite closely, though the number of samples used is often small, e.g., 6 to 20. If such results can be accepted, the fatigue variability is typically less than 5%, using modern strain-controlled test techniques. It seems possible that this scatter would increase if additional test data was obtained. This variability applies for the basic material strain-life curve, and it does not include the effect of corrosion, or creep under high temperature conditions. Both corrosion and creep have been shown to cause significant changes in the material strength where long-term exposure to either condition was involved. Insufficient data appears to be available at present for precise estimates of creep-fatigue and corrosion-fatigue life values to be made.

The linear life prediction law given earlier is one method by which estimates can be obtained for the effects of errors in fatigue parameters on blade life values. Using average values for the parameters listed in table 2 leads to the following result:

$$L_B = L\{\sigma_S, \sigma_D(\delta, S(\omega), A(\omega)G), \Delta\varepsilon, \sum(n_i/N_i), H(t)\}$$

$$= 1.03x(1.30x1.50x1.02)x1.15 \qquad (11)$$
$$x1.10x1.30x1.0$$

$$= 3.37$$

where H(t) =1.0 for identical load cycle blocks.

This blade life result suggests that there may be ~337% variability between measured blade life and calculated blade life. Such variability is consistent with results obtained in the SAE Fatigue Test Program [42]. If the variability of the given input data for the SAE program is estimated from the data given in [42] as σ_S = 1.03, σ_D = 1.10, G = 1.03, $\Delta\varepsilon$ = 1.10, $\sum(n_i/N_i)$ = 1.3, and H(t) = 1.0, the comparable value of variability of specimen life can be estimated using the same procedure as:

$$L_S = 1.03x1.10x1.03x1.10x1.30x1.0 \qquad (12)$$
$$= 1.69$$

The observed range of extreme variability in the SAE program was between 200-300%, and so the above L_S value represents an average value for the observed program results. The greater variability with the turbine blade life estimate is due to the larger number of parameters which contribute to the total error in life estimates, i.e., less controlled conditions.

Further supporting data is available from recent fatigue test results on turbine blade materials reported by Morrow [44]. With σ_S = 1.0, σ_D = 1.0, $\Delta\varepsilon$ = 1.05 (est.), G = 1.0, $\sum(n_i/N_i)$ = 1.5, H = 1.0, the results show a scatter from 0.63 to 1.43, which compares well with the value assumed above for the Miner's law factor (1.3), which was the primary variable under strictly controlled test conditions involved. In these tests also, the predicted blade life was 63 years. The specimen lives ranged from 40 years to 90 years (of accelerated testing), with a mean life of 65 years. Such correlation between calculated life and test life is encouraging, but it should not be considered common at present.

Finally, some comments on cumulative damage evaluation procedures are needed. The best known procedure is the Palmgren-Miner linear damage law [43]. From experimental

comparisons this procedure is known to be imprecise but it provides a useful approximation, given the inaccuracy which is typical of much calculation input data. Manson et al [45] mentioned two specific limitations which are evident from various studies of Miner's Law. First, no order-of-failure effect is implicit within the law, although it is known that high-load first exposures lead to shorter lives. Second, damage acquired at stress levels below the elastic limit can lead to failure if it is preceded by high-load damage in certain instances.

An excellent survey of cumulative damage has recently been published by Conway, Stentz and Berling [46], in which attention is drawn to studies of the Double-Linear-Damage Law by Grover [47], Manson [48], Manson et al [49], and many others. This procedure is illustrated in figure 18. An extension to a Multiple-Level-Damage rule has been proposed and studied by Battacharya [50] who compared his experimental results for impact loading with predictions by Miner's rule, and with Corten and Dolan's rule, and found improved correlation with the Multiple-Damage Rule for low carbon steel at room temperature. Conway et al also mentioned an extensive review of cumulative damage procedures by Dubec et al [51], which focused on mathematical procedures, and on strain controlled fatigue studies by several authors. Dubec described the development of a Unified Theory of Cumulative Damage, which contained concepts from previous strain-life fatigue studies by Shanley [52], Valluri [53], and Gatts [54]. The survey by Conway et al also included a review of recent work on cumulative creep failure studies for high temperature turbine blades.

CONCLUSIONS

- The effect of blade geometry details on stresses and natural frequencies is accurately and conveniently accounted for within the blade finite element model.
- Finite element blade average steady stresses typically agree with strain gage stress results to within 1-2%. Peak steady stresses typically agree to within 2-5%.
- Finite element blade natural frequencies typically agree with test frequencies to within 1-6% depending on the mode involved. Such agreement for the first 6 to 10 natural frequencies is desirable for calculations, to validate the blade dynamic model, and to ensure accurate dynamic stress results.
- Detuned blade dynamic stresses can be correlated with measured dynamic stresses to within 5-10% when the excitation spectrum is known. Resonant stresses can be correlated to within 30-50% when suitable excitation and damping data are available.
- Material fatigue initiation life estimates can be typically made to within 200-300% of measured material life values, where the stresses and material fatigue properties are available.
- Blade life estimates to within 300-400% or less of measured life values are currently possible given the current state of knowledge for material properties, excitation, damping and cumulative damage estimates.
- Improved methods for obtaining blade life estimates are needed. Such methods will involve more sophisticated life estimation technology than that proposed herein, together with improved input data on excitation, damping, materials technology and life history.
- Records of blade loading history which include all loading data should be developed. Such data should be used to calculate blade life expenditure to date. Improved procedures for estimating future load cycle histories, based on machine class operating statistics, are needed.

REFERENCES

1. O. C. Zienkiewicz, "The Finite Element Method," McGraw-Hill Book Company, Inc., New York, NY, 3rd Edition, 1977.
2. J. M. Steele, T. Lam, "Stress and Fatigue Analysis of Steam Turbine Blades," Second ANSYS Conference Proceedings, Pittsburgh, PA, April, 1983.
3. M. A. Prohl, "Method for Calculating Vibration Frequency and Stress of Banded Group of Turbine Buckets," Trans. ASME, Vol. 80, pp. 169-180, Jan. 1958.
4. N. F. Rieger, "Diagnosis and Correction of Vibration Problems in Turbine Generator Units," Proceedings, EPRI Workshop on Power Plant Availability, Dearborn, MI, August, 1982.

5. P. Kelen, L. E. Cave, "Calculated and Measured Natural Frequencies of Low Pressure Steam Turbine Blades and Wheels With Arch-Coverbands," Third International Conference on Vibrations in Rotating Machinery, Inst. Mech. Engrs., York, England, Sept., 1984.

6. Proprietary Blade Excitation Computer Code SPACEX, Stress Technology Incorporated, Rochester, NY, 1984.

7. R. Kroon, "Turbine-Blade Vibration Due to Partial Admission," Jnl. of Appl. Mechanics, Dec. 1940. 1940

8. H. K. Heen, R. W. Mann, "The Hydraulic Analogy Applied to Non-Steady Two-Dimensional Flow in the Partial-Admission Turbine," Trans. ASME, Jnl. Basic Eng., Series D., pp. 408-421, Sept. 1961.

9. A. J. Partington, "Vibration analysis of Steam Turbine Pinned Root Control Blades," Proceedings IFTOMM Intl. Conference, "Rotordynamic Problems in Power Plants," Rome, Italy, Sept. 28-Oct. 1, 1982.

10. N. H. Kemp, W. R. Sears, "Aerodynamic Interference Between Moving Blade Rows," Jnl. of the Aeronautical Sciences, Vol. 22, No. 7, pp. 585-597, 1953.

11. N. H. Kemp, W. R. Sears, "The Unsteady Forces Due to Viscous Wakes in Turbomachines," Jnl. of the Aeronautical Sciences, Vol. 22, No. 7, pp. 478-483, 1955.

12. J. H. Horlock, "Fluctuating Lift Forces on Aerofoils Moving Through Transverse and Chordwise Gusts," Trans. ASME, Jnl. Basic Eng., Series D, pp. 494-500, Dec. 1968.

13. H. Naumann, H. Yeh, "Lift and Pressure Fluctuations of a Cambered Airfoil Under Periodic Gusts and Applications to Turbomachinery," Trans. ASME, Jnl. of Eng. Pwr., Series A, pp. 1-10, Jan. 1973.

14. C. Osborne, "Compressible Unsteady Interactions Between Blade Rows," AIAA Journal, Vol. 11, No. 3, pp. 340-346, March 1973.

15. R. Mani, "Compressibility Effects in the Kemp-Sears Problem," Presented at International Symposium on the Fluid Mechanics and Design of Turbomachinery, Penn State University, 1970.

16. S. S. P. Rao, V. Mukhopadhyay, and J. S. Rao, "Lift and Moment Fluctuations of a Cambered Aerofoil Under Non-Connecting Streamwise Gust," Jnl. of Royal Aeronautical Society, p. 83, Feb. 1977.

17. J. S. Rao, V. V. R. Rao, and V. Seshadri, "Non-Steady Forces in Turbomachine Stage," Third International Conference on Vibrations in Rotating Machinery, Inst. Mech. Engrs., York, England, Sept. 1984.

18. D. S. Whitehead, "Vibration of Cascade Blades Treated by Actuator Disk Methods," Proc. Inst. of Mech. Eng., Vol. 173, No. 21, pp. 555-574, 1959.

19. D. S. Whitehead, "Force and Moment Coefficients for Vibrating Aerofoils in Cascade," Aeronautical Research Council, RaM 3254, 1960.

20. S. Smith, "Discrete Frequency Sound Generation in Axial Flow Turbomachines," Aeronautical Research Council, RaM 3684, 1972.

21. D. W. Holmes, "Lift and Measurement in an Airfoil in Unsteady Flow," Trans. ASME, Jnl. Eng. Pwr., Series A, 1974.

22. R. E. Henderson, J. H. Horlock, "An Approximate Analysis of the Unsteady Lift on Airfoils in Cascade," Trans. ASME, Jnl. Eng. Pwr., Series A, pp. 223-240, Oct. 1972.

23. J. H. Horlock, E. M. Greitzer, and R. E. Henderson, "The Response of Turbomachine Blades to Low Frequency Inlet Distortions," Trans. ASME, Jnl. of Eng. Pwr., Series A, 1976.

24. S. Fleeter, "On the Unstalled Subsonic, Sonic and Supersonic Aerodynamic Coefficients Necessary for Aeroelastic Calculations," Proc., Workshop on Aeroelasticity in Turbomachines, Office of Naval Research Program ONR Project Squid, Detroit Diesel Allison, Indianapolis, IN, June 1972.

25. N. F. Rieger, A. L. Wicks, A. B. Dodd, "Design and Development of a Rotating Water Table for Flow Studies in Turbomachine Stages," ASME Preprint Number 78-WA/DE-16, 1978.

26. N. F. Rieger, A. L. Wicks, "Non-Steady Forces and Observations of Flow in Three Turbine Stage Geom-

etries," Turbomachinery Developments in Steam and Gas Turbines, Trans. ASME, Vol. 100, p. 525, Presented at ASME Winter Annual Meeting, Atlanta, GA, Oct. 1978.

27. N. F. Rieger, A. L. Wicks, J. Crofoot, W. J. Nowak, "Experiments and Theories for Non-Steady Forces on Turbine Blades," Stress Technology Incorporated Report for Naval Ship Engineering Center, Turbine and Gear Branch, Arlington, VA, Feb. 1978.

28. N. F. Rieger, A. L. Wicks, "Measurement of Excitation Force Levels for SSME HPFTP Turbine Rotor Blades Using Water Table Hydraulic Analogy," Report PA001, Stress Technology Incorporated, Prepared for Rocketdyne Division, North American Rockwell Division, Sept. 1979.

29. B. J. Lazan, "Damping of Materials and Members in Structural Mechanics," Pergammon Press, Inc., New York, 1968.

30. J. T. Wagner, "Blade Damping Tests," Westinghouse Engineering Report, EC-401, NOBS N00024-67-C-5494, May, 1969.

31. Hidemi Gotoda, "An Analysis on Resonant Stress and Damping in Turbine Blades," Turbine Designing Department, Kawasaki Heavy Industries, Ltd., Kobe, Japan, 1974.

32. N. F. Rieger, "Damping Properties of Steam Turbine Blades," Proceedings WPAFB Materials Laboratory, Vibration Damping Workshop, Queen Mary Hilton, Long Beach, CA, Feb. 1984.

33. A. Wilkinson, Publications on Assessment of Material Damping, Jnl. of Strain Technology, Texas A&M University, Dept. of Mech. Eng., College Station, TX, 1984.

34. D.I.G. Jones, A. Muszynska, "Vibrations of a Compressor Blade with Slip at the Root," The Shock and Vibration Bulletin, Washington, DC, The Shock and Vibration Center, pp. 53-61, Sept. 1978.

35. D.I.G. Jones, A. Muszynska, "Design of Turbine Blades for Effective Slip Damping at High Rotational Speeds (U)," Reprinted from The Shock and Vibration Bulletin, Part 2, Washington, DC, The Shock and Vibration Information Center, pp. 87-96, Sept., 1979.

36. A. Muszynska, D.I.G. Jones, "On Discrete Modelisations of Response of Blades with Slip and Hysteretic Damping," Proceedings of the Fifth World Congress on Theory of Machines and Mechanisms, ASME, pp. 646-649, 1979.

37. A. V. Srinivasan, D. G. Cutts, and S. Sridhar, "Turbojet Engine Blade Damping," United Technologies Report No. R. 81-91441031, Submitted to NASA (Report No. CR 165406), July 1981.

38. A. V. Srinivasan, Paper on Blade Damping Analysis, Proceedings WPAFB Materials Laboratory, Vibration Damping Workshop, Queen Mary Hilton, Long Beach, CA, Feb., 1984.

39. D. F. Socie, J. D. Morrow, "Review of Contemporary Approaches to Fatigue Damage Analysis,", Chpt. 8, Risk and Failure Analysis for Improved Performance and Reliability, Edited by John J. Burke and Volker Weiss, Plenum Publishing Corporation, 1980.

40. D. F. Socie, "Fatigue Life Prediction Using Local Stress-Strain Concepts," Paper Presented at 1975 SESA Spring Meeting, Chicago, IL, May, 1975.

41. N. E. Dowling, W. R. Brose, and W. K. Wilson, "Notched Member Fatigue Life Predictions by the Local Strain Approach," Fatigue Under Complex Loading: Analyses and Experiments, SAE, Vol. 6, 1977.

42. SAE Cumulative Fatigue Damage Test Program, Fatigue Under Complex Loading: Analysis and Experiments, R. M. Wetzel, Editor, SAE Publ., 1977.

43. M. A. Miner, "Cumulative Damage in Fatigue," Trans. ASME, Series E, Jnl. Appl. Mech., 67:A159-A164, 1945.

44. J. M. Morrow, "Laboratory Simulation of the Low Cycle Fatigue Behavior of the Hook Region of a Steam Turbine Blade Subjected to Start Stop Cycles," ASME Proceedings, Fourth National Congress on Pressure Vessel and Piping Technology, Portland, Oregon, June, 1983.

45. S. S. Manson, A. J. Nachtigall, C. R. Ensign, and J. C. Freche, "Further Investigation of a Relation for Cumulative Fatigue Damage in Bending," Trans. ASME, Series B, Jnl. Eng. Ind., 87:25-35, 1965.

46. J. B. Conway, R. H. Stentz, J. T.

Berling, "Cumulative Damage Concepts," Chapter 5, Fatigue, Tensile, and Relaxation Behavior of Stainless Steel, TID-26135 U.S. Atomic Energy Commission, Technical Information Center, Oak Ridge, TN, 1974. (Also Mar-Test, Inc., Cincinnati, OH).

47. H. J. Grover, "An Observation Concerning the Cycle Ratio in Cumulative Damage," Fatigue in Aircraft Structures, ASTM, Special Publication No. 274, pp. 120-124, 1960.

48. S. S. Manson, "Interfaces Between Fatigue, Creep, and Fracture," Proceedings of the International Conference on Fracture, Sendai, Japan, Sept. 14, 1965; also Int. J. Fracture Mech., 2(1): 327, March, 1966.

49. S. S. Manson, J. C. Freche, and C. R. Ensign, "Application of a Double Linear Damage Rule to Cumulative Fatigue," ASTM, Special Technical Publication No. 415, p. 384, 1967.

50. A. Battacharya, "Cumulative Damage of Carbon Steel Specimens in Tension-Impact Fatigue," Ph.D. Thesis, Banaras Hindu University, Varanasi, India, 1984.

51. J. Dubec, B. Q. Thang, A. Bazergui, and A. Biron, "Unified Theory of Cumulative Damage in Metal Fatigue," Weld. Res. Counc. Bull., No. 162, June, 1971.

52. F. R. Shanley, "A Theory of Fatigue Based on Unbounding During Reversed Slip," The Rand Corp., Report P-350, 1953.

53. S. R. Valluri, "A Unified Engineering Theory of High Stress Level Fatigue," Aerosp. Eng., 20L 18-19, 68-89, 1961.

54. R. R. Gatts, "Application of Cumulative Damage Concept to Fatigue," Trans., ASME, Series D, Jnl. Basic Eng., 83: 529-540, 1961.

55. J. Sohre, "Steam Turbine Blade Failures, Causes and Correction," Proceedings, Texas A&M Fourth Turbomachinery Symposium, College Station, TX, 1974.

56. J. Montoya, "Coupled Bending and Torsional Vibrations in a Twisted Rotating Blade," The Brown Boveri Review, Col. 53, No. 3, pp. 216-230, March, 1966.

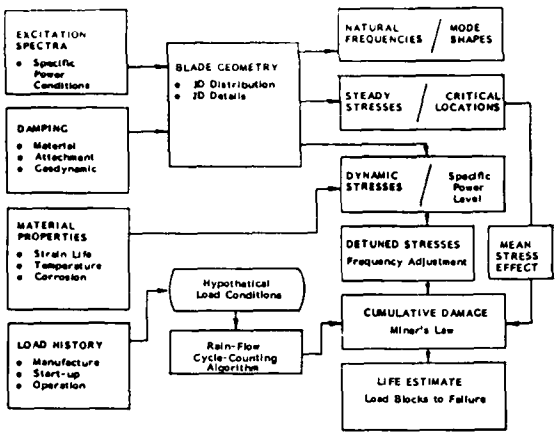

Fig. 1 Interrelationship Between Factors Influencing the Fatigue Life of Turbine Blades

Fig. 2 High-Pressure Steam Turbine Blade

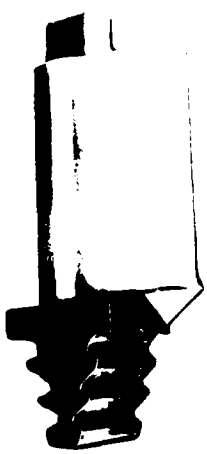

Fig. 3 Intermediate Pressure Steam Turbine Blade

Fig. 4 Low-Pressure Steam Turbine Blade

Fig. 5 High-Pressure Steam Turbine Blade

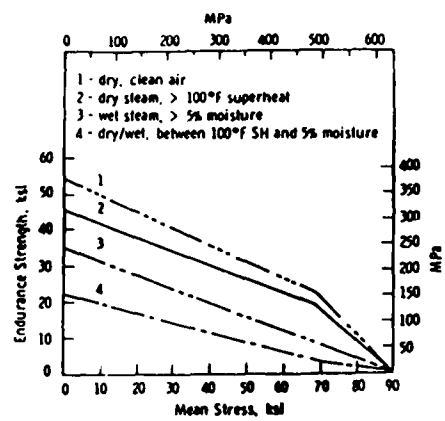

Fig. 6 Goodman Diagram for ASM 403 Stainless Steel. Sohre [55]

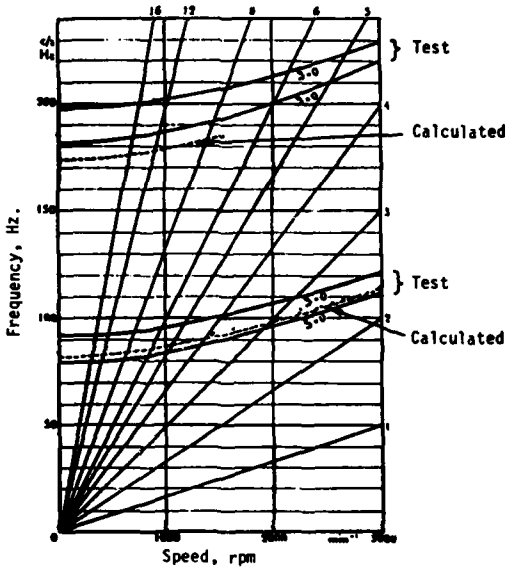

Fig. 7 Campbell Diagram for Free-Standing Low-Pressure Blade. Montoya [56]

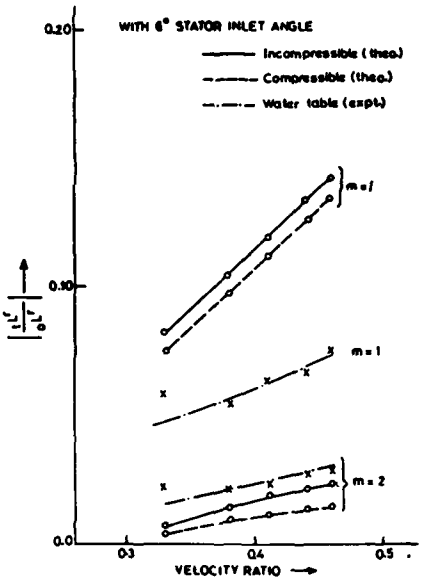

Fig. 10 Comparison of Calculated Results and Test Data for Non-Steady Left on Turbine Blade (shallow camber). Rao et al [16]

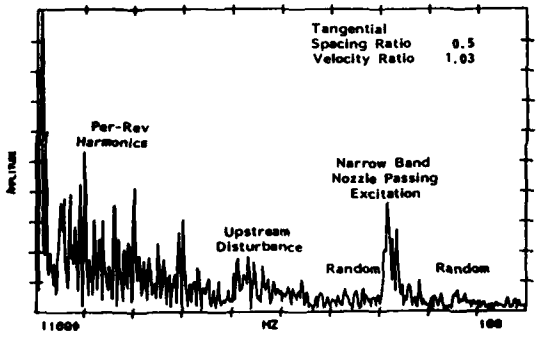

Fig. 8 Excitation Spectrum. Non-Steady Tangential Force vs. Frequency. Tangential Direction. Water Table Test Data. Rieger [28]

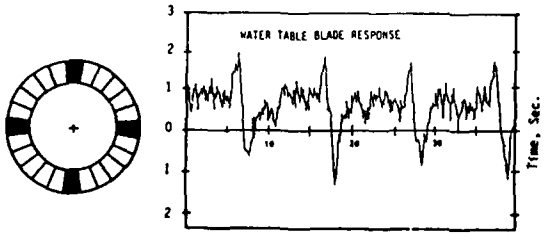

Fig. 9 Partial Admission Transient Loading. Tangential Direction. Water Table Test Data. Rieger [4]

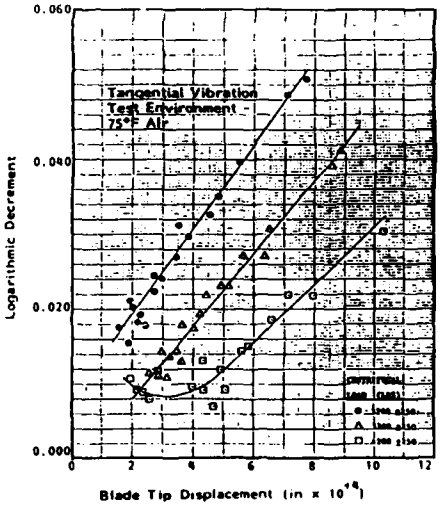

Fig. 11 Damping Log. Dec. vs. Tip Displacement for Turbine Blade. ASM 403 Stainless Steel. Tangential Vibration. Air 75°F

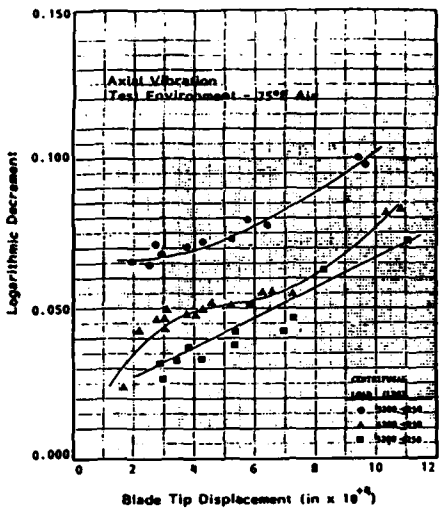

Fig. 12 Damping Log. Dec. vs. Tip Displacement for Turbine Blade. ASM 403 SS. Axial Vibration. Air 75°F

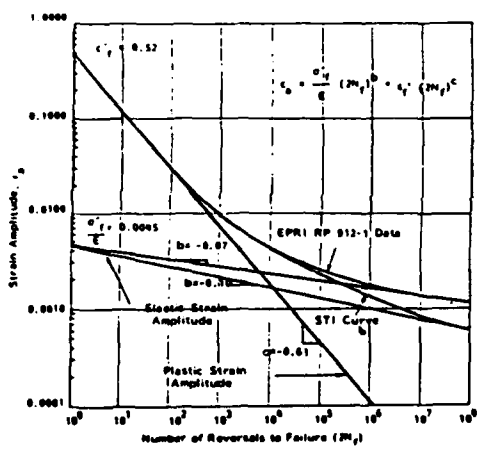

Fig. 13 Strain Life vs. Number of Cycles for ASM 403 SS

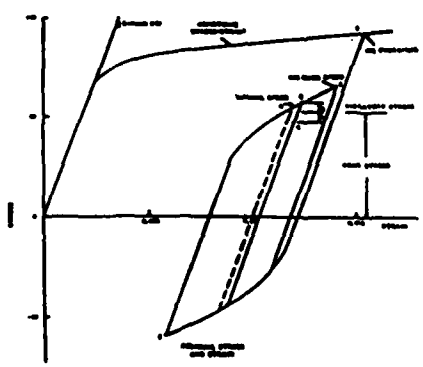

Fig. 14 True Stress vs. True Strain for ASM 403 SS

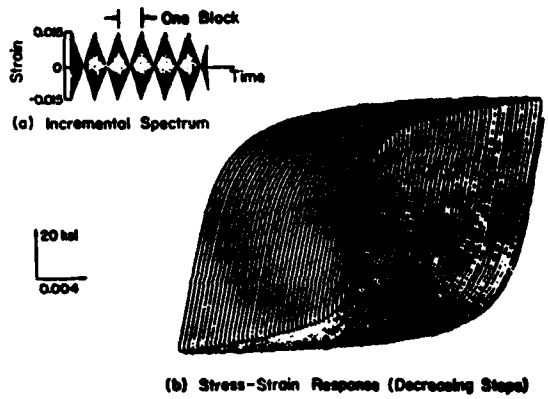

Fig. 15 Development of Cyclic Stress-Strain Curve, Socie and Morrow [39]

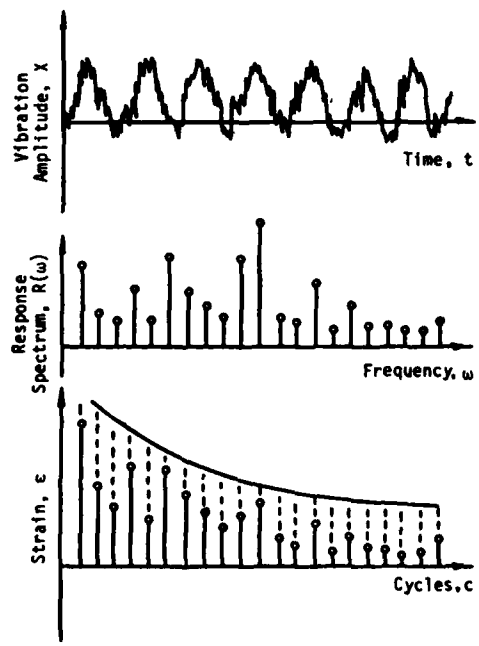

Fig. 16 Development of Cumulative Damage from Multi-Component Blade Response

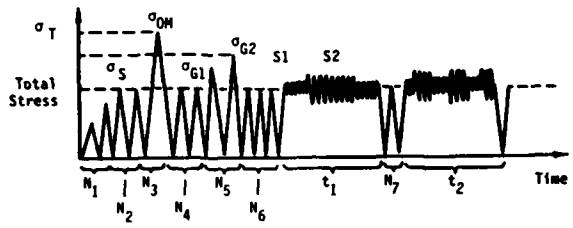

σ_T	Total Stress	N_1	Preliminary, Balancing Runs
σ_{OM}	Overspeed max.	N_2	Full Speed Balancing
σ_{G1}	Governor Overspeed 1	N_3	Max. Overspeed
σ_{G2}	Governor Overspeed 2	N_4	Trim Balance, Installation
S_1	Spectrum 1	N_5	Governor Settings
S_2	Spectrum 2, etc.	N_6	Process Trials
t_1	Time, Process Run 1	N_7	Start-up Checkouts
t_2	Time, Process Run 2		

Fig. 17 Typical Loading History for Blade Application

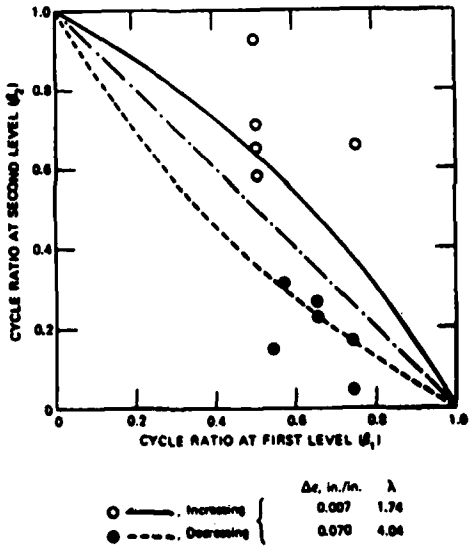

Fig. 18 Double Linear-Damage Concept. Conway et al [46]

Table 1 Material Properties of ASM 403 SS at 635°F. Morrow [44]

Elastic Modulus, E, ksi	28,000
Fatigue Strength Coefficient Exponent σ'_f ksi	131.0
Fatigue Strength Exponent, b	-.083
Fatigue Ductility Coefficient ε'_f	0.381
Fatigue Ductility Exponent, c	-.58
Cyclic Strength Coefficient, K', ksi	151.0
Cyclic Strain Hardening Exponent n'	0.143

Table 2 Estimates of Accuracy to Which Various Fatigue Parameters are Known

Steady Stress σ_S	Damping Log. Dec. δ	Excitation $\Delta F/F$ $S(\omega)$	Dynamic Magnifier $A(\omega)$	Assembly Tolerance G	Strain Life $\Delta\varepsilon$	Miner's Law Sum $\sum(n_i/N_i)$	Load History H(t)	Life Variation Estimate L_B
$\frac{1.01}{1.05}$	$\frac{1.10}{1.50}$	$\frac{1.30}{1.70}$	$\frac{1.02}{1.05}$	$\frac{1.05}{1.25}$	$\frac{1.05}{1.15}$	$\frac{1.10}{1.15}$	$\frac{1.00}{1.50}$	$\frac{1.786}{9.093}$

DISCUSSION

Mr. Huang (University of Wisconsin): Is the computational accuracy of the finite element method 1%?

Mr. Rieger: I think I said we can measure the geometry to within 1%.

Mr. Huang: Not the finite element method?

Mr. Rieger: Not the finite element method. I think I said 10% to 20% for three dimensional calculations using the BLADE code, and 2% to 5% for two dimensional calculations based on the three dimensional results. That is the computational accuracy.

Mr. Huang: Then the finite element method is not that accurate.

Mr. Rieger: Not to 1%, no. I think most of us can measure to 1% or to less than 1%. But the accuracy of the calculations using the code depends on whether a two-dimensional calculation backing up a three-dimensional calculation is accurate to 2% to 5% on stress.

SPIN PIT TEST OF BLADED DISK WITH BLADE PLATFORM FRICTION DAMPERS

R. J. Dominic
University of Dayton
Research Institute
Dayton, Ohio

A turbine blade friction damping study, involving both analytical and experimental evaluations, has been performed for a high speed bladed disk of the high pressure fuel turbopump of the space shuttle main engine. The results of the analytical study were presented last year at the 54th Shock and Vibration Symposium [1]. The recently completed experimental study involved spin pit testing of an instrumented bladed disk assembly. The study was performed to evaluate the effectiveness and operational characteristics of blade platform friction dampers designed to limit damaging resonance vibrations of the turbine blades in their lower order flexural vibration modes. The test program will be described and the test results will be presented. A brief comparison will be made between the results of the analytical and experimental studies. This program was funded by Marshall Space Flight Center of NASA at Huntsville, Alabama.

INTRODUCTION

An analytical and test evaluation were conducted to determine the performance of turbine blade platform friction dampers used to control the lower order flexural modes of a blade. The configuration used in the study was the first stage turbine of the high pressure fuel turbopump (HPFTP) of the space shuttle main engine (SSME) as shown in Fig. 1. The analytical study used the lumped parameter method developed by Jones and Muszynska [2] as implemented on a VAX 11/780 computer. It showed that the primary parameters affecting the friction damper performance are: the damper-blade coefficient of friction; the normal force applied to the friction interface; the amplitude of the periodic forcing function; the relative phase angle between the excitation forces for adjacent blades bridged by a damper (effectively, the engine order of the forcing function); and the amount of hysteretic damping that acts to limit the vibration amplitude of the blade in its resonance modes. In addition, the analytical study showed that over-damping of the blade, resulting in fixity at the platform and a consequent lightly-damped flexural resonance mode of the blade airfoil section alone, is likely to occur in a high-speed turbine such as the HPFTP because of the high normal force applied to the friction interface by the centrifugal force acting on the damper. A test study was performed in a high speed spin pit to evaluate the low order flexural resonance vibration modes of HPFTP blades without dampers, with production dampers, and with two types of lightweight experimental dampers. The test program results agreed with the results of the analytical study in that blades fitted with production friction dampers experienced the airfoil-alone flexural resonance mode, while those without dampers or with lighter weight dampers did not. Likewise, no blades fitted with dampers experienced the whole blade flexural resonance mode during high speed tests, while those without dampers did.

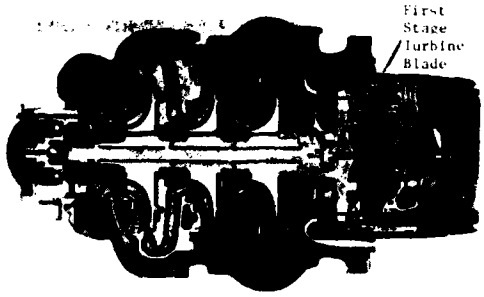

Fig. 1 Section, SSME High Pressure Fuel Turbopump

BACKGROUND

Three catastrophic failures of HPFTP first stage turbine blades occurred during test stand runs early in the SSME development program. These failures were attributed to lockup of the platforms of adjacent blades, in one case due to welding of the underplatform friction dampers to the platforms because of overtemperaure conditions during the run, in another case due to extrusion of a nickleplate antifriction coating on the dampers into the interplatform gap, and in a third case due to an out of tolerance build that reduced or eliminated the interplatform gap for some blades in the stage. The mechanism of the failures was determined to be high cycle fatigue caused by excessive vibration of the blades. Failures occurred near the base of the airfoil section of the blades, just above the platform. Fig. 2 shows two of the subject blades and the friction dampers

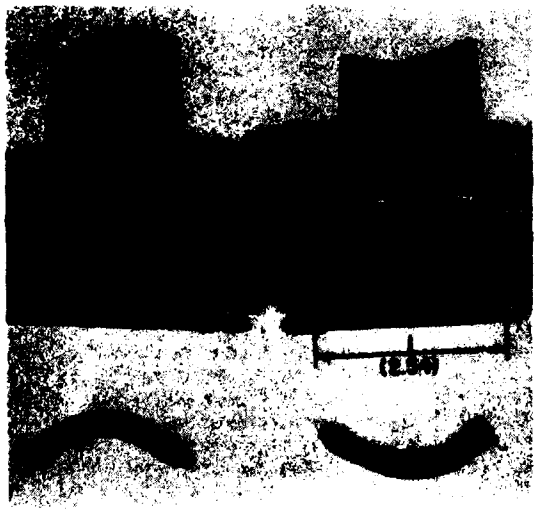

Fig. 2 HPFTP 1st Stage Blades and Dampers

that are placed in slots below the platforms and act on the bottom surface of the platforms to reduce the flexural vibrations of the blades through the dissipation of energy by friction heating. During pump operation the dampers also act to limit the eakage of cooling hydrogen, which is routed over the blade roots, into the turbine drive fluid stream. The dampers are forced against the under surface of the platforms by a combination of centrifugal force and the differential pressure between the cooling hydrogen and the turbine drive fluid.

The 63 blade turbine wheel is fed by 41 first stage nozzles. Thirteen shaft front bearing support struts are aligned with 13 of the nozzles in a necessarily unsymmetrical arrangement with 11 struts spaced three nozzles apart and two struts spaced four nozzles apart. Pressure pulses caused by the wakes off the nozzles, and particularly the higher amplitude pulses for the nozzles aligned with struts, excite vibrations in the blades that cause the high cycle fatigue problems. The repetition frequencies for these pulses are 10-1/4 per rev for the two struts spaced four nozzles apart, 13-2/3 per rev for the eleven struts spaced three nozzles apart, and 41 per rev for the symmetrically spaced nozzles. Sum and difference frequencies of these excitation components and their harmonics occur also to provide wide band excitation of the blades. The 13-2/3 per rev (14E) excitation of the blades is shown later to be a critical excitation frequency in the operating regime of the blades.

The nature of the blade fatigue failures caused them to be attributed to flexural resonance modes of the blades. Modal studies of the blades showed that the first two bending modes of the blade occurred at approximately 4,500 and 18,000 Hz. Later, during a whirligig spin test program [3] conducted by Rocketdyne, a resonance condition near 8,500 Hz was found. This resonance condition was first described as the first torsional mode of the blade (which actually occurs at approximately 11,000 Hz), but it was later identified by the University of Dayton Research Institute (UDRI) as the first flexural mode of the airfoil section of the blade when the platform is constrained from motion. The 14E excitation pulses occur at this airfoil-alone flexural resonance frequency of the blade during the long (relatively) time periods of engine operation at RPL.

As a result of the early studies the strut contour was changed to reduce the energy in the excitation pulses and the platform friction damper weight was reduced to provide more optimum damping. However, fatigue cracking continued to occur near the airfoil root with the platform at much lower than the specified and predicted life for the blade. Subsequently, UDRI contracted with NASA to evaluate the operation of the blade-damper system analytically, using the lumped parameter analysis, and to evaluate the operation of a test system in a high speed spin pit.

TEST EVALUATION IN THE SPIN PIT

A vibration test evaluation of a simulated HPFTP first stage bladed disk was conducted in a high speed spin pit. For purposes of test, a used set of blades and dampers was furnished by NASA and a titanium disk and two types of experimental dampers were fabricated. Blade vibration responses were measured with strain gages as the blades were excited magnetically during high speed spins in vacuum.

Twelve blades were instrumented with 1/16 inch square strain gages on the suction side of the airfoil. The gages were centered 1/4 inch above the platform and 1/8 inch from the trailing edge, a high stress region of the blade. Leadwires were routed down the aft face of the blade through a slot cut in the platform to terminals on the aft face of the firtree area. A photograph of a strain gage installation is shown in Fig. 3.

Fig. 3 HPFTP Strain Gaged Blade

The blades were installed in a test disk fabricated from a forged and heat-treated 6A14V titanium blank. The firtree slots in the disk were cut by computer controlled wire EDM, which achieved production tolerance of the slot configuration and of the blade to disk firtree fit. The test disk was fabricated with 64 slots in order that a symmetrical test specimen configuration could be obtained.

In addition to the disk, two types of lightweight experimental platform friction dampers wee fabricated. These dampers were formed of nichrome wire on bending jigs designed for the purpose. Fig. 4 shows the production 0.56 gram dampers and the experimental 0.20 gram and 0.10 gram dampers.

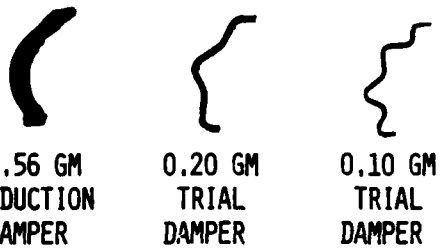

Fig. 4 Test Dampers

After 0.5 gram magnetic cobalt weld beads were added to the blade tips, the blades were tested in a broach block to identify the first flexural and first torsional mode resonance frequencies of each blade. They were subsequently x-rayed to verify the adequacy of the welds and the absence of serious cracks. They then were weighed and were installed in the test disk in the scheme shown in Fig. 5. As shown, eight groups of eight blades were installed in test octants consisting of oppositely balanced octants of each of the three test damper types and two opposite groups of blades without dampers. Two primary strain gaged blades and one spare gaged blade were included for each configuration type. In addition, two gages were installed to measure radial strain on the test disk. The blade strain gages were connected to leadwire pairs on the disk with jumpers over the firtree gap.

The bladed disk was installed to an arbor assembly and the strain gage leadwires were routed from terminals on the disk up through the hollow arbor shaft. The disk-arbor assembly was

precision dynamically balanced and then was installed in the spin pit test assembly shown in Fig. 6. The strain gage leads were routed from the arbor shaft through the quill shaft to the high speed slip ring on top of the spin assembly. They then were routed through strain signal amplifiers to an FM recorder. Two channels were always monitored by an oscilloscope and a frequency analyzer.

Octant	Damper Type
1,5	None
2,6	0.56 gram production
3,7	0.10 gram wire
4,8	0.20 gram wire

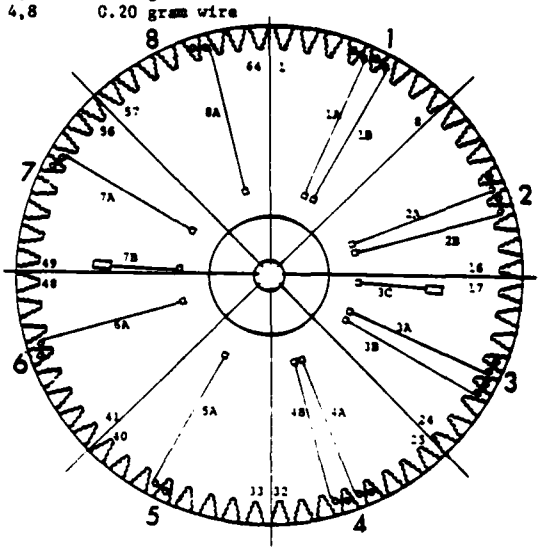

Fig. 5 Test Disk Layout

As shown in Fig. 6, the blades were excited by radially mounted samarium cobalt permanent magnets that were spaced symmetrically around the disk with an at-rest gap of 0.12 inch between the magnets and the cobalt weld beads on the blade tips. The magnet support fixture was provided with 28 magnet mounts and tests were conducted with both 28 and 14 magnets installed, providing 28E or 14E excitation of the bladed disk for two series of test runs. Whether 28 or 14 magnets were installed, adjacent magnets were always installed with opposite polarity, i.e. if a magnet had its north magnet pole facing the blade tips the magnets on either side had their south magnet pole facing the blade tips. The blades were excited primarily by the magnet drag pulses as the blade tips passed through the fields of the permanent magnets. A photograph of the spin pit test setup with 14 magnets installed is shown in Fig. 7.

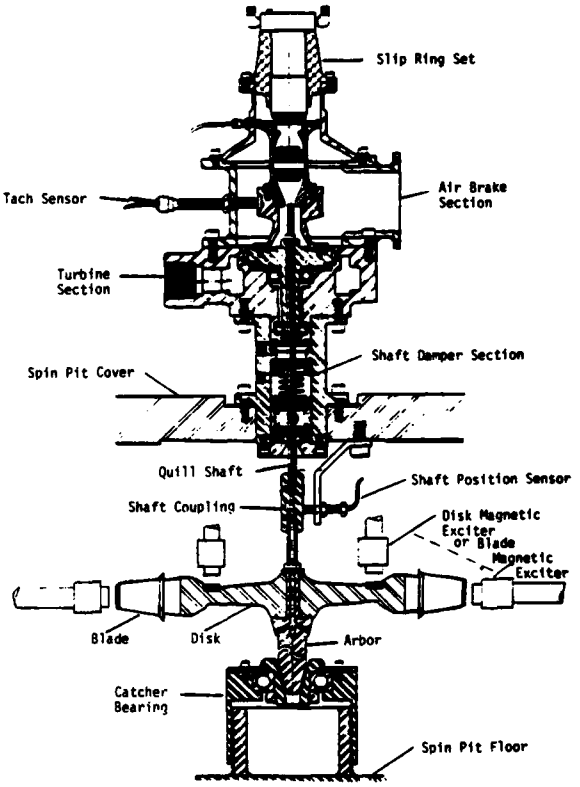

Fig. 6 Spin Test Assembly

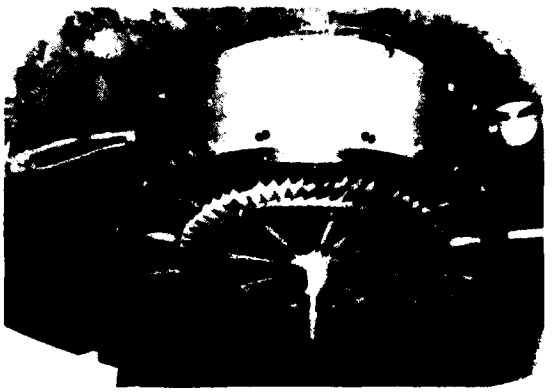

Fig. 7 Spin Test Set-up

The test assembly was always spun in a vacuum that ranged from 2.5 to 3.0 torr for various test spins. In early testing, high whirl modes of the test assembly were encountered but these were reduced to tolerable levels by redesigning the arbor to quill shaft coupling. The first spin test was conducted with 28 excitation magnets installed. It was expected that this 28E excitation would induce the first flexural resonance mode of the blades

(4,800 Hz was the mean frequency for 64 blades hard clamped in the broach block) at about 10,000 rpm and that the 8,500 Hz airfoil-alone first flexural mode might occur near 18,000 rpm, at least on the blades with the heaviest (production 0.56 gram) dampers since frequency increases linearly with rpm and normal force of the dampers increases with the square of the rpm.

The first test spin covered the range from 0 to 23,000 rpm. The only significant test data from this spin are shown in Fig. 8, 9, 10 and 11.

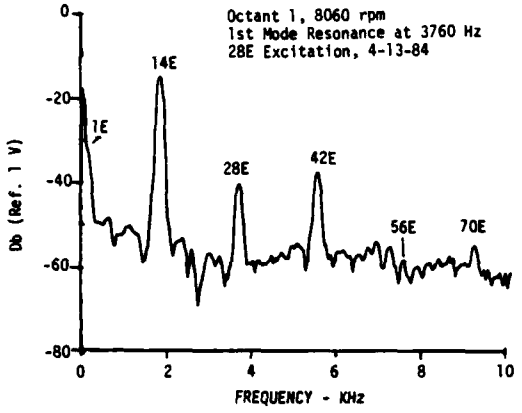

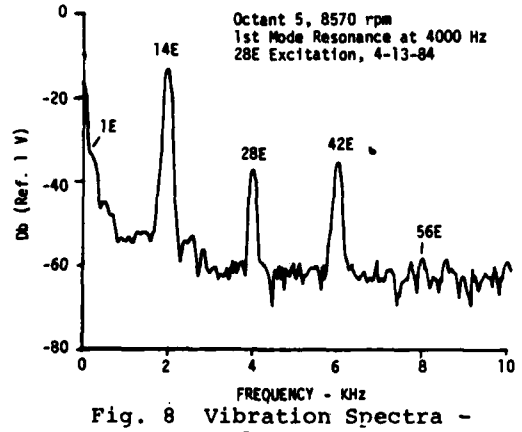

Fig. 8 Vibration Spectra - Undamped Blades

First flexural resonance vibration of all the monitored test blades is shown clearly at the 28E excitation frequency. The peaks at 14E and 42E are due to magnetically induced EMF in the strain circuits and the 1E peak and its harmonics are due to one-per-rev unbalance-induced strain and to EMF generated by the whirl mode shaft displacement. The signal noise floor is caused by sum and difference frequencies of the one-per-rev signal and its harmonics with the other major signal components.

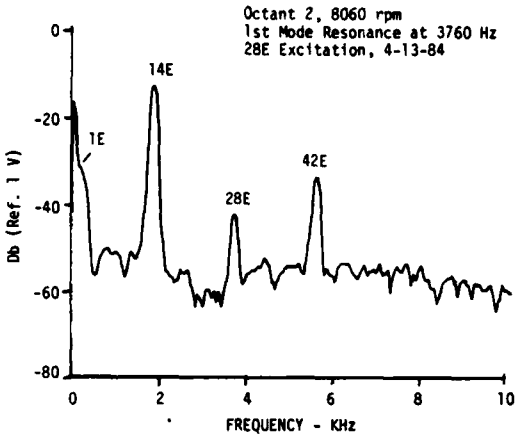

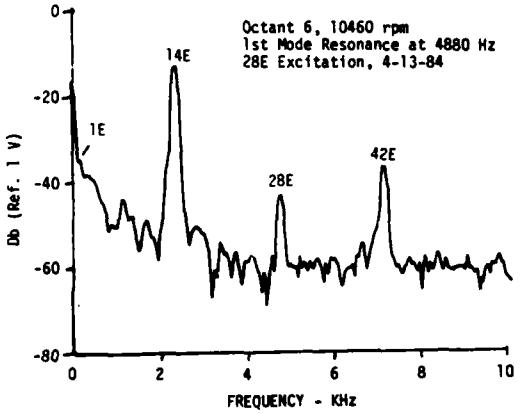

Fig. 9 Vibration Spectra-Production 0.56 Gram Dampers

By contrast, Fig. 12 shows strain gage signals for 28E and 14E excitation spins when no blade resonance vibration is occurring.

The significant factors shown by the low speed spin data of Fig. 8 through 11 are that the blade first flexural mode resonance occurred at lower than expected frequencies for all four test configurations and that no airfoil-alone resonances occurred for any of the instrumented blades. The first torsional mode resonance was found for two blades near 10,700 Hz at a rotational speed near 23,000 rpm, but at a relatively low amplitude. The surprisingly low first flexural mode blade resonance frequencies found during this spin test are attributed to a relatively soft cantilever mount condition of the blades at the firtree root for this low speed spin condition.

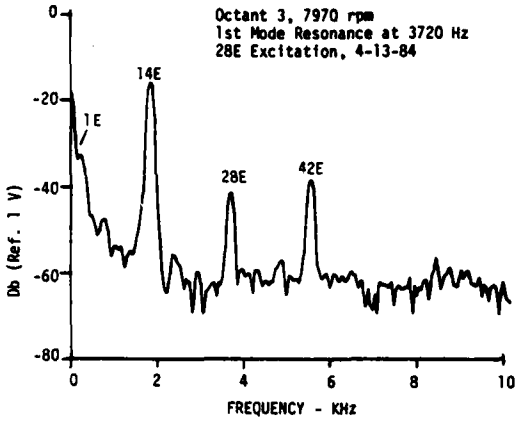

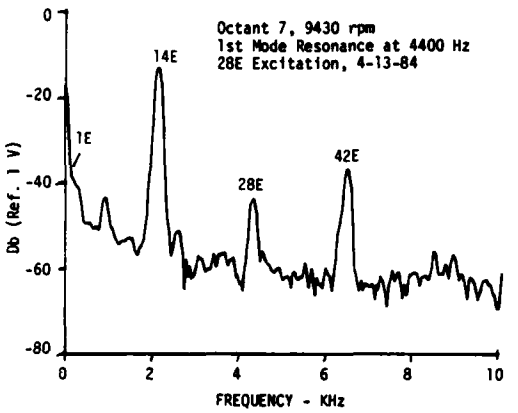

Fig. 10 Vibration Spectra-Experimental 0.10 Gram Dampers

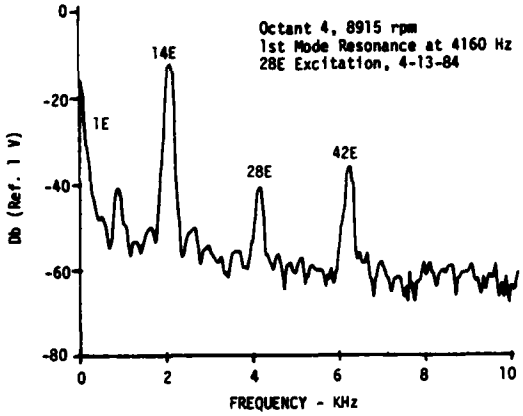

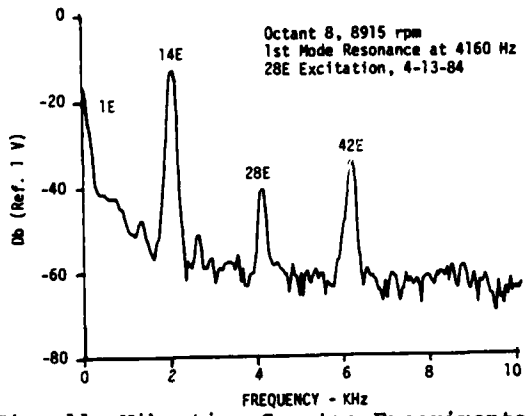

Fig. 11 Vibration Spectra-Experimental 0.20 Gram Dampers

After the magnets were configured for 14E excitation, a high speed spin test to 38,000 rpm was performed. The only significant blade resonance vibrations found during this test are shown in Fig. 13 and 14. Fig. 13 shows the first flexural mode vibration of the whole blade for the blades with no friction dampers and Fig. 14 shows the airfoil-alone flexural resonance mode for blades with production 0.56 gram dampers. Neither mode was found for the blades with lightweight experimental dampers indicating vibrations of these blades occurred at very low amplitude in the transitional region between the two resonance modes. The lightweight friction dampers obviously worked very well at the excitation force levels produced by the permanent magnets. Conversely, the production 0.56 gram dampers caused an airfoil-alone resonance vibration strain signal in test octant 6 that was more than 6 dB higher, or double the strain amplitude, than any of the resonance vibrations that occurred in the undamped blades or in any of the blades in the whole blade first flexural resonance mode.

The resonance vibrations shown for undamped blades in Fig. 13 again occurred at a lower than expected frequency but at a higher frequency than in the low speed spin test. This shows a still soft but hardening root fixity at the firtree. The airfoil-alone flexural resonance modes shown in Fig. 14 also occurred at a lower than expected frequency. This is attributed to the 0.5 gram magnetic cobalt weld bead masses added to the blade tips and to the belief that the maximum response at the center frequency of this resonant mode was not reached before the strain gage circuits failed.

The following conclusions are drawn from the test program.

1. Low speed spin conditions are not adequate to seat the blades and dampers firmly enough to produce

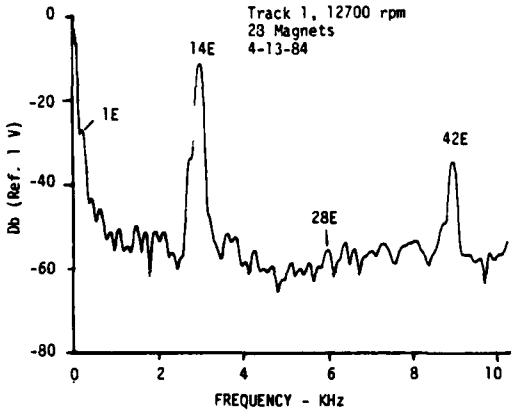

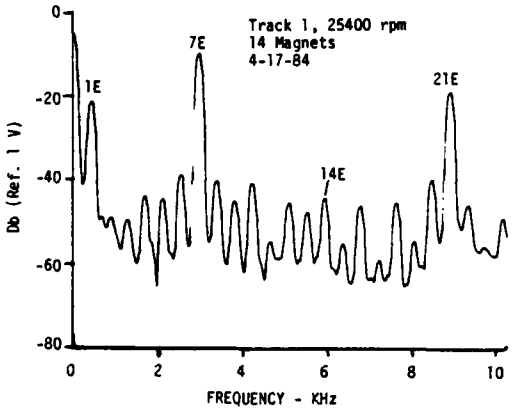

Fig. 12 Octant 1 Frequency Spectra-No Resonance

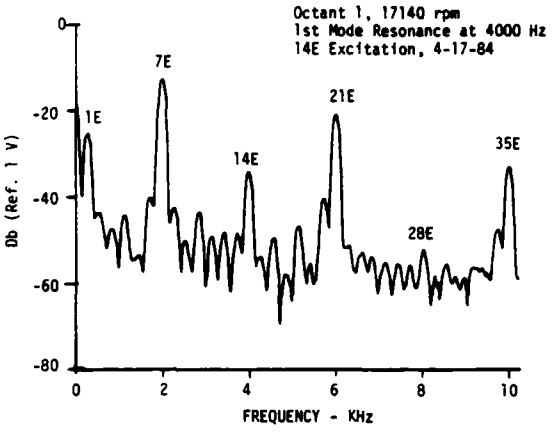

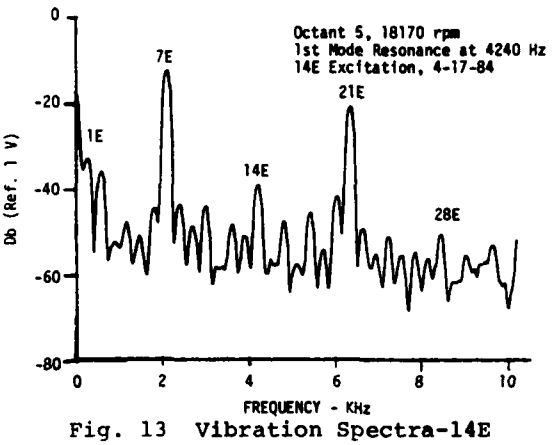

Fig. 13 Vibration Spectra-14E Excitation of Undamped Blades

data related to conditions during operational speeds of the HPFTP.

2. The production 0.56 gram dampers did constrain the platforms at operational spin speed and caused airfoil-alone first flexural mode resonance vibration, probably at a lower response amplitude than that which occurs during operational conditions at the 14E excitation frequency that is known to occur in the HPFTP at operational speed.

3. Lightweight experimental dampers eliminated both lower order flexural modes of the blade for the excitation level that occurred in the test.

4. The test data confirmed the results of the analytical study as shown generally in Figures 15 and 16. In these two figures: S is the excitation force; η_1 and η_2 are the hysteretic damping in the outboard and inboard sections of the blade, respectively; μ is the coefficient of friction for the coulomb damping force, N is the normal force on the damper to platform friction surface; and θ is the phase angle between the forces applied to adjacent blades bridged by a damper. Examination of these two figures shows that as the platform is restricted by greatly increasing friction force opposing platform motion, due to the effect of increase in the normal force (N), the reponse of the blade changes from the whole blade flexural mode at 4500 Hz to the airfoil alone flexural mode at 8500 Hz. Studies of the effects of interactions of the various blade system parameters are presented in [1] and in [4]. More complete details of the analysis and test programs are presented in [5] and additional background information is presented in [6], [7] and [8].

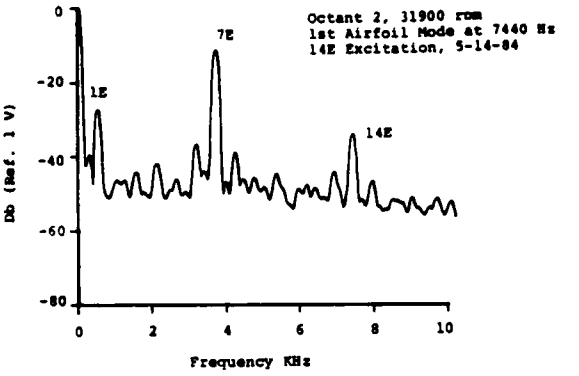

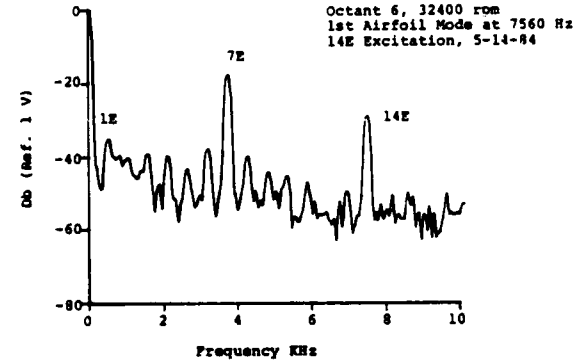

Fig. 14 Vibration Spectra-Airfoil Flex Mode-Production 0.56 Gram Dampers

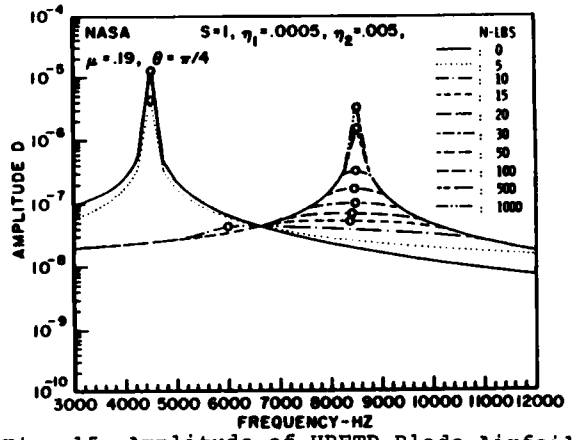

Fig. 15 Amplitude of HPFTP Blade Airfoil Mass VS Frequency of Excitation

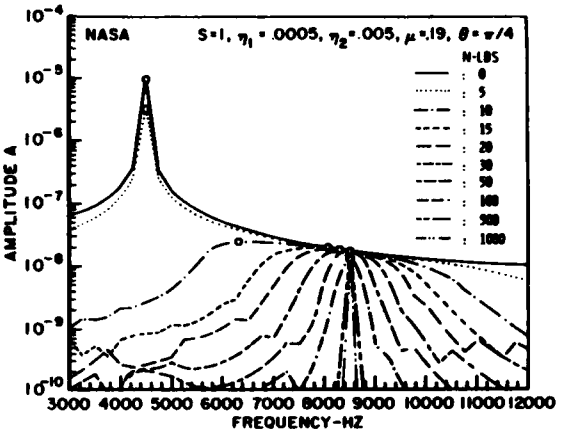

Fig. 16 Amplitude of HPFTP Blade Platform VS Frequency of Excitation

ACHNOWLEDGEMENT

This work was performed for Marshall Space Flight Center (MSFC) of NASA under Contract NAS8-34682. Mr. Larry Kiefling, the project technical monitor, of the Structural Dynamics Division of MSFC, was very helpful in providing data and guidance for the work.

REFERENCES

1. R.J. Dominic, "The Analysis by the Lumped Parameter Method of Blade Platform Friction Dampers Used in the High Pressure Fuel Turbopump of the Space Shuttle Main Engine," Shock and Vibration Bulletin, Vol. 54, May 1984.

2. A. Muszynska, D.I.G. Jones, T. Lagnese, and L. Whitford, "On Nonlinear Response of Multiple Blade Systems," Shock and Vibration Bulletin Vol. 51, No. 3 May 1981.

3. R.F. Sutton, "NASA, High Speed Rotating Diagnostic Laboratory Testing, SSME High-pressure Fuel Turbopump Blade/Damper Evaluation," Rocketdyne Division of Rockwell International Rept. RSS-8626, Nov. 1978.

4. R.J. Dominic, "Parametric Study of Turbine Blade Platform Friction Damping Using the Lumped Parameter Analysis," ASME Paper 84-GT-109, 1984.

5. R.J. Dominic, "Turbine Blade Damping Study," University of Dayton Research Institute Rept. UDR-TR-84-87, Nov. 1984.

6. E.O. Dickerson, "Turbine Blade Structural Dynamic Analysis," AIAA Paper 80-0782, 1980.

7. L.P. Scott, J.E. Pond, C.C. Myers, G.A. Teal, G.F. Lewis and J.K. Robinson, "Assessment of HPFTP Turbine Blade Environment and Fatigue Life Study on the SSME, Volumes I and II," Lockheed Missiles and Space Company, Inc., Huntsville Research and Engineering Center Rept. LMSC-HREC TR D784198, May 1981.

8. R.J. Dominic, P.A. Graf and B.B. Raju, "Analytical and Experimental Investigation of Turbine Blade Damping - Final Report," University of Dayton Research Institute Rept. UDR-TR-82-39, (AD-A120470, AFOSR-82-0911TR, or NTIS HC A04/MF A01), Aug 1982.

DISCUSSION

Mr. Belcher (General Motors - Allison Gas Turbine Div.): You said the turbo pump for the Space Shuttle engine, or the engine itself, was throttleable from approximately 65% to 109% rated power level. Will this correlate with a range of turbo pump speeds to supply the fuel for that?

Mr. Dominic: Yes. The range of turbo pump speeds to cover that power output level of the rocket engine is about 28,000 to 38,000 rpm. While I am here, I would like to say I did not really summarize that paper. The study did show the lighter weight dampers will avoid the "air foil alone" resonance mode. We would recommend they change from a super alloy damper material to beryllium since there are already a number of beryllium parts in that engine.

Mr. Belcher: Did you test in a spin facility at room temperature?

Mr. Dominic: At room temperature and in a vacuum.

Mr. Belcher: Did you make any kind of a temperature correction calculation to take into account the operating environment in the turbo pump?

Mr. Dominic: No.

Mr. Belcher: In the frequency data you presented, did you come up with fairly consistent first bending and torsional modes for that blade with the two speeds you were using; the two magnet configurations?

Mr. Dominic: We never got to the speed that would represent the first torsional mode at the high speed run condition. That would have been very much of an over-speed condition for that turbine disk.

Mr. Belcher: With the configuration where you drove the free platform fundamental mode of the blade, did you see fairly close frequencies in the two speed ranges?

Mr. Dominic: They were fairly close, but it was obvious during the higher speed run, where we only used half as many magnets, all of the first bending mode frequencies were 200 to 300 Hz higher. We attributed that to the increased lock-up in the "fir tree" giving closer to an ideal cantilever condition at the root.

Mr. Belcher: Was that in addition to speed stiffening effects on the blade itself?

Mr. Dominic: Possibly. But, we think it was really more of a root effect than the speed stiffening effect.

Mr. Belcher: Do you think the modes you were trying to test for would have been present in the operating range as a function of that differential order of the upstream struts rather than the downstream vanes?

Mr. Dominic: Obviously, that mode causes the high cycle fatigue failure in that blade right above the platform, and also the 13 2/3 or 14 E excitation mode occurs at the rated power level of the engine. That engine runs about eight and a half minutes during each launch, and it runs at rated power level 95% of the time. The only throttleable portion of the engine operation is for acceleration control, primarly for injection into orbit at the end of the launch mode.

Mr. Belcher: Did you do any kind of a bench test, or a preliminary study, for locating the instrumentation on the blade?

Mr. Dominic: Rocketdyne collected a great deal of modal strain data, and they performed many finite element analyses of that blade. A blade was also extensively instrumented with strain gages for an acoustic test; the location we chose to monitor was the highest strain area of the blade.

A DIFFERENT VIEW OF VISCOUS DAMPING

P. J. Torvik
Department of Aeronautics and Astronautics
Air Force Institute of Technology
Wright-Patterson Air Force Base, Ohio

and

Major R. L. Bagley
4950th Test Wing
Aeronautical Systems Division
Wright-Patterson Air Force Base, Ohio

INTRODUCTION

The linear viscous damper, or dashpot, has proven to be an extremely useful concept in the modelling of vibrating systems. One usually justifies the inclusion of such elements in models of mechanical systems through the following argument: Consider two flat plates (or cylinders), parallel, infinite in extent, and separated by a distance h. Assume that the region between the two plates (or cylinders) is filled with a Newtonian fluid of viscosity μ. Assume that one plate (cylinder) is displaced parallel to the other at a speed V, or, in terms of a displacement coordinate, $\dot{x}$. Assume further that the resulting velocity distribution between the two plates (cylinders) in linear. Then, the average shear stress in the fluid is proportional to the average velocity gradient, or:

$$\sigma = \mu \frac{v}{h} \tag{1}$$

If A represents the wetted area of the moving plate (cylinder), then the resisting force on that surface is

$$F = A\sigma = A\mu \frac{v}{h} \tag{2}$$

From this we deduce the value of a dashpot constant to be

$$C = A\mu/h \tag{3}$$

ANALYSIS

Let us now consider a somewhat different problem, generated by relaxing three assumptions implicit in the foregoing: (1) that the viscous layer is thin, (2) that the velocity distribution is linear, and (3) that the inertia of the viscous fluid may be neglected. The configuration is now that of a moving plate, wetted on one side by a semi-finite domain of Newtonian fluid of density ρ. The velocity distribution in the fluid must satisfy the diffusion equation. After certain manipulations, it can be shown (see Appendix) that the stress at any point in the viscous fluid can be written in terms of a fractional derivative:

$$\sigma(z,t) = \sqrt{\mu\rho}\, \frac{d^{1/2} v(z,t)}{dt^{1/2}} = \sqrt{\mu\rho}\, D_t^{1/2}\{v\} \tag{4}$$

The force resisting the motion of the plate is again determined from

$$F = A\,\sigma \tag{5}$$

but is now of a very different form. Here, we find

$$F = A\,\sqrt{\mu\rho}\, D_t^{1/2}\{v(z,t)\} \tag{6}$$

We regard this development as being cogent to the explanation of the effectiveness of fractional derivatives in modelling real materials. Just as equation 1 has led to families of useful models constructed from Kelvin and Maxwell units, each built up from springs and dashpots, equation 6 suggests the development of models from elements involving fractional derivatives. Although equation 6 implies restoring forces proportional to the 3/2 derivative of displacement, we have found that fractional derivatives of orders near to 1/2 to be more promising. Nonetheless, the above argument demonstrates that the fractional derivatives are present in physical systems. With this established, the process of developing models may go forward with some degree of confidence.

It then becomes of interest to explore the nature of the response of systems containing such restoring forces. In particular, if a plate of

mass m and area A is suspended by a linear spring, k, and immersed in an infinite Newtonian fluid as above and subjected to a force F(t), the differential equation for the displacement x(t) is easily found to be:

$$m\ddot{x} + 2A\sqrt{\mu\rho}\, D^{3/2}\{x\} + kx = F(t) \qquad (7)$$

By first finding the response to an impulsive loading, $F(t) = \delta(t)$, the response to other external forces may be obtained by convolution. We will use Laplace transforms to solve for the impulse response. Taking the transform of the equation of motion leads to the transform of the impulse response, X(s).

$$\hat{X}(s) = (ms^2 + 2A\sqrt{\mu\rho}s^{3/2} + k)^{-1} \qquad (8)$$

Using theorems on the properties of Laplace transforms [2], we can immediately conclude that the inverse transform, $\hat{x}(t)$, is a real, continuous and causal function of time. Proceeding to calculate the inverse transform we need first to solve for the roots of the auxiliary equation

$$ms^2 + 2A\sqrt{\mu\rho}s^{3/2} + k = 0 \qquad (9)$$

or

$$m\lambda^4 + 2A\sqrt{\mu\rho}\lambda^3 + k = 0 \qquad (10)$$

where

$$\lambda = s^{1/2} \qquad (11)$$

The roots of this auxiliary equation are the poles of the transform of the impulse response. The expressions for the roots are

$$\lambda_{1,2} = \frac{-\beta\sqrt{\tilde{\omega}}}{2} + \frac{\sqrt{\tilde{\omega}}}{2}\sqrt{\beta^2+\cos\theta} \pm \frac{i\sqrt{\tilde{\omega}}}{2}\sqrt{\cos\theta - 2\beta^2\left(1-\frac{\beta}{\sqrt{\beta^2+\cos\theta}}\right)} \qquad (12)$$

and

$$\lambda_{3,4} = \frac{-\beta\sqrt{\tilde{\omega}}}{2} - \frac{\sqrt{\tilde{\omega}}}{2}\sqrt{\beta^2+\cos\theta} \pm \frac{i\sqrt{\tilde{\omega}}}{2}\sqrt{\cos\theta - 2\beta^2\left(1+\frac{\beta}{\sqrt{\beta^2+\cos\theta}}\right)} \qquad (13)$$

where

$$\tilde{\omega} \equiv \frac{4}{\sqrt{3}}\sqrt{\frac{k}{m}} \qquad (14)$$

$$\beta^2 \equiv \frac{A^2\mu\rho}{\tilde{\omega}\, m^2} \qquad (15)$$

and

$$\theta \equiv \frac{1}{3}\cos^{-1}(3\beta^2). \qquad (16)$$

When $3\beta^2$ is greater than one, θ is defined as

$$\theta \equiv \frac{1}{3}\cosh^{-1}(3\beta^2) \qquad (17)$$

and the $\cos\theta$ terms in (12 and (13) are replaced by $\cosh\theta$.

We are now in a position to evaluate the inverse transform of the response by contour integration [3] and the residue theorem from the calculus of a complex variable. The results are

$$\hat{x}(t) = A_1 e^{\lambda_1^2 t} + A_2 e^{\lambda_2^2 t} + \frac{1}{\pi}\int_0^\infty \frac{A\sqrt{2\mu\rho}\; e^{-rt}\; r^{3/2}}{A_3}\, dr \qquad (18)$$

where

$$A_1 = \frac{2\lambda_1}{m}\left[(\lambda_1-\lambda_2)(\lambda_1-\lambda_3)(\lambda_1-\lambda_4)\right]^{-1} \qquad (19)$$

$$A_2 = \frac{2\lambda_2}{m}\left[(\lambda_2-\lambda_1)(\lambda_2-\lambda_3)(\lambda_2-\lambda_4)\right]^{-1} \qquad (20)$$

$$A_3 = (mr^2+k-A\sqrt{2\mu\rho}\; r^{3/2})^2 + (A\sqrt{2\mu\rho}\; r^{3/2})^2 \qquad (21)$$

and

$$\lambda_{1,2}^2 = \frac{\tilde{\omega}}{2}(\sqrt{\beta^2+\cos\theta} - \beta)^2\left(-\frac{\beta}{\sqrt{\beta^2+\cos\theta}} \pm i\sqrt{1+\frac{2\beta}{\sqrt{\beta^2+\cos\theta}}}\right) \qquad (22)$$

As before, when $3\beta^2$ is greater than one, $\cos\theta$ is replaced by $\cosh\theta$.

DISCUSSION

The response of the system as given in (18) contains three functions of time. The first two are exponentially decaying sinusoidal functions that are seen to be complex conjugates. Hence, their sum produces a real function of time. The third function, the integral term in the response, describes the non-oscillatory response of the system, which for t large is asymptotic to $t^{-5/2}$. Since the first two functions decay exponentially, the integral term dominates the response of the system when t is large. Amplitude decay, or damping, which is not exponential, but which is proportional to fractional powers of time, for large time, is a general characteristic of systems containing dissipative elements described by fractional derivatives.

The total response of the system is the sum of decaying monotonic and oscillatory motions. For implusive loading the classical viscously damped oscillator exhibits either monotonically decaying exponential motion in the overdamped and critically damped cases or decaying sinusoidal motion in the underdamped case. The analysis we have given here simultaneously exhibits overdamped and underdamped behavior. The amount of overdamped behavior relative to the amount of underdamped behavior increases as the damping measure β increases, which is what one might expect.

Posing the original equation of motion (7) in terms of the algebraic parameters appearing for the roots of the auxiliary equation, β and $\tilde{\omega}$, yields

$$\ddot{x}(t) + 2\beta\sqrt{\tilde{\omega}}D^{3/2}\{x(t)\} + \frac{3}{16}\tilde{\omega}^2 x(t) = \frac{f_e(t)}{m} \quad (23)$$

This form is convenient for comparison to the equation of motion for an oscillator having classical viscous damping.

$$\ddot{x}(t) + 2\zeta\omega_n\dot{x}(t) + \omega_n^2 x(t) = \frac{F_e(\omega)}{m} \quad (24)$$

Taking the Fourier transform of (23) yields:

$$(i\omega)^2 X(\omega) + 2\beta\sqrt{\tilde{\omega}}\,(i\omega)^{3/2} X(\omega) + \frac{3}{16}\tilde{\omega}^2 X(\omega) = \frac{F_e(\omega)}{m} \quad (25)$$

which indicates that the contribution of the viscous damping is proportional to $\omega^{3/2}$, instead of ω as in the case in the more traditional view of viscous damping (equation 24). The reason for this difference is that in the problem under consideration here the thickness of the boundary layer in the fluid varies as $\omega^{-1/2}$. Thus, the velocity gradient and the shear stress in the fluid are proportional to $\omega^{1/2}$. A combined factor of $\omega^{3/2}$ appears when we pose the equation of motion in terms of displacement instead of velocity.

Through this example, we have seen that Newtonian viscous fluids are capable of producing damping forces considerably different from the viscous damping forces traditionally assumed to be proportional to velocity. The difference appears when the thickness and inertia of the fluid are significant. The difference leads to a response which is qualitatively different from that of the traditional damped oscillator.

CLOSURE

In a series of papers, beginning with the Proceedings of the 1978 Shock and Vibration Symposium, we have applied material models involving the fractional derivative to problems in vibration. These works have shown that the fractional derivative has utility as a means of modelling the behavior of elastomeric materials. Specifically, it has been shown that such models are not only useful for describing the behavior of real materials, but that the inclusion of such constitutive equations in engineering analyses leaves problems which may be solved analytically, and that those solutions are real, continuous and causal [5]. We have also shown that such models, determined from experimental data obtained under sinusoidal oscillation, may be used to successfully predict the results of a transient phenomenon [1]. That such models are more than very effective empirical fits has also been demonstrated, as it has been shown that they can be developed from accepted theories of the behavior of dilute polymers [6]. It has also been shown that the use of the fractional derivative model of material behavior does not remove the possibility of using the powerful tools of finite element analysis in the solution of structural problems [4], and that the use of such models produces results in good agreement with results from continuum solutions [6].

REFERENCES

1. Torvik, P. J. and Bagley, R. L., "On the Appearance of the Fractional Derivative in the Behavior of Real Material," Journal of Applied Mechanics, Vol. 51, p 295, June 1984.

2. Churchill, R. V., Operational Mathematics, 3rd ed., McGraw-Hill, 1972, p 195.

3. Bagley, R. L., and Torvik, P. J., "Fractional Calculus - A Different Approach to the Analysis of Viscoelastically Damped Structures," AIAA Journal, Vol. 21, No. 5, May 1983, pp 747.

4. Ross, B., "A Brief History and Exposition of the Fundamental Theory of Fractional Calculus," Fractional Calculus and Its Applications, Lecture Notes in Mathematics, Vol. 457, Springer Verlag, Berlin, 1974, pp 1-36.

5. Bagley, R. L., and Torvik, P. J., "A Generalized Derivative Model for an Elastomer Damper," Shock and Vibration Bulletin, No. 49, Part 2, pp 135-143, Sept 1979.

6. Bagley, R. L., and Torvik, P. J., "A Theoretical Basis for the Application of Fractional Calculus to Viscoelasticity, Journal of Rheology, Vol. 27, No. 3, pp 201-210, June 1983.

APPENDIX

The derivation of this different view of viscous damping begins with the equation that governs the response of a semi-infinite domain of fluid, set in motion by the displacement of a bounding plate at z = 0.

$$\rho \frac{\partial v}{\partial t} = \mu \frac{\partial^2 v}{\partial z^2} \qquad (A1)$$

Here ρ is the fluid density, μ is the viscosity and V is the velocity profile of the fluid which depends upon time, t, and the distance from the "wetted" plane, z. Solving this equation using Laplace transforms

$$L[v(t,z)] = \int_0^\infty e^{-st}\, v(t,z)\, dt = \bar{v}(s,z) \qquad (A2)$$

and applying the boundary conditions that the velocity of the fluid at the plate match the velocity of the plate and that the velocity of the fluid be bounded away from the plate produces

$$\bar{v}(s,z) = \bar{v}_p(s) e^{\frac{\rho s}{\mu} z} \qquad (A3)$$

Here $v_p(s)$ is the transform of the velocity of the plate.

Having obtained the transform of the velocity profile, the stress in the fluid, $\bar{\sigma}_{xz}(s,z)$, may be found by using the standard shear stress relationship for the Newtonian fluid.

$$\bar{\sigma}_{xz}(s,z) = \mu \frac{d\bar{v}(s,z)}{dz} \qquad (A4)$$

The resulting transform of the stress is

$$\bar{\sigma}_{xz}(s,z) = \sqrt{\mu\rho}\, \sqrt{s}\, \bar{v}\,(s,z) \qquad (A5)$$

We now note that the fractional order derivative, defined in the time domain as [4]

$$D^{\alpha}_{(t)}[v(t,z)] \equiv \frac{1}{\Gamma(1-\alpha)} \frac{d}{dt} \int_0^t \frac{v(\tau,z)}{(t-\tau)^{\alpha}}\, d\tau \qquad (A6)$$

may be simply expressed in the Laplace transform domain if the transform of the definition is written:

$$L\left[D^{\alpha}[v(t,z)] \right] = S^{\alpha}\, L[v(t,z)] \qquad (A7)$$

Using this, we may return equation A5 to the time domain, finding

$$\sigma_{xz}(t,z) = \sqrt{\mu\rho}\, D_t^{\frac{1}{2}}\, [v(t,z)] \qquad (A8)$$

the desired result. Although equation A8 may resemble a constitutive equation, it is not. The constitutive equation is that of the Newtonian fluid

$$\sigma_{xz}(t,z) = \frac{\mu \partial v(t,z)}{\partial z} \qquad (A9)$$

Equation A8 is merely an expression for the shear stress distribution in terms of a time derivative rather than a partial derivative, obtained by making use of the velocity distribution for this particular flow.

TEMPERATURE SHIFT EFFECTS ON COMPLEX MODULUS

James A. Eichenlaub and Dr Lynn C. Rogers
Air Force Flight Dynamics Laboratory
Wright-Patterson Air Force Base, Ohio

The first step in using viscoelastic materials to control vibration is the accurate determination of the material properties. Since polymer properties exhibit a strong dependence on frequency and temperature, it is necessary to characterize samples over a wide range of temperatures and frequencies. It is impractical to measure all points of interest in the temperature and frequency ranges, therefore, some type of curve fitting is required to allow extrapolation of data at other temperatures and frequencies. To plot the modulus and loss factor in two dimensions, these properties must be functions of one variable which contains the two independent variables mentioned. The two independent variables may be combined using a temperature shift parameter to give a reduced frequency. In most material tests, experimental data cannot be collected over a sufficiently wide frequency range to define the temperature shift parameter equation. Therefore, an alternate method of defining the shift parameter is required. This paper presents a method of defining the temperature shift parameter equation when the frequency range is inadequate to find it by inspection of the experimental data.

INTRODUCTION

This paper deals with the shear modulus as a dynamic mechanical property of viscoelastic damping materials (VEM). The modulus will be treated as a complex-valued function of temperature and frequency. It is assumed that, at least as a first approximation, the behavior of the VEM is thermorheologically simple, i.e., the complex modulus is a function of reduced frequency defined as a product of frequency and temperature shift function

$$f_r = f \cdot \alpha_T(T) \qquad (1)$$

This allows the real component, imaginary component, and ratio of these parts of the complex modulus function to be plotted in two dimensions. This permits curve fitting which is required to efficiently and accurately calculate modulus and loss factor for any temperature and frequency of interest. It has been determined that the shift parameter, $\alpha_T(T)$, equations are dependent only on temperature and they are relative to a reference temperature, T_0, of the material of concern.

Strictly speaking, full experimental characterization of the VEM complex modulus requires data at a sufficient size of increments and range of temperature and at least three decades of frequency coverage at each temperature. This would define the temperature shift function, $\alpha_T(T)$, for the VEM. This is rarely practical because of the expense.

Shift parameter equations have been empirically determined by comparing the

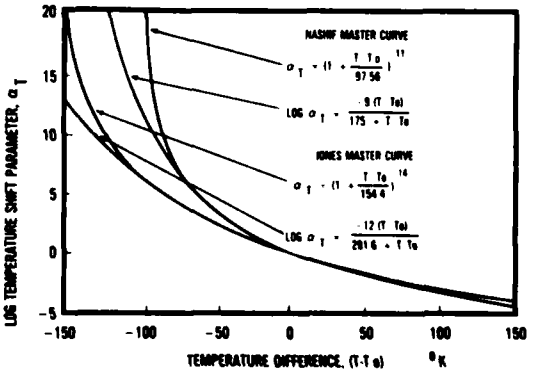

Fig. 1 - Temperature Shift Parameter Versus Temperature Difference

results of many materials. Historically, the temperature shift functions in Fig. 1 have been used. In fitting the complex modulus data with mathematical expressions, separate empirical equations have been used for the real component and for the material loss factor. While this has been satisfactory for past applications, a need exists for improved accuracy and efficiency for more demanding future work.

APPROACH

The availability of data over a wide range of frequencies makes it possible to accurately determine the shift parameter by choosing a value of T_0 which results in the smoothest representation of the data on a superimposed master curve, avoiding overlap and excessive scatter. In most material tests experimental data cannot be collected over a sufficiently wide frequency range to define the temperature shift parameter equation. When the range of frequency is lacking in the experimental complex modulus data, recent developments in the mathematical expressions for complex modulus as a function of reduced frequency may be used to infer certain information about the shift parameter. First of all, it is a conceptual error to consider the real modulus and the loss factor as separate functions. The complex modulus is a single complex-valued function of reduced frequency. The simplest such expression is included in Fig. 2.

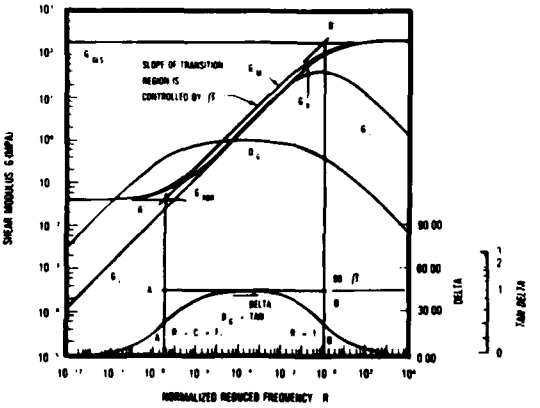

Fig. 2 - Complex Shear Modulus Quantities

The expression for the complex modulus is

$$G^*(j\omega_R) = [Ge + Gg(jR)^\beta]/[1 + (jR)^\beta] \quad (2)$$

where $R = \omega_R/\omega_{Ro}$. This is a good approximation for many VEMs. It may be shown that the slopes of the real, the imaginary and the magnitude near the center of the transition region depend only on the exponent β. The imaginary slope will be used in this paper.

$$\beta = \frac{d(\log G_I)}{d(\log f_r)} \quad (3)$$

It may also be shown that the maximum loss factor depends largely on β, but also on the ratio of the glassy asymtote to the rubbery asymptote according to the following equation

$$\eta_{max} = \frac{(1 - 1/A)\tan\frac{\beta\pi}{2}}{1 + 1/A + 2/A^{\frac{1}{2}}\cos\beta\pi/2} \quad (4)$$

Where A = Gg/Ge.

We now assume that the temperature shift function may be represented

$$\alpha_T(T) = a\left(\frac{1000}{T} - \frac{1000}{T_0}\right) \quad (5)$$

for an as yet unspecified range of temperature. The slope of the imaginary component of the modulus, G_I, is now a function of the parameter a. This relationship will be used to evaluate a.

The slope of G_I for any particular value of a is somewhat subjective. Presently, a straight line fit of (log G_I) versus (log f_r) starting with the lowest 10 values of reduced frequency and adding points one at a time is performed. A plot of n points versus slope of G_I is plotted for different values of a. This is shown in Fig. 3 for one arbitrary value of a. By taking a value representative of the maximum slope f G_I from each of several plots of different a values, a plot showing slope of G_I versus a can be generated for a particular material.

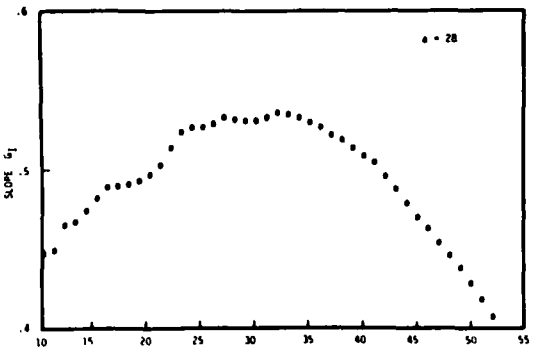

Fig. 3 - Slope G_I Versus n

ILLUSTRATION

The procedure outlined above is shown in Fig. 4 for two materials. The value of a is selected from Fig. 4 to give the desired value of β which is established separately.

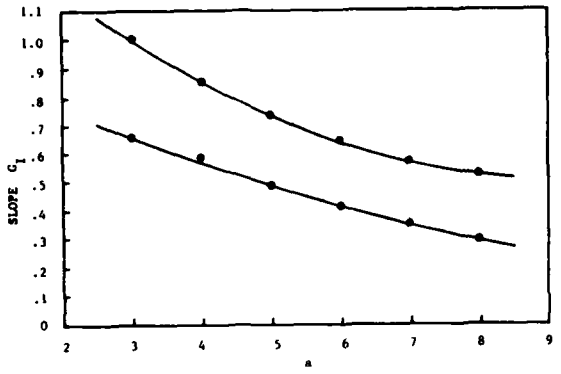

Fig. 4 - Slope G_I Versus a

The experimental imaginary component versus the real component can be used to estimate the ratio of glassy to rubbery modulus. This is shown in Fig. 5. The modulus ratio is then used to determine the slope β in conjunction with the maximum loss factor, η_{max}.

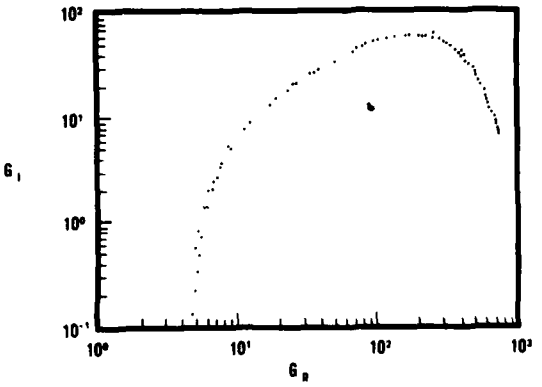

Fig. 5 - G_I Versus G_R

For this paper, a plot of loss factor versus temperature is plotted as in Fig. 6. A quadratic is fit to the experimental data to find an analytic η_{max} and reference temperature, T_o, which is the temperature at the analytic η_{max}.

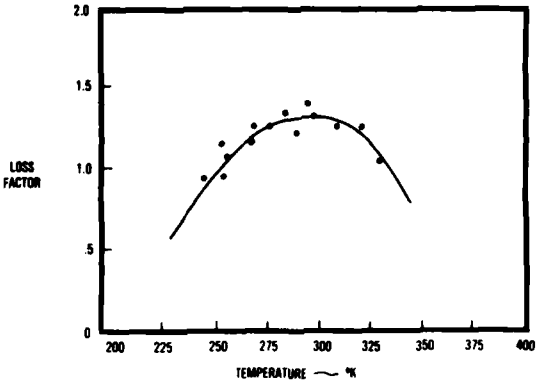

Fig. 6 - Loss Factor Versus Temperature

Fig. 7 is a plot of η_{max} versus β for different ratios of A = Gg/Ge. These curves are based on Eqn. 4. After η_{max} and A are determined, then β can be found from Fig. 7. The slope of G_I and β are equivalent so Fig. 4 can be used to find a value of the parameter a for Eqn. 5.

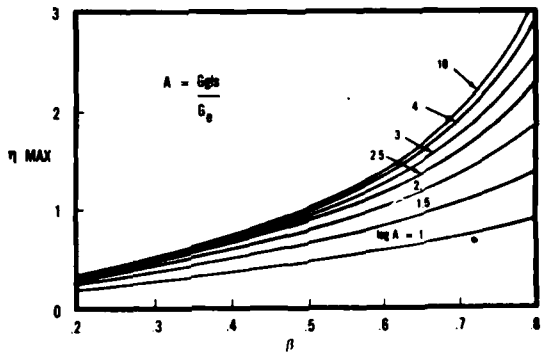

Fig. 7 - Maximum Loss Factor Versus β for Different Values of A

The temperature shift curve is now defined as a function of temperature. A flow diagram of this process is illustrated in Fig. 8. Actually this procedure only defines the shift function in the neighborhood of the temperature of maximum loss factor.

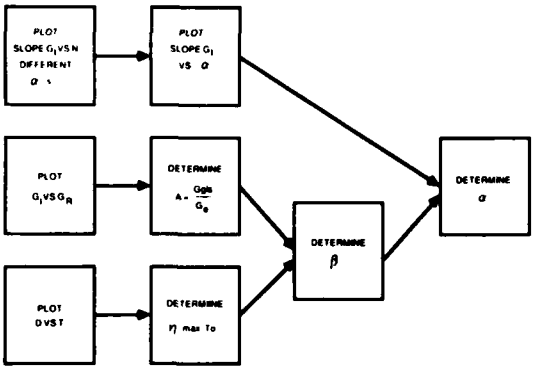

Fig. 8 - Process Flow Diagram

DISCUSSION

Certain sets of experimental complex modulus data currently available make it obvious that the above $\alpha_T(T)$ is inappropriate for the full range of temperature. Future work will focus on the Williams-Landell-Ferry (WLF) equation

$$\log \alpha_T(T) = \frac{-C(T - T_o)}{C_2 + T - T_o} \qquad (6)$$

and its slope at T_o

$$\left.\frac{d(\log \alpha_T)}{dT}\right|_{T=T_o} = -\frac{C_1}{C_2} \qquad (7)$$

Equating the slopes of Eqn. 5 and Eqn. 6 gives

$$\frac{C_1}{C_2} = \frac{1000a}{To^2} \qquad (8)$$

or

$$\log \alpha_T = \frac{\frac{-1000aC_2}{To^2}(T - To)}{C_2 + T - To} \qquad (9)$$

Procedures to evaluate C_2 will be investigated as well as procedures of using still other expressions for the temperature shift function. This procedure, or some evolution, is mandatory until experimental complex modulus data covering an adequate range of frequency is available.

PASSIVE DAMPING - SONIC FATIGUE - AND THE KC-135

P. A. Graf, M. L. Drake, M. P. Bouchard, R. J. Dominic
University of Dayton Research Institute
Dayton, Ohio

High noise levels occurring during maximum-thrust takeoff have caused sonic fatigue cracking of the aft fuselage skin and stringers of the KC-135A aircraft. The University of Dayton Research Institute has conducted a program to solve this problem through the design and evaluation of a passive damping system for the aft fuselage of the KC-135A. The paper presents a detailed description of the program results. The program was sponsored by the Air Force Wright Aeronautical Laboratories' Materials Laboratory and the Oklahoma City Air Logistics Center.

BACKGROUND

Early in the life of the KC-135 aircraft, sonic fatigue problems developed. These early problems were corrected by adding "belly bands" to the skin panels which were placed between the frames and ran parallel with the frames around the fuselage. This fix to the problem was both costly and heavy.

Recently, sonic fatigue cracks have begun appearing in the KC-135A. These cracks are occurring aft of fuselage body station (BS) 1370 (see Fig. 1) which is the frame location where the belly bands stopped. In an effort to find a more cost and weight effective solution to the fatigue problem the University of Dayton Research Institute undertook a program funded by the Air Force to design and evaluate a passive damping system which would eliminate the problem.

The program was divided in the following three efforts:

1. Dynamic response tests of the undamped fuselage.
2. Damping system design.
3. Damping system application and evaluations.

Each task is detailed in the following paragraphs.

DYNAMIC RESPONSE TESTS, UNDAMPED FUSELAGE

Dynamic response tests were conducted on an aircraft at Wright-Patterson Air Force Base, Ohio. The testing consisted of modal analysis and engine operating acoustic and structural response data.

Analysis of the data acquired from these tests provided the dynamic behavior baseline parameters required for the design optimization of an effective passive damping system for decreasing dynamic stresses causing the fatigue problem.

Modal data was acquired to identify the dominant resonant modes. The portion of the fuselage tested contained nine panel sections bounded by fuselage body stations (BS) 1380 and 1440 and stringers 9 and 12. The data were acquired with a GenRad 2510 micromodal analyzer and associated signal conditioners. The instrumentation system is described in the block diagram presented in Fig. 2. The force impulse-response transfer function method was used in collecting the data [1-3].

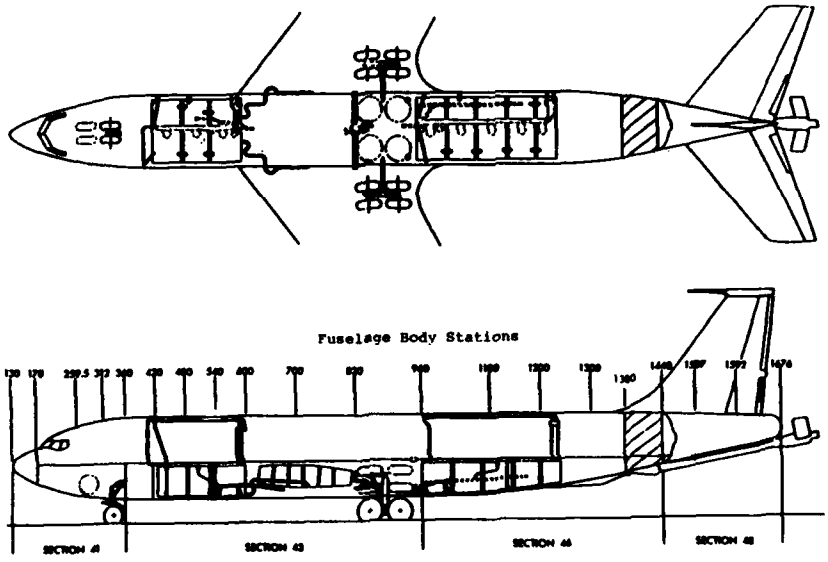

Fig. 1 - Definition of the region of interest

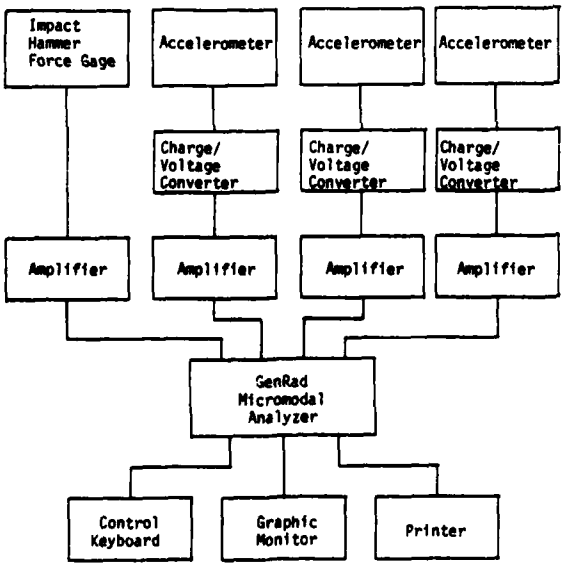

Fig. 2 - Block diagram of modal data acquisition system

The test points surveyed are identified in Figs. 3, 4, and 5. The modal data included 113 points on the skin, 40 points on stringers 10 and 11, and 62 points on the frame ribs at BS 1400 and BS 1420. The force impulse was imparted at stringer data point 196 which was directly over skin panel data point 59. Three response accelerometers were used simultaneously resulting in three transfer functions taken at a time.

The GenRad analyzer received amplified outputs from the force transducer on the impact hammer and the accelerometers on the structure. A fast fourier transform (FFT) converted each signal from the time domain to the frequency domain from D.C. to 800 Hz having sampling bandwidths of 4 Hz. The data for each transfer function was then stored as an accelerance (acceleration/force) frequency response function (FRF). Typical FRF's are shown in Figs. 6 through 8.

Analysis of the data indicated one modal frequency dominating the band under study. The resonance at approximately 300 Hz appears on the data from skin, stringers, and frames. Resonances at other frequencies between 300 and 800 Hz appear to be plate modes in the skin and structural modes of the skin stringer structure. Response of points on the frame ribs were minimal except at the stringer-frame attachments.

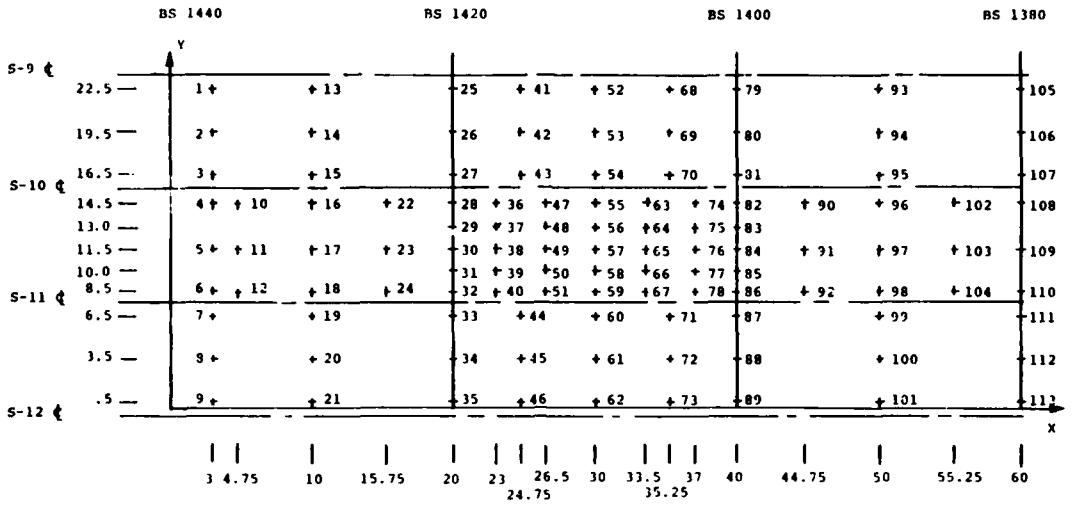

Fig. 3 - Location of modal data points on skin

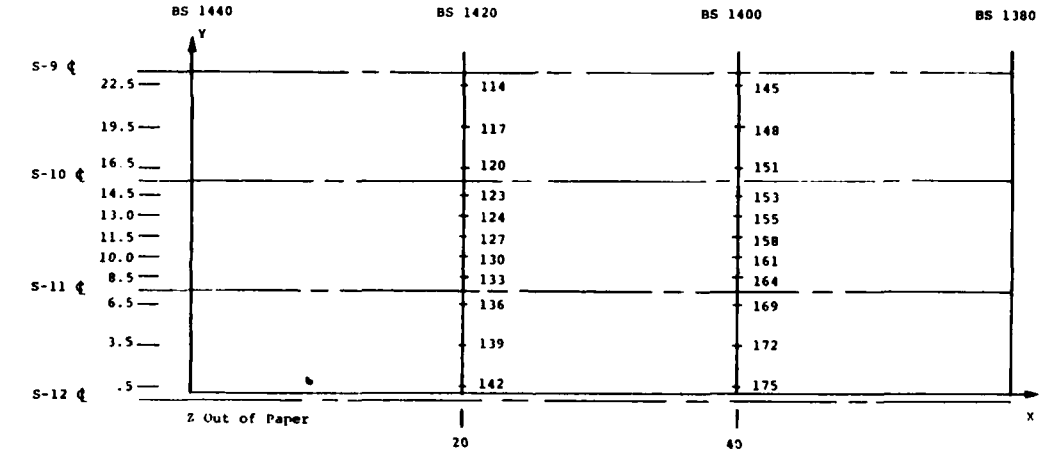

Fig. 4 - Location of modal data points on frames

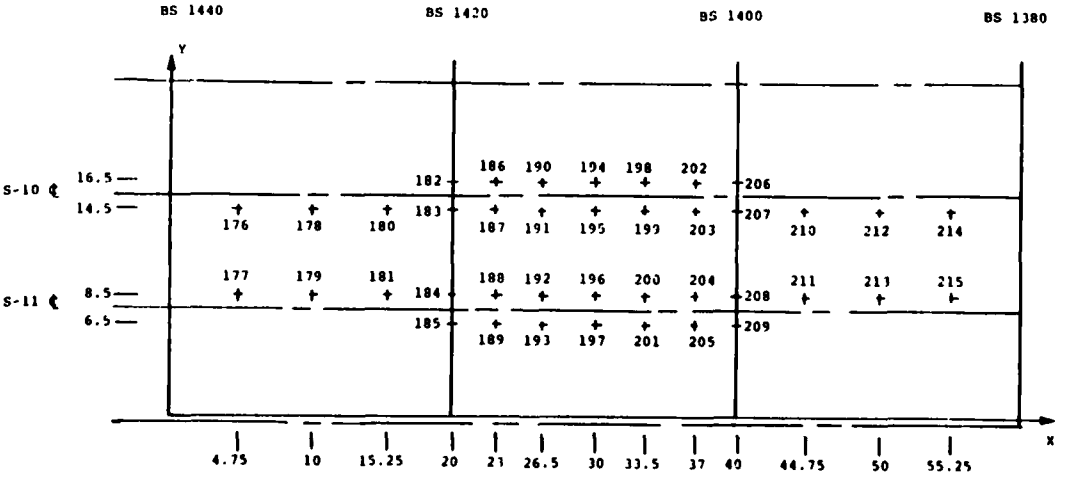

Fig. 5 - Location of modal data points on stringers

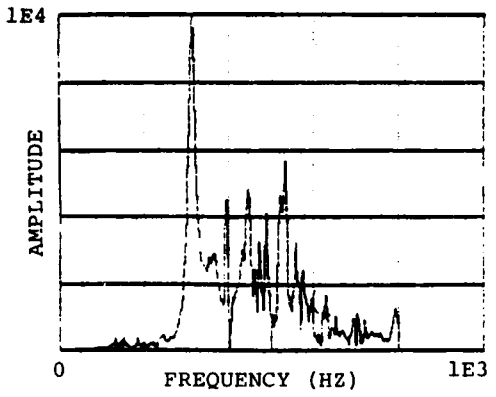

Fig. 6 - FRF skin data point 77

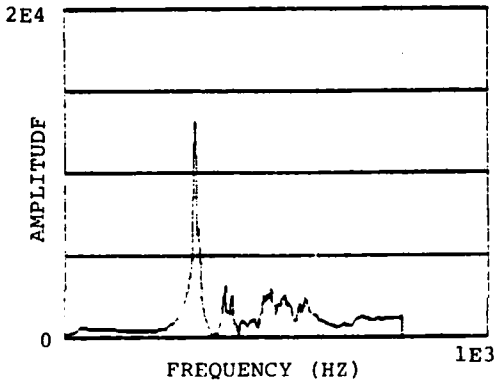

Fig. 7 - FRF stringer data point 196

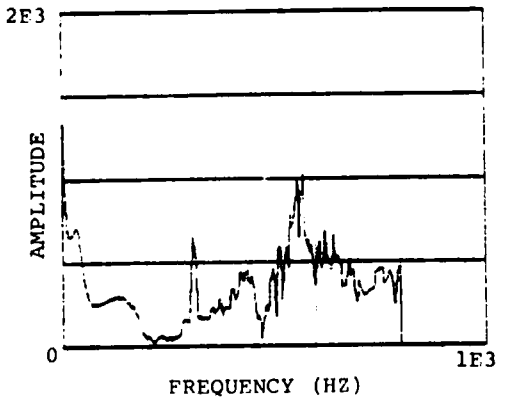

Fig. 8 - FRF frame data point 158

A review of the available literature indicated that the RMS sound pressure level (SPL) of the maximum wet thrust engine impingement noise on the KC-135 fuselage was 152 dB, at approximately 400 Hz, the half-power bandwidth extending from approximately 230 Hz to 650 Hz (see Figs. 9 and 10).

Sonic tests were conducted at maximum wet thrust with the aircraft stationary and the flaps set to 20 degrees to simulate takeoff configuration. SPL was monitored at stringer 12 at BS 1400 and on the pod three inches below the pod-body intersection at BS 1350 (Fig. 11). Vibratory responses were acquired with accelerometers located at modal test points 57, 77, 158, 196, and 208. All signals were recorded in real time on an FM tape recorder (Fig. 12). The recorded signals were played back and analyzed on a Hewlett-Packard Model 3582A sepctrum analyzer.

Analysis of the frequency response spectra of the five points surveyed during the engine run showed modal frequencies which agreed closely with those acquired during the modal testing. The SPL was recorded to be 157 dB.

DESIGN OF THE DAMPING SYSTEM

Proper design of a damping system requires detailed information on the structure to which the damping system is to be applied. The tasks previously discussed provided the required input for the damping design, namely: the structural configuration, the frequency range of concern, the mode shapes of concern, and the temperature range of concern [4].

The first step in a damping design is to construct an analytical model of the structure being investigated. From the modal analysis, it was determined that all the modes of concern involved skin deformations which were amenable to constrained layered damping systems. It was, therefore, decided to design a damping system to be applied to the skin only. Further review of the modal analysis determined that a skin panel bordered by two adjacent frames and two adjacent stringers would be a suffcient structural subsystem to model (see Fig. 13). The analytical method used to develop the model was fourth-order plate theory [4]. The constrained layer model system is shown in Fig. 14. The boundary conditions chosen for the model were all edges fully clamped. This resulted in slightly higher

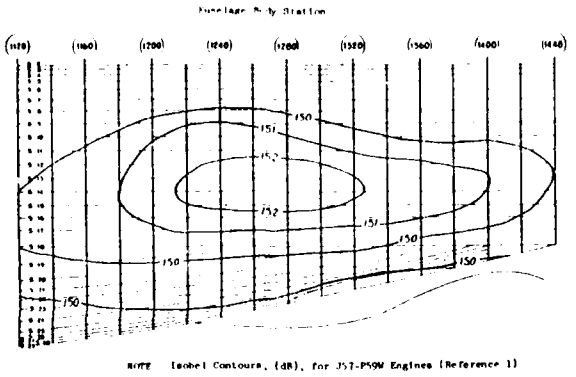

Fig. 9 - C/KC-135 aft fuselage maximum wet thrust engine impingement noise isobel contours

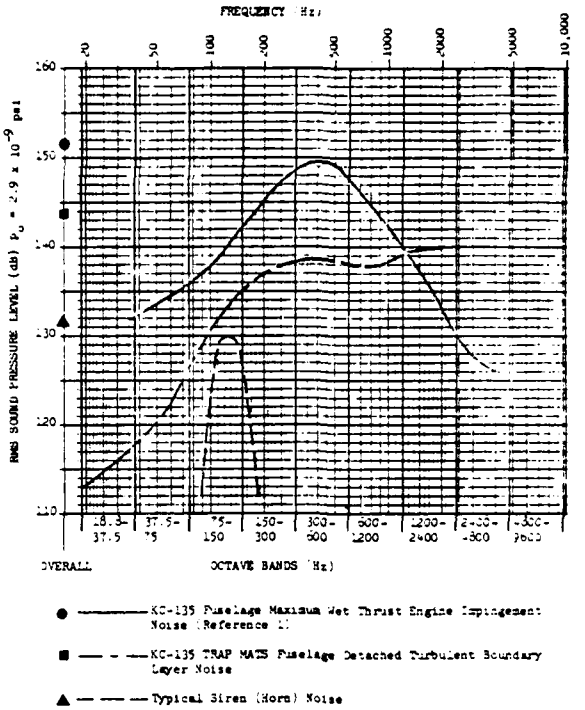

Fig. 10 - RMS sound pressure level versus frequency

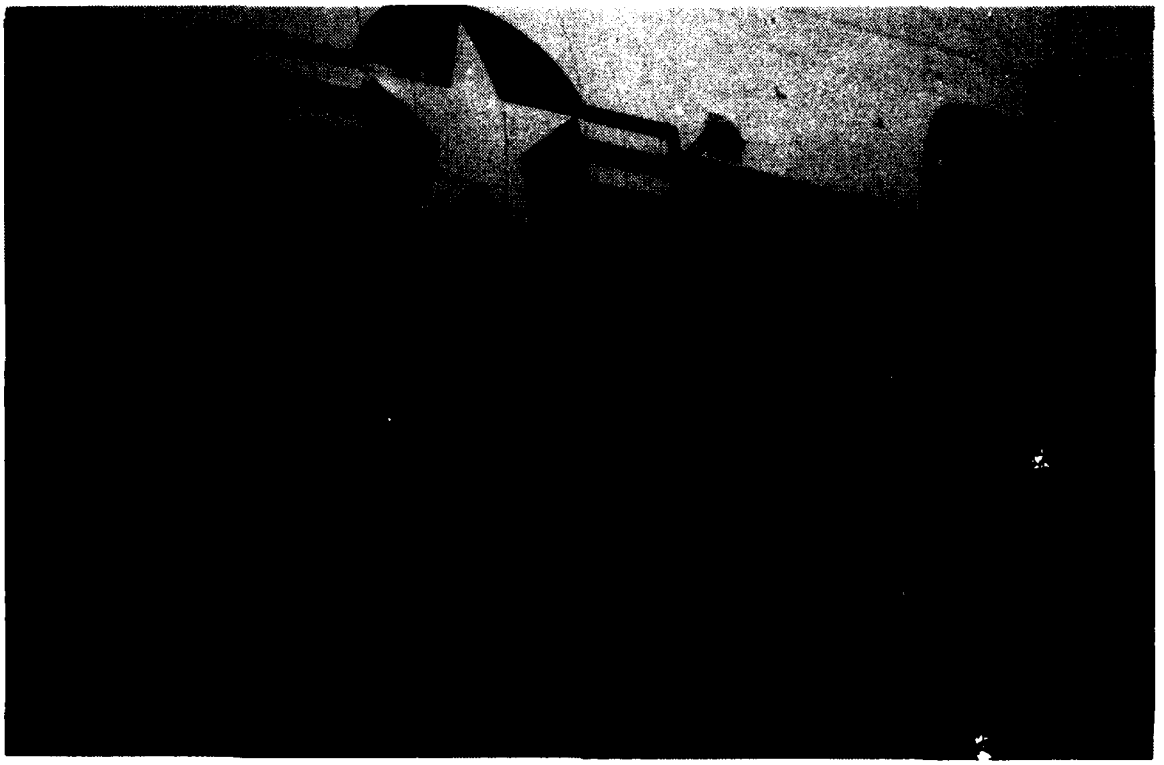

Fig. 11 - Sound pressure level monitor microphones installation

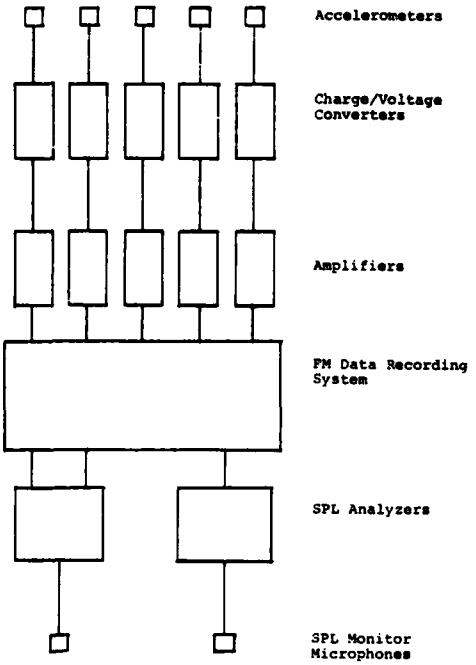

Fig. 12 - Block diagram of sonic response data acquisition system

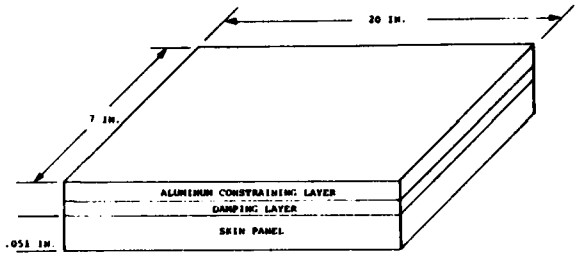

Fig. 14 - Constrained layer damping model

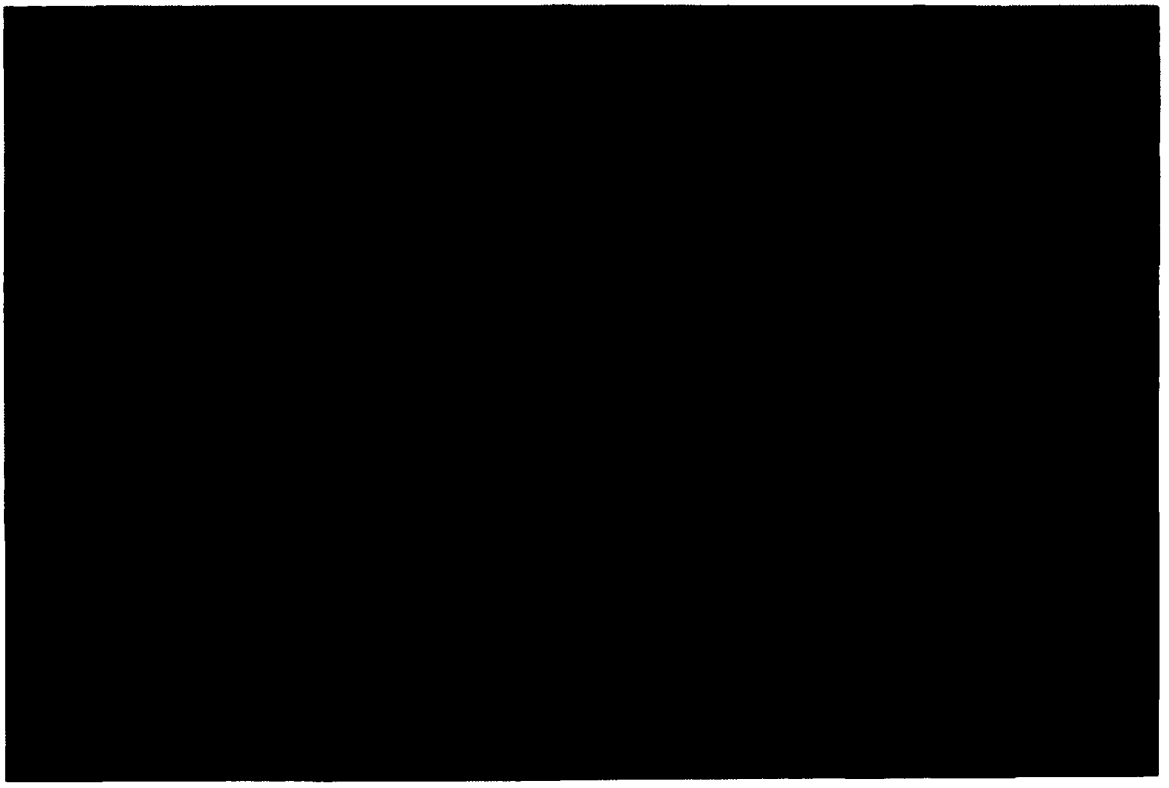

Fig. 13 - Typical view of skin/stringer/frame structure

predicted resonance frequencies from the model than what was measured on the aircraft; however, the damping design developed from the model would function properly for the actual aircraft panels.

Based on the frequency response data, the modal analysis, and the engine ground tests it was decided that the primary mode of concern was a panel mode with a frequency near 300 Hz and a deformed mode shape of one-half sine wave between the stringers and a complete sine wave between the frames (see Fig. 15). The analytical model predicted this mode (the 1,2 mode) had an undamped frequency of 473 Hz.

The next major consideration was the temperature range over which damping is required. Water assist takeoffs are not made below 20°F. The upper design temperature was taken to be 100°F. Based on various aircraft data reviewed, it is believed that the temperature range of 20°F to 100°F will encompass 80 to 95 percent of all the takeoffs. Effective damping over this range will eliminate the cracking problem.

The final input into the design process was the choice of damping material and constraining layer material to be used in the design. The choice of damping material is dictated by the temperature and frequency of interest for the design. For this project, two 3M damping materials and two Soundcoat damping materials were evaluated. The constraining layer was chosen to be aluminum because of its light weight, availability, low cost, and to avoid dissimilar metal problems between the fuselage and the constraining layer.

The design process first generated a "carpet plot." This plot depicts the effects of varying both the damping material thickness and the constraining layer thickness on both the maximum structural loss factor (η_{max}) attainable and the temperature at which η_{max} occurs. Fig. 16 illustrates a carpet plot generated for 3M's ISD 113. From the carpet plot the designer can easily decide what geometric configuration provides the peak damping at the desired temperature required for the particular problem to be solved.

For the design on the KC-135, two objectives were set: (1) a predicted system loss factor of approximately 0.1 over the required temperature range, and (2) a constraining layer no thicker than 0.020 inches. (The thinner the constraining layer the smaller the weight penalty for the damping system.)

Three damping configurations using ISD 113 were evaluated from the carpet plot. The configurations were:

1. ISD 113 0.002 inch thick with a 0.012 inch thick aluminum constraining layer.

2. ISD 113 0.004 inch thick with a 0.012 inch thick aluminum constraining layer.

3. ISD 113 0.004 inch thick with a 0.015 inch thick aluminum constraining layer.

The structural loss factor for each of the damping configurations as a function of temperature is shown in Fig. 17. The recommended damping system for fleet implementation is the 0.004 inch ISD 113 and the 0.012 inch aluminum constraining layer. The increase in damping gained by increasing the constraining layer thickness to 0.015 inch does not appear to be worth the 25 percent weight penalty which results.

In order to avoid placing the Air Force in a single source procurement situation, another damping system was designed using a Soundcoat damping material. Using the same process as completed for the 3M design, the final design chosen was a damping system consisting of a 0.006 inch thick layer of MN damping material with a 0.015 inch thick aluminum constraining layer. Fig. 18 illustrates the predicted damping of this Soundcoat damping design compared to the 3M design.

Fig. 18 shows the overall damping of the Soundcoat system to be slightly higher than the 3M system; however, the Soundcoat system weighs approximately 28 percent more than the 3M system.

EVALUATION OF INSTALLED DAMPING TREATEMENT

The final step in the design effort was to install and evaluate the damping system. The temperature of the fuselage of KC-135 which was tested at Wright-Patterson Air Force Base was between 70°-80°F. In this temperature range, either of the damping systems using the 0.012 inch thick aluminum constraining layer provide the same level of damping. Therefore, the 0.002 inch ISD 113 treatment was used in the evaluation test.

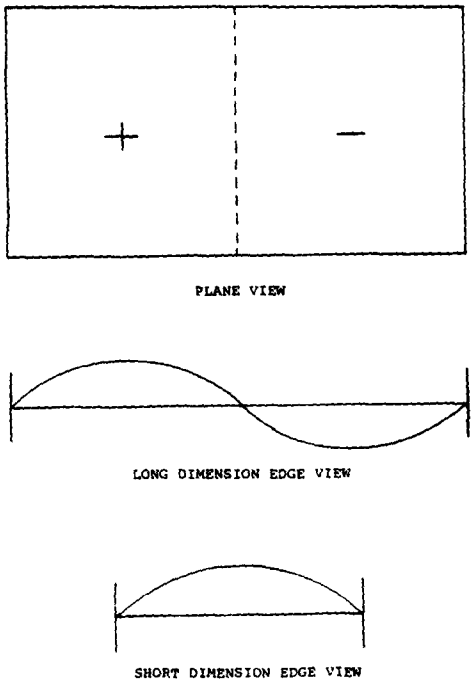

Fig. 15 - Modal model used for damping design

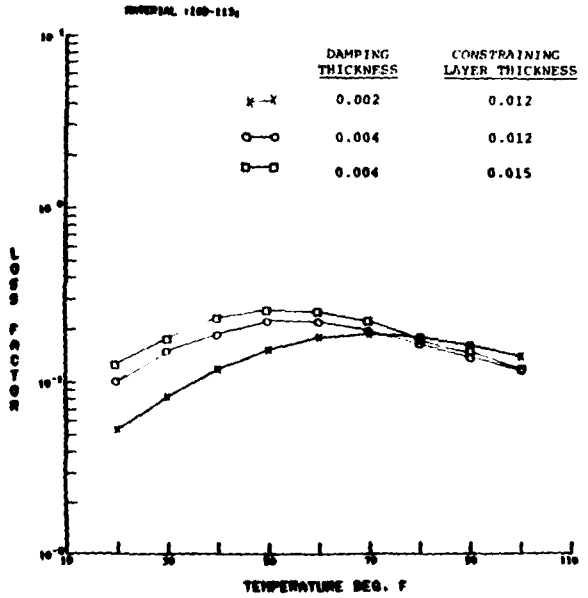

Fig. 17 - Structural loss factor versus temperature for three ISD 113 damping configurations

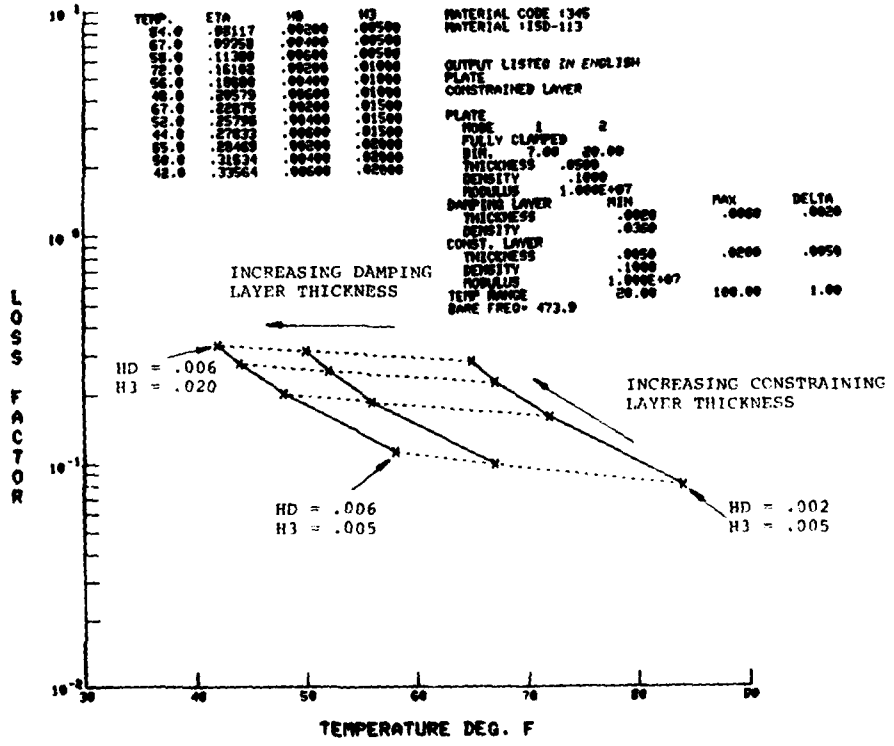

Fig. 16 - Carpet plot for ISD 113

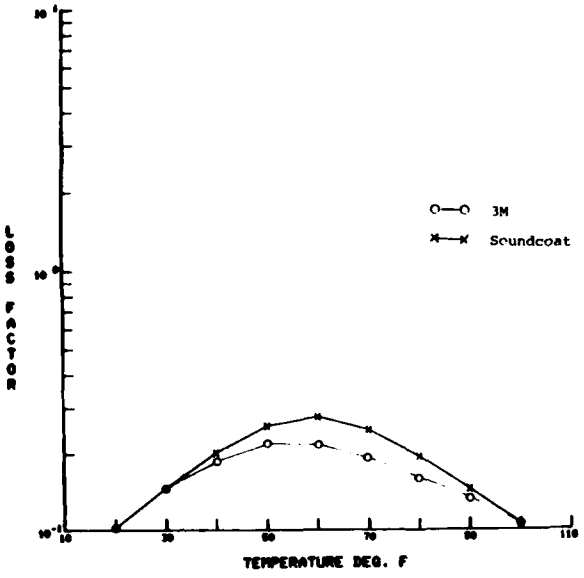

Fig. 18 - Comparison of 3M and Soundcoat recommended damping design

The damping material (ISD 113 and MN) in this design has excellent adhesive properties and, therefore, no additional adhesive is necessary. The installation consisted of degreasing the inside fuselage surface and applying the six inch (6.0) by twenty inch (20.0) damping patch to the skin.

After installation of the prototype damping system was completed, tests were conducted to evaluate its effectiveness. The modal data survey was partially replicated, data being acquired from the skin panel bounded by BS's 1400 and 1420 between stringers 10 and 11, and data points 158, 184, and 196 on stringer and frames. Also engine run sonic response data were acquired during water-injected maximum thrust conditions. Conditions during these tests were held constant with the exception of ambient and skin temperatures, which were uncontrollable. During the damped and undamped tests, temperatures were between 70°F and 80°F and interior monitored skin temperatures were between 73°F and 83°F. These variations are small enough to allow direct comparison of undamped and damped data.

The effectiveness of the applied damping system was evaluated by comparison of levels of response experienced by the skin, stringers, and frames in the damped skin structure, relative to the responses experienced by the same components in the undamped skin structure. Representative comparisons of FRF responses are illustrated in Figs. 19 through 21. While these comparisons indicated a significant reduction in responses of certain points, they serve more as a model for the anticipated sonic test results than as a conclusive stand alone set of results.

Comparison of responses of the skin, stringer, and frame structure to the impingement of engine-generated noise over the surface of the skin is of primary interest in the evaluation of damping effectiveness. Noise impingement on the fuselage skin fore and aft of, and above and below, the treated area excite resonances borne through the stringer and frame components to the monitored area. Aware of this, we can proceed with our analysis of the comparison of the treated skin responses to sonic excitation relative to the untreated responses, illustrated in Figs. 22 through 24, which illustrate the RMS levels of representative points to the sonic inputs. (The recorded SPL was 155 dB.)

As predicted by the comparative FRF data, skin responses were reduced significantly (Figs. 22 and 24) while stringer and frame responses were reduced to a lesser degree. The reductions in vibratory response levels are summarized in Table 1.

It should be noted that all the FRF responses were acquired with the fuselage insulation pads and liners removed, while all the sonic test data were acquired with the insulation pads and liners installed.

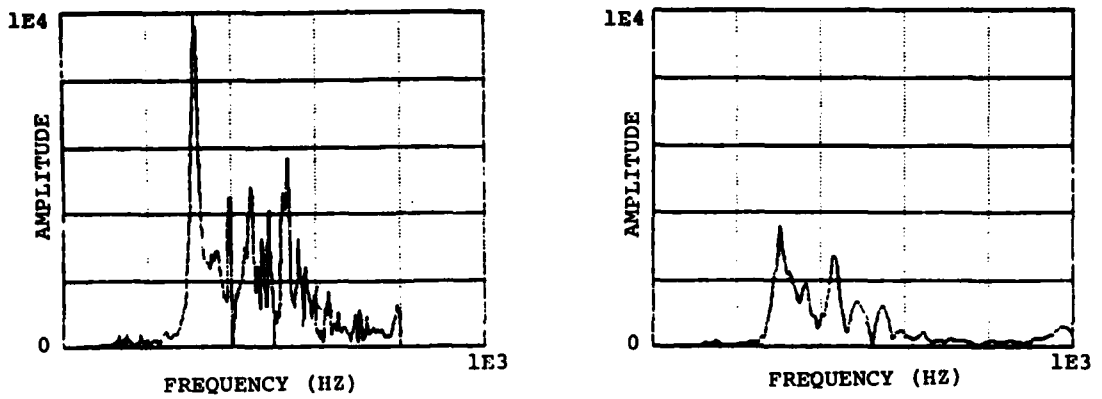

Fig. 19 - FRF's skin data point 77 before (left) and after damping installation

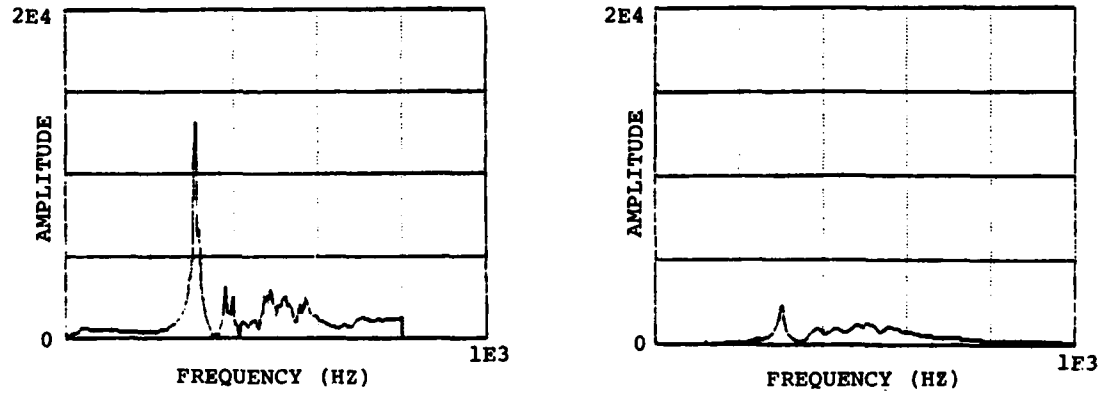

Fig. 20 - FRF's stringer data point 196 before (left) and after damping installation

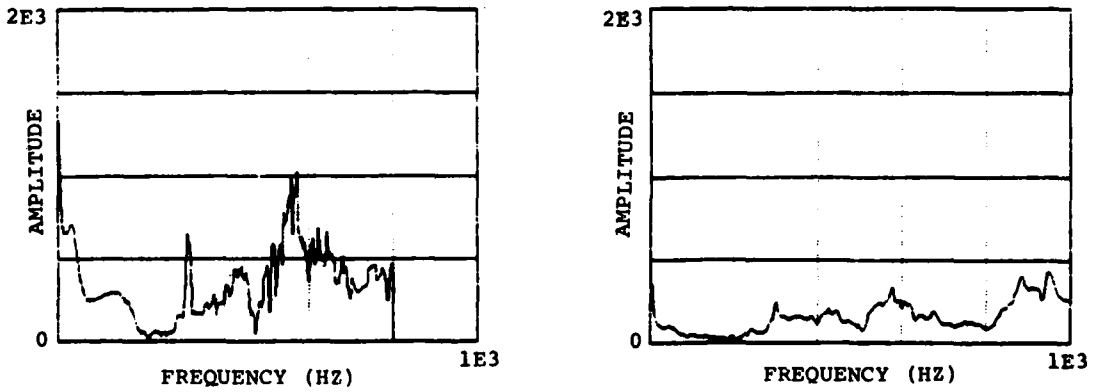

Fig. 21 - FRF's frame data point 158 before (left) and after damping installation

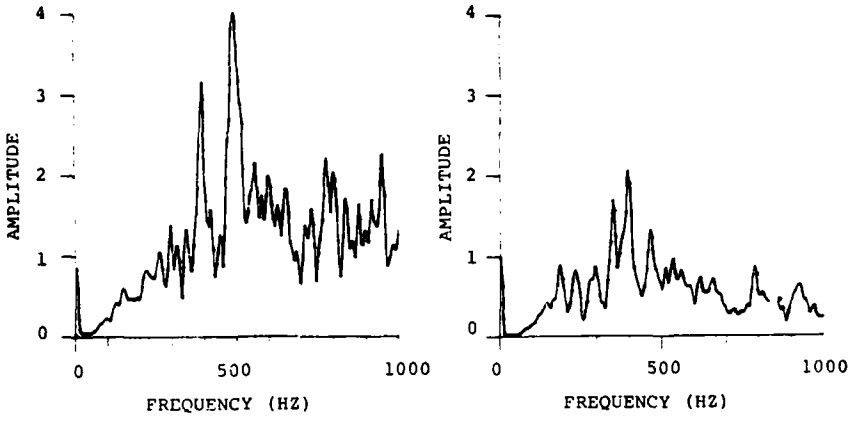

Fig. 22 - Response of test point 77 to sonic excitation before (left) and after damping installation

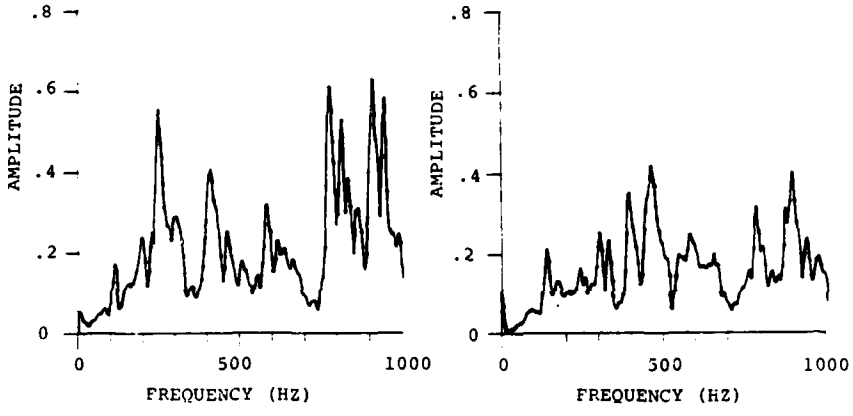

Fig. 23 - Response of test point 158 to sonic excitation before (left) and after damping installation

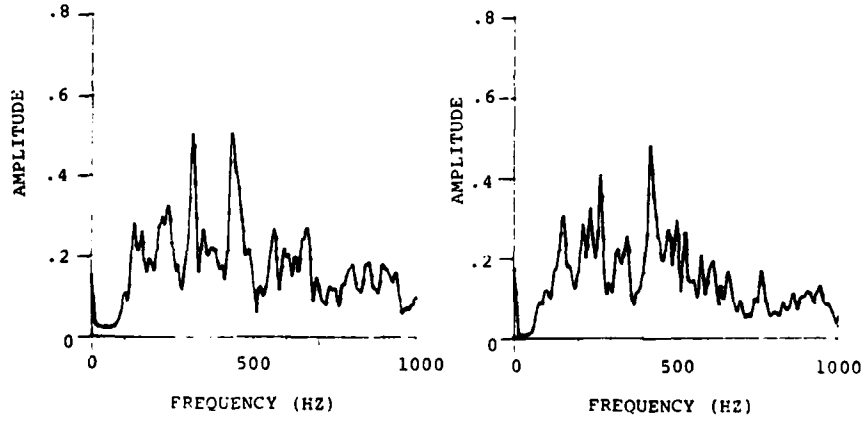

Fig. 24 - Response of test point 196 to sonic excitation before (left) and after damping installation

TABLE 1

Summary of Engine Test Results

RESPONSE LOCATION	RMS AMPLITUDE (V)		% RESPONSE REDUCTION
	UNDAMPED	DAMPED	
SKIN	12.0	5.5	54
SKIN	12.5	6.0	52
STRINGER	--	--	15*
FRAME	2.25	1.65	27
FRAME-STRINGER JOINT	1.7	1.5	18

*PEAK RESPONSE REDUCTION

SUMMARY

Design of an effective passive viscoelastic damping system is dependent upon several parameters among which are the resonant frequencies of concern and the operating temperature range.

Resonant frequencies of structural responses were characterized during ground tests on a KC-135 aircraft. Modal data were acquired with engines shut down, and responses to noise impingement were acquired during maximum wet thrust engine runs with the aircraft stationary. Results from these tests were used to establish the frequency parameters for design of the damping treatment.

After the constrained layer damping treatment was designed, fabricated, and installed, the ground tests were replicated.

Significant response reductions were observed for the skin, stringers, and frames. These results are summarized as follows:

- Noise level during maximum wet thrust engine tests was 155-157 dB (rel. 2.9×10^{-9} PSI).
- RMS response of skin reduced by more than 50 percent.
- RMS response of frames reduced by 20 to 25 percent.
- Peak response of stringers reduced by 15 percent.

CONCLUSIONS

The designed passive viscoelastic damping system applied to a very limited area of the skin was effective in reducing the damaging vibrations induced by impingement on the fuselage skin of engine generated noise during conditions simulating water augmented maximum thrust takeoff environment.

Implementation of the recommended skin damper system design would result in an expected ten-fold increase of fatigue life in the skin and at least a doubling of fatigue life for the frame/stringer substructure. These predictions are based upon the curves presented in Fig. 25 which is from Ref. [5]. The predicted fatigue life increases are gained at a weight penalty of less than 21 pounds added weight.

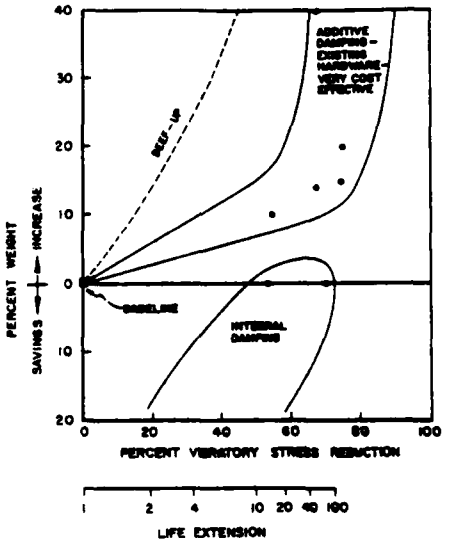

Fig. 25 - Comparison of approaches to extension of resonant fatigue life (Ref. [3])

ACKNOWLEDGMENTS

The authors would like to express their appreciation of the support from the 4950 test wing at Wright-Patterson Air Force Base, especially Lt. W. Norton for all the cooperation in completing the aircraft testing, and to Miss C. Gran for typing the manuscript.

REFERENCES

1. J. O. Litz, "Improving the Accuracy of Structural Response Measurements - Part I and II," Test, August/September and October/November, 1979.

2. W. G. Holvorsen and D. L. Brown, "Impulse Technique for Structural Frequency Response Testing," Sound and Vibration, November 1977, pp. 8-21.

3. University of Cincinnati and Hewlett-Packard, "Modal Analysis - Theory and Measurement Techniques," Short Course Notebook, D. L. Brown Editor.

4. University of Dayton, "Vibration Damping," Short Course Notebook, M. L. Drake, Editor.

5. AFFDL-TR-74-112, "Sonic Fatigue Design Guide For Skin Panels."

DISCUSSION

Mr. Binder (Hamilton Standard): Did most of the curves show data taken at a room temperature of 70 degrees?

Mr. Bouchard: Yes.

Mr. Binder: What degradation in the loss factor would you expect if you made measurements over a 20 degree to 180 degree temperature range?

Mr. Bouchard: I am not exactly sure what it would be for 160 degrees. Our analysis showed we would have a structural loss factor of approximately .05 at 120 degrees. Going to 100 degrees the loss factor might run from 0.1 to .14.

DESIGN OF INTEGRALLY DAMPED SPACECRAFT PANELS

C. V. Stahle and J. A. Staley
General Electric Space Systems Division
Valley Forge Space Center
P.O. Box 8555
Philadelphia, PA 19101

The purpose of this paper is to present the results of preliminary design and analysis studies of damped spacecraft equipment mounting panels. Increased vibroacoustic reliability and reduced program development costs can be achieved by controlling spacecraft equipment vibration during launch. To reduce the significant number of anomalies which occur shortly after launch, component vibration requirements have been increased to provide larger margins. This has resulted in a large number of vibroacoustic test failures during qualification and acceptance tests. A $40 million cost saving is estimated using the OCTAVE code if the equipment vibration environment is reduced 50 percent for an operational satellite system using a MIL-STD-1540 test program. To realize this high payoff, the RELSAT project has been initiated through USAFWAL to develop and demonstrate damping control of satellite launch vibration. A typical satellite equipment panel has been selected and analyzed. The resulting panel design will be fabricated and tested in the near future.

1. INTRODUCTION

Vibration is a major cause of failures occurring during ground vibration tests of spacecraft, spacecraft subsystems, and spacecraft components. A trend of increasing severity of spacecraft launch vibration environments is related to increased acoustic pressure levels at launch. In particular, the Space Transportation System (STS) or shuttle exhibits an increase in sound pressure levels in the low frequency range (below 200 Hz) compared to earlier expendable launch vehicles. A cost/reliability model computer program called OCTAVE (Optimized Cost of Testing for Acoustic and Vibration Environments [1, 2] indicates that significant savings in development and operational costs of a communication satellite system can be achieved if a satellite's launch vibroacoustic environment can be reduced by 50 percent. For a global communication satellite system involving a total production quantity of 14 satellites, this cost savings is estimated to be $40M.

Damping materials have been available and have been used for controlling satellite vibration levels during launch since the early 1970s. Extensive applications have been made to printed wire boards in electronic components to reduce deflections and increase reliability [3, 4]. However, damping treatments have only been applied to a limited number of satellite secondary structures for the purpose of reducing the environments of components attached to these secondary structures [5].

Optimization of damping treatment designs is accomplished using two methods of analysis. Closed form solutions are available which can be implemented on a computer to rapidly examine alternate design configurations [6]. Based on panel cross section geometry, material extensional and shear moduli, damping material loss factor and a wavelength parameter, expressions for system natural frequency and loss factor are obtained. After initial design sizing and establishing trends, more accurate Finite Element Models (FEMs) are used to determine the damping performance and to refine the damped panel design. A NASTRAN modal strain energy method is used to determine the system loss factor [7]. The FEM analysis provides a detailed structure analysis that accurately predicts the dynamic characteristics of the damped panel configuration.

Demonstration programs (RELSAT and PACOSS) are currently underway to show the benefits of damping for improved satellite reliability by reducing launch vibration and shock environments [8, 9] and for increasing orbital damping to assist in control of spacecraft

motions on orbit [10]. These programs, sponsored by USAFWAL, are expected to build on the experience gained to date in applications of damping to spacecraft and other aerospace structures.

2. PAYOFFS FROM EQUIPMENT PANEL DAMPING

Benefits of damping are exhibited in a significant decrease in the large number of ground test and flight failures associated with the launch environment. A significant number of on-orbit failures or malfunctions have been observed during the initial month of spacecraft operation which are believed to be traceable to the vibration environment. Data from a number of NASA spacecraft are shown in Figure 1 obtained from the evaluation of early flight failures [11]. As indicated by the bar graph, approximately half the failure/malfunctions are considered to be traceable to vibration. A significant reduction in the random vibration qualification requirements for components is anticipated. The quantification of damping payoffs is estimated using the OCTAVE code. Figure 2 indicates the models used in OCTAVE for the reliability and cost analyses. Figure 2 indicates that the three major portions of the reliability model are the housekeeping components, structure, and payloads. The housekeeping components are represented by 64 elements made up of 32 pairs of redundant components. The payload is represented by 42 elements which correspond to seven communication channels made up of six elements each.

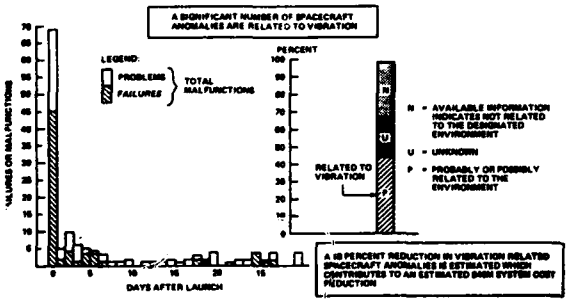

Fig. 1. Spacecraft Flight Failures

The cost model consists of cost elements related to vibroacoustic effects. These include direct costs of design, testing, and weight, as well as probabilistic costs of failures during ground testing and launch. The cost model is based on a decision tree structure of test options, severity of test levels, component strength, and flight stress levels. These options affect the overall system cost and reliability and a design/development test strategy can be developed which minimizes the probable total system cost.

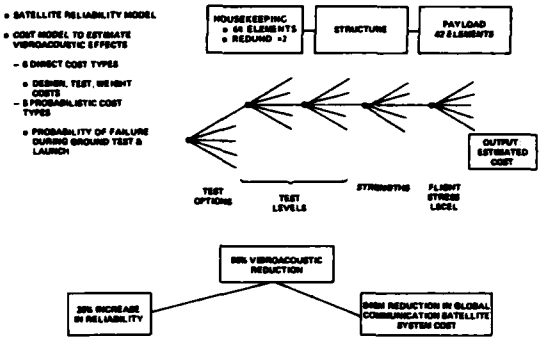

Fig. 2. Quantification of Payoffs

The damping payoff was estimated using OCTAVE with the vibroacoustic changes being reflected in a reduction in the environment. For a reference, the OCTAVE code was used to estimate the Expected Program Cost using a 145 dB acoustic environment. The damping effect was included by reducing the vibration and acoustic environment by 6 dB, i.e., to an effective 139 dB environment.

The flight failure probability (i.e., the probability of losing data from one or more payloads) is estimated to be reduced approximately 20% (0.0048 to 0.0040) by a 50 percent reduction in the launch vibroacoustic environment. The expected cost is shown to be reduced by $2.8M per spacecraft. Considering this savings to be applicable to a complete series of 14 satellites, a total savings on the order of $40M is estimated. Within the modeling simplification constraints of OCTAVE, the dollar payoff should be a valid estimate of the savings that will be obtained.

3. FEASIBILITY OF DAMPED EQUIPMENT PANEL DESIGNS

The feasibility of controlling vibroacoustic response of an equipment panel is illustrated by the analysis and test of a satellite equipment panel. A NASTRAN analysis of a graphite/epoxy constrained layer damping strip applied to a panel which had originally been designed without damping is shown to provide composite loss factors on the order of 0.2 to 0.5 for varying material thicknesses using a modal strain energy estimate (Figure 3). Acoustic tests of the satellite with and without the damping treatment installed showed that the damping treatment reduced the vibroacoustic response at component mounting points by approximately an order of magnitude. Because the damping treatment was added directly to the structure without any modifications of the original structure, a significant weight penalty was imposed. Figure 4 shows the test results for the panel

shown in Figure 3. Results are for response to acoustic tests of two similar panel structures except for the addition of the damper strip. The random vibration response shown near one of the components mounted on the panel is seen to be significantly reduced with the addition of the damper strip.

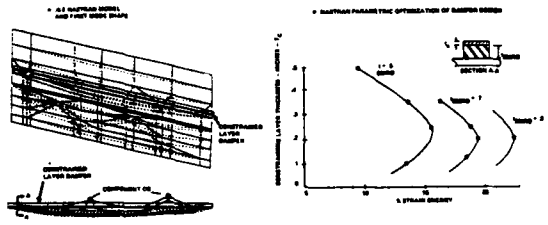

Fig. 3. Optimization of Damping Treatment Using the Modal Strain Energy Method and NASTRAN

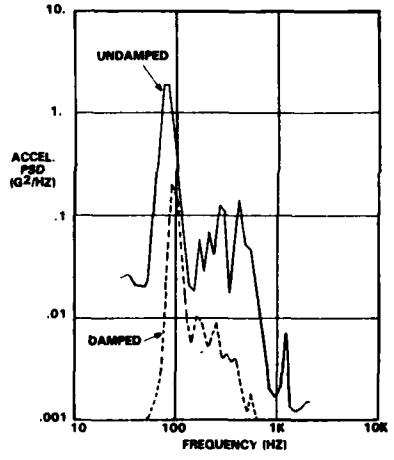

Fig. 4. Panel Acoustic Response With and Without Damping Treatment

4. DESIGN CRITERIA FOR DAMPED EQUIPMENT PANELS

Three types of design criteria are considered for use in design of satellite equipment panel structures. Panel structures designed to criteria based on the assumption of no damping treatment are relatively rigid structures. These panels must be designed for steady accelerations, transient accelerations, and lightly damped vibroacoustic response during launch. Adding damping to these designs after they have been developed is difficult and usually results in large weight penalties. These "add-on" designs are conservative, however, in that the inherent load carrying capability and damping capability are designed separately.

Design criteria for integrally damped panel designs take into account the reduced dynamic loads for the damped structure. A reduction in the weight of the panel structure and the damping treatment (compared to an add-on damping treatment) results.

Design criteria which include both reduced damped panel loads and load sharing by the damping treatment enable least weight designs.

Specific design criteria used to develop panel designs and their damping treatments discussed below are shown in Table 1. For Criterion I, the total design load factor for panels designed ignoring damping is 35G and the resulting panel deflection is 0.105 inches maximum (for the panels discussed in Section 5 below). If damping is added to this design, the component environment will be reduced but the structure will be over designed for the loads it will actually see. For Criterion II, damping is included in the initial panel design and the total load factor is reduced to 23.3G. The damping treatment is not considered to carry any of this 23.3G load, however. For Criterion III, both the reduced load factor due to the damping treatment and any load carrying capability of the damping treatment are taken into account. Damped panels designed using Criterion III should have the least weight.

TABLE 1
Panel Design Criteria

A. LOAD FACTORS

CRITERION	LOAD FACTOR (G)				DEFLECTION
	STEADY (ZERO FREQ)	TRANSIENT (2 HZ)	VIBRO-ACOUSTIC	TOTAL	
I. ADD-ON DAMPING – BASIC PANEL DESIGNED ASSUMING LOW DAMPING	3.0	8.5	23.5	35.0	ABOUT 0.10 INCH
II. INTEGRAL DAMPING – 50% REDUCTION IN VIBROACOUSTIC LOAD – NO LOAD CARRYING CAPABILITY OF DAMPING TREATMENT ASSUMED	3.0	8.5	11.8	23.3	SAME AS I
III. INTEGRAL DAMPING – 50% REDUCTION IN VIBROACOUSTIC LOAD – DAMPING TREATMENT CARRIES TRANSIENT AND VIBROACOUSTIC LOADS	3.0	8.5	11.3	23.3	SAME AS I

B. DAMPING
– FUNDAMENTAL PANEL MODE LOSS FACTOR AT LEAST 0.3
– LOSS FACTOR FOR OTHER MODES UP TO 600 HZ AT LEAST 0.1

5. PRELIMINARY DESIGNS FOR RELSAT

Under the General Electric RELSAT contract with AFWAL, damped panel designs are being developed to simulate an equipment panel which represents Bay 3 of the North Equipment Panel of the Defense Communication System Satellite DSCS-III. Figure 5 shows the North Panel and Bay 3. The primary components on Bay 3 are three traveling wave tube amplifiers (TWTAs). Under the RELSAT contract damped panel designs which represent this panel (Bay 3) will be developed and tested to demonstrate the

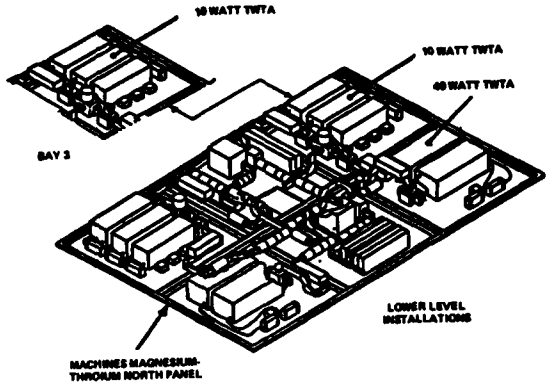

Fig. 5. DSCS-III North Equipment Panel

effectiveness of damping treatments by obtaining performance data under static, low frequency transient, vibroacoustic, and shock loading conditions. Six damped panel designs will be developed and tested along with a baseline panel without damping for reference. Figure 6 shows the results of a study using a simplified method [6] to perform parametric studies to obtain trends for damping treatment sizing. Results are shown in the form of a plot of system loss factor and natural frequency for the fundamental mode of a damped panel which corresponds to Bay 3 of the DSCS-III North Panel mentioned earlier. Results are shown as a function of viscoelastic layer and constraining layer thicknesses for five constrained layer damper strips attached to the panel. The possibility of achieving fundamental mode loss factors of the order of 0.70 is indicated for a 0.50 inch thick viscoelastic layer and a graphite/epoxy constraining layer of the order of 0.10 inch thick. The surface area used by this damping treatment is about 5 percent of the area of the panel which is about 25 by 25 inches square.

5.1 Damped Stiffener Concepts

Figure 7 shows a finite element model for the same panel without any damping treatment. The TWTAs are connected to the panel by rigid elements and are represented as lumped masses at their CGs. The baseline panel is essentially made up of a plate with two stiffeners. Figure 8 shows the same baseline panel with constrained layer damper strips added to the stiffeners and two additional constrained layer damper strips attached directly to the plate and running parallel to the long axis of the TWTAs. This design is an add-on damped stiffener design.

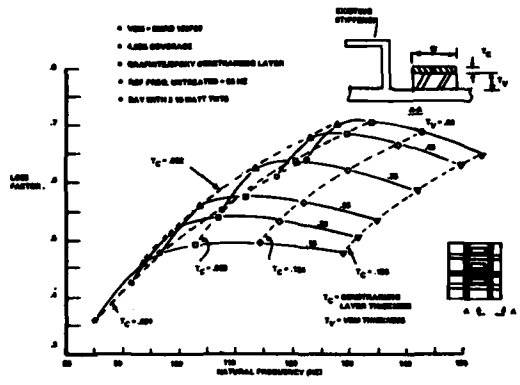

Fig. 6. Parametric Results for Loss Factor and Natural Frequency

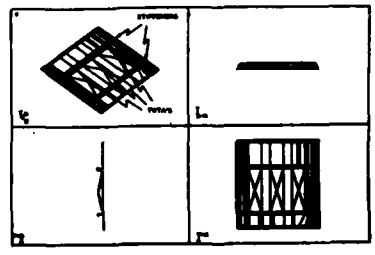

Fig. 7. Undamped Panel With Stiffeners

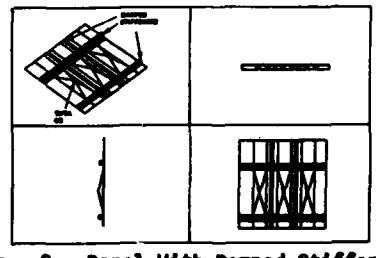

Fig. 8. Panel With Damped Stiffeners

Figure 9 shows a typical detail of the integrally damped stiffeners developed using Criterion II. The basic panel stiffener is a hat section. On top of this is attached a thin viscoelastic layer of SMRD 100F90. On top of this layer is a graphite/epoxy constraining layer. SMRD 100F90 has a shear modulus of about 4000 psi and a loss factor of about 1.0 at room temperature and 100 Hz.

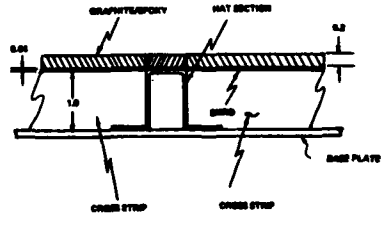

Fig. 9. Damped Stiffener Details

Figure 10 shows the damping performance for North Panel Bay 3 designs with stiffeners designed to the three criteria in Table 1. The damping levels achieved indicate that the damping criteria can generally be met and that reductions of vibroacoustic response of 50 percent can be expected. The panel structure weights including damping treatment indicated in Figure 10 show that damping can be included in integrally damped panel designs without producing a weight penalty.

5.2 Damped Sandwich Panel Concepts

Figure 11 shows a damped sandwich panel concept for the North Panel Bay 3. This concept used a sandwich base panel which supports the three TWTAs. A thin layer of a viscoelastic damping material 3M ISD112 is attached to the base panel. ISD112 has a shear modulus of about 100 psi and a loss factor of about 1.0 at room temperature and 100 Hz. A constraining sandwich is then attached to the viscoelastic material. The base sandwich has aluminum face sheets and an aluminum honeycomb core. The constraining panel has graphite/epoxy face sheets with an aluminum honeycomb core. Figure 12 shows the damping achieved using the damped sandwich concept using Criteria II and III of Table 1.

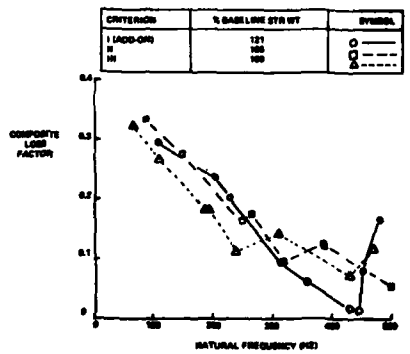

Fig. 10. Damping Performance - Panel With Damped Stiffeners

6. CONCLUSIONS

The conclusions from material presented in this paper are that:

1. A need exists for reducing the vibration related failures which occur during launch and ground vibration testing;
2. The OCTAVE code shows that application of damping treatments can significantly reduce the development cost and increase the reliability of satellites;
3. The analytical tools are available for performing preliminary and detailed designs of damping treatments for spacecraft equipment support structures;
4. Preliminary designs have been developed for damped equipment panels which meet structural load carrying and damped requirements; and
5. Both damped stiffener concepts and damped sandwich concepts can be used to meet these requirements.

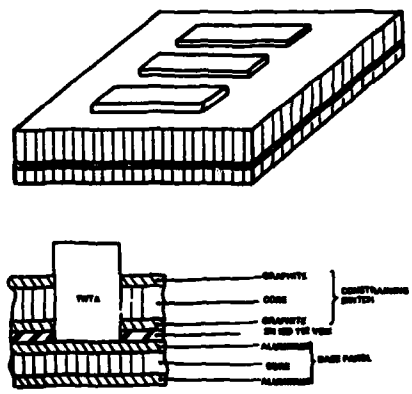

Fig. 11. Damped Sandwich Panel Concept

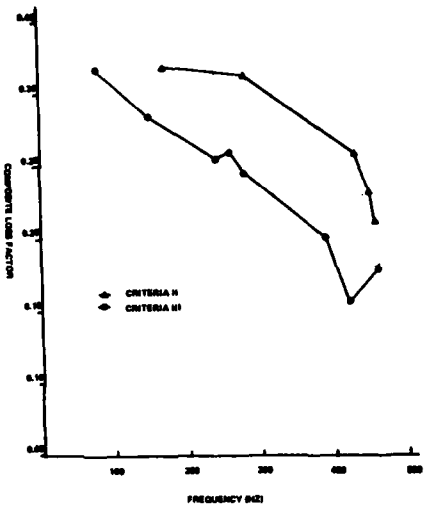

Fig. 12. Graph of Composite Loss Factor Vs. Frequency For the Two Integrally Damped Sandwich Panels

REFERENCES

1. C. V. Stahle, H. R. Gongloff, J. P. Young, and W. B. Keegan, "Shuttle Payload Minimum Cost Vibroacoustic Tests," Proc. 1977 Annual Rel. and Maint. Symp.

2. C. V. Stahle, "Cost Effectiveness of Spacecraft Vibration Qualification Testing," Proc. of Inst. of Env. Sci., 20th Annual Mtg., May 1974.

3. J. M. Medaglia, "Dynamic Integrity Methods Including Damping for Electronic Packages in Random Vibration," 50th Shock and Vib. Bull., 1980.

4. C. V. Stahle, A. T. Tweedie, and T. M. Gresko, "Viscoelastic Epoxy Shear Damping Characteristics," Shock and Vib. Bull., No. 43, 1973.

5. J. M. Medaglia and C. V. Stahle, "SMRD Damping Applications," SAMPE Series Volume 25, 1980, pp. 90-102.

6. F. Abdulhadi, "Transverse Vibrations of Laminated Plates With Viscoelastic Layer *Damping*," *Shock and Vib. Bull., No. 4, Dec.* 1969.

7. L. C. Rogers, C. Johnson, and D. A. Kienholz, "Finite Element Predictions of Damping in Beams With Constrained Viscoelastic Layers," Proc. of 22nd Struct. Dyn. and Mat. Conf., May, 1981.

8. J. A. Staley and C. V. Stahle, "Damping in Support Structures for Equipment Reliability - RELSAT," Vibration Damping Workshop, Feb., 1984.

9. R. Ikegami, W. J. Walker, and C. J. Beck, "Application of Damping to Improve Reliability of IUS Type Satellite Equipment - RELSAT Program," Vibration Damping Workshop, Feb., 1984.

10. C. W. White and G. Morosow, "Passive and Active Control of Space Structures (PACOSS)," Vibration Damping Workshop, Feb., 1984.

11. A. R. Timmins and R. E. Heuser, "A Study of First Day Space Malfunctions," NASA TND-6474, 1971.

A DIFFERENT APPROACH TO "DESIGNED IN" PASSIVE DAMPING

M. L. Drake
University of Dayton
Research Institute
Dayton, Ohio

In the past, most damping applications were additive designs used to solve field problems [1,2,3]. Today, designers are beginning to consider integral (designed in) damping systems [4,5,6,7]. This change in emphasis in damping design will change the market in damping materials. Soon the damping material vendor will be supplying damping materials in bulk form (sheets, rolls, uncured gum) to the structural system manufacturers. Since the damping materials will be required in bulk form, the possibility of ordering a custom formulated material exits. This paper will demonstrate a method to develop the required damping material properties, discuss formulation changes usable to adjust the damping material properties, and discuss the benefits of such design procedures.

Background

The author has assumed that the reader has a basic understanding of constrained layer damping systems and the design of these system [8]. However, there are two equations which add understanding and meaning to what follows. The first equation is the strain energy representation of modal loss factor [9].

$$\eta_s = \frac{\sum_{i=1}^{n} \eta_i W_i}{\sum_{i=1}^{n} W_i} \qquad (1)$$

where W_i = energy stored in component i

η_i = loss factor for component i

in most cases, only a single component has appreciable damping, then Eq. 1 simplifies to

$$\eta_s = \frac{\eta_D W_D}{\sum_{i=1}^{n} W_i} = \frac{D_s}{U} \qquad (2)$$

Eq. 2 simply tells us that for any successful damping design the damping system must store a reasonable amount of the total system energy.

The second equation to be reviewed is the equation for the energy dissipated per cycle [10]

$$D_s = \pi \int_{vol} \eta_D G_D \gamma^2 \, dV \qquad (3)$$

where G_D is the damping material shear modulus, and γ is the instantaneous strain. There are two types of terms in Eq. 3. η_D and G_D are material terms; while, γ^2 is related to a geometry term (also a function of mode shape).

Damping Design Methods

Eq. 2 states that the greater the energy dissipated, the higher the modal loss factor. From Eq. 3, there are two ways to optimize D_s:

1) fix the material properties and optimize D_s through geometric consideration or,

2) fix the geometry and optimize the material parameter.

By enlarge, the first approach is the "standard approach" and the one used most often for the "solve the field problem" damping design. The basic steps in this design approach are:

1) Develop an analytical model of the system or component of interest;

2) determine the temperature and frequency range of interest;

3) choose a damping material with good damping across the temperature and frequency range required; and

4) use analysis to determine damping system configuration to obtain required system damping.

Referring to equation 3, and realizing that η_D and G_D are now defined, it can be seen that the essence of this design effort is adjusting the geometry of the constrained layer system until the shear energy term is sufficient to provide the required system loss factor. It is a proven fact that there is a combination of a specific G_D and damping system geometry which results in an optimum shear parameter [11]. The problem may be solved before this optimum is obtained. The standard design approach has proven successful in the past, but there are two primary disadvantages. First the damping design geometry required for sufficient system damping may not meet the non-damping system constraints, such as; (1) total system weight, 2) dimensional fit, 3) aerodynamic shape, etc. Second, since strain energy is mode shape dependent and η_D and G_D are frequency dependent, the damping design is usually useful over a limited frequency range.

The second approach to optimize the energy dissipated will be called the "Alternate Approach." This approach consists of the following steps:

1) Develop a damping design window or geometry which meets all the non-damping system requirements;

2) develop analytical model of the damped system and determine maximum system damping possible for that design;

3) if step 2 indicates sufficient damping, use the analytical model to determine damping material properties as a function of frequency required;

4) find or formulate the required material.

The alternate approach immediately appears more practical because at the outset the design will meet the nondamping requirements. Several other advantages which at this point are not so obvious are:

1) a single constrained layer design provides near optimum damping over a large frequency range,

2) the damping system is a minimum weight design,

3) a single constrained layer design reduces installation costs.

Alternate Approach Illustrations

The following example problems illustrate the use of the alternate design approach through the development of the required damping material properties.

The first example is for a symmetric sandwich beam pinned at both ends as shown in Fig. 1. The beam is

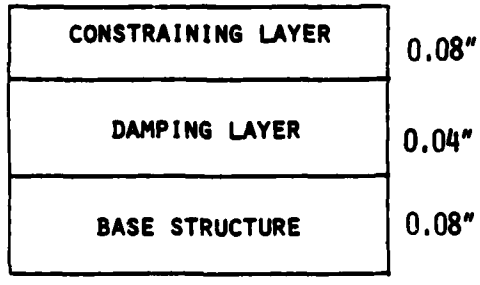

Fig. 1 First Damping System Model

twelve inches long with aluminum face sheets 0.08 inches thick. The damping layer is taken to be 0.04 inches thick. The analysis technique used here will be fourth order beam theory; however, finite elements or any other analysis technique will provide similar results [12,13,14]. In the analysis, the damping material loss factor is assumed to be one and the shear modulus is varied. The results of the analysis for the first five resonant modes of the beam are shown in Fig. 2. Note that the maximum modal damping for each mode is the same 0.299; however, the damping material shear modulus required for maximum damping increases with

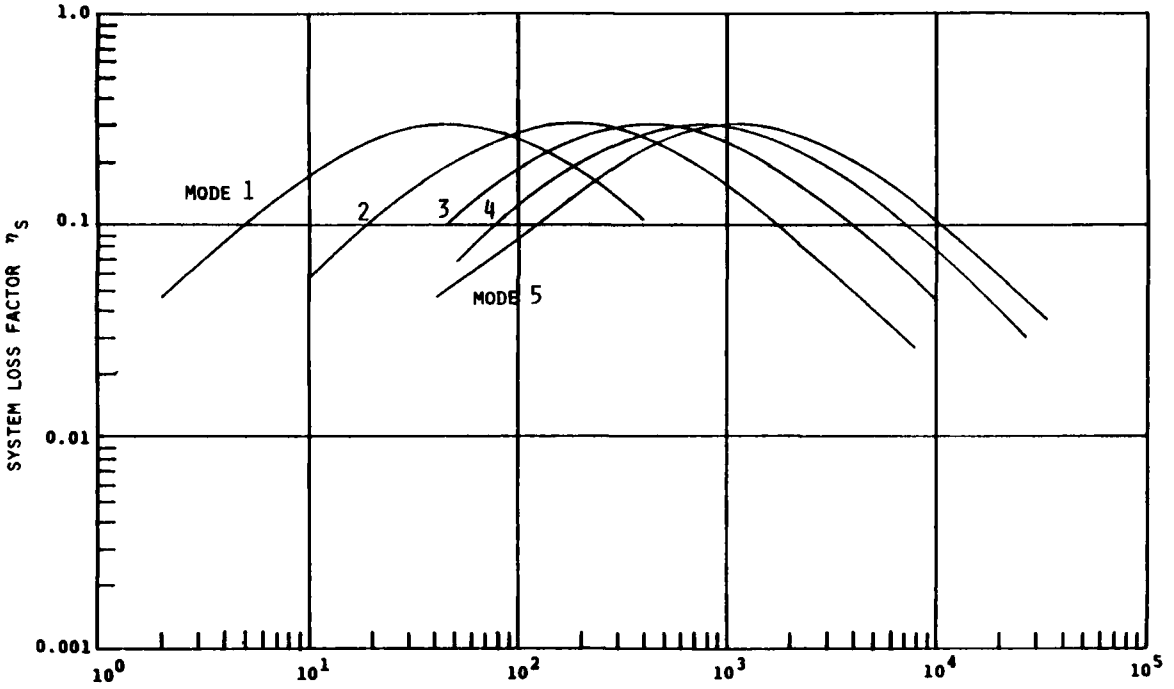

Fig. 2 Damp Material Shear Modulus (PSI)

Table 1
Loss Factor, Modulus and Frequency Data For Model 1

MODE NUMBER	η_{MAX}	FREQUENCY AT η_{MAX}	SHEAR MODULUS (PSI) AT η_{MAX}
1	0.299	67.7	40.0
2	0.299	267.4	150.0
3	0.299	630.0	425.0
4	0.299	1,118.4	750.0
5	0.299	1,740.9	1,150.0

frequency. Table 1 presents the resonant frequency data for the first five modes. Obviously, if a damping material could be found with the proper modulus versus frequency characteristics, optimum damping could be obtained in all five modes. In most problems, the maximum possible damping is not required, if one assumes that 80 percent of η_{max} is sufficient to solve the current problem then Fig. 3 can be generated. Fig. 3 defines the damping material shear modulus as a function of frequency for both the maximum damping attainable for this configuration and the modulus limits within which a minimum of 80 percent maximum damping will occur. With this data the search

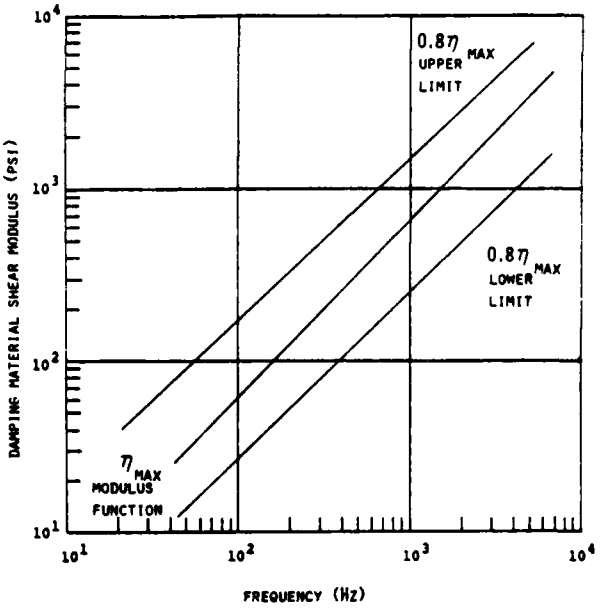

Fig. 3 Shear Modulus - Frequency Characteristics For Maximum Damping

for or development of the required damping material can begin. To illustrate the use of this data in the material selection procedure, four materials will be evaluated. Fig. 4 shows shear modulus versus frequency

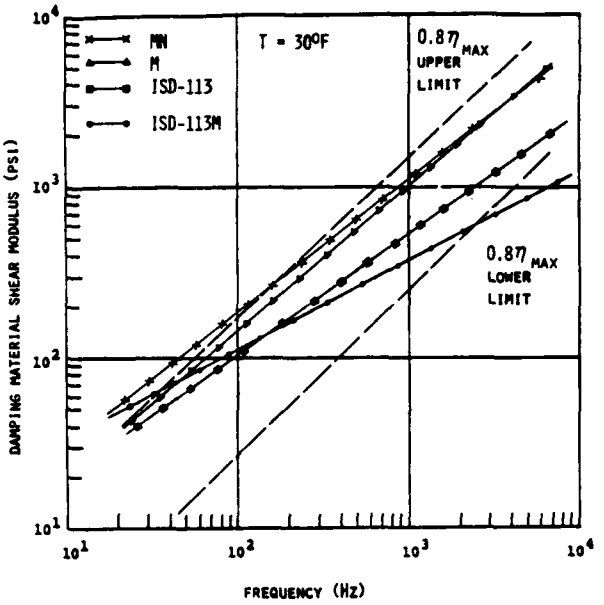

Fig. 4 - Shear Modulus - Frequency Characteristics For Maximum Damping

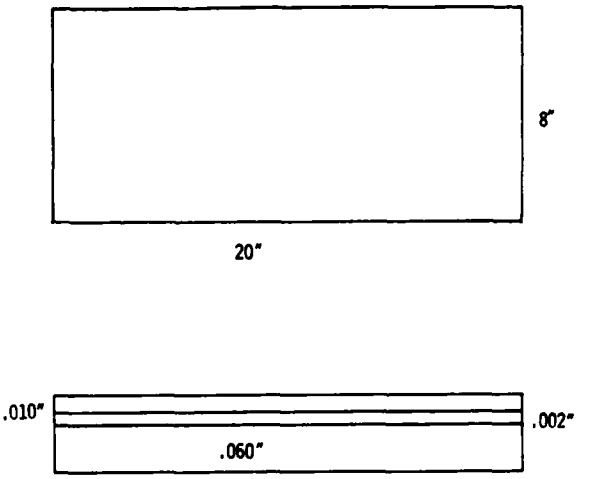

Fig. 5 Model for Second Example

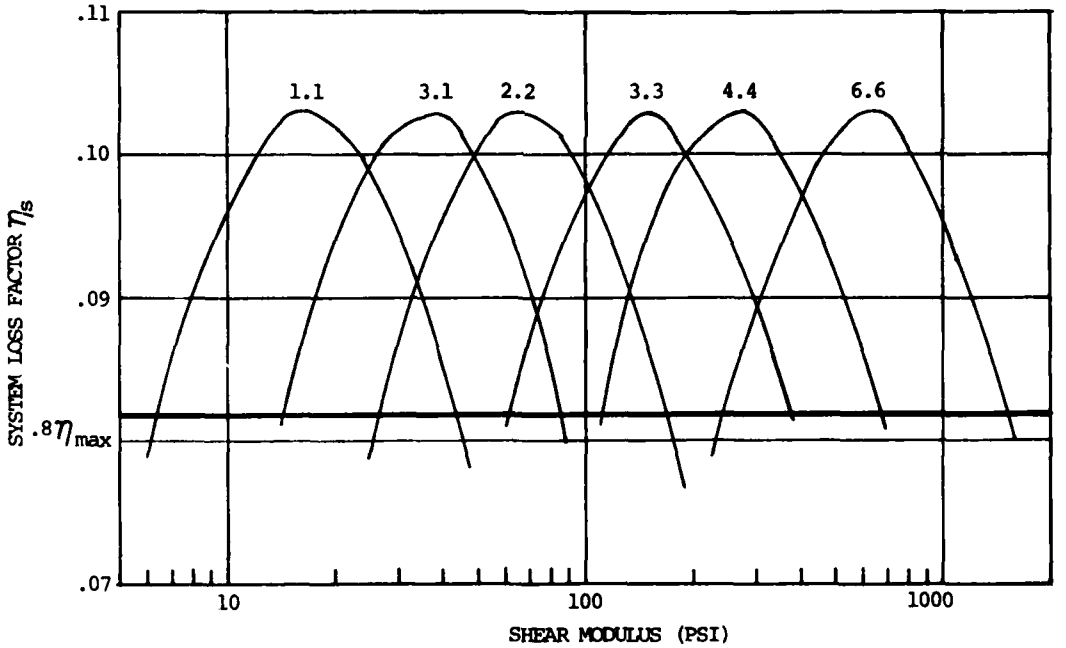

Fig. 6 System Loss Factor VS Damping Material Shear Modulus for Example Number 2.

plots of the four commercial damping materials superimposed on the modulus limits just established. Soundcoat MN is a modified version of Soundcoat M, while 3M ISD-113M is a modified version of ISD-113. For this example, the unmodified materials are inside the modulus limits over the frequency range of interest and, providing the loss factors are acceptable, should provide the required system damping.

The second example problem is shown in Fig. 5. The system is an aluminum flat plate 20.0 inches long, 8.0 inches wide and 0.06 inches thick. The damping layer is 0.002 inches thick with an aluminum constraining layer

0.01 inches thick. The analysis was again completed using fourth order theory and assuming a damping material loss factor value of one. Fig. 6 shows the modal loss factor for several plate modes as a function of damping material shear modulus. Note that the maximum modal damping is again equal for all modes and as the frequency increases so does the shear modulus for maximum damping. Table 2 further illustrates

Table 2
Loss Factor, Modulus and Frequency Data For Model 2

MODE NUMBER	η_{MAX}	FREQUENCY AT η_{MAX}	SHEAR MODULUS (PSI) AT η_{MAX}
1,1	.103	105.1	15
2,1	.103	150.3	25
3,1	.103	224.9	40
4,1	.103	326.0	55
2,2	.103	422.5	65
5,1	.103	450.5	65
3,2	.103	499.5	85
7,1	.103	793.2	120
3,3	.103	953.0	150
4,4	.103	1697.0	275
5,5	.103	2639.0	400
6,6	.103	3831.0	650

these points for the plate modes given. Using the data given in Fig. 6 and Table 2, a damping material could be chosen such that all the modes between 100 Hz and 3900 Hz were damped to the maximum level possible by the current damping configuration. If one again assumes that eighty percent of η_{max} is sufficient, a set of modulus limits as a function of frequency can be generated as shown in Table 3. Plotting the data in Tables 2 and 3 results in Fig. 7. Fig. 7 defines the damping material shear modulus required for acceptable damping as the problem is defined. Now the search for a material or material modification can begin.

The results of comparing the same four material used in the first example to this example are considerably different. Fig. 8 shows the shear modulus versus frequency of the four materials and the second example modulus requirements. As can be seen, none of the materials are acceptable over the entire frequency range. The modification to ISD-113 has improved the materials performance; however,

Table 3
Modulus Range For $\eta_s \geq .8\eta_{max} = .0824$

MODE NUMBER	LOWER MODULUS LIMIT (PSI)	UPPER MODULUS LIMIT (PSI)
1,1	6.4	43.5
2,1	10.0	60.0
3,1	14.4	85.0
4,1	20.0	130.0
2,2	26.5	170.0
3,2	30.0	200.0
3,3	61.0	375.0
4,4	112.0	670.0
5,5	175.0	1050.0
6,6	241.0	1500.0

additional changes are definitely in order. The change from M to MN is in the wrong direction for this particular problem; however, note the modulus line slope of M. If M could be softened it would appear that the modification would fit the entire frequency range.

Material Modification Techniques

Once the designer has defined the required damping material properties the rest is up to the chemists. Only in special cases would the cost of a completely new material development program be justified. The intent here is to discuss general methods for minor tailoring of the modulus properties.

There are three primary ways to tailor the damping materials [15]. These are:

1) addition or reduction of fillers,

2) addition or reduction of crosslinking agents, and

3) addition or reduction of plasticizers.

The effects of adding fillers to a material are shown in Fig. 9. Increasing filler level increases the modulus across the temperature range and also causes an increase in the glass transition temperature. Fig. 10 illustrates the effects of filler level on the modulus of a butyl rubber compound. Fig. 11 shows the effects on loss factor for the same material. Note the positive effect of the filler through the broadening of the loss factor peak [16].

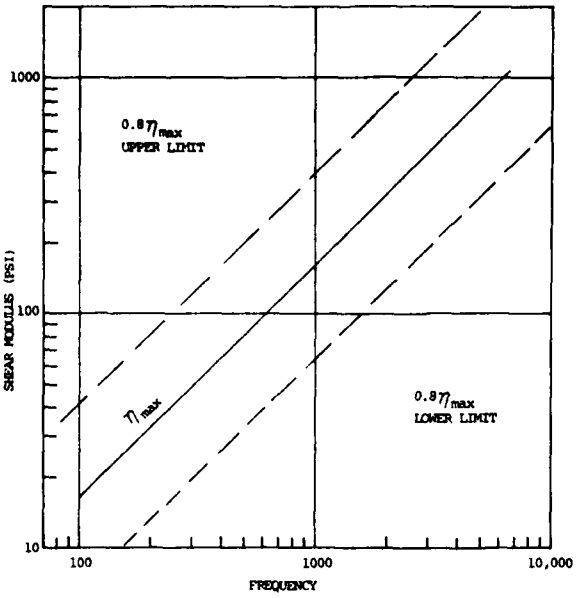

Fig. 7 Damping Material Shear Modulus VS Frequency For Maximum and 80% Maximum System Damping

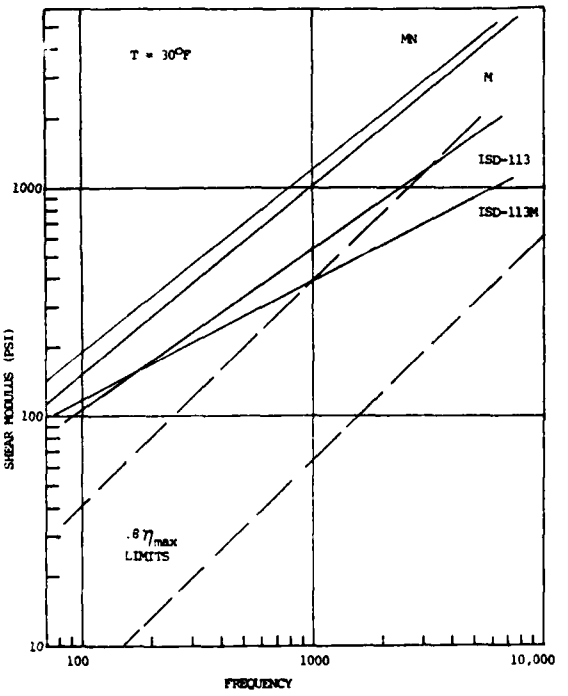

Fig. 8 Commercial Damping Material Modulus Data Compared to Design Modulus Limits

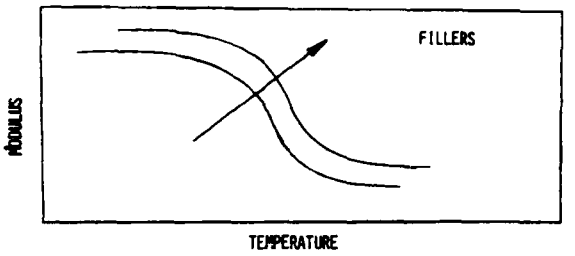

Fig. 9 The Effects of Fillers on Modulus

The effects of varying crosslinking in a material is shown in Fig. 12. The primary effect is to adjust the rubber modulus value, however, it is a known fact that increasing crosslinking reduces the material loss factor [16].

The effects of adding plasticizers is illustrated in Fig. 13. Plasticizers can be used to adjust the glass transition temperature; however, the addition of large amounts of plasticizers often makes a material unstable.

Summary and Conclusions

An alternate design procedure has been discussed which is very useful for either developing an integrally damped system or for developing a damping design where nondamping constraints limits the geometric size of the damping system.

The design approach determines the maximum system damping possible and the required damping material modulus as a function of frequency. A distinct advantage of this approach is that a single constrained layer damping design can provide maximum damping for all the resonant modes of concern which is impossible using the standard design approach. A disadvantage of the procedure is that no two damping designs use the same material; however, the same base material would form the starting point for many designs.

As damping design moves in to the initial design procedure and structural system are built with damping incorporated, damping materials will be supplied in bulk form. The advantages of custom formulated materials are:

1) complete frequency coverage from a single constrained layer damping system,

2) reduced damping system weight,

3) reduced damping system manufacturing costs and,

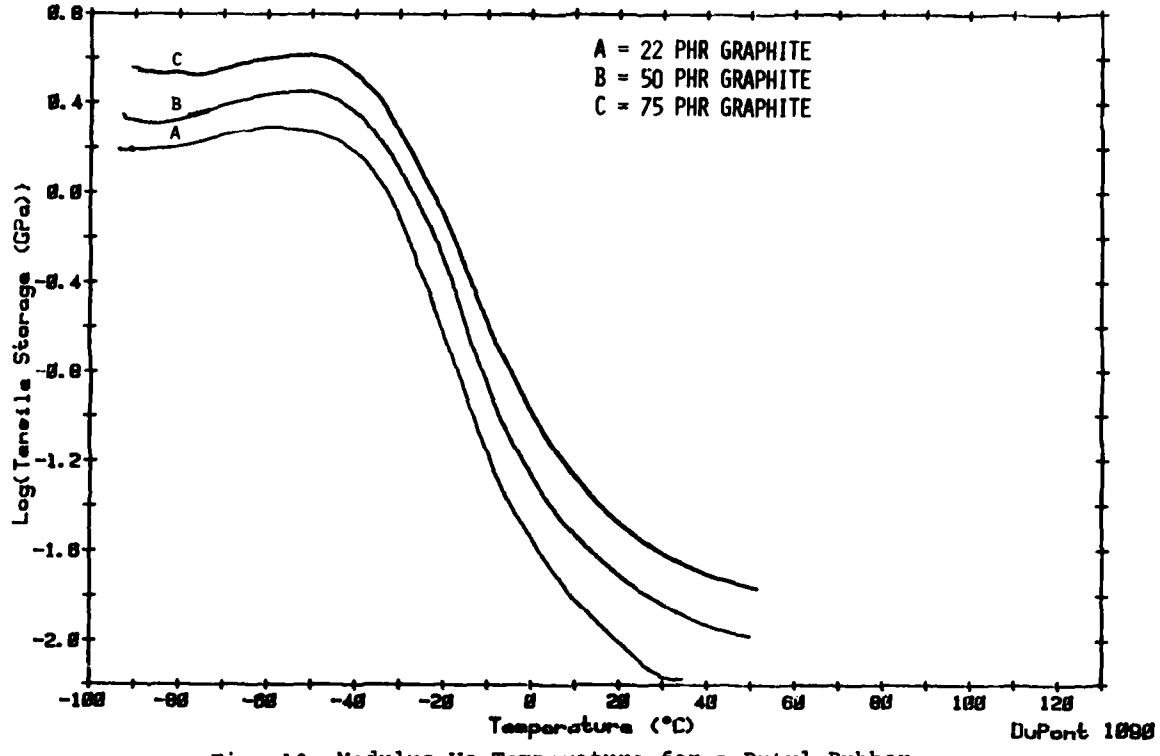

Fig. 10 Modulus Vs Temperature for a Butyl Rubber with Three Different Levels of Fillers

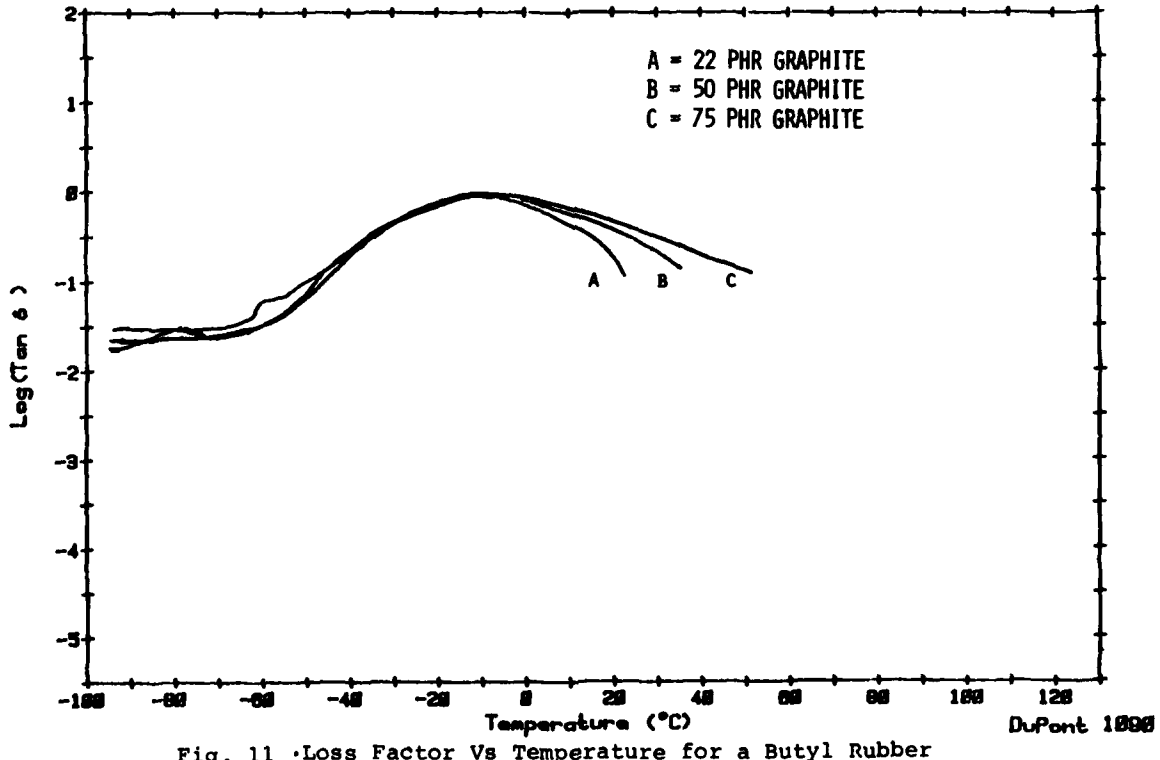

Fig. 11 Loss Factor Vs Temperature for a Butyl Rubber with Three Different Levels of Fillers

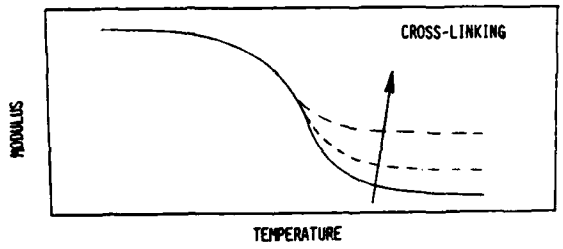

Fig. 12 The Effects of Cross-Linking on Modulus

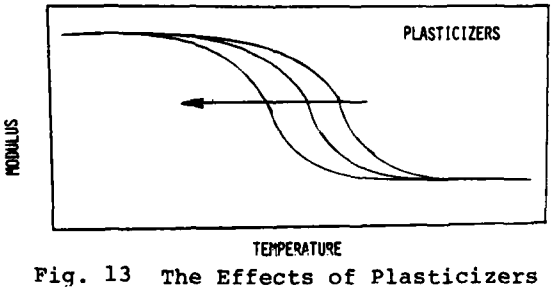

Fig. 13 The Effects of Plasticizers on Modulus

4) reduced damping system application costs. The disadvantages is increased damping material costs.

Acknowledgements

The author wishes to acknowledge the help of Dr. R. P. Chartoff and Mr. I. Salyer in developing many of the ideas expressed in this paper. The author also wishes to thank Mrs. J. Glover for turning my hieroglyphics into this manuscript and Howard Watkins for completing the artwork.

References

1. L.C. Rogers And M.L. Parin, "A Thoroughly Engineered Application of Damping Technology to Jet Engine Inlet Guide Vanes," (L. Rogers, ed.) from Conference on Aerospace Polymeric Viscoelastic Damping Technology for the 1980's. AFFDL-TM-780 78-FBA, July 1978.

2. M.L. Drake and J.D. Sharp, "An Example of Additive Damping as a Cost Savings Alternative to Redesign," presented at Winter Annual Meeting ASME Turbine Division, Atlanta, Georgia, Nov. 27-Dec. 2, 1977.

3. R.N. Miles, "Beam Dampers for Skin Vibration and Noise Reduction in the 747," presented Vibration Damping Workshop sponsored by AFWAL, Long Beach, California, February 17-19, 1984.

4. Charles W. White, "Passive and Active Control of Space Structures (Pacoss) presented Vibration Damping Workshop sponsored by AFWAL, Long Beach, California, February 17-19, 1984.

5. J.A. Staley and C.V. Stahle, "Damping in Support Structures for Satellite Equipment Reliability - Relsat presented Vibration Damping Workshop sponsored by AFWAL, Long Beach, California, February 17-19, 1984.

6. R. Ikegami, C.J. Beck, and W.J. Walker, "Application of Damping To Improve Reliability of IUS-Type Satellite Equipment - Relsat Program presented Vibration Damping Workshop sponsored by AFWAL, Long Beach, California, February 17-19, 1984.

7. M.F. Kluesener, and D.R. Oeth, "The Dynamic Behavior of Advanced Fan Materials," - A Review and Summary of the Air Force Materials Laboratory Damped Fan Blade Program,"presented at ASME Conerence on Mechanical Vibration and Noise, Cincinnati, Ohio, Sept. 11-13, 1985.

8. University of Dayton Vibration *Damping Short Course* Notebook, 1983.

9. C.D. Johnson, D.A. Kienholz, and L.C. Rogers, "Finite Element Prediction of Damping in Beams with Constrained Viscoelastic Layers," The Shock and Vibration Bulletin, Vol 51, part 1 pp.71-82, May 1981.

10 B.J. Lazan, Damping of Materials and Members in Structural Mechanics. Pergamon Press, New York 1968.

11. D.K. Rao, "Frequency and Loss Factors of Sandwich Beams Under Various Boundary Conditions," Journal of Mechanical Engineer Science, Vol. 20, No. 5, 1978.

12. D. Ross, E.E. Ungar, and E.M. Kerwin, Jr.,"Damping of Plate Flexural Vibrations by Means of Viscoelastic Laminae," Section III of Structural Damping, ASME, pp. 49-88, 1959.

13. M.F. Kluesener, "Practical Methods of Applying Finite Element Analysis to the Design of Complex Damped

Structures," AIAA paper No. 84-0971-CP, Presented at the SDM Conference, Palm Springs, California, May 14-16, 1984.

14. C.D. Johnson and D.A. Kienholz, "Finite Element Design of Viscoelastically Damped Structures-- Methods presented Vibration Damping Workshop sponsored by AFWAL, Long Beach, California, February 17-19, 1984.

15. D. Klempner, H.K. Yoon, K.C. Frisch, and H.L. Frisch, "Chemistry and Properties of Crosslinked Polymers," p. 243. Ed. S.S. Labana, Academic Press, New York, 1977.

16. L.E. Nielson, "Damping and Mechanical Properties of Filled Polymeric Systems," in Proceedings of the Workshop on Acoustic Attenuation Materials Systems, National Maerials Advisory Board, National Academy of Sciences, Report No. NMAB-339, p. 63, Washington, D.C., 1978.

ANALYSIS OF DAMPED TWIN TOWERS

C. W. White
Martin Marietta Denver Aerospace
Denver, Colorado 80201

This paper presents the procedure used to design two viscoelastically damped 60-ft tall generic test towers. It describes how the Modal Strain Energy (MSE) approach was used to identify favorable locations in these towers for viscoelastic structural members and for discrete viscoelastic damper mechanisms. The use of standard viscoelastic material (VEM) property data to design the discrete dampers is illustrated. Testing procedures and data reduction required for theoretical experimental correlation are described at both the VEM element and truss system levels.

INTRODUCTION

The next generation of orbital spacecraft will be very large, have low mass density, and be highly flexible. As a result, they will have many low frequency modes. It is likely that mission requirements will produce control system designs that couple strongly with the structure in the low frequency region. Suppression of structural vibration by use of passive damping can be a great aid in the design of a stable control system.

Viscoelastic material has been used to suppress vibration in many structures. Most of these, however, have been small and stiff by comparison to large space structures (LSS), and the method of application has been either free or constrained layer. Existing technology may not be readily adaptable at LSS frequencies and in a space environment. Therefore, before funds are committed to passively damp a specific large spacecraft, the successful applicability of existing technology to a less expensive, but convincingly similar structure, must be demonstrated. It is the purpose of this paper to provide that demonstration and to record the technology used so that it may be applied in the design of a real large space structure.

ORGANIZATION SUMMARY

A brief discussion of the demonstration structure and why it was selected is given. Then, the modal characteristics of the undamped structure are presented, along with application of the Modal Strain Energy (MSE) method of selecting effective locations for discrete viscoelastic material (VEM) dampers. Having selected the damper locations, the method of damper design using existing VEM modulus and loss factor data is shown. Next, hysteresis testing of component structure performed to aid in system structure theoretical/experimental correlation is presented. Finally, the system structure test and the correlation of those results with the theoretical predictions are discussed.

THE DEMONSTRATION STRUCTURE

The first step was to choose a structure that would economically allow the side-by-side damping comparison test of two structural materials with measurably different damping exercised in the frequency range expected on LSS. The chosen structure was the small truss described by Fig. 1. This configuration has been named the Small Generic Test Article (SGTA). Lexan and Plexiglas were the low and high damping materials, respectively. The log decrement method [1] of determining damping of each truss from the response to an initial tip displacement (Fig. 2) was used to determine that the Plexiglas truss has 7.1% damping, but the Lexan truss has only 0.75% damping.

This result encouraged continuation to the second step which was construction of the Large Generic Test Article (LGTA), a large-scale version of Fig. 1 trusses. This larger version was required to demonstrate that construction tolerances, higher joint loads, and near buckling conditions did not introduce additional damping of the order of magnitude produced by the high damping material. It also provided a convincing demonstration that significant damping can be designed into large structures. A modification of the SGTA damper arrangement was made on the LGTA. All dampers were placed in two parallel planes on the truss. No dampers were placed on the remaining two planes. This arrangement of two trusses allowed evaluation

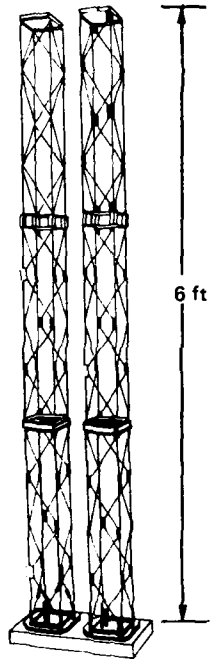

Fig. 1 - Small Generic Test Article

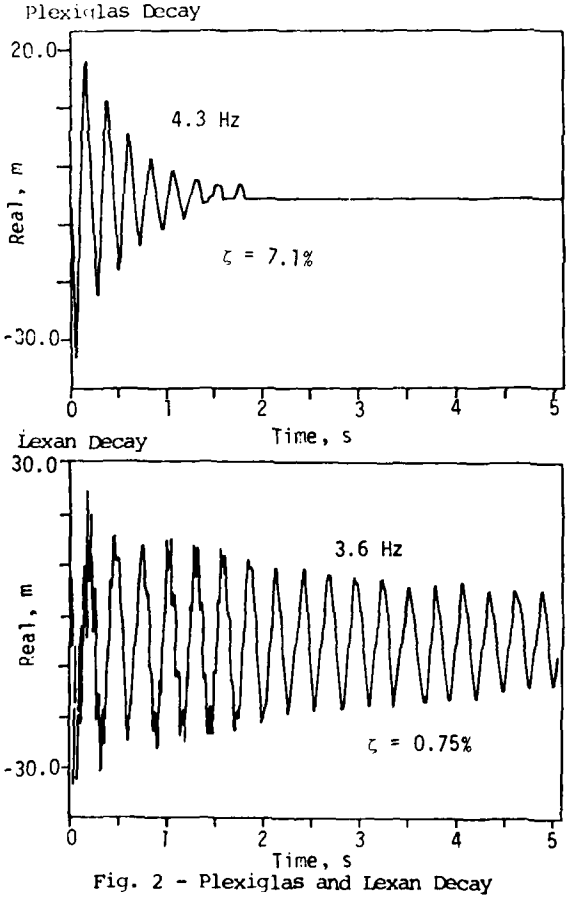

Fig. 2 - Plexiglas and Lexan Decay

of four configurations: low damping material, high damping material, low damping material with discrete dampers, and high damping material with discrete dampers. Fig. 3 shows the LGTA truss which is 60-ft tall.

One additional deviation from the SGTA was required to produce a LGTA that would survive in Earth's gravity field: the vertical members of the truss had to be constructed of aluminum rather than Lexan or Plexiglas, because those materials would not support their own weight in the LSS-like configuration. (Most LSS would not survive in Earth's gravity.) The discussion of modal strain energy, given below, will show that this necessary concession greatly reduced the amount of damping achievable in the structure.

MODAL CHARACTERISTICS OF UNDAMPED STRUCTURE

A standard finite element modeling program was used to model the Plexiglas LGTA truss using beam elements with 6 degrees-of-freedom (DOFs) displacement matching of all beams at all joints. This fixity was judged representative, as all joints were either welded, cemented, or double bolted. Plexiglas diagonals were modeled using handbook values for the modulus of elasticity. Various section properties were used until one was found which resulted in a model with acceptably low frequency (in the LSS range) and significant strain energy in the Plexiglas elements. These requirements were satisfied using 1.5-in. tube with 1/8-in. thickness. No discrete damper elements were modeled at this time.

The reason for the requirement of significant strain energy in the VEM (Plexiglas) becomes clear by a brief review of the Modal Strain Energy method of VEM application [2, 3]. Its mathematical statement is simply stated in Ref. [3] and is repeated here for convenience.

$$n_{sr} = n_v V_{vr}/V_{sr} \qquad (1)$$

where

n_{sr} = loss factor for the r^{th} mode of the composite structure

n_v = material loss factor for the viscoelastic material

V_{vr} = elastic strain energy stored in the viscoelastic material when the structure deforms in its r^{th} undamped mode shape

V_{sr} = elastic strain energy of the entire composite structure in the r^{th} mode shape.

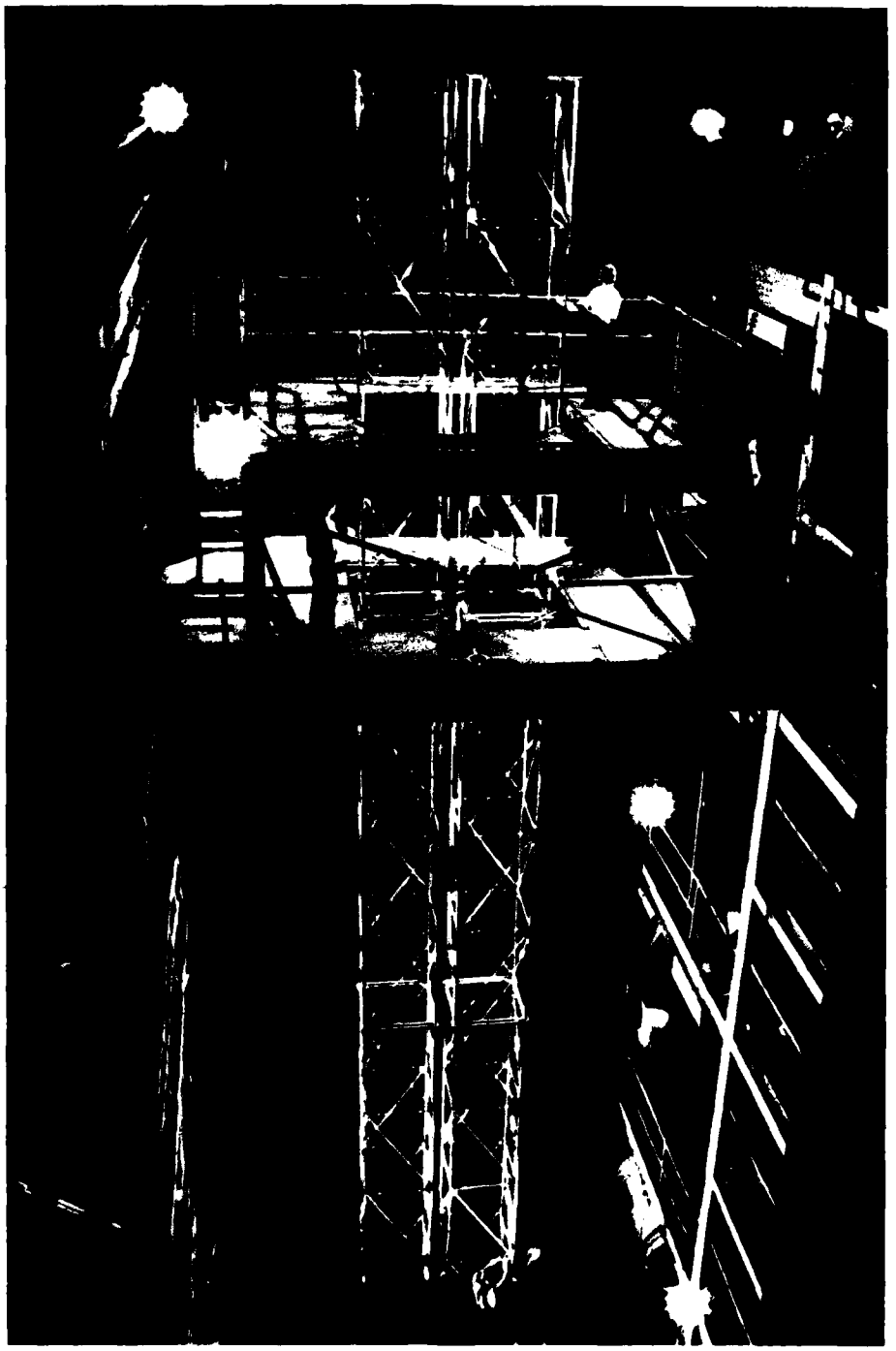

Fig. 3 - Large Generic Test Article
60-ft Tall Truss

That is, the greater the percentage of total strain energy that is stored in the VEM, the more effective the damping treatment. A detailed explanation of the calculation of strain energy distribution is given in Ref. [4]. The calculation of strain energy in this model was provided by an output option of a finite element program used to calculate modal characteristics. Fig. 4 depicts the percentage of fundamental mode strain energy in the diagonal Plexiglas elements in each bay of the truss. Two important observations are made from this figure:

1) The total Plexiglas strain energy is only 34.68%, therefore, the remaining energy, 65.30% in the vertical aluminum truss members, is not available for dissipation via the higher loss modulus of the Plexiglas. (Further application of constraint layer damping on the aluminum members is possible, but has not been done.)

2) Most of the Plexiglas member strain energy is, as one would expect, in the lower diagonals; thus, the lower diagonals are the most effective locations for discrete dampers which introduce VEM having a larger loss factor than that of Plexiglas. The following section addresses the design of such a damper.

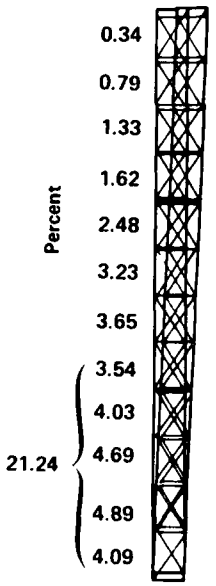

Fig. 4 - Percent Strain Energy Distribution in Diagonals, Fundamental Bending Mode of LGTA Without Discrete Dampers

DISCRETE VEM DAMPER DESIGN

Fig. 5 presents a sketch of the discrete damper configuration chosen to replace the Plexiglas (and Lexan) links in parallel planes of the five lowest truss bays. Thus, ten of these dampers were installed in each truss. The damper configuration was an obvious choice, after it was determined that the truss diagonals operated primarily in tension and compression. It was only necessary to convert the longitudinal diagonal motion into shear strain in a VEM. The choice of material required a search through VEM damping properties available from existing test data. The object of the search was to find a material with high loss factor in the predicted fundamental truss frequency range and in the expected room temperature range (60°F to 90°F). Fig. 6 is the result of that search. The data is presented in a format that is becoming a standard in the VEM industry. However, in the frequency range of interest, the data is an extrapolation. It is satisfactory for preliminary design but is superseded by new test data as discussed below in the component testing section.

The next step was to choose the dimensions of VEM that would produce a diagonal member stiffness close to that of the Plexiglas tube it is to replace so that the strain energy it contains remains the same as that predicted for the Plexiglas link. That is, it was desired to produce an A/t such that:

$$K_p = G_v A_v/t_v \qquad (2)$$

where

K_p = longitudinal stiffness of Plexiglas diagonal

G_v = shear modulus of selected VEM

A_v = shear area of VEM damper design

t_v = thickness of VEM in damper design.

This approach resulted in a design having the VEM dimensions shown in Fig. 5. Direct substitution of the VEM damper stiffness into the LGTA analysis predicted a truss damping much greater than that observed by log decrement of preliminary decay traces obtained by "twang testing" (excitation by step release of initial tip displacement) the fundamental mode in the plane of discrete damper activity. From this datum point it became apparent that the stiffness of the tube in series with the VEM damper cannot be ignored. Thus, Eq. (2) was replaced by:

$$K_D = (G_v A_v/t_v) K_p/[(G_v A_v/t_v) + K_p] \qquad (3)$$

where

K_D = longitudinal stiffness of the series combination of discrete VEM damper and Plexiglas tube

K_p = longitudinal stiffness of the Plexiglas tube ($= A_p E_p/[L_1 + L_2]$ where L_1 and L_2 are shown in Fig. 5.)

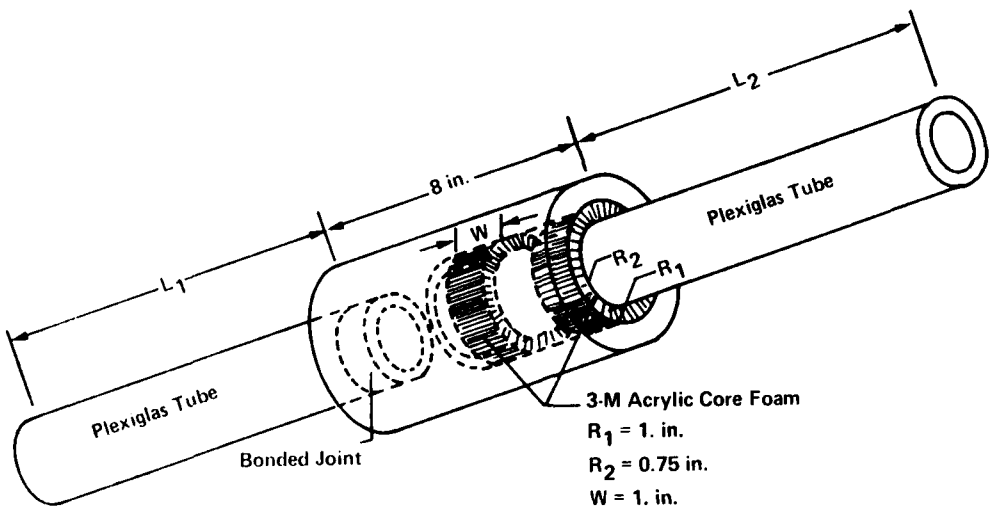

Fig. 5 - Discrete Damper Configuration

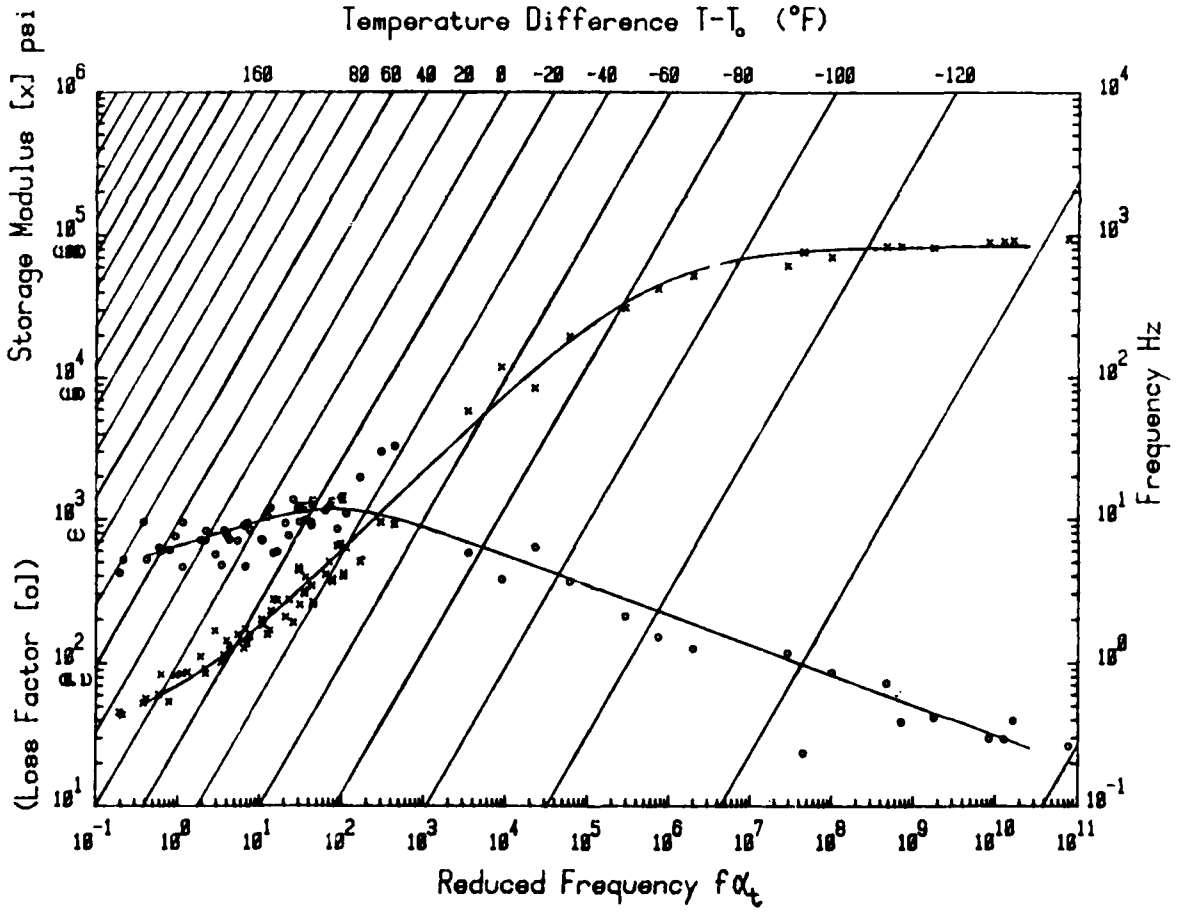

Fig. 6 - 3-M Acrylic Core Foam
Reference Temperature 75°F

Because the numerical value of $G_V A_V / t_V$ was approximately equal to that of K_D, the resultant K_D value was approximately half the intended value. The hardware, unfortunately, had been built by the time of this discovery. As will be shown in the theoretical/experimental correlation discussion, the opposite trends of frequency and strain energy help mollify this oversight.

HYSTERESIS TESTING OF COMPONENT STRUCTURE

Because of the known extrapolation of 3-M acrylic core foam into the low frequency range and the poor preliminary correlation of analysis and twang test results, it was decided that individual testing of the discrete damper mechanism, the Lexan tubing, and the Plexiglas tubing was required. Hysteresis testing was selected as the test method. It consists of applying an oscillatory force to the component structure while recording the force and resulting displacement as shown in Fig. 7. The information contained in a hysteresis plot is easily identified by a discussion of the elementary diagram of the rotating force vectors that describe the force balance in a sinusoidally excited single-degree-of-freedom system. Fig. 8 shows such a diagram. (The mathematics leading up to the diagram are detailed in many elementary vibration textbooks, e.g., Ref. [1].) At a constant excitation frequency the diagram in Fig. 8 rotates at ω radians per second with a constant phase angle, θ, between applied force, F, and displacement, X_o. The values of F and X recorded by the hysteresis plot of Fig. 7 are:

$$F = F_o \sin \omega t \tag{4}$$

and

$$X = X_o \sin (\omega t - \theta) \tag{5}$$

Therefore, when

$\omega t = \theta$

$$F = F_o \sin \theta = C\omega X_o \tag{6}$$

and

$$X = 0 \tag{7}$$

Thus, in Fig. 7 the force, $F = C\omega X_o$ at $X = 0$ is highlighted as of special interest. Furthermore, it is clear from Fig. 8 that:

$$F_o \cos \theta = KX_o - M\omega^2 X_o \tag{8}$$

At the low frequencies at which the truss (and most LSS) vibrate the contribution of $M\omega^2 X_o$ will be negligible, so Eq. (8) gives:

$$K \approx F_o \cos \theta / X_o \tag{9}$$

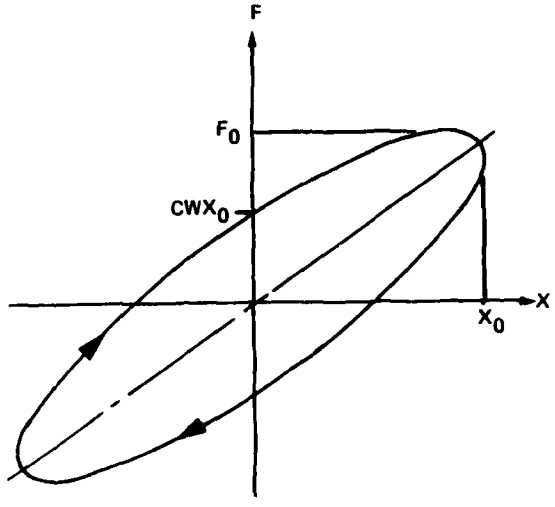

Fig. 7 - Viscoelastic Damping Hysteresis Loop

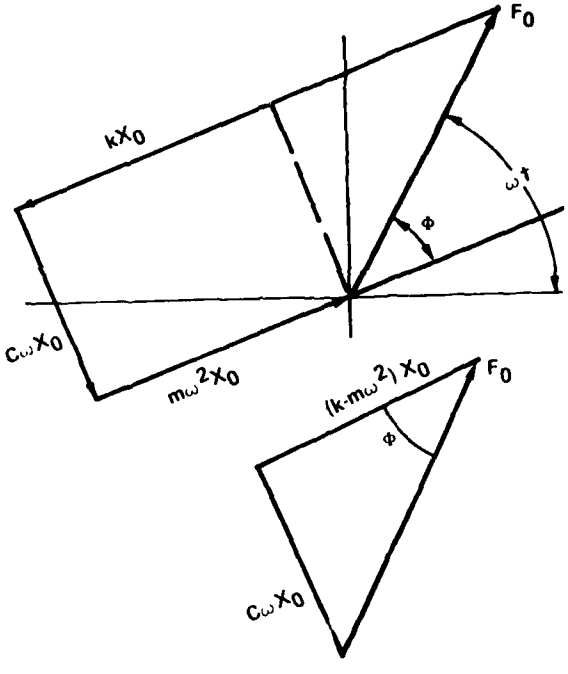

Fig.8 - Vector Representation of Forced Vibration with Viscous Damping

By reading the peak force, F_o, (when $\omega t = 0$) and maximum displacement, X_o, (when $\omega t - \theta = 0$) as indicated on Fig. 7, one can determine θ from Eq. (6) and then K from Eq. (9). Finally, using the definition that the component loss factor, n, is the ratio of the energy lost over the energy stored the equivalent ratio can be obtained from Fig. 8 as:

$$n = C\omega X_o / [KX_o - M\omega^2 X_o] = \tan \theta \tag{10}$$

Since each of the components is composed of some type of VEM, we require characterization of each component in a form similar to that given for 3-M acrylic core foam shown by Fig. 6. We elected to conduct the tests over the temperature range of 50°F to 100°F and over the frequency range 0.5 Hz to 1.5 Hz. The addition parameter, strain, was varied from 0.01-in. into 0.03-in. to determine linearity over the expected range of operation in the truss.

Because of test fixture limitations, full-size components could not be tested. The Plexiglas and Lexan tube test articles were 30-in. long. The damper component had 13-in. of Plexiglas on either end of the VEM housing (i.e., $L_1 = L_2 = 13$-n. in Fig. 5). The effective length of full-scale diagonal elements in the LGTA is 60-in. Table 1 summarizes the results of these tests for the discrete damper, Plexiglas tube and Lexan tube, respectively. The trend of loss factor for both the Plexiglas and Lexan tubes is not very definite. An average loss factor of 0.05 was used for Plexiglas tubes and an average loss factor of 0.01 was used for Lexan tubes in all subsequent analyses. As can be seen from the examination of these tables, temperature is by far the most important parameter for all components. This outcome suggests that one might expect reasonably accurate prediction of LGTA test results using a linear analysis at any given temperature. However, the component test data must be adjusted to the LGTA length to provide input to that analysis.

Adjusting the Plexiglas and Lexan tube data is simple. Because the loss factor is a ratio and the material is homogenous, no adjustment is required. Since,

$$K = AE/L \tag{11}$$

for each tube the LGTA stiffness values, K_{LGTA}, are obtained from

$$K_{LGTA} = L_{CT}K_{CT}/L_{LGTA} \tag{12}$$

where the subscript CT refers to component test results at any temperature.

Adjusting the damper component test data is slightly more complicated. Because the tubing and VEM are in series, both the measured loss factor and spring rate are a combination of the two materials. First of all, consider the spring rate adjustment. No measurement of the VEM stiffness alone was made, therefore, this value had to be backed out from the available data. This was done by using Eq. (3) to solve for:

$$G_vA_v/t_v = [K_DK_p/(K_p - K_D)]_{CT} = K_v \tag{13}$$

With this value of VEM stiffness, K_v, Eq. (3) again was used along with a spring rate, K_{LGTAp}, which reflects the length of Plexiglas in LGTA damper. (This length is 8-in. less than the effective LGTA diagonal length, or 52-in.) That is, the LGTA damper spring rate is:

$$K_{LGTAD} = K_vK_{LGTAp}/(K_v + K_{LGTAp}) \tag{14}$$

Secondly, following the definition of loss factor given by Eq. (1), the component test damper loss factor, n_{CT}, is the sum of the Plexiglas loss factor, n_p, times its fraction of component strain energy and the VEM loss factor, n_v, times its fraction of component strain energy. This can be written:

$$n_{CT} = n_pV_p/V_{CT} + n_vV_v/V_{CT} \tag{15}$$

Or, expressing strain energy ratio in terms of end load, L, e.g.,

$$V_p/V_{CT} = (L^2/2K_p)/(L^2/2K_{CT}), \tag{16}$$

loss factor can be written in terms of stiffness ratio as:

$$n_{CT} = n_pK_{CT}/K_p + n_vK_{CT}/K_v \tag{17}$$

Knowing all other terms, Eq. (17) can be used to determine n_v. Reapplication of Eq. (17) using LGTA spring rates produces the desired LGTA damper loss factor:

$$n_{LGTAD} = n_pK_{LGTAD}/K_{LGTAp} + n_vK_{LGTAD}/K_v \tag{18}$$

It is evident from Eqs. (14) and (18) that it is highly desirable to make the structural link in series with VEM as stiff as possible, i.e.,

$$\lim_{K_{LGTAp} \to \infty} n_{LGTAD} = n_v \tag{19}$$

Finally, the truss loss factor is the sum of the products of corresponding loss factors times fraction of modal strain energy from all components. Thus, the Plexiglas truss loss factor is:

$$n_{LGTAp} = n_{LGTAD}\,(S.E._D) + n_p(S.E._p) + n_{AL}(S.E._{AL}) \tag{20}$$

where,

n_{AL} = aluminum loss factor (0.005 used here)

$S.E._i$ = summation of fractions of modal strain energy in all of the i^{th} type components (e.g., S.E.p is strain energy fraction in Plexiglas diagonals)

TABLE 1 - Hysteresis Test Results

	Strain in.	freq Hz	50° F		75° F		100° F	
			n	K lb/in.	n	K lb/in.	n	K lb/in
Damper, Includes 26 in. Plexiglas Tube	0.01	0.5	0.51	4607	0.58	1815	0 45	1039
		1.0	0.46	5743	0.61	2158	0 44	1273
		1.5	0.41	6589	0.63	2417	0.53	1415
	0.02	0.5	0.49	4554	0.58	1732	0.51	933
		1.0	0.42	5833	0.55	2257	0 48	1287
		1.5	0.38	6909	0.59	2528	0 47	1506
	0.03	0.5	0.48	4583	0.49	1988	0 51	1038
		1.0	0.45	5737	0.53	2464	0 51	1307
		1.5	0.44	6401	0.59	2782	0 59	1428
30 in. Plexiglas Tube	0.01	0.5	0.062	10137	0.060	9075	0 029	8527
		1.0	0.058	10516	0.055	9894	0 034	8622
		1.5	0.046	10422	0.046	9990	0 056	8627
	0.02	0.5	0.049	9797	0.049	9139	0.046	8304
		1.0	0.048	10036	0 048	9389	0 051	8450
		1.5	0.048	10183	0.054	9527	0 037	8540
	0.03	0.5	0.058	9350	0.0517	9143	0 044	8292
		1.0	0.050	10310	0.050	9452	0 039	8430
		1.5	0 038	10350	0.044	9549	0 078	8569
30 in. Lexan Tube	0.01	0.5	0	6442	0	6100	0	6176
		1.0	0	6346	0	6100	0	6176
		1.5	0	6311	0	6100	0	6176
	0.02	0.5	0	6300	0.008	6262	0	6000
		1.0	0.0079	6300	0 016	6105	0.008	6050
		1.5	0.016	6249	0.020	6194	0.017	6049
	0.03	0.5	0.010	6387	0.011	6166	0.011	6100
		1.0	0.015	6419	0.022	6165	0 028	5998
		1.5	0.005	6290	0.022	6207	0 028	5998

Fig. 9 plots the variation of 60-in. LGTA diagonal elements stiffness versus temperature. Solid lines cover the component test temperature range. Dashed lines are used to extrapolate the curves to 150°F and -25°F using end points calculated using the 3-M Acrylic Core Foam data in Fig. 6 and linear extrapolation of 0.03-in., 1.5 Hz Plexiglas tube component test data scaled to LGTA length.

A finite element analysis of each truss was made at 50°F, 75°F, and 100°F by inputting the element stiffness shown in Fig. 9 at those temperatures. For example, for the 50°F Plexiglas LGTA, K_p = 5200.0-lb/in. and K_D = 4120.0-lb/in. were input to the Finite Element Program which calculated frequency and mode shapes and calculated the total strain energy in all Plexiglas diagonal elements, all damper elements, and all aluminum elements. Using the relationship between damper stiffness and temperature shown in Fig. 9, the frequency, damper strain energy, and Plexiglas tube strain energy results were plotted versus damper stiffness as shown in Fig. 10a. Similar results for the Lexan truss are shown in Fig. 10b.

Vibration analysis results for both trusses are presented for the first two modes. As the legend indicates, a solid line was used to plot results in the mode which moves parallel to the truss planes in which the dampers are installed. A dashed line was used to plot results in the mode perpendicular to the truss planes in which the dampers are installed. Truss motion parallel to the plane of the dampers works the dampers. Thus, the strain energy in the dampers, indicated by the solid lines labeled Dampers in Fig. 10a, is generally higher than the strain energy in the Plexiglas diagonals indicated by the solid lines labeled Plexiglas in Fig. 10a. Note that as the damper stiffness increases the dampers strain energy decreases while Plexiglas diagonals strain energy increases. This is due to the fact that stiffness increases as temperature decreases and damper stiffness approaches Plexiglas tube stiffness as temperature decreases. (This was shown in Fig. 9.) That is, at low temperatures, the truss acts as if all diagonals were Plexiglas. This trend can be seen in the frequency plots. As the dampers stiffen (cool) the frequency of both planes of truss vibration approach the same value. This is most apparent in the Lexan truss data, Fig. 10b, as the frequencies cross where the damper and Lexan tube stiffness are equal (as seen in Fig. 9). Strain energy in aluminum elements can be obtained by subtracting the sum of the Plexiglas and damper strain energy in a mode from 100%.

The loss factor is given by Eq. (20). The strain energy values for this equation were discussed above. A loss factor of 0.005 was used for aluminum elements. Average values of 0.05 for Plexiglas and 0.01 for Lexan were taken from

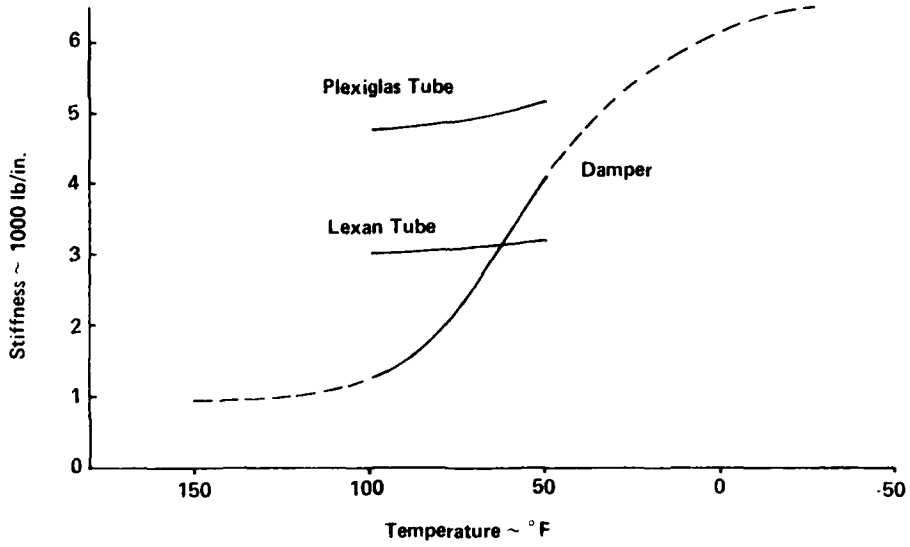

Fig. 9 - Stiffness Properties from Component Testing

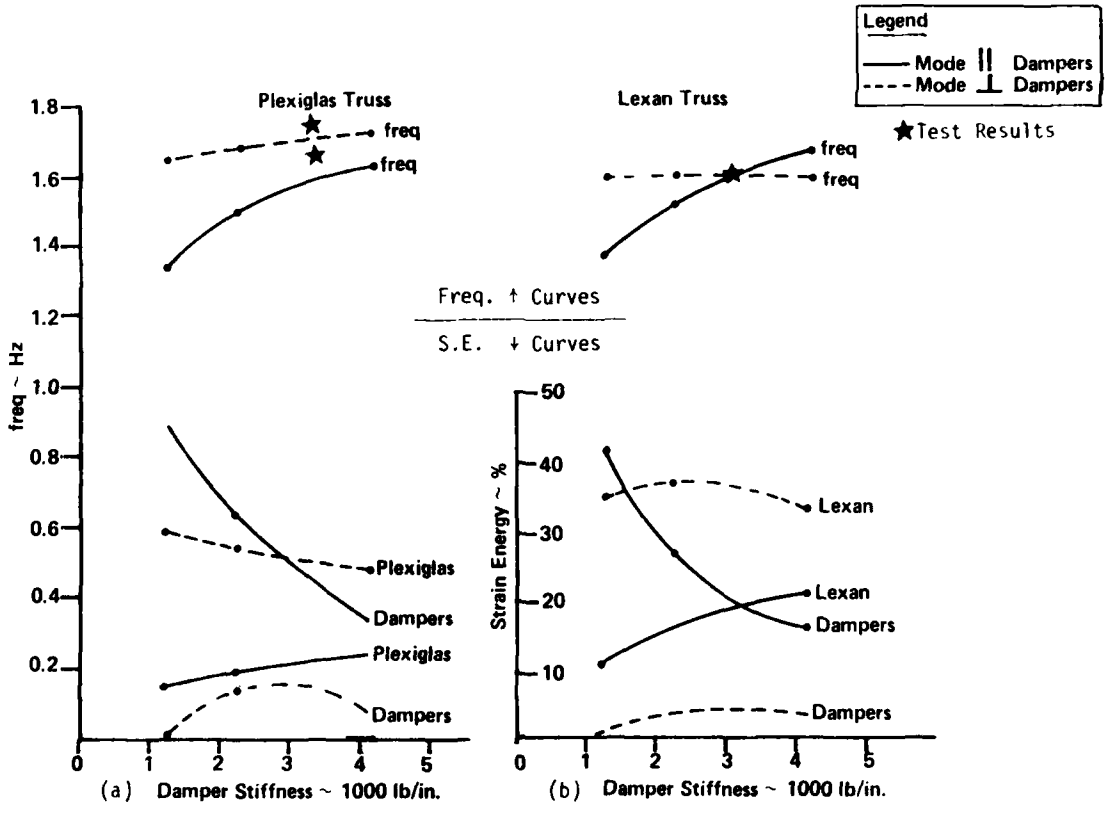

Fig. 10 - Vibration Analyses Results

the component test data. Fig. 11 superimposes the plot of damper loss factor (obtained using Eq. (18)) on the plot of damper stiffness versus temperature. Damper loss factor was extrapolated to 150°F and -25°F (dashed lines) in the same way, as described above, for the damper stiffness. The extrapolations illustrate that the damper component properties vary with temperature in a manner similar to that of the VEM alone. However, if the low frequency 3-M acrylic core foam properties of Fig. 6 were used directly, the damper component properties in the 100°F to 50°F range would be quite different. (This comparison is shown in Fig. 12.) The damper loss factors of Fig. 11 and those for aluminum, Plexiglas and Lexan identified above were used in Eq. (20), along with strain energy in the mode parallel to the damper plane from Fig. 10 to calculate truss loss factors shown as a function of temperature on Fig. 11. The truss loss factor in the mode perpendicular to the plane of the dampers is predicted to be 0.02 in both the Plexiglas and Lexan trusses at all temperatures within the operating range.

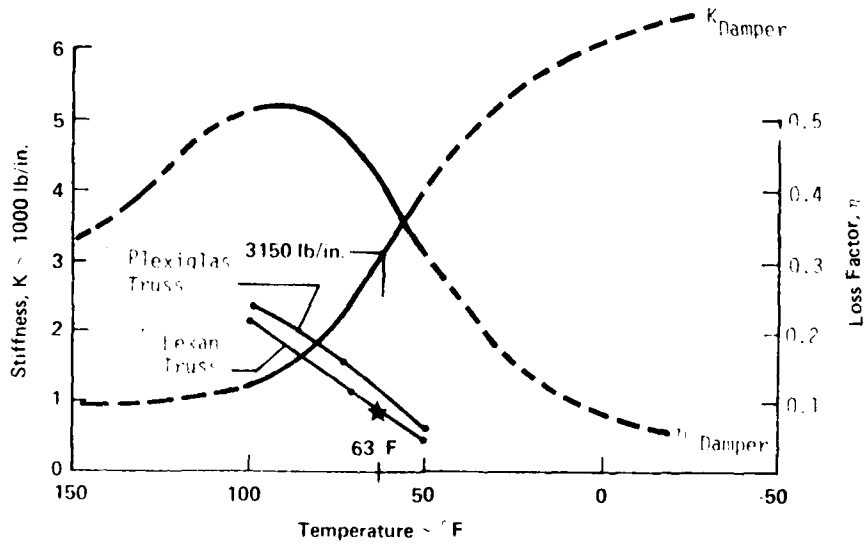

Fig. 11 - IGTA Damper Properties and Truss Loss Factor

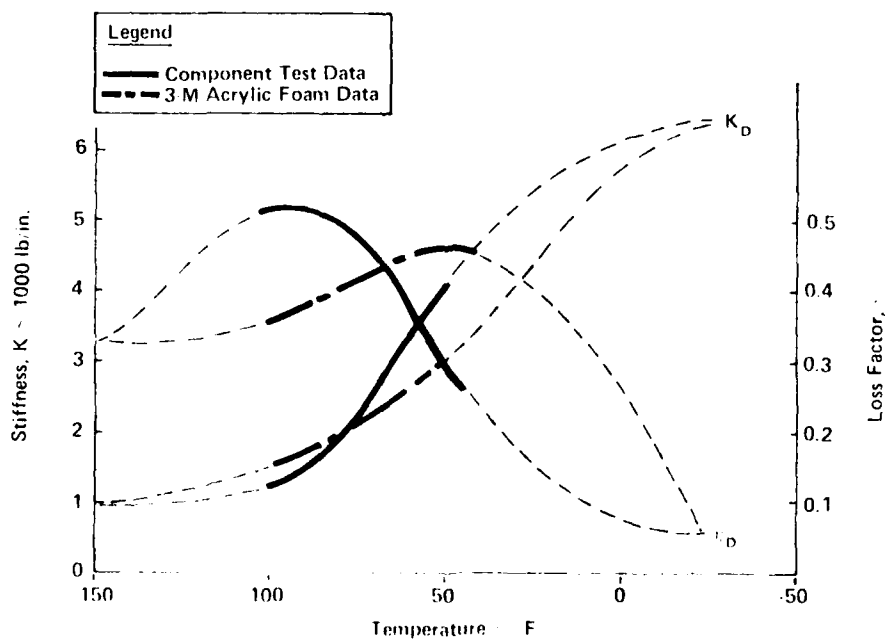

Fig. 12 - IGTA Damper Properties

SYSTEM STRUCTURE TEST

The final step was to determine the actual frequencies and loss factors of the LGTA trusses. This was done by applying single point random excitation at the 40-ft level of each truss in each direction (four separate tests were conducted) while acquiring input force and response acceleration in each direction. Fast Fourier Transform techniques were used to generate frequency response functions defining the response in two perpendicular directions per force input. The frequency response method of modal parameter estimation requiring both single and multiple DOFs curve fitters was used on this data. Table 2 presents the results of this data analysis along with corresponding analytical predictions. The stars shown on Figs. 10 and 11 superimpose the damper mode test data from Table 2 to show the comparison of LGTA analytical and test results. Only one star appears on Fig. 11, since the damper mode loss factor is the same in both trusses.

Correlation of the Lexan truss test and analysis is excellent in both frequency and loss factor. Plexiglas truss correlation is not bad and may be even better than shown. This is because the laboratory temperature where LGTA tests were conducted are not controlled and temperature is manually recorded. Plexiglas truss testing perpendicular to the plane of the dampers was conducted on a Friday when 51°F was recorded in the laboratory. Testing in the other plane was conducted the following Monday when 63°F was recorded in the laboratory. Both tests yield two frequency response curves from which frequency and damping are extracted; one in each truss plane. The results of both tests are similar. Had the Plexiglas truss loss factor been plotted on Fig. 11 at 51°F and the Plexiglas truss frequency been plotted on Fig. 10 at a damper stiffness of 4167.0-lb/in. (corresponding to 51°F) the correlation test and analysis for the Plexiglas truss would be very good, as indicated by the open circles, o, on Figs. 10 and 11.

CONCLUSIONS

A. It has been demonstrated that current passive damping design technology can be applied successfully to produce a large structure which has significant damping when operated in the design environment. The procedure for designing such a highly damped structure can be summarized as follows:

   1. Generate a finite element model of the structure being considered and calculate mode shapes and frequencies.

   2. Calculate the strain energy distribution among the elements of the model in each of the modes [4].

   3. Examine the strain energy distributions to identify structural elements containing a large percentage of strain energy in the modes in which high damping is desired.

   4. Select a method of VEM application (e.g., shear damper, constraint layer, etc) which will not compromise the integrity of the structural load paths.

   5. Select a VEM having a high loss factor at the expected operating temperature and calculated frequency of the structure. Some testing to validate the VEM application method and/or low frequency properties may be required.

   6. Revise the finite element model of the structure to include the mechanical properties of the selected VEM and calculate new mode shapes and frequencies. (Finite element models at more than one VEM temperature may be required.)

   7. Calculate the strain energy distribution among the elements of the revised model in each of the modes [4].

   8. Calculate the loss factor of the structure in each mode at each temperature using Eq. (20).

B. The most efficient series installation of VEM dampers is obtained when very stiff structural elements are used in the series.

ACKNOWLEDGMENTS

The analyses and testing described in this paper were performed at Martin Marietta Denver Aerospace under Contract No. F33615-83-C-3222, Passive and Active Control of Space Structures (PACOSS).

REFERENCES

1. W.T. Thomson, Mechanical Vibrations, p. 52, Prentice-Hall, Inc., Englewood Cliffs, New Jersey, 1956

2. E.E. Unger and E.M. Kerwin, Jr., "Loss Factors of Viscoelastic Systems in Terms of Energy Concepts," J. Acoust. Soc. Am., Vol. 34, p. 954, 1962

3. C.D. Johnson, D.A. Kienholy, and L.C. Rogers, "Finite Element Prediction of Damping in Beams with Constrained Viscoelastic Layers," Shock and Vib. Bul., No. 50, Part 1, p. 71, May 1981

4. C.W. White and B.D. Maytum, "Eigensolution Sensitivity to Parametric Model Perturbations," Shock and Vib. Bul., No. 46, Part 5, p. 123, Aug. 1976

TABLE 2 - Comparison of Test and Analysis

	PLEXIGLAS		LEXAN	
	TEST	ANALYSIS	TEST	ANALYSIS
Frequency Loss Factor (Mode ∥ Dampers)	1.67 Hz 0.081	1.59 Hz 0.12	1.60 Hz 0.080	1.60 Hz 0.080
Frequency Loss Factor (Mode ⊥ Dampers)	1.73 Hz 0.031	1.70 Hz 0.02	1.59 Hz 0.006	1.60 Hz 0.02

PASSIVE LOAD CONTROL DAMPERS

David M. Eckblad, Patrick James Schirmer
Boeing Aerospace Company
Seattle, Washington

The need to accommodate greater nuclear groundshock threats for a larger and heavier missile/canister within an existing underground site has led to a unique damper requirement which is satisfied using the passive load control damper. The design approach to develop this passive load control damper is described. Details in modeling the passive load control damper valve dynamics are given. Dynamic analysis is compared with various levels of tests, showing good correlation.

INTRODUCTION

The passive load control damper (PLCD) is a high performance damper for the vertical shock isolation system (VSIS) used on a large missile in an underground silo basing system. Through transient analysis, it was concluded that severe groundshock environments along with multiple attacks had to be accommodated in the VSIS design. Thus, optimization for a specific groundmotion was not possible, rather the design was developed with the goal of accommodating many different groundshock waveforms.

It was evident through optimization studies that an ideal damper for the VSIS should develop a damping force independent of stroke position and limit the damping force above a threshold velocity. The optimal damping performance goals for the VSIS are shown for both extension and compression velocities in Fig. 1.

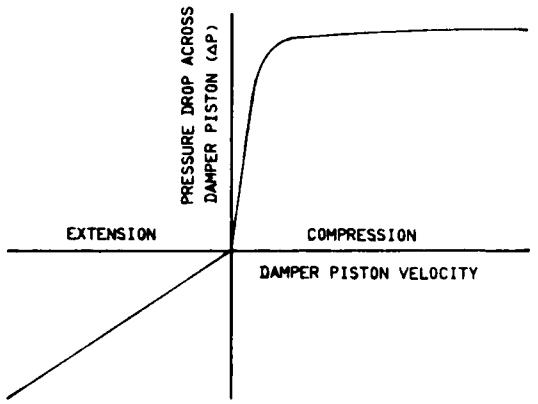

FIGURE 1 OPTIMAL PASSIVE LOAD CONTROL DAMPER PRESSURE REGULATION RELATIONSHIP

With this damping characteristic, it was demonstrated through analysis that 30 to 50 percent reduction in the liquid spring length and dynamic excursions could be achieved while maintaining the same peak missile/canister loads.

Conventional fixed orifice area dampers produce a damping force nearly proportional to the square of the damper piston velocity. This is a very inefficient system for dissipating kinetic energy from a dynamic system subjected to load and excursion limitations particularly when many different groundshock velocity waveforms as well as liquid spring stroke velocity conditions must be considered.

In the past, typical approaches to obtain this damping performance have involved changing the damper orifice area as a function of damper stroke by using variable-diameter needle valves or exposing a varying number of holes in the damper sleeve. This technique is not satisfactory in the present case, because of the wide range of operating groundshock environments that require different orifice areas at the same damper stroke.

The combined requirements of a variable damper orifice area dependent on the damping force and a reliable passive system has motivated the development of the PLCD.

DESIGN APPROACH

The PLCD concept is a self-contained, passive, pressure feedback system that governs the differential pressure of the system.

To illustrate the general operation of the PLCD valve, consider motion of the damper in the positive direction shown in Fig. 2a. This motion will cause the upstream pressure (P_2) to be greater than the downstream pressure (P_1). The differential pressure loading in the valve forces it to displace until it is in equilibrium with the valve spring load. By appropriate selection of the valve orifice area and valve spring rate as a function of the valve displacement, it is possible to get any desired damping force which increases monotonically with damper piston velocity.

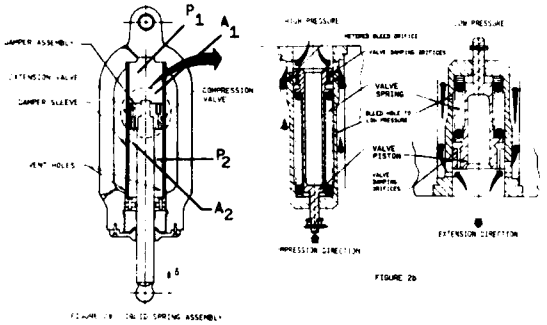

FIGURE 2 GENERAL REPRESENTATION OF A LIQUID SPRING WITH INSTALLED PASSIVE LOAD CONTROL DAMPERS

This procedure is illustrated in Fig. 3 for quasi-steady incompressible flow. The transient behavior of the valve is controlled by the valve damping, valve mass, valve piston/orifice overlap, and control of the fluid dynamics. These parameters can be adjusted to control valve oscillations and transient valve overshoot.

In practice, the PLCD is initially sized for desired liquid spring performance requirements using the quasi-steady incompressible flow assumptions as shown in Fig. 3. More detailed dynamic analysis and tests are then used to refine valve performance through consideration of higher order effects such as valve friction, fluid flow forces, and unsteady flow through the valve.

ANALYSIS

The primary transient forcing function of the PLCD valve is caused by the pressure differential acting on the valve areas. This pressure differential is calculated assuming turbulent flow through the valve orifice as follows.

$$P_1 - P_2 = \frac{1}{2} \rho_2 V_2^2 \qquad (1)$$

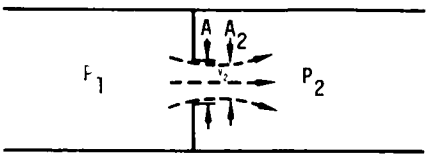

FIGURE 4 FLOW THROUGH AN ORIFICE

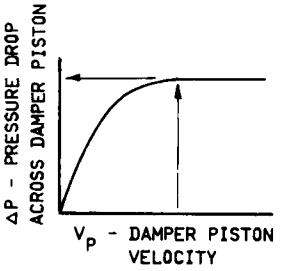

FIGURE 3a

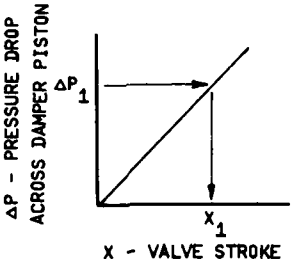

FIGURE 3b

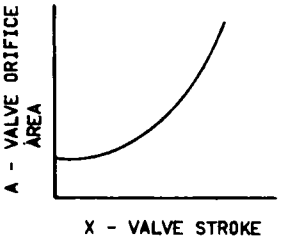

FIGURE 3c

IT CAN BE SHOWN THAT:

$$A = \sqrt{\frac{\rho V_P^2 A_P^2}{2 C_d^2 \Delta P}} \qquad (3.1)$$

ORIFICE AREA STROKE FUNCTIONAL

FIG 3a FIG 3b EQ 3.1

SELECT $V_P \Rightarrow \Delta P \Rightarrow X_1 \Rightarrow A_{o_1}$ $\Rightarrow$ FIGURE 3c

FINE TUNE WITH DYNAMIC ANALYSIS AND TEST

NOMENCLATURE

- A = GEOMETRIC ORIFICE AREA
- C_d = ORIFICE DISCHARGE COEFFICIENT
- A_p = AVERAGE DAMPER PISTON AREA
- V_p = DAMPER PISTON VELOCITY
- ρ = FLUID DENSITY
- X = VALVE DISPLACEMENT

FIGURE 3 PROCEDURE FOR DEVELOPING PASSIVE LOAD CONTROL PROPERTIES

where P_1 is the upstream pressure, P_2 is the downstream pressure, ρ_2 is the downstream density, and V_2 is the velocity of the fluid at A_2.

In an effort to model the restriction of the orifice area due to the boundary layer presence, an orifice discharge coefficient is incorporated. The discharge coefficient is simply the ratio of the minimum area of the moving fluid (A_2) to the geometric area of the orifice (A). Traditionally, orifice discharge coefficients vary in value from .6 to .8 depending on the orifice shape, orifice sharpness, and Reynold's number of the fluid moving through the orifice.

Thus, in a simple piston-cylinder system, the rate of mass flow is the product of the downstream fluid density (ρ_2), fluid velocity (v), and effective area (A_2). So,

$$\dot{m} \equiv \rho A v = \rho_2 \sqrt{\frac{2}{\rho_2}(P_1 - P_2)}\, C_d\, A \qquad (2)$$

where m is the mass flow rate, A is the geometric area of the orifice, and c_d is the orifice discharge coefficient.

Integrating the mass flow rate, the transfer of fluid mass can be calculated. Thus, the density can be computed for the i-th volume of the liquid spring using the following relationships,

$$\text{and} \qquad \rho_i(t) = \left(\frac{M_{oi} + M_i(t)}{v_i(t)}\right) \qquad (3)$$

$$\left(\frac{\Delta V}{V}(t)\right)_i = \left(1 - \frac{\rho_{oi}}{\rho_i(t)}\right) \qquad (4)$$

where the (o) subscript refers to initial condition properties, ρ is the fluid density, m is the fluid mass, v is the fluid volume, and $\Delta V/V$ is the state of the fluid compressibility. Thus, from actual fluid $\Delta V/V$ versus pressure data, the pressure in each volume is obtained.

Valve damping was estimated using one dimensional, incompressible fluid relationships. Referring to Fig. 5 below, it is seen that

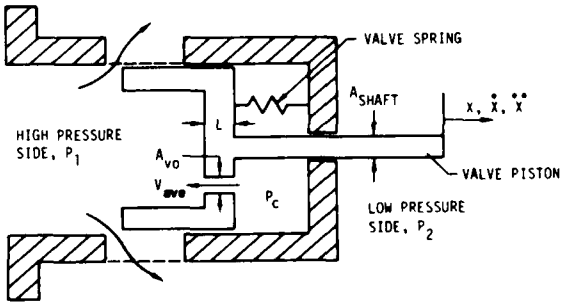

FIGURE 5 VALVE SCHEMATIC DETAILING VALVE DAMPING GEOMETRY

motion of the valve results in fluid moving through the valve damping area (A_{VO}) in the direction indicated. The Reynold's number associated with the fluid flowing from the P_1 face of the valve piston to the valve damping chamber (P_C) has been less than 2000 for the PLCD's considered in this paper. This implies the flow through this damping orifice is laminar, which results in viscous damping of the valve motion, thus a linear relationship of valve damping to valve velocity. In one-dimensional laminar flow, the relationship between shear stress and the velocity gradient is given by Newton's law of viscosity. It can be shown that

$$P_1 - P_C = \frac{8\mu}{r_o^2}\, L\, V_{ave} \qquad (5)$$

where P_1 is the high pressure, P_c is the chamber pressure, μ is the fluid viscosity, r_o is the radius of the orifice, L is the length of the orifice, and V_{ave} is the average fluid velocity (Ref. 1). Multiplying the pressure differential by the valve piston area (Ap) and using continuity to solve for the fluid velocity yields the following valve viscous damping expression (F_{vd}):

$$F_{vd} = k_{vd} \cdot \dot{X} \qquad k_{vd} = 8\pi\mu L \left(\frac{d}{dc}\right)^4 \qquad (6)$$

where d is the piston diameter and d_c is the valve orifice diameter.

To model the pressure loss on the face of the valve piston due to fluid motion, the fluid streamlines in the region of the orifice were assumed as shown in Fig. 6 below.

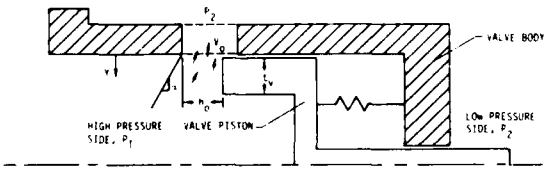

FIGURE 6 VALVE SCHEMATIC ILLUSTRATING ASSUMED FLUID STREAMLINES

Prescribing the velocity streamlines and permitting only two-dimensional flow allows an approximation of the drop in pressure on the high pressure face of the valve.

Using continuity and assuming the flow to be incompressible, the following can be shown,

$$v(y) = \frac{v_o}{\left(1 + \frac{\alpha y}{h_o}\right)} \qquad (7)$$

where v_o is the maximum fluid velocity at the orifice opening, h_o is the orifice opening height, and α is an empirical constant (determined from flow tests) that prescribes the fluid streamlines near the face of the valve.

Thus, using a simplified energy relationship and substituting the $v(y)$ expression into the equation, the following is obtained:

$$\Delta P(y) = \frac{\Delta P_o}{\frac{(1+\alpha y)^2}{h_o}} \quad (8)$$

where

$$\Delta P_o = \frac{1}{2} \rho V_o^2 \quad (9)$$

Integrating the resulting pressure differential distribution over the thickness of the valve and subtracting this quantity from the resulting force if no fluid were moving over the valve yields the following expression for the total resulting force on the high pressure side of the valve (F_H).

$$F_H = P_1 A_v - (P_1 - P_2)\left(\frac{w h_o t_v}{h_o + \alpha t_v}\right) \quad (10)$$

Where t_v is the thickness of the valve, w is the width of the orifice, and A_v is the area of the valve piston.

In the transient modeling the PLCD valve, the spring force, viscous damping, flow loss, and estimated friction are summed to obtain the valve acceleration shown below.

$$\ddot{X} = [X \cdot K_v + F_{PL} + \dot{X} \cdot K_{vd} + F_H + P_C \cdot (A_v - A_{SHAFT}) + P_2 \cdot A_{SHAFT} + F_F]/M_v \quad (11)$$

where K_v is the valve spring constant, F_{PL} is the valve spring preload, A_{SHAFT} is the valve shaft area, F_F is the valve friction force, and M_v is the valve mass.

This result is numerically integrated to obtain the velocity and the displacement of the valve.

Using equations (2), (3), and (4) the liquid spring fluid pressures are calculated. These pressures are integrated over all of the volume surfaces illustrated in Fig. 2.a to yield the liquid spring reaction (F_{LS}),

$$F_{LS} = P_1 A_1 - P_2 A_2 - \text{FRICTION} \quad (12)$$

The above analysis outlines the procedure to determine the liquid spring force time history which is incorporated in the full scale dynamic model of the VSIS for the canister/missile system.

A drop test was conducted primarily to evaluate the system performance and to assess uncertainties associated with suspension cable slack, cable guide friction, and liquid spring friction. Application of the analysis technique for modeling the PLCD has been incorporated into a full scale drop test transient model. A general schematic of this transient model that consists of a missile, canister, liquid springs, lever arms, and suspension cables is shown in Fig. 7.

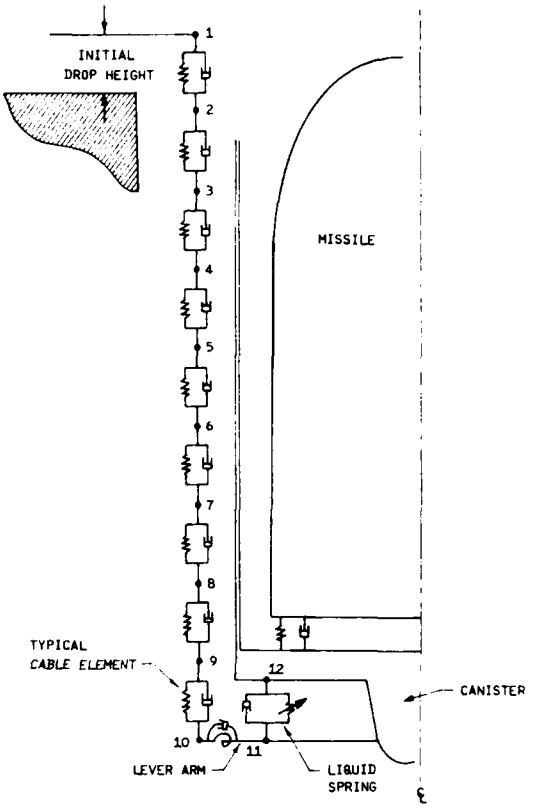

FIGURE 7 SCHEMATIC DIAGRAM OF VERTICAL DROP TEST DYNAMIC MODEL

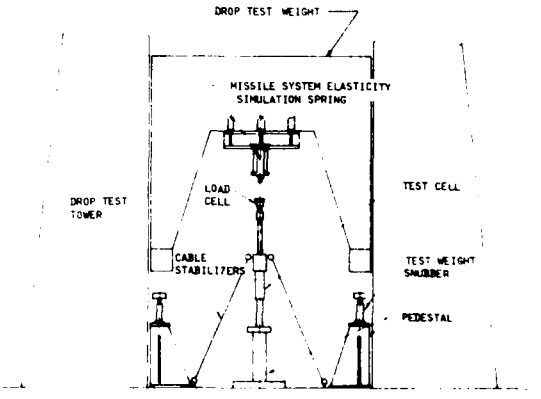

FIGURE 8 PLCD SINGLE VALVE DROP TEST FACILITY

TEST/ANALYSIS CORRELATION

During development, individual PLCD valves were tested instead of entire damper assemblies. Individual valve testing was accomplished using two different techniques: a drop test tower and a driven actuator facility. Fig. 8 shows details of the drop test tower while Fig. 9 shows a schematic of the driven actuator single valve test fixture.

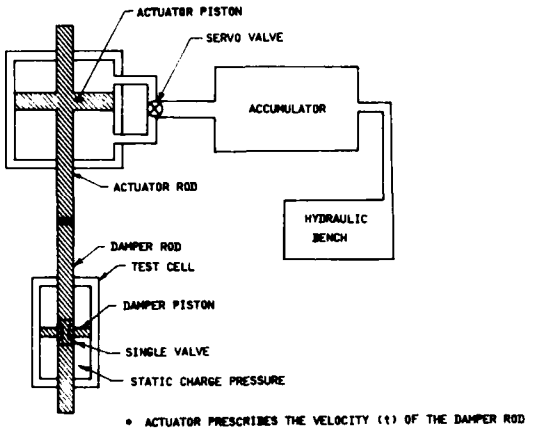

FIGURE 9 ACTUATOR DRIVEN PLCD SINGLE VALVE TEST FIXTURE

The valve test cells for both methods of testing were identical. This test cell consisted of a damper piston with a rod extending out both sides the cylinder assembly, thus only damping forces resulted--no liquid spring reaction. Both methods of PLCD valve testing were found to be adequate for development testing. The ability to prescribe the damper rod velocity was an added advantage of the driven actuator test method. This feature aided in a more direct assessment of the valve steady state performance.

Initially, the transient behavior of the valve was a concern. If valve chatter or high overshoot in pressure regulation occurred, the

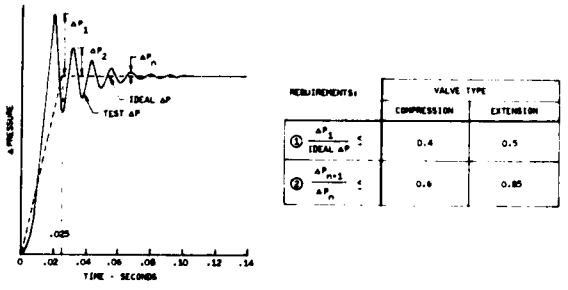

REQUIREMENTS:	VALVE TYPE	
	COMPRESSION	EXTENSION
① $\frac{\Delta P_1}{\text{IDEAL } \Delta P} \leq$	0.4	0.5
② $\frac{\Delta P_{n+1}}{\Delta P_n} \leq$	0.6	0.85

FIGURE 10 PLCD VALVE TRANSIENT RESPONSE LIMITS

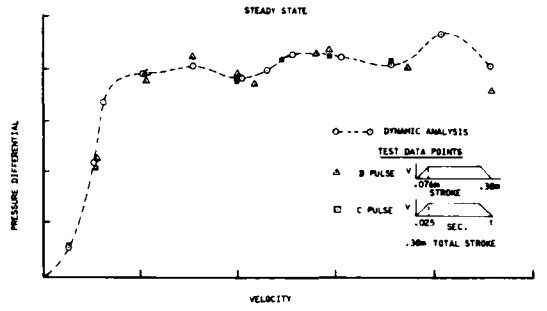

FIGURE 11 PRELIMINARY COMPRESSION PLCD VALVE ANALYSIS/TEST CORRELATION

resulting high frequency and/or load environment could be detrimental to the mechanical system. Through careful design and testing, it was found that the imposed transient limits for the PLCD valves were not difficult to satisfy. Fig. 10 shows the transient regulation limits developed for the VSIS PLCD valves.

A comparison between analysis and actual test steady state performance of one of the initial PLCD designs is shown in Fig. 11. The waving characteristic of the damping force with piston velocity was caused by the discontinuous orifice area/valve stroke relationship. The close correlation between actual test and dynamic analysis resulted from the development of the methodology for estimating the reduction in fluid pressure due to fluid flow on the valve piston face as outlined in the analysis section.

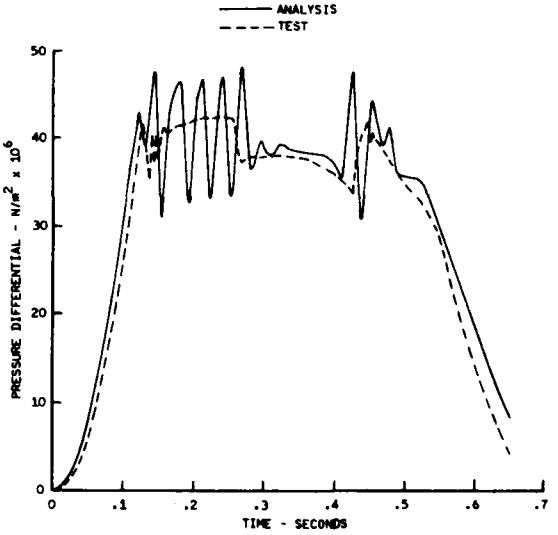

FIGURE 12 PRELIMINARY COMPRESSION PLCD VALVE ANALYSIS/TEST COMPARISON

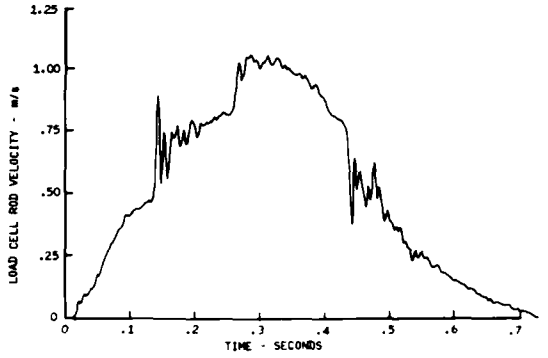

FIGURE 13 PRELIMINARY COMPRESSION PLCD VALVE VELOCITY TIME HISTORY

The measured load cell (damping force) response time history for the same valve, using the driven actuator test fixture, is compared with transient model in Fig. 12. Fig. 13 shows the measured load cell rod velocity time history that was used for the transient model rod velocity. The oscillation seen in Fig. 9 is attributed to discontinuities in the valve orifice area versus stroke relationship and the oscillatory character of the prescribed velocity (Fig. 11). This discontinuous valve area relationship was subsequently avoided in future PLCD valve designs.

Multi-valve tests were performed to assess the behavior of many valves regulating together. Steady-state data from tests for a six-valved PLCD assembly are compared with

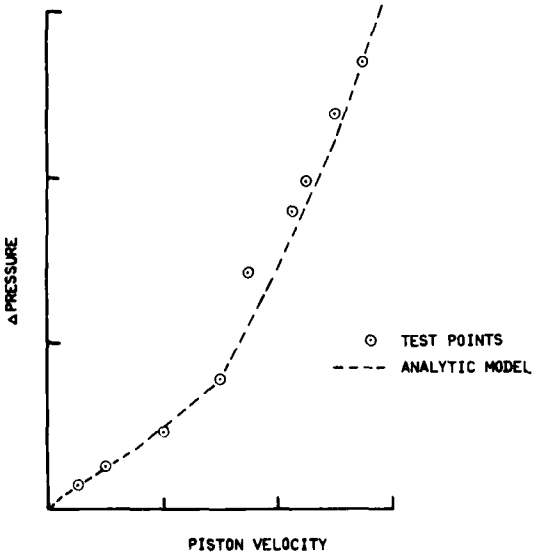

FIGURE 14 EXTENSION PLCD VALVE STEADY STATE BEHAVIOR

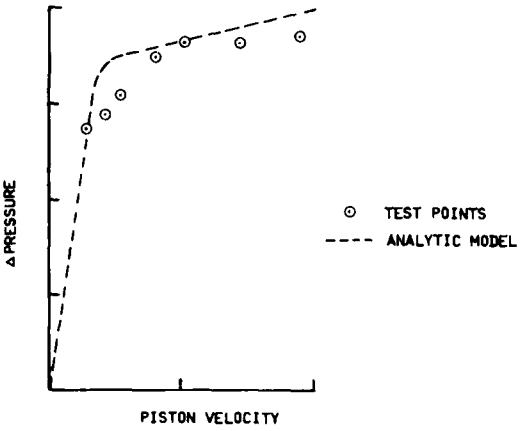

FIGURE 15 COMPRESSION PLCD VALVE STEADY STATE BEHAVIOR

dynamic analysis predictions in Figs. 14 and 15. Tests showed that the six-valved PLCDA performed nearly identical to the single valve tests. It was concluded that single valve testing is adequate for predicting system behavior.

The final test employed in evaluation of the ability of the PLCD valve to regulate the pressure differential in the liquid springs was accomplished through a full scale drop test. In this test, the canister/missile was mass simulated, but the actual lower launch support, lever arms, liquid springs, and suspension cables of the VSIS were used. Fig. 13 describes the actual test apparatus.

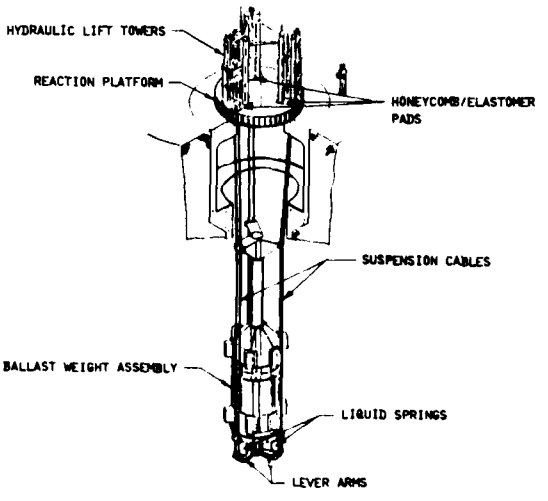

FIGURE 16 VERTICAL DROP TEST OF SHOCK ISOLATION SYSTEM

The drop test was commenced by explosive charges which released the statically loaded cables a predetermined height above honeycomb/ elastomer pads. Time histories comparing actual test responses and dynamic analysis from the full scale drop test are shown in Fig. 17 and 18.

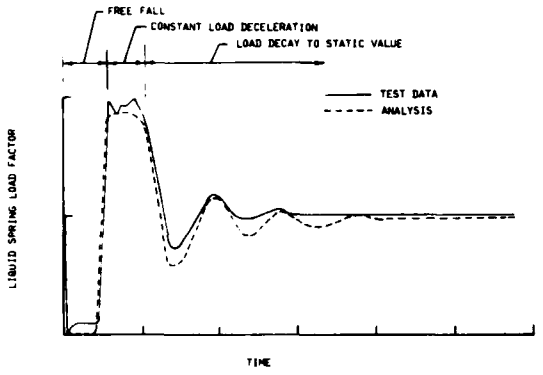

FIGURE 17 DROP TEST CORRELATION

During the free-fall phase of the test, the liquid springs extend due to the liquid spring preload generated by the initial static charge pressure reacting on liquid spring rod areas to resist the static load of the suspended weight. The liquid spring extension is primarily resisted by the extension damping provided by the PLCD valve assembly.

When the cable ends impact the honeycomb/ elastomer pads, the cables begin to stretch due to loading and the liquid springs begin to compress. During this phase, the PLCD valves provide a nearly constant damping force to resist the relative motion between the cable ends and the canister/missile mass.

After the high load phase, the PLCD valve assembly continues to regulate the pressure to provide a rapid decay of the missile/canister motion.

CONCLUSIONS

The PLCD concept is a very efficient method of dissipating kinetic energy through unique non-linear damping characteristics. This

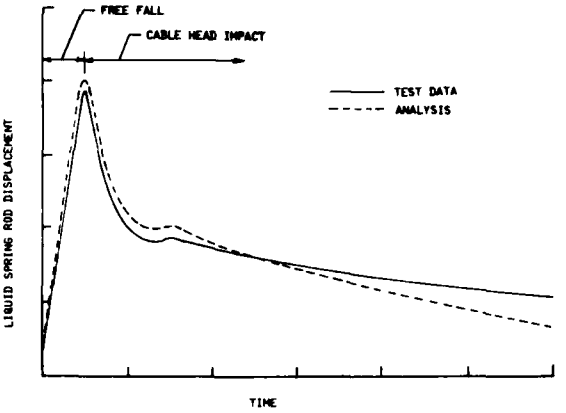

FIGURE 18 DROP TEST CORRELATION

increased efficiency allows for physically smaller shock isolation systems which reduces system costs (Ref. 2).

It has been demonstrated that PLCD pressure regulation can be tailored in a fashion to give any monotomically increasing damping force with piston velocity.

Close correlation between transient analysis and test gives confidence in the ability to predict actual system performance in an actual nuclear weapons effect groundshock environment.

Although the unique damping relationship was specifically optimized for criteria groundmotion, the passive nature of the damping load control valves allows for substantial increase in waveform amplitude as well as change in waveform shape with satisfactory dynamic responses.

REFERENCES

(1) Ovid Wiesnbach, Handbook of Engineering Fundamentals, 2nd Ed. John Wiley & Sons, Inc., New York, 1952

(2) Robert M. Foster, Brian A. Moravec, and Pierre M. Mirande, "The Design and Development of the Liquid Spring/Damper for the Peacekeeper Shock Isolation System," 19th Aerospace Mechanisms Symposium, NASA Ames Research Center, 1985

DISCUSSION

Mr. LeKuch (Aeroflex Corporation): You went ahead with this development program because the devices which were commercially available did not suit your requirements. In what way were they unsuitable, as a generalization? Was it size? Was it load capability? Was it efficiency?

Mr. Schirmer: A particular valve was available, but it was not suitable because of its regulation, its shape and its size; also it could not accommodate the large mass flows that we needed, so we had to develop our own.

RESPONSE OF A SYMMETRIC SELF-DAMPED PNEUMATIC SHOCK ISOLATOR TO AN ACCELERATION PULSE

M. S. Hundal
Department of Mechanical Engineering
University of Vermont
Burlington, Vermont

and

D. J. Fitzmorris
General Electric Co.
Burlington, Vermont

Pneumatic damping offers several advantages in shock and vibration applications including cleanliness, light weight and few moving parts. Large deflections of pneumatic shock absorbers make their behavior nonlinear and thus difficult to analyze. This paper details the analysis and response of a symmetric pneumatic absorber with orifice damping. With proper design such an absorber can provide a response to a shock pulse similar to that of a (theoretically) linear absorber. The response to a rectangular acceleration pulse is determined, which is the most severe pulse shape for a given duration. Results are given in the form of graphs and empirical formulas which can be used for design. An important conclusion reached is that there is a trade-off between optimum shock isolation and optimum damped response.

INTRODUCTION

This is a study of the response of a symmetric self-damped pneumatic shock isolator to an acceleration pulse. A diagram of the system is shown in Figure 1. Throughout the analysis, nonlinear behavior is assumed for both the pneumatic spring rate and the damping characteristics. The isolator receives an acceleration pulse of $\ddot{U}a(t)$ and duration t_f at its base. The piston, rigidly attached to the mass requiring isolation, upon excitation will

1. compress gas in chamber A forcing it through the orifice into surge tank A, and
2. extract gas out of surge tank B through an identical orifice into chamber B.

Damping for this system results from pressurized gas expanding across both orifices and dissipating its pressure energy as heat. A rectangular acceleration pulse was chosen as the best pulse to analyze since it represents the most severe pulse possible for any particular maximum shock strength $\ddot{U}$ and time duration. The object of the report is to determine what conditions and design yield optimum shock attenuation and dynamic response in terms of dimensionless ratios.

The application of pneumatic elements as vibration isolators is well established and analyzed [3,4,6,7,9]. They are characterized by relatively spongy nature, clean environment, and for small displacements they can be easily analyzed. Hundal [10] compared response to shock for linear and quadratic damping. Results showed that the quadratic response was most sensitive to any changes in system inputs and characteristics. Optimum damping ratio for linear damping is constant for any type of shock input, but in quadratic and pneumatic damping the optimum damping ratio always changes with time for a dynamically nonlinear response.

Studies of pneumatic systems undergoing

vibration have been done by Cavanaugh [4] and Andersen [1] for capillary and orifice damping, respectively. Both works treated the damping as nonlinear, but assumed small displacements to linearize dynamic response. By linearization a damping ratio may be computed analytically for response to forced vibration. Both authors determined optimum damping ratios which were functions of system parameters and not constants.

The system shown in Figure 1 represents an extension of the work by Hundal [11,12] which analyzed the response of asymmetric systems utilizing a single orifice. In [12], the dependency of optimum shock isolation on orifice area and volume ratio is shown and optimum area is shown not to be constant for particular system parameters of inertia and pulse duration. This report attempts to correlate this phenomenon as it pertains to the system in Figure 1.

Other studies on pneumatics used for shock isolation include Fox and Steiner [8] who presented both analytical and experimental results for passive pneumatic isolators and have shown that a specific geometry yields ideal system response. Bachrach and Riven [2] have examined the complex dynamic stiffness of a damped spring.

DERIVATION OF SYSTEM EQUATIONS

The mathematical analysis of this system is based on the following assumptions:

1. The ideal gas law prevails.
2. Coulomb friction between the piston and chamber wall is negligible.
3. There is no gas flow between chambers A and B.
4. The system is adiabatic.
5. The surge tank and chamber are rigidly attached to each other.
6. The chamber and tank dimensions in the unexcited state are equal between sections A and B.
7. The orifice area, configuration and efficiency are equal between sections A and B.

The equations for the system model require a mass flow analysis of the gas through the orifices and an equation of motion analysis of the piston. First, the equation of motion is derived for the system in Figure 1. Summation of forces on the piston yields:

$$M\ddot{x} = S(P_A - P_B) \tag{1}$$

Upon substituting $\ddot{d} = \ddot{x} - \ddot{U}a(t)$, the relative motion, equation (1) becomes

$$M\ddot{d} = S(P_A - P_B) - M\ddot{U}a(t) \tag{2}$$

where $\ddot{U}$ is the pulse strength and a(t) defines its shape. Upon dividing by $M\ddot{U}$ we get

$$\ddot{d}/\ddot{U} = S(P_A - P_B)/M\ddot{U} - a(t) \tag{3}$$

Now, the mass flow rates through the orifices shall be computed by using thermodynamic and empirical relations. From the Ist law of thermodynamics, the enthalpic relation describing the rate of mass change in a chamber is

$$\dot{m}h = dU_e/dt + dE/dt \tag{4}$$

where U_e is the internal energy of the gas, h the specific enthalpy and E the external energy provided to the gas, represents PV work. Using the relations $h = c_pT$, $c_p/c_v = n$ and $c_p - c_v = R$ the above equation becomes

$$\dot{m} = [PdV/dt + (V/n)dP/dt]/RT \tag{5}$$

The mass flow rate through an orifice is, [12]

$$\dot{m} = C_oC_2AP_u/\sqrt{RT_u}, \text{ for } P_u/P_d > 1.894$$

$$= C_oC_3AP_u/\sqrt{RT_u}, \text{ for } P_u/P_d < 1.894 \tag{6}$$

where the constants C_2 and C_3 are defined as

$$C_2 = \{n/[(n+1)/2]^{(n+1)/(n-1)}\}^{1/2} \tag{7}$$

$$C_3 = [n/(n-1)]^{1/2}(P_d/P_u)^{1/n} \cdot \{1-(P_d/P_u)^{(n-1)/n}\}^{1/2} \tag{8}$$

Mass flow rates given by equations (5) and (6) must be equal at all times; hence, they can be equated to give

$$(PdV/dt+(V/n)dP/dt)/RT = C_oC_{2,3}AP_u/\sqrt{RT_u} \tag{9}$$

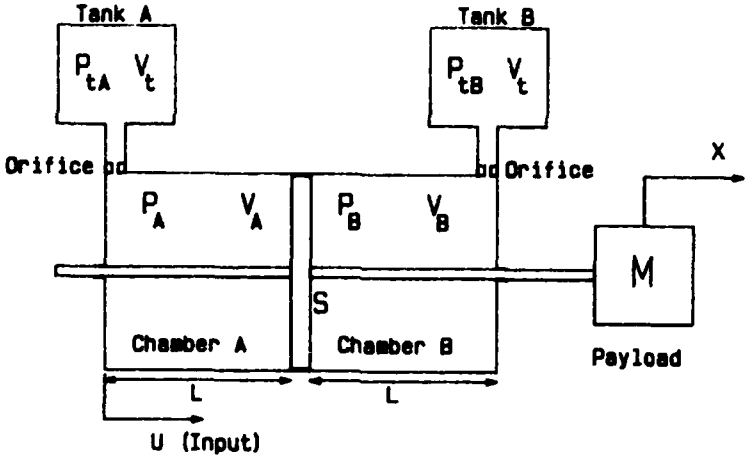

Figure 1. Symmetric Pneumatic Shock Isolator

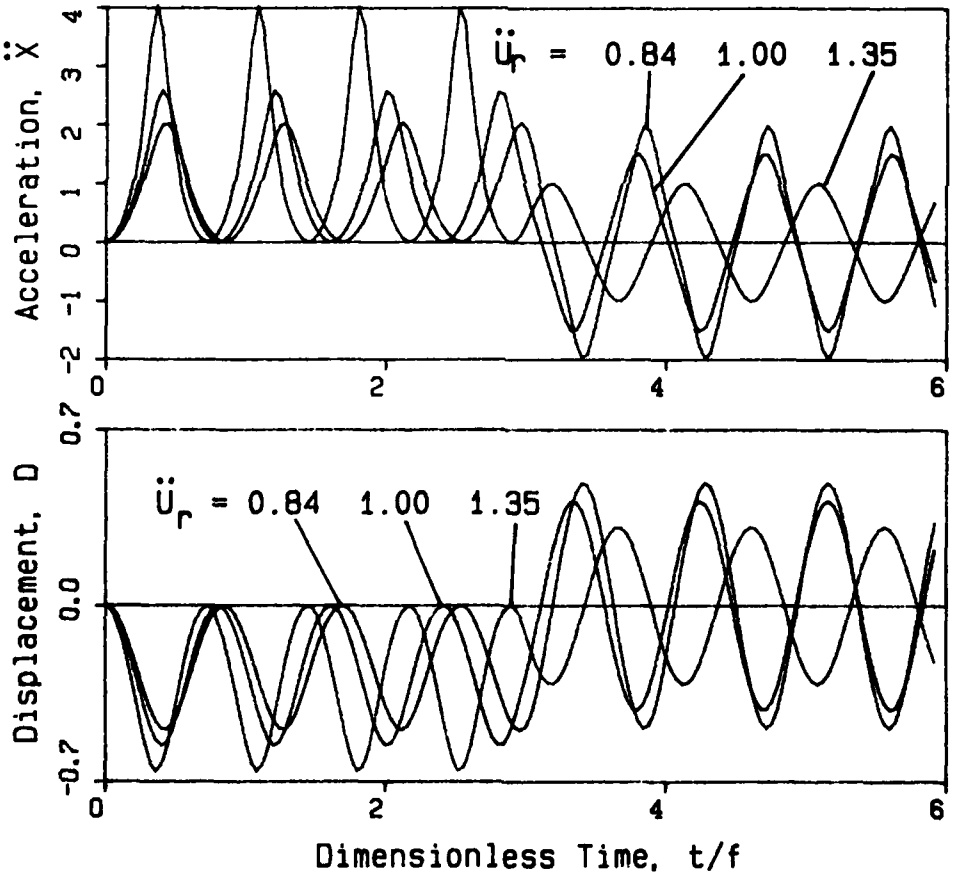

Figure 2. Nonlinear Undamped System Response

The gas volumes in the chambers and volume rates may be expressed in terms of S and d as

$$V_A = V_c + S\,d; \quad dV_A/dt = S\,\dot{d} \tag{10a}$$

$$V_B = V_c - S\,d; \quad dV_B/dt = -S\,\dot{d} \tag{10b}$$

$$dV_{tA}/dt = dV_{tB}/dt = 0 \tag{10c}$$

Next, temperatures may be expressed in terms of the pressure ratios and ambient temperature T_o using the adiabatic relation

$$T_i = T_o(P_i/P_o)^{(n-1)/n} \tag{11}$$

We next define the following quantities: Pressure ratio $P_{io} = P_i/P_o$, where i = A, B, tA or tB; pulse strength ratio $\bar{U}_r = (\ddot{U}/L)^{1/2}$; N = (n-1)/n and the following ratios:

$$\text{Force Ratio} = F_r = P_oS/M\ddot{U} \tag{12a}$$

$$\text{Volume Ratio} = V_r = V_t/V_c = V_t/SL \tag{12b}$$

$$\text{Area Ratio} = A_r = C_o n\sqrt{RT_o}(A/S)L \tag{12c}$$

We now introduce the relative displacement ratio D = d/L. Combining the equations given above yields the following final set of equations used to model the system.

$$dP_{Ao}/dt = [C_{2,3}A_rP_{uAo}^{(1-.5N)} \cdot P_{Ao}^{N} - P_{Ao}n\dot{D}\ddot{U}_r]/(1+D) \tag{13a}$$

$$dP_{tAo}/dt = -C_{2,3}A_rP_{uAo}^{(1-.5N)} \cdot P_{tAo}^{N}/V_r \tag{13b}$$

$$dP_{Bo}/dt = [C_{2,3}A_rP_{uBo}^{(1-.5N)} \cdot P_{Bo}^{N} + P_{Bo}n\dot{D}.\ddot{U}_r]/(1-D) \tag{13c}$$

$$dP_{tBo}/dt = -C_{2,3}A_rP_{uBo}^{(1-.5N)} \cdot P_{Bo}^{N}/V_r \tag{13d}$$

$$\ddot{D} = [F_r(P_{Ao} - P_{Bo}) - a(t)]\ddot{U}_r \tag{13e}$$

$$D = \int_0^t\int_0^t \ddot{D}\,dt\,\ddot{U}_r \tag{13f}$$

LINEAR, UNDAMPED SYSTEM

Before the system response is investigated, the study of the undamped, linearized system will prove useful towards understanding the nonlinear system. The effects of shock pulse strength and duration will become especially evident. If the orifice is closed (A=0) equation (5) becomes

$$P_i dV_i/dt + (V_i/n)dP_i/dt = 0 \tag{14}$$

Since equation (14) applies to both chambers, we can write

$$P_A\dot{V}_A - P_B\dot{V}_B = (V_B\dot{P}_B - V_A\dot{P}_A)/n \tag{15}$$

Now, using equation (10) and since for small deflections $d \approx 0$ and $P_A + P_B = 2P_o$ equation (15) takes the form

$$2nSP_o\dot{d} = V_c(\dot{P}_B - \dot{P}_A) \tag{16}$$

Integrating (16) we get

$$P_A - P_B = -2nP_o d/L \tag{17}$$

Substituting this in equation (2) the equation of motion for small oscillations becomes

$$M\ddot{d} + (2nSP_o/L)\,d = -M\ddot{U}\,a(t) \tag{18}$$

Therefore the spring rate of the linear system is

$$k = 2\,n\,S\,P_o/L \tag{19}$$

and the natural frequency is

$$w_n = (2nSP_o/ML)^{1/2} = (2nF_r\ddot{U}/L)^{1/2} = \ddot{U}_r(2nF_r)^{1/2} \tag{20}$$

after using the definitions of F_r and $\ddot{U}_r$. The period of the linear undamped system is $f = 2\pi/w_n$. In terms of D = d/L and for a rectangular pulse, i.e., a(t) = 1, equation (18) becomes

$$\ddot{D} + w_n^2 D = -\ddot{U}_r^2 \text{ for } t < t_f$$

$$= 0 \text{ for } t > t_f \tag{21}$$

Solution of equation (21) for $t < t_f$ and $D(0) = \dot{D}(0) = 0$ is

$$D = \ddot{U}_r^2/w_n^2(\cos w_n t - 1) \tag{22}$$

or as a function of F_r

$$D = (1/2nF_r)(\cos w_n t - 1) \qquad (23)$$

As is well established in published literature [13], a linear system has the following properties:

1. The maximum possible shock transmission is 2 times the pulse strength for a pulse duration of $t_f > 0.5f$.
2. The maximum shock transmission is dependent on natural frequency and pulse duration for $t_f < 0.5f$ and is independent of either for $t_f > 0.5f$.
3. The maximum deflection is directly proportional to pulse strength for $t_f > 0.5f$. One can also conclude that maximum deflection is proportional to the dimensionless constant $[1/(2nF_r)]$.

A shock isolator would be useless if the transmitted acceleration were greater than the input shock. For this reason, the pulse duration must be less than a certain time, based on natural frequency, that ensures shock transmission less than the input. It has been shown [13] that the maximum pulse duration must be less than 1/6 of the system period, i.e., $t_f < f/6$ for $\ddot{X}_{max} < 1$.

NONLINEAR, UNDAMPED SYSTEM

When piston deflections become large, the assumptions used to derive the linearized equations are no longer valid. The overall effect of nonlinearity is to increase the pneumatic force on the piston for increased displacements. The increasingly harder spring rate will cause the shock transmission to rise above values found using linearity and the higher natural frequency will likewise raise the peak acceleration expected for a particular pulse duration. For a nonlinear, undamped system, plots were made of $\ddot{X}$ and D versus time for increasing pulse strengths with all other characteristics kept equal. These plots are shown in Figure 2. The graphs were then reduced to generate two plots of w/w_n and $\ddot{X}_{max}$ versus D_{max}, respectively and are shown in Figure 3. These demonstrate the exponential character of the system for increasing D. If one can accept up to 10% error, then for peak displacement ratios of less than 0.35 the system can be analyzed as a linear second order system. The limits for safe performance are taken as D greater than 0.8, where the pneumatic spring essentially bottoms out. Both of these observations apply to the undamped system only. By using orifice damping, both of these limits can be raised and shock transmission lowered.

THE DAMPED SYSTEM

The linearized equations for natural frequency, displacement and shock isolation can show the design extremes at opening and closing the orifice when the damped system is analyzed. Referring to Figure 1, if limits of orifice opening are A=0 and A=S, then the effective chamber volume ranges from V_c to V_c+V_t. The effective natural frequency w_e, according to equation (20) in terms of volume ratio V_r becomes

$$w_e = \sqrt{2nP_oS^2/M[SL(1+V_r)]} \qquad (24)$$

or in terms of the closed orifice natural frequency w_n, the lower extreme of system natural frequency (A=S) becomes

$$w_e = w_n/\sqrt{(1+V_r)} \qquad (25)$$

It is seen that a wide open orifice can drastically lower the natural frequency depending on the value of V_r. Also the peak shock transmission will decrease with increasing volume ratio as will the system period. A graph of this phenomenon is shown in Figure 4. This also shows the extreme that for V_r equal to infinity, the system provides perfect isolation, i.e. the piston will not move with respect to ground during excitation. The adverse effect of low V_r's is that displacement ratio D may increase up to D=1 (piston bottomed out in chamber) which may result in damage to the system. This will happen only if t_f is less than $\sqrt{2/U_r}$.

The damping of this isolator results from pressurized gas expanding through two orifices. Since damping removes kinetic energy from the system somewhere between the design extremes of A=0 and A=S, an orifice area providing maximum shock attenuation must exist and was shown in [12]. For any linear, damped second order system, a constant damping ratio exists and can be defined. In this nonlinear system, damping is a function of several variables. In studies by Andersen [1], the damping ratio for the dead-ended orifice chamber undergoing vibration is found to be a function of amplitude, frequency and spring rate of the system. Andersen determines the time constant, τ defining the pressure decay of gas in the upstream source as it depletes into a lower pressure tank to be

$$\tau = [V/(1.198n\sqrt{2RT}\,A)](\Delta P/P)^{1/2} \qquad (26)$$

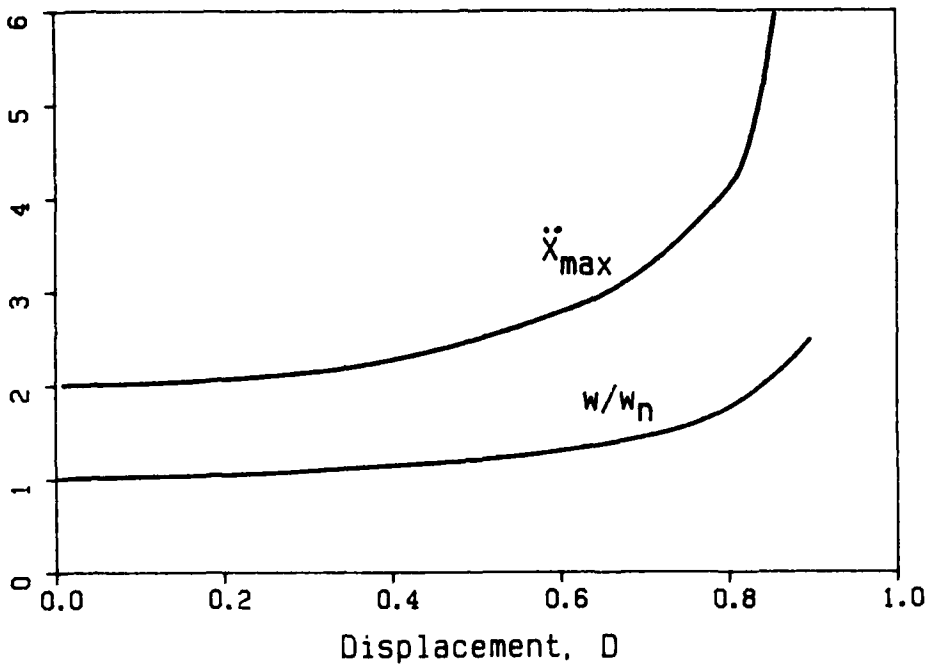

Figure 3. Nonlinear Progression of System Response

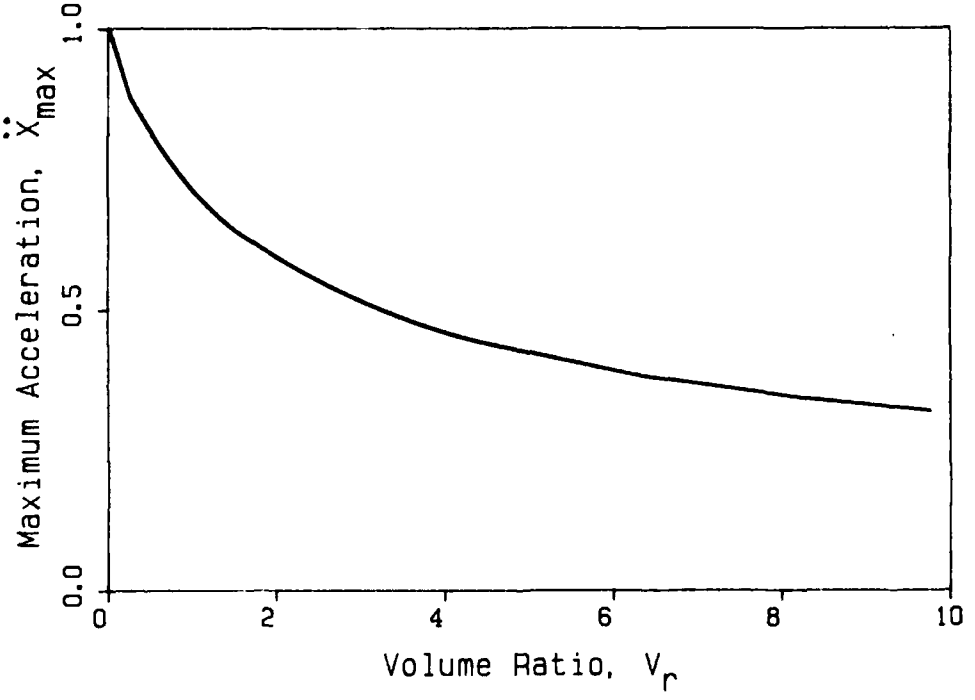

Figure 4. Change in Shock Isolation with Volume Ratio

This equation is for instantaneous chamber volume of V, upstream pressure P, and pressure difference ΔP. Further theoretical and experimental studies of dead-ended orifice systems undergoing small amplitude forced vibrations showed [1] that the damping ratio may be defined as

$$d_a = nP_oS^2\tau/V\ [0.5\sqrt{1 + 4(w_n\tau)^4} - 1]^{3/2}/(w_n\tau)^5$$

or, in terms of spring rate,

$$d_a = k\tau\ [0.5\sqrt{1 + 4(w_n\tau)^4} - 1]^{3/2} /(w_n\tau)^5 \qquad (27)$$

and the optimum damping occurs at

$$w_n\tau = 1 \qquad (28)$$

For the isolator in Figure 1, one can expect that the product $w_n\tau$ would likewise equal one for optimum damping. This damping factor shows that for a system of a particular natural frequency and spring rate, the orifice area and volume ratio (which determines the magnitude of ΔP) will have the greatest impact on damping. We can now state the rule that at any instant of time during the dynamic response of the system, there exists an area ratio that provides maximum damping. Too small an opening will not allow enough gas flow, and too wide an opening will only cause the gas in both chamber and tank to either compress or expand. From equations (28) and (26), it can be said that the greater the amplitude or frequency of the piston, the greater the orifice area must be for optimum isolation.

When considering the second order damped time response to a shock input, a sinusoidal, exponentially decaying function is expected. This is also true for nonlinear pneumatic damping except for one important fact. Since the damping ratio will always change as piston motion decays, the damping ratio will approach zero and the motion will not die out. This is proof of the statement that the area ratio yielding the best time response, as defined later, will be smaller than the area ratio yielding the best shock isolation. The relationship between the two will be demonstrated in detail in the next section and will be analyzed in reference to the damping ratio in equation (27).

DETERMINATION OF OPTIMUM SHOCK ISOLATION

The preceding analysis showed that the area ratio A_r has the greatest effect on system damping and isolation. In this section we will determine what the area ratios for optimum damping and isolation will be for varying shock input strengths and durations. First, consider the effect of increasing $\ddot{U}_r$ on the system while leaving the force ratio and the volume ratio unchanged. The first set of plots are for system characteristics of $F_r = 1$, $V_r = 1$, $t_f = 1/8$ of linear system period , and gas coefficient for air of $n = 1.4$. Now, when $\ddot{U}_r$ increases, the linearized natural frequency will change proportionally according to equation (20). Since F_r will remain unchanged, either P_o or S must proportionally change in order to reflect a change in shock strength $\ddot{U}$. Hence, a stiffer pneumatic spring results. Altering $\ddot{U}_r$ also implies a change in cylinder length L. This would necessitate adjusting V_t. The plots of A_r versus X_{max} for the above conditions and varying $\ddot{U}_r$ are shown in Figure 5. From these graphs, one can conclude that the percent reduction in transmitted acceleration is constant for all $\ddot{U}_r$. In Table 1, a compilation of X_{max} versus A_r for different pulse durations is given.

These graphs were then reduced to show the area ratio for optimum isolation, A_{roi} versus $\ddot{U}_r$ and are shown in Figure 6. We notice from this figure that a linear relationship exists between these variables. The slope of these curves is an exponential function of t_r. The area ratio for optimum shock isolation for varying $\ddot{U}_r$ and the previously given F_r and V_r is, approximately,

$$A_{roi} = 3.2\ U_r(t_r/f)^{0.560} \qquad (29)$$

From this equation it can be said that for any system excited for a particular pulse duration, the dimensionless ratio of $A_{roi}/\ddot{U}_r$ must be constant. The relationship between piston displacement D_{max} and $\ddot{U}_r$ offers a reason for the constant nature of $A_{roi}/\ddot{U}_r$. The plots of D_{max} versus A_r in Figure 7 correspond to the plots in Figure 6. These graphs have been marked with an "x" at the point where A_r yields optimum shock isolation. Now notice that D_{max} is the same at optimum isolation regardless of $\ddot{U}_r$. Since the natural frequency changes with $\ddot{U}_r$ in this analysis, the time constant defined in equation (26) must change proportionally to obtain the same damping ratio for a different strength pulse. The best way to describe what happens in this system is to take an energy perspective. The energy input to the system increases in proportion to $\ddot{U}$. Also, by nature of the defined natural frequency, the initial pressure P_o and mass of gas must also increase by equal proportions. Now, the energy dissipation may be assumed directly proportional to the mass of gas passing through the orifices. From this, it may be concluded that for an equally proportional change in energy input and amount of gas, the volume of

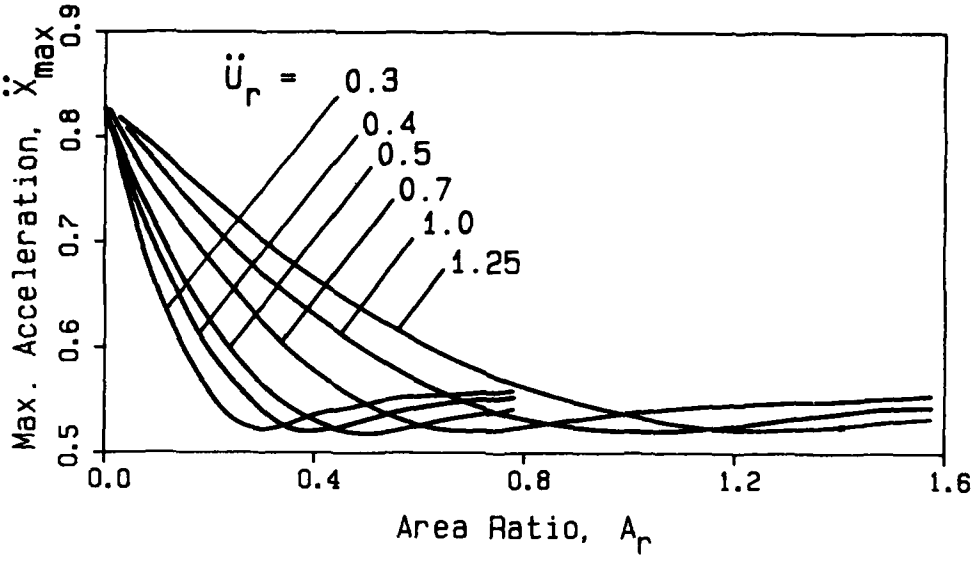

Figure 5. Shock Isolation for Different Area Ratios

TABLE 1

$\ddot{X}_{max}$ versus $\ddot{U}_r$ for Optimum Isolation

t_f	0.0625f		0.125f		0.167f		0.25f	
$\ddot{U}_r$	$\ddot{X}_{max}$	A_r	$\ddot{X}_{max}$	A_r	$\ddot{X}_{max}$	A_r	$\ddot{X}_{max}$	A_r
0.3	0.259	0.22	0.527	0.30	0.713	0.36	1.105	0.47
0.4	0.256	0.27	0.520	0.41	0.714	0.49	1.090	0.60
0.5	0.259	0.36	0.527	0.52	0.704	0.60	1.105	0.77
0.7	0.256	0.49	0.520	0.71	0.713	0.85	1.090	1.07
1.0	0.259	0.68	0.527	1.01	0.704	1.18	1.105	1.53
1.25	0.259	0.88	0.527	1.26	0.704	1.48	1.105	1.90

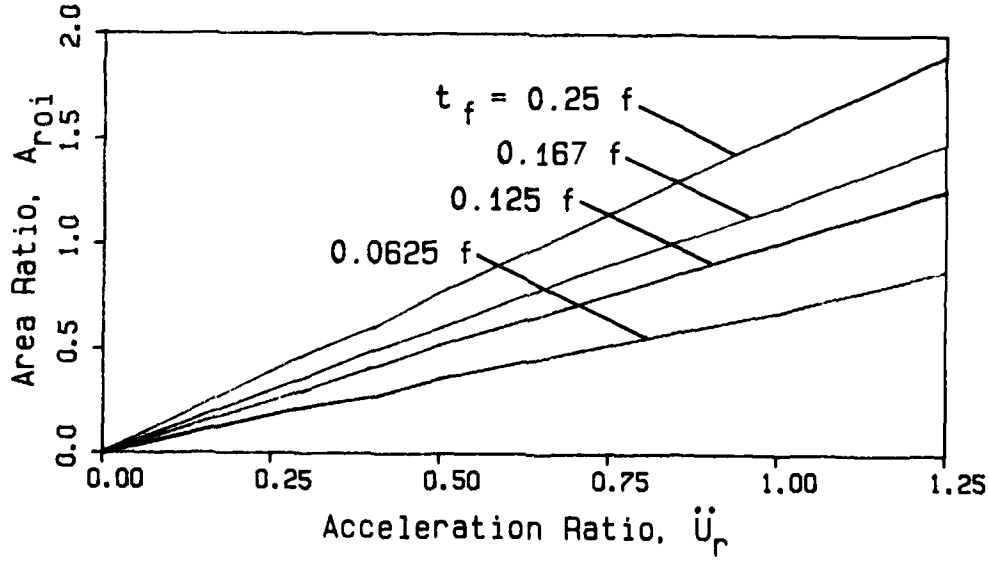

Figure 6. Area Ratios for Optimum Shock Isolation

displaced gas must be the same to achieve the same energy dissipation. Thus the relation $\Delta P/P$ in equation (26) must not change in order to attain the same energy dissipation rate over the first half cycle of the system's response. Referring back to equations (26) and (28), since w_n changes proportionally with $\ddot{U}_r$, the only factor in ζ that can change to provide equivalent damping is A. Hence, any increase in $\ddot{U}_r$ requires an equal increase in area ratio A_r to achieve optimum shock isolation. The corresponding displacement at A_{roi} for the studied pulse durations are shown in Table 2.

DETERMINATION OF OPTIMUM TIME RESPONSE

The analysis presented thus far deals with the first half cycle of the system response. It was stated before that as piston amplitude and frequency decrease, the damping ratio will change and the orifices will provide less damping capabilities. To improve time response the area ratio must be decreased from that required for best shock isolation to compensate for the loss of damping experienced with lower optimum response. Thus a criterion for amplitude decay must be established. Through trial computer runs, the lowest amplitude one and one-half periods after the first peak in the acceleration curves is used as a criterion to evaluate effect of area ratio on damped response.

Time response for the system was determined using different area ratios and by observation, the optimum area ratio was then ascertained. The optimum area ratios for various $\ddot{U}_r$'s and t_f's are listed in Table 3.

A plot of A_r for optimum time response, A_{ror} versus $\ddot{U}_r$ is shown in Figure 8. Once again, a linear relationship exists between A_{ror}, $\ddot{U}_r$ and an exponential relation between their slope and t_f as was the case for optimum shock isolation. The equation relating A_{ror} to t_f and $\ddot{U}_r$ is, approximately,

$$A_{ror} = 1.2\, \ddot{U}_r (t_f/f)^{0.550} \qquad (30)$$

Figures 6 and 8 reveal that the area ratio for optimum isolation and area ratio for optimum response are related to each other for any t_f. The relation is found to be

$$A_{ror} = 0.375\, A_{roi} \qquad (31)$$

Furthermore, comparing the time-response curves at optimum damping for a particular t_f reveals that the shape of the optimum response is identical for any $\ddot{U}_r$ for the same reasons as the maximum deflection at optimum isolation being the same for any $\ddot{U}_r$.

The preceding study demonstrates the trade-off which must be made in deciding whether to obtain the most shock isolation possible or provide a faster settling time. To show the extent of the trade-off, time response curves for $\ddot{U}_r = 0.5$ and corresponding area ratios yielding optimum isolation and damping are shown in Figure 9. Notice that for $A_r = A_{roi}$ the systems shows very low damping. The shock transmission for $A_r = A_{ror}$ is approximately 20% higher than that obtained using $A_r = A_{roi}$. For this reason, the best design should have the area ratio provide optimum response rather than optimum isolation.

EFFECT OF VARYING PULSE STRENGTH

The preceding work studied the effects of varying $\ddot{U}_r$, but it did not tell us how a particular system would respond to a pure change in shock strength $\ddot{U}$. Previously, it was mentioned that a change in $\ddot{U}_r$ inherently produced a change in natural frequency and spring rate. Studying the change in $\ddot{U}$ will reveal the operating range for the system based on pulse duration. Operating range is defined as the limiting $\ddot{U}$ that at either optimum isolation or response will cause the pneumatic spring deflect to D = 0.8. For this purpose $\ddot{U}_r$ and t_f were varied and $V_r = 1$ and $f = 1/1.172$ were used. F_r was computed for each particular $\ddot{U}_r$. Plots of $\ddot{X}_{max}$ versus A_r and D_{max} versus A_r were generated for varying $\ddot{U}_r$ and $t_f = 0.125f$ and are shown in Figure 10. Comparing these curves to those in Figure 5 reveals that the transmitted shock at optimum area ratio varies exponentially with $\ddot{U}$. The percent of shock absorption attainable also varies with $\ddot{U}$. Plotting A_{ror} and A_{roi} versus $\ddot{U}_r$ for different pulse durations is done in Figure 11. The results are more indicative of a nonlinear system where over a band of low inputs the relationships between A_{roi} and A_{ror} versus $\ddot{U}_r$ are linear and for large inputs they increase exponentially until the pneumatic spring bottoms out. The displacement data obtained show that the system becomes nonlinear for D > 0.35. Another result obtainable from these plots is that their exists a maximum A_{roi}, independent of pulse duration above which the system will bottom out. These area ratios are found to be

$$\max A_{roi} = 1.3$$

$$\max A_{ror} = 0.47 \qquad (32)$$

Since this is the limiting area ratio, obviously there is a limit on the range of $\ddot{U}_r$ that the system can withstand before bottoming out and the extent of this range is a function of pulse duration. By curve fitting the data this range can be expressed as

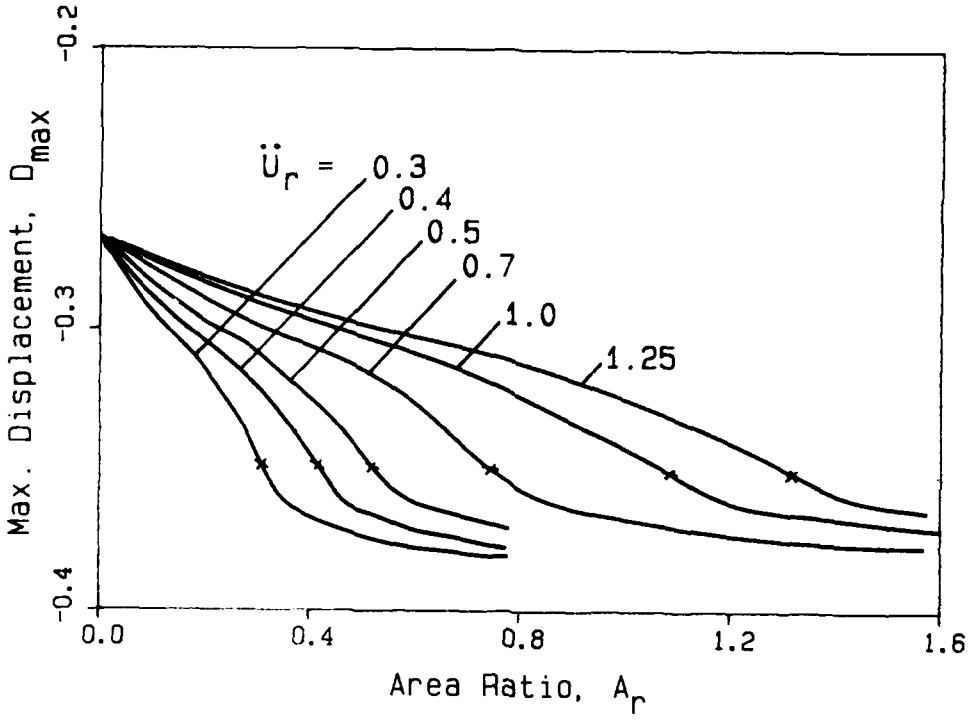

Figure 7. Maximum Displacement vs. Area Ratio

TABLE 2

Maximum Displacement at Optimum Isolation

t_f	0.0625f	0.125f	0.167f	0.25f
$\ddot{U}_r$	D_{max}	D_{max}	D_{max}	D_{max}
0.3	0.18	0.35	0.45	0.65
0.4	0.18	0.35	0.46	0.64
0.5	0.18	0.35	0.45	0.65
0.7	0.18	0.35	0.46	0.64
1.0	0.18	0.35	0.45	0.64
1.25	0.18	0.35	0.45	0.65

TABLE 3

Area Ratio Versus Acceleration Ratio

t_f	0.0625f	0.125f	0.167f	0.25f
$\ddot{U}_r$	A_r	A_r	A_r	A_r
0.3	0.08	0.11	0.14	0.16
0.4	0.11	0.16	0.18	0.22
0.5	0.14	0.20	0.24	0.27
0.7	0.19	0.27	0.30	0.38
1.0	0.27	0.38	0.44	0.55
1.25	0.34	0.51	0.55	0.66

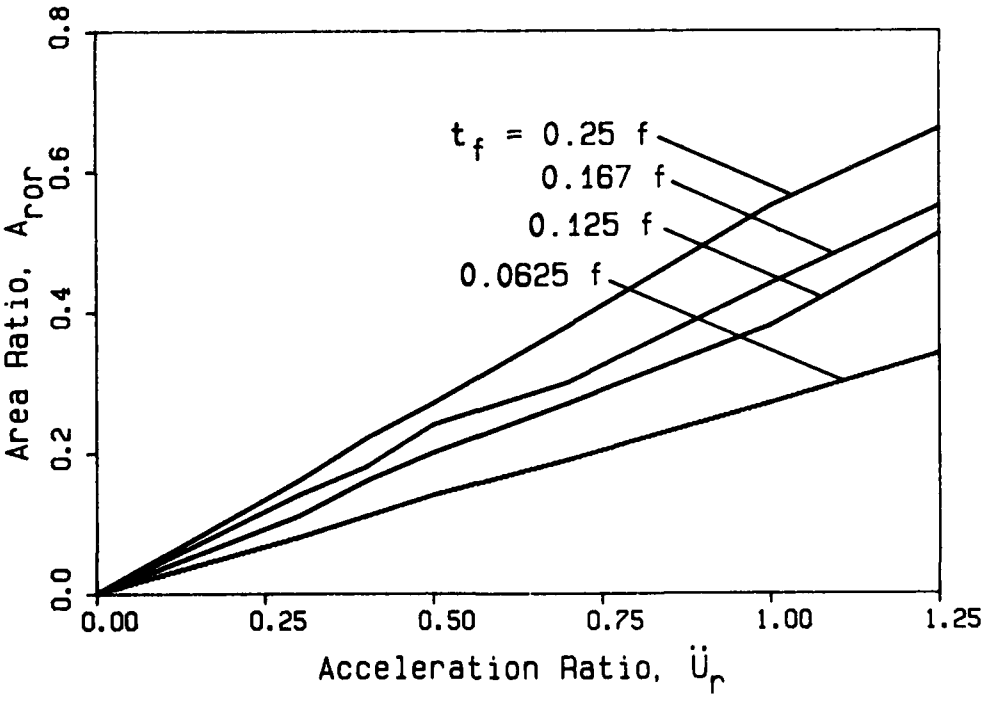

Figure 8. Area Ratios for Optimum Response

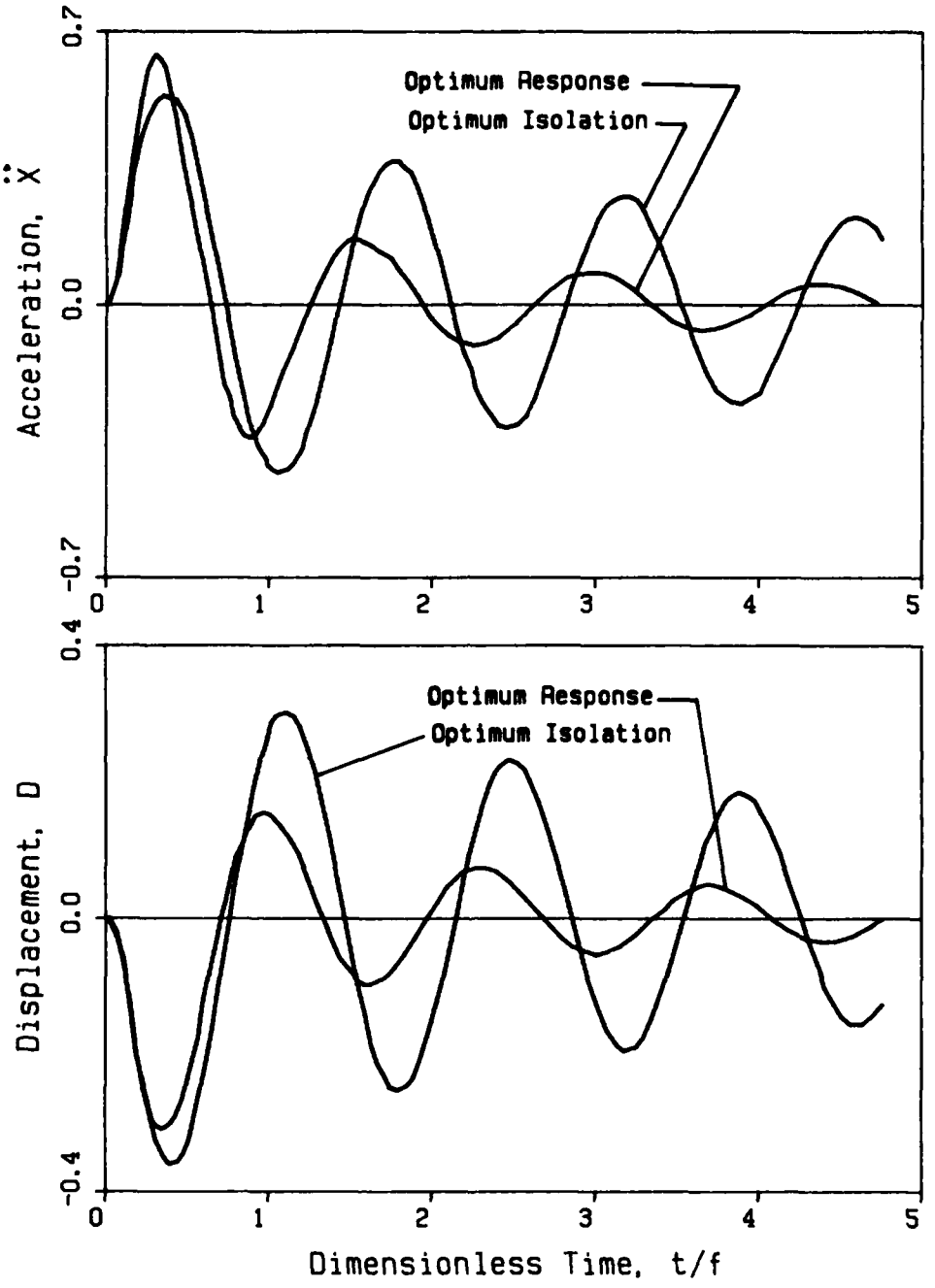

Figure 9. Use of Area Ratios for Optimum Response and Isolation

$$\text{Range of } \ddot{U}_r = 0.375/(t_f/f)^{0.550}$$

for optimum isolation

$$\text{Range of } \ddot{U}_r = 0.462/(t_f/f)^{0.49}$$

for optimum response (33)

In the linear range of Figure 11, the relationships between A_r for optimum isolation and response, as functions of $\ddot{U}_r$ and t_f are

$$A_{roi} = 2.63\ \ddot{U}_r(t_f/f)^{0.476} \quad (34)$$

$$A_{ror} = 1.047\ \ddot{U}_r(t_f/f)^{0.495} \quad (35)$$

and the relationship between A_{roi} and A_{ror} in the linear range is approximately

$$A_{ror} = 0.398\ A_{roi} \quad (36)$$

The relationships stated in equations (32) and (33) will be of great importance to a designer since the size of his system will be dependent on the range of pulse duration and pulse strength of the shock environment.

DESIGN CONSIDERATIONS AND DISCUSSION

With the information provided in this study, a methodical approach can be used to design a pneumatic shock absorber such as the one just studied. First, the designer must gather information on the shock environment, the pneumatic properties and the dimensional constraints. If all of the above are known, the designer should begin the design having already ascertained the factors M, $\ddot{U}$, t_f, n, R, T_o and the range of shock strengths and durations that the mass may encounter. The design criteria should be based on the expected pulse with allowances made for handling more severe pulses without bottoming. The design is an iterative process and the iteration should provide the optimum parameters.

One of the first steps is to determine the linearized natural frequency of the isolator. Knowing t_f and the range of pulses encountered the frequency may be ascertained by referring to equation (33) for range, then choosing the fraction of system period necessary to provide for the range of pulse strengths encountered. Calling this fraction Y, the linearized natural frequency may be expressed as

$$w_n = 2\pi Y/t_f = \ddot{U}_r(2nF_r)^{1/2} \quad (37)$$

Now recalling that the force ratio controls displacement, the force ratio may be determined, equation (23), and knowing the maximum displacement desirable for the expected shock pulse. This displacement should be less than 0.35 to assure linearity.

Obtaining the desired force ratio F_r, allows determination of the static pneumatic force on the piston, SP_o, which is from equation (12a)

$$SP_o = F_r M\ddot{U} \quad (38)$$

Now, knowing F_r and Y allows solutions to $\ddot{U}_r$ and subsequently L to be, from (37),

$$\ddot{U}_r = 2\pi Y/t_f(2nF_r)^{1/2} \quad (39)$$

and

$$L = \ddot{U}/\ddot{U}_r^2 \quad (40)$$

The final solutions for S, P_o and L are obtained by considering the envelope requirements of the isolator. If requirements on length are satisfied, then the length found in equation (40) should be used and if requirements on S are satisfied, then S should be determined using equation (38) and set P_o equal to 1 atm. for simplicity. If envelope requirements prohibit S and L from being values chosen using equations (38) and (40), respectively, then the following alterations should be made: If S is constrained, determine the largest piston area possible and compute the P_o necessary to satisfy equation (38). If L is constrained, choose the longest L possible, then recalculate $\ddot{U}_r$ per equation (40) and recalculate F_r for the higher value of $\ddot{U}_r$ using equation (39), then solve for P_o using the higher value of F_r. This compensates for the increased chance of bottoming as a result of decreasing the chamber length. Finally, using the plots in Figure 8, determine the area ratio necessary to provide optimum response to the expected pulse for the computed $\ddot{U}_r$. From this plot, the desired orifice area may be determined using equation (14) for A_r and the product C_oA may now be computed as

$$C_oA = A_rSL/n(RT_o)^{1/2} \quad (41)$$

CONCLUSIONS

The response of a symmetric, self-damped shock isolator has been modelled and its response predicted. The sensitivity of pneumatic damping is shown in detail here and is an important consideration in design. Because of this any design of a pneumatic shock

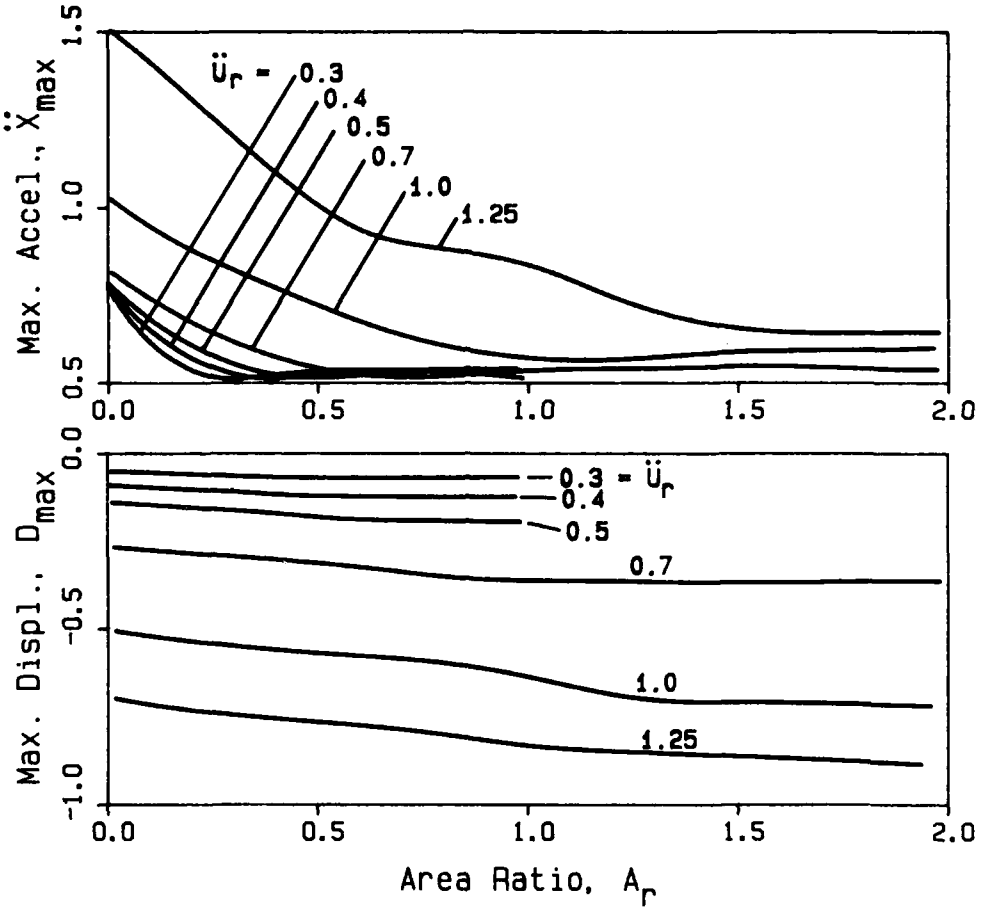

Figure 10. Determining Area Ratio for Maximum Shock Isolation

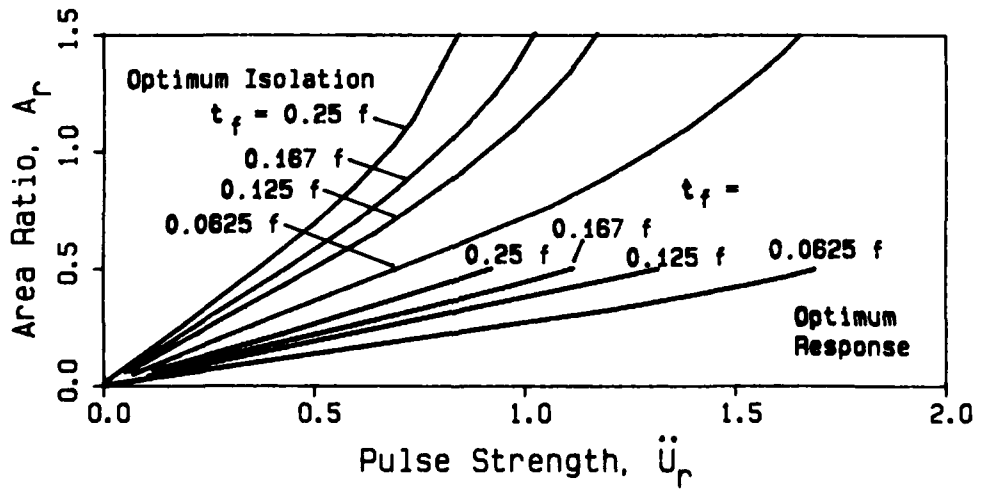

Figure 11. Optimum Area Ratios for Varying Pulse Strength

isolator of this type should not focus just on optimum shock attenuation, but also on dynamic response. The trade-off between shock attenuation and motion decay definitely favors designing for motion decay using the criterion of most decay one and one-half cycles following the first acceleration peak. Although theoretically the oscillating motion should continue almost indefinitely, coulomb friction between the piston and chamber wall will become dominant at small deflections and would bring the piston to a stop. The ideal design should keep displacements in the dynamically linear range of $D < 0.35$. This is for predictability and to provide allowance for unexpectedly severe shocks. For any type of shock pulse, the natural frequency of the system should be such that the shock duration is less than 1/6th the natural period so as to ensure shock attenuation and not amplification. If a volume ratio of unity is used, linearity can be assured by maintaining a force ratio greater than one [14].

The five factors F_r, A_r, $\ddot{U}_r$, V_r and t_f are adequate for describing the behavior of the system in the general sense. The constant relationship of $A_{ror}/\ddot{U}_r$ and $A_{roi}/\ddot{U}_r$ provides the capability of quick analysis of any changes to a design. Although a volume ratio of unity is recommended due its favorable compromise between space and dynamic constraints, it can be made larger if a specific acceleration pulse is expected. This could provide greater shock attenuation with a small trade-off for higher displacement and additional space.

Further details of this study, including the effects of varying force and volume ratios and response to other pulse shapes may be found in reference [14].

REFERENCES

1. B. Anderson 1967 The analysis and design of pneumatic systems. J. Wiley & Sons. Chapter 4.

2. B. I. Bachrach and E. Rivin 1983 Shock and Vibration Bulletin. Vol 86, pp 191-197. Transient Response of Passive Pneumatic Shock Isolators.

3. W. S. Berry 1958 Transactions of the Society of Automotive Engineers vol 66, p. 471. The air coil spring.

4. R. D. Cavanaugh 1976 in Shock and Vibration Handbook (editors C. M. Harris and C. E. Crede). New York: McGraw-Hill, second edition, Chapter 33. Air suspension and servo-controlled isolation systems.

5. R. E. Eshleman and P. N. Rao 1969 Shock and Vibration Bulletin vol 40(5), pp. 217-234. The responses of mechanical shock isolation elements to high rate input loading.

6. E. Esmailzadeh 1978 Transactions of the American Society of Mechanical Engineers, Journal of Mechanical Design vol 100, pp. 500-506. Optimization of pneumatic vibration isolation system for vehicle suspension.

7. E. Esmailzadeh 1979 Journal of Mechanical Engineering Science vol 21, pp. 7-18. Servo-valve controlled pneumatic suspensions.

8. G. L. Fox and E. Steiner 1972 Shock and Vibration Bulletin vol 42(4), pp. 85-91. Transient response of passive pneumatic isolators.

9. A. B. Hirtreiter 1965 Machine Design vol 37, p. 104. Air springs.

10. M. S. Hundal 1981 Journal of Sound and Vibration. vol 76(2), pp 273-281. Response of Shock Isolators with Linear and Quadratic Damping.

11. M. S. Hundal 1982 Shock and Vibration Bulletin vol 52(4), pp. 161-168. Response of a pneumatic isolator to standard pulse shapes.

12. M. S. Hundal 1983 Shock and Vibration Bulletin vol 53(4), pp. 73-83. Damped pneumatic spring as shock isolator: generalized analysis and design procedure.

13. W. T. Thomson 1972 Theory of Mechanical Vibration. Prentice Hall, chapter 4.

14. D. J. Fitzmorris 1984 Analysis of a Symmetric Self-damped Pneumatic Shock Absorber. M.S. Thesis, University of Vermont.

NOMENCLATURE

$a(t)$ = input acceleration shape function

A = orifice area

A_r = area ratio, A/S

A_{roi} = area ratio for optimum shock isolation

A_{ror} = area ratio for optimum system response

C_2 = orifice constant for sonic flow

C_3 = orifice constant for subsonic flow

C_o = orifice discharge coefficient

c_p = specific heat at constant pressure

c_v = specific heat at constant volume

d = piston displacement relative to

D = displacement ratio, d/L

f = period of linearized system

F_r = force ratio

h = specific enthalpy

k = spring rate of linearized system

m = mass of gas

M = mass of piston and payload

n = c_p/c_v

N = $(n-1)/n$

P_i = pressure in chamber or tank i

P_o = static fluid pressure

P_{io} = pressure ratio, P_i/P_o

P_d = downstream pressure

P_{ui} = upstream pressure in chamber i

R = gas constant

S = piston area

t = time

t_f = shock pulse duration

τ = exponential time constant

T_i = temperature in chamber or tank i

T_o = static gas temperature

T_d = downstream temperature

T_{ui} = upstream temperature in chamber i

U = base motion

V_c = chamber volume at rest

V_i = volume of chamber or tank i

V_r = volume ratio

w_n = natural frequency, linearized system

x = absolute motion of piston and payload

X = absolute displacement ratio, x/U

Subscripts on P, T and V:

i = A: chamber A

= B: chamber B

= tA: tank A

= tB: tank B

VIBRATION AND DAMPING ANALYSIS OF CURVED SANDWICH PANEL WITH VISCOELASTIC CORE

J. Vaswani, N.T. Asnani and B.C. Nakra
Mechanical Engineering Department
I.I.T. Delhi-110016 INDIA

Equations of motion for flexural vibrations of curved sandwich panel, consisting of elastic face layers sandwiching a viscoelastic core have been derived considering extension and bending deformations in the face layers and shear deformation in the core layer, using variational principles. A solution for panel with simply supported edges is taken in series summation form and the correspondence principle of linear viscoelasticity is applied for evaluating the resonant frequencies and associated system loss factors. Effects of the variations of the geometric and the material parameters on the resonant frequencies and the system loss factors are reported.

NOTATIONS

CR	Curvature Parameter ($=t_3/2R$)
E_i	Youngs Modulus of ith layer
FPR	Frequency parameter
G_2	Shear modulus of core
l	length along straight edge of panel
m	Number of half waves in ϕ direction
n	Number of half waves in y direction
p_{mn}	Resonance Frequency for m-n mode
R_i	Radius of curvature of ith layers
t_i	Thickness of ith layer
u_i	Displacement of midsurface of ith layer along ϕ direction
v_i	Displacement of midsurface of ith layer along y direction
w	Displacement along z direction
y	Coordinate along straight edge of panel
z	Coordinate perpendicular to ϕ and y coordination
η_2	Loss factor of core
η_s	System loss factor
ν_i	Poissons ratio of ith layer
ϕ	Coordinate along curved edge of panel
ρ_i	Density of ith layer
δ_{23}	Shear parameter
β_{23}	Length parameter
θ_{13}	Elastic layer thickness ratio ($=\frac{t_1}{t_3}$)
θ_{23}	Core layer thickness ratio ($=\frac{t_2}{t_3}$)
γ	Aspect ratio ($=\frac{R_2\theta}{l}$)

INTRODUCTION

Considerable work, has been reported on vibration and damping analysis of flat sandwich panels with elastic face layers sandwiching viscoelastic core [1,2,3]. However in many applications, curved rather than straight panels are encountered, especially in aerospace structures. Sewall [4], Petyt and Debnath [5] have reported vibration analysis of a curved homogeneous panel and Mead and Pretlove [6] have analyzed vibrations of a curved sandwich panel with elastic core. In the present paper, governing equations of motion for a curved sandwich panel consisting of elastic face layers sandwiching a viscoelastic core have been derived, considering extension and bending deformations of the face layers and shear deformations of the core layer, using the variational principles. A solution for simply supported sandwich panel is taken in series summation form and the correspondence principle of linear viscoelasticity is applied for evaluating the resonant frequencies and the associated system loss factors.

EQUATIONS OF MOTION

Figure (1) shows the configuration and the displacement pattern of the curved sandwich panel. Assuming all the displacements to be small and continuous with no slip at interfaces, the strains at a point distance z from the midsurface

of ith layer (i=1,3) are given by [7],

$$\epsilon_{\phi i} = \frac{u_i'}{R_i} + \frac{W}{R_i+Z} - \frac{ZW''}{R_i(R_i+Z)}$$

$$\epsilon_{y_i} = v_i^* - ZW^{**}$$

$$\gamma_{\phi y_i} = \frac{R_i}{R_i+Z}\, u_i'' + \frac{R_i+Z}{R_i^2} v_i' - \left(\frac{Z}{R_i} + \frac{Z}{R_i+Z}\right) W'^*$$

and the shear strains in the core are given by

$$\gamma_{\phi z} = \frac{R_2}{R_2+z} \frac{1}{t_2} \left(\frac{w'h_1}{R_2} + b_1 u_1 - b_2 u_3 \right)$$

where

$$b_1 = \left(1 - \frac{t_2}{2R_2}\right)\left(1 - \frac{t_1}{2R_2}\right), \quad b_2 = \left(1 + \frac{t_2}{2R_2}\right)\left(1 + \frac{t_3}{2R_2}\right)$$

$$h_1 = \frac{t_1}{2}\left(\frac{R_2}{R_1} - \frac{t_2}{2R_1}\right) + \frac{t_3}{2}\left(\frac{R_2}{R_3} + \frac{t_3}{2R_3}\right) + t_2$$

$$\gamma_{yz} = \frac{1}{t_2}\left(v_1 - v_3 + h_2 w''\right)$$

where $h_2 = \frac{t_1+t_3}{2} + t_2$

The strain energy of the panel is given by

$$U = \sum_{i=1,3} \int_{-\frac{t_i}{2}}^{+\frac{t_i}{2}} \int_0^1 \int_0^\theta \frac{E_i}{2(1-\nu_i^2)} \left\{ \epsilon_\phi^2 + \epsilon_y^2 + 2\nu_i \epsilon_\phi \epsilon_y - \frac{1-\nu_i}{2} \gamma_{\phi y}^2 \right\} (R_i+z)\, d\phi\, dy\, dz$$

$$+ \int_{-\frac{t_i}{2}}^{+\frac{t_i}{2}} \int_0^1 \int_0^\theta \frac{G_2}{2} \left(\gamma_{\phi z}^2 + \gamma_{yz}^2\right)(R_2+z)\, d\phi\, dy\, dz \qquad \ldots(2)$$

Taking only transverse inertia the kinetic energy of the panel is given by

$$T = \sum_{i=1}^{3} \int_{-\frac{t_i}{2}}^{+\frac{t_i}{2}} \int_0^1 \int_0^\theta \frac{\rho_i}{2} \dot{w}^2 (R_i+z)\, d\phi\, dy\, dz \qquad \ldots(3)$$

The potential energy of the radial loading $q(\phi,y)$ Sin pt on the panel is given by

$$V = \int_0^1 \int_0^\theta q(\phi,y) \sin pt\, WR\, d\phi\, dy \qquad \ldots(4)$$

Taking the variations and applying Hamilton's principle, following equations of motion are obtained

$$\frac{C_1}{R_1R_2} u_1'' + \frac{C_1R_1}{R_2} \frac{(1-\nu_1)}{2} u_1^{**} + \frac{3D_1}{R_1R_2} \frac{(1-\nu_1)}{2} u_1^{**} - G_2 A b_1^2 u_1 + G_2 A b_1 b_2 u_3$$

$$+ \frac{C_1}{R_2} \frac{(1+\nu_1)}{2} v_1'^* + \frac{C_1}{R_1R_2} w' - \frac{3D_1}{R_1R_2} \frac{(1-\nu_1)}{2} w'^{**} - \frac{D_1\nu_1}{R_1R_2} w'^{**} - \frac{G_2 A b_1 h_1}{R_2} w' = 0 \qquad \ldots(5)$$

$$\frac{C_3}{R_2R_3} u_3'' + \frac{C_3R_3}{R_2} \frac{(1-\nu_3)}{2} u_3^{**} + \frac{3D_3}{R_2R_3} \frac{(1-\nu_3)}{2} u_3^{**} - G_2 A b_2^2 u_3 + G_2 A b_1 b_2 u_1$$

$$+ \frac{C_3}{R_2} \frac{(1-\nu_3)}{2} v_3'^* + \frac{C_3}{R_2R_3} w' - \frac{3D_3}{R_2R_3} \frac{(1-\nu_3)}{2} w'^{**} - \frac{D_3}{R_2R_3} w'^{**} + \frac{G_2 A b_2 h_1 w'}{R_2} = 0 \qquad \ldots(6)$$

$$\frac{C_1R_1}{R_2} v_1^{**} + \frac{C_1}{R_1R_2} \frac{(1-\nu_1)}{2} v_1'' + \frac{D_1}{R_1^3R_2} \frac{(1-\nu_1)}{2} v_1'' - \frac{G_2\nu_1}{t_2} + \frac{G_2\nu_3}{t_2} + \frac{C_1}{R_2} \frac{(1+\nu_1)}{2} u_1'^*$$

$$+ \frac{C_1}{R_2} \nu_1 w^* + \frac{D_1}{R_1^2R_2} \frac{(1-\nu_1)}{2} w''^* - \frac{D_1}{R_2} w^{***} - \frac{G_2h_2}{t_2} w^* = 0 \qquad \ldots(7)$$

$$\frac{C_3R_3}{R_2} v_3^{**} + \frac{C_3}{R_2R_3} \frac{(1-\nu_3)}{2} v_3'' + \frac{D_3}{R_2R_3^3} \frac{(1-\nu_3)}{2} v_3'' - \frac{G_2}{t_2} v_3 + \frac{G_2}{t_2} v_1 + \frac{C_3}{R_2} \frac{(1+\nu_3)}{2} u_3'^*$$

$$+ \frac{C_3}{R_2} \nu_3 w^* + \frac{D_3}{R_2R_3^2} \frac{(1-\nu_3)}{2} w''^* - \frac{D_3}{R_2^2} w^{***} + \frac{G_2 h_2}{t_2} w^* = 0$$

$$\frac{C_1}{R_1R_2}u_1' - \frac{3D_1}{R_1R_2}\frac{(1-\nu_1)}{2}u_1'^{**} - \frac{D_1\nu_1}{R_1R_2}u_1'^{**} - \frac{G_2Ab_1h_1}{R_2}u_1' + \frac{C_3}{R_2R_3}u_3' - \frac{3D_3R_3}{R_2}\frac{(1-\nu_3)}{t_2}u_3'^{**}$$

$$- \frac{D_3\nu_3}{R_2R_3}u_3'^{**} + \frac{G_2Ab_2h_1}{R_2}u_3' + \frac{C_1}{R_2}\nu_1v_1^* + \frac{D_1}{R_1^2R_2}\frac{(1-\nu_1)}{2}v_1''^* - \frac{D_1}{R_2}v_1^{***} - \frac{G_2h_2}{t_2}v_1^*$$

$$+ \frac{C_3}{R_2}\nu_3v_3^* + \frac{D_3}{R_2R_3^2}\frac{(1+\nu_3)}{2}v_3''^* - \frac{D_3}{R_2}v_3^{***} + \frac{G_2h_2}{t_2}v_3'' + \left(\frac{C_1}{R_1R_2} + \frac{C_3}{R_2R_3}\right)w$$

$$+\left(\frac{D_1}{R_1^3R_2} + \frac{D_3}{R_2R_3^3}\right)(w''''+2w'') - \frac{G_2Ah_1^2}{R_2^2}w'' - \frac{G_2h_2^2}{t_2}w^{**} = q - \rho tw^{\cdot\cdot} \qquad \ldots(9)$$

where $C_i = \frac{E_i t_i}{1-\nu_i^2}$ and $D_i = \frac{E_i t_i^3}{12(1-\nu_i^2)}$

(for i = 1 and 3)

Simply Supported Panel

The solution for a curved sandwich panel with simply supported edges is taken in series summation form as follows

$$w = \sum_{m=1}^{\infty}\sum_{n=1}^{\infty} W_{mn} \sin\left(\frac{m\pi\phi}{\theta}\right)\sin\left(\frac{n\pi y}{\ell}\right)\sin pt$$

$$u_i = \sum_{m=1}^{\infty}\sum_{n=1}^{\infty} U_{imn} \cos\left(\frac{m\pi\phi}{\theta}\right)\sin\left(\frac{n\pi y}{\ell}\right)\sin pt \qquad \ldots(9)$$

(for i = 1 and 3)

$$v_i = \sum_{m=1}^{\infty}\sum_{n=1}^{\infty} V_{imn} \sin\left(\frac{m\pi\phi}{\theta}\right)\cos\left(\frac{n\pi y}{\ell}\right)\sin pt \quad \text{(for i = 1 and 3)}$$

and radial loading is expressed in series summation form as

$$q(\phi,y) = \sum_{m=1}^{\infty}\sum_{n=1}^{\infty} q_{mn} \sin\left(\frac{m\pi\phi}{\theta}\right)\sin\left(\frac{n\pi y}{\ell}\right)\sin pt$$

Substituting eqns (9) in eqns (5 to 8), the resulting algebraic eqns. may be written in matrix form as

$$\begin{bmatrix} & & & & \\ & & A & & \\ & & & & \end{bmatrix} \begin{Bmatrix} u_{imn} \\ u_{3mn} \\ V_{1mn} \\ V_{3mn} \\ W_{mn} \end{Bmatrix} = \begin{Bmatrix} 0 \\ 0 \\ 0 \\ 0 \\ q_{mn} - \rho^2 W_{mn} \end{Bmatrix} \qquad \ldots(10)$$

where elements of the matrix are as follows

$$A_{11} = \left[\frac{-\alpha_{13}\theta_{13}}{1-2\psi_{13}\nu_3^2}\left\{\frac{m\beta}{R_{12}} + \frac{(1-\psi_{13}\nu_3)}{2}\frac{n^2\beta\gamma^2R_{12}}{m}\right\} - \frac{\alpha_{13}\theta_{13}^2}{2(1+\psi_{13}\nu_3)\theta_{23}^2}\frac{\xi_1^2\gamma^2n^2\beta R_{12}}{} - \frac{\delta_{23}\xi_2^2}{\theta_{23}m\beta}\frac{(1+\xi_1^2)}{3}\right]\frac{E_3m\beta}{t_3}$$

$$A_{12} = \left\{ \frac{\delta_{23}}{m\beta\ \theta_{23}} \left(1 + \frac{\xi_1^2}{3}\right) \xi_2 \xi_3 \right\} \frac{E_3 m\beta}{t_3}$$

$$A_{13} = -\frac{\alpha_{13}\ \theta_{13} n\beta\gamma}{2(1-\nu_3 \gamma_{13}^3)} \quad \frac{E_3 m\beta}{t_3} \quad , \quad A_{14} = 0$$

$$A_{15} = \left\{ \frac{2\alpha_{13}\xi_1\theta_{13}}{\theta_{23}(1-\gamma_{13}^2\nu_3^2)R_{12}} + \frac{\alpha_{13}}{4\theta_{13}} \frac{n^2\beta^2\gamma^2\xi_1}{(1+\gamma_{13}\nu_3)R_{12}} + \frac{\gamma_{13}\nu_3\alpha_{13}\ n^2\theta_{13}^2\xi_1\beta^2\gamma^2}{-6(1-\gamma_{13}^2\nu_3^2)\ R_{12}\theta_{23}} \right.$$

$$\left. -\delta_{23}\xi_2 H_1 \left(1+\frac{\xi_1^2}{3}\right) \right\} \frac{E_3 m\beta}{t_3}$$

$$A_{21} = A_{13}, \quad A_{22} = 0$$

$$A_{23} = -\frac{\alpha_{13}\theta_{13}\ n^2\beta\gamma^2 R_{12}}{(1-\gamma_{13}^2\nu_3^2)m} - \frac{\alpha_{13}\theta_{13}\ m\beta}{2(1+\gamma_{13}\nu_3)R_{12}} - \frac{\alpha_{13}\theta_{13}^3\xi_1^2 m\beta}{6(1+\gamma_{13}\nu_3)R_{12}^3\theta_{23}^2}$$

$$\left. -\frac{\delta_{23}}{\theta_{23}^2 m\beta} \right\} \frac{E_3 m\beta}{t_3}$$

$$A_{24} = \frac{\delta_{23}}{\theta_{23} m} \quad \frac{E_3 m\beta}{t_3}$$

$$A_{25} = \left\{ \frac{2\gamma_{13}\nu_3\alpha_{13}\theta_{13}\xi_1 n\gamma}{(1-\gamma_{13}^2\nu_3^2)\ m\ \theta_{23}} - \frac{\alpha_{13}\theta_{13}^3\xi_1 n\gamma m\beta^2}{12(1+\gamma_{13}\nu_3)\ R_{12}^2} + \frac{\alpha_{13}\theta_{13}^3\xi_1\gamma^3 n^3\beta^2}{6m\theta_{23}(1-\nu_3^2\gamma_{13}^2)} \right.$$

$$\left. -\frac{\delta_{23} n\gamma H_2}{m} \right\} \frac{E_3 m\beta}{t_3}$$

$$A_{31} = A_{12}$$

$$A_{32} = \left[-\frac{1}{(1-\nu_3^2)} \left\{ \frac{m\beta}{R_{32}} + \frac{(1-\nu_3)}{2} \frac{n^2\beta\gamma^2}{m} R_{32} \right\} - \frac{\xi_1^2\ n^2\beta\gamma^2 R_{32}}{2(1+\nu_3)\theta_{23}^2 m} \right.$$

$$\left. -\frac{\delta_{23}\xi_3^2}{\theta_{23} m} \left(1+\frac{\xi_1^2}{3}\right) \right] \frac{E_3 m\beta}{t_3}$$

$$A_{33} = 0$$

$$A_{34} = \frac{-n\beta\gamma}{2(1-\nu_3)} \frac{E_3 m\beta}{t_3}$$

$$A_{35} = \left\{ \frac{2\ \xi_1}{\theta_{23}(1-\nu_3^2)R_{32}} + \frac{n^2\beta^2\gamma^2\xi_1}{4\theta_{23}^2\ (1-\nu_3)R_{32}} + \frac{\nu_3\ n^2\ \xi_1\ \beta^2\ \gamma^2}{6\theta_{23}\ R_{32}\ (1-\nu_3^2)} \right.$$

$$\left. +\delta_{23}\xi_3 H_1\ \left(1+\frac{\xi_1^2}{3}\right) \right\} \frac{E_3 m\beta}{t_3}$$

$$A_{41} = 0 \ , \ A_{42} = A_{34} \ , \ A_{43} = A_{24}$$

$$A_{44} = \left\{ - \frac{n^2\beta\gamma^2 R_{32}}{m(1-\nu_3^2)} - \frac{m\beta}{2(1+\nu_3)\,R_{32}} - \frac{\xi_1^2\, m\beta}{6(1+\nu_3)\,R_{32}^3\theta_{23}^2} - \frac{\delta_{23}}{\theta_{23}^2} - m\beta \right\} \frac{E_3 m\beta}{t_3}$$

$$A_{45} = \left\{ \frac{2\nu_3\xi_1 n\gamma}{(1-\nu_3^2)m\theta_{23}} - \frac{\xi_1 n\gamma m\beta^2}{12(1+\nu_3)R_{32}^2} + \frac{\xi_1\gamma^3\beta^2 n^3}{6m\theta_{23}(1-\nu_3^2)} + - \frac{\delta_{23}H_2 n\gamma}{m} \right\} \frac{E_3 m\beta}{t_3}$$

$$A_{51} = - A_{15},\ A_{52} = - A_{35},\ A_{53} = - A_{25},\ A_{54} = - A_{45}$$

$$A_{55} = \left[\frac{4\xi_1^2}{m\beta\theta_{13}^2} \left\{ \frac{\alpha_{13}\theta_{13}}{(1-\Psi_{13}^2\nu_3^2)R_{12}} + \frac{1}{(1-\nu_3^2)R_{32}} \right\} + \frac{\alpha_{13}\theta_{13}^3}{12(1-\Psi_{13}^2\nu_3^2)} \left\{ \frac{16\xi_1^4}{R_{12}^3 m\beta} \right.\right.$$

$$\left. + \frac{m^3\beta^3}{R_{12}^3} + \frac{2n^2 m\beta^3\gamma^2}{R_{12}} + \frac{n^4\beta^3\gamma^4 R_{12}}{m} - \frac{8m\beta\xi_1^2}{R_{12}^3\theta_{23}^2} \right\}$$

$$+ \frac{1}{12(1-\nu_3^2)} \left\{ \frac{16\xi_1^4}{R_{32}^3\theta_{23}^4 m\beta} + \frac{2n^2 m\beta^3\gamma^2}{R_{32}} - + \frac{n^4\beta^3\gamma^4 R_{32}}{m} + \frac{m^3\beta^3}{R_{23}^3} + \frac{8m\beta\xi_1^2}{R_{23}^2\theta_{23}^2} \right\}$$

$$\left. + \delta_{23}\left(1+\frac{\xi_1^2}{3}\right) H_1^2 m\beta\theta_{23} + \frac{\delta_{23}H_2^2 n^2\gamma^2\beta\,\theta_{23}}{m} \right] \frac{E_3 m\beta}{t_3}$$

Where the non dimensional parameters are given by

$$\xi_1 = \frac{t_2}{2R_2}\ ,\quad R_{12} = \frac{R_1}{R_2}\ ,\quad R_{23} = \frac{R_3}{R_2}$$

$$R_{12} = 1+\xi_1 + \frac{\theta_{13}}{\theta_{23}}\xi_1\ ,\ R_{23} = 1 - \xi_1 - \frac{\xi_1}{\theta_{23}}\ ,\ \delta_{23} = \frac{G_2}{E_3}$$

$$\alpha_{13} = \frac{E_1}{E_3}\ ,\ \theta_{13} = \frac{t_1}{t_3}\ ,\ \theta_{23} = \frac{t_2}{t_3}\ ,\ \beta = \frac{\pi t_3}{R_2\theta}\ ,\ \gamma = \frac{R_2\theta}{1}$$

$$\Psi_{13} = \frac{\nu_1}{\nu_3}\ ,\quad CR = \frac{t_3}{2R_2}\ ,\ \xi_2 = (1-\xi_1)\left(1 - \frac{\theta_{13}\xi_1}{\theta_{23}R_{12}}\right)$$

$$\xi_3 = (1+\xi_1)\left(1 + \frac{\xi_1}{R_{32}\theta_{23}^2}\right)\ ,$$

$$H_1 = 1 + \left\{ (1+\xi_1)\frac{\theta_{13}}{R_{12}} + \frac{(1+\xi_1)}{R_{23}} \right\} \frac{1}{2\theta_{23}}\ ,$$

$$H_2 = 1 + \frac{(\theta_{13}+1)}{2\theta_{23}}$$

Applying the correspondence principle of linear viscoelasticity, the shear modulus of the viscoelastic core is taken as complex i.e. $G_2 = G_2(i+ i\eta_2)$ where G_2 and η_2 are the in phase shear modulus and loss factor of the core material respectively. This results into five simultaneous equations (10) with complex coefficients. Eliminating u_{1mn}, u_{3mn}, V_{1mn} and V_{3mn} and on siplification these equations are reduced to the form.

$$(R_{mn}+i\ I_{mn})\ \frac{E_3 m\beta}{t_3} - \bar{\rho} p^2\ W_{mn} = q_{mn} \quad ..(12)$$

here R_{mn} and I_{mn} are real and imaginary parts of the resulting term. The resonating frequency and the associated system loss factor are given by

$$p^2_{mn} = \frac{R_{mn}\ E_3\ m\beta}{\bar{\rho}\ t_3}$$

$$\eta_s = \frac{I_{mn}}{R_{mn}} \quad ..(13)$$

The above procedure has been programmed on ICL 2960 computer to study the effects of the variations of various geometric and material parameters on the resonant frequencies and the associated system loss factors of the curved sandwich panel and are given in next section. Resonant frequency has been expressed as a nondimensional parameter

$$FPR = \frac{\rho_3 t_3 p^2_{mn}}{E_3}$$

RESULTS AND DISCUSSIONS

The face layers 1 and 3 of the curved sandwich panel are taken to be of the same elastic material with Poisson's ratio 0.3, giving $\rho_{13}=\alpha_{13}=\gamma_{13}=1.0$. Mass density of viscoelastic material of the core is taken as half of that of the elastic material of the faces, giving $\rho_{23}=0.5$. Values of other parameters, are specified in graphs and tables. Variation of the resonant frequency parameter FPR and the system loss factor η_s with other parameters has been reported.

The variation of FPR with the curvature parameter CR at various values of the corethickness ratio θ_{23} for a curved simply supported sandwich panel are shown in figure (2). FPR increases with an increase of CR at all values of θ_{23}. Increasing slope of these curves with CR indicates that rate of increase of resonating frequencies goes on increasing with the curvature of the panel. This effect is similar to that observed by Sewall [4] and Petyt and Debnath [5] for a homogeneous curved panels. Further it may be noted that upto certain curvature value, an increase in core thickness increases the resulting resonant frequencies, but the behaviour is reversed beyond this curvature value ie for panel with thinner core layers, the resonant frequencies are higher. The variation of associated system loss factor η_s with CR at the same set of values of θ_{23} is shown in figure (3). η_s decreases with an increase of CR for all values of θ_{23} and this decrease is quite steep beyond certain value of CR. This may be due to the fact that increase in CR results in increased stiffness, which in turn results lesser energy dissipation, and so the smaller η_s.

Figure (4) shows the variation of η_s with the shear parameter δ_{23} at various values the core thickness ratio θ_{23}. From the study of damping analysis of sandwich structures[2,3], it is established fact that corresponding to some optimum shear parameter, the value of the product of stiffness and deformation of the core are maximum, resulting in maximum energy dissipation and so the maximum η_s. Similar expected behaviour is observed in these curves. The maximum system loss factor $\eta_{s,max}$ increases with an increase of θ_{23} and occurs at higher values of δ_{23}.

Figure (5) shows the variation of η_s with δ_{23} at various values of the elastic layers thickness ratio θ_{13} and the nature of the curves is similar to those in figure (4). $\eta_{s,max}$ increases with an increase of θ_{13} from 0.1 to 5.0, but further increase in θ_{13} results in a decrease of $\eta_{s,max}$. For straight sandwich beams and panels, it is an established fact [3], that the highest $\eta_{s,max}$ may be obtained with symmetric arrangement i.e. for $\theta_{13}=1$. This fact does not apply to the curved panels, as in this particular curved panel, the highest $\eta_{s,max}$ is obtained for an unsymmetric arrangement with $\theta_{13}=5.0$. In general the highest $\eta_{s,max}$ may be achieved for an unsymmetric arrangement for the curved sandwich panels.

Figure (6) shows the variation of η_s with δ_{23} at various values of the length parameters β. It is observed that $\eta_{s,max}$ increases with an increase of δ_{23} and occurs at higher values of δ_{23}, and this increase goes on decreasing at higher values of β.

Figure (7) shows the variation of η_s with δ_{23} at various values of the aspect ratio γ. It is observed that $\eta_{s,max}$ for γ=0.5 and for γ=2.0 are the same, occuring at different δ_{23} values. $\eta_{s,max}$ value for γ=1 is the lowest, and for any other value of γ less or more than 1, $\eta_{s,max}$ is more than the lowest.

Figure (8) shows the variation of η_s with δ_{23} at various values of circumferential modal numbers m. It is observed that $\eta_{s,max}$ increases with m and occurs nearly at the same values of δ_{23}. Thus the optimum choice of the shear parameter for first mode (m=1, n=1) may also ensure nearly maximum system loss factors for other higher circumferential modes (m=1,2,3 and n=1). $\eta_{s,max}$ values are not same for various modes (m=1 to 3, n=1) and in this respect, behaviour of the curved plate is different from that of the flat plate.

The variation of FPR and associated η_s for various modes (m and n values) of a plate are tabulated in tables (1) and (2), at two values of CR, the other parameters remaining the same. It may be observed that at low values of curvature parameter CR = 0.00005, the curved sandwich plate behaviour is similar to that of straight sandwich plate. The resonant frequency increases with an increase in number of modal numbers m and n. For relatively higher curved plates with curvature parameter CR = 0.0005, the resonant frequency for mode m=2, n =1 is less than that for mode m =1, n=1, and the resonant frequency for mode m = 3, n = 1 is same as that for mode m =1, n =1 . Similar effects have been observed by Mead and Pretlove [6], in case of elastic sandwich plate.

CONCLUSIONS

On the basis of present investigation, it is concluded that the resonant frequency of a curved sandwich panel increases and its associated system loss factor decreases with an increase of curvature. For a given geometric configuration, the maximum system loss factor may be achieved with an optimum shear parameter. It has been found that in general, the maximum obtainable system loss factor for a curved sandwich panel may be highest for an unsymmetric arrangement and in this respect its behaviour is different from that of a straight sandwich panel.

REFERENCES

1. Yu,Yi-Yuan, "Damping of Flexural Vibration of Sandwich Plates" Journal of the Aerospace Sciences. Vol. 29, No.7, July, 1962, pp. 791-803.

2. Mead, D.J. "The Damping Properties of Elastically supported Sandwich Plates". Journal of Sound and Vibration, 24 (3), 1972, pp. 275-

3. Rao, Y.V.K.S. and Nakra B.C., "Vibration of Unsymmetrical Sandwich Beams and Plates with Viscoelastic Cores", Journal of Sound and Vibration 34 (3), 1974, 309-326.

4. Sewall, J.L., "Vibration Analysis of Cylindrical Curved Panels with Simply Supported and Clamped Edges and Comparison with Experiment", NASA report TND 3971, 1967.

5. Petyt, M. and Debnath, J.B., "Vibrations of Curved Plate" Journal of Sound and Vibration, Vol.13, 1970, pp. 485-497.

6. Mead, D.J. and Pretlove, A.J., "On the Vibration of Curved Sandwich Plate". Aeronautical Research Council London Report R and M 3363, 1964.

7. Flugge. W., "Stresses in Shells" Springer Verlag Publication, 1962.

Table (1) FREQUENCY PARAMETER AND ASSOCIATED SYSTEM LOSS FACTOR FOR VARIOUS MODES

$\theta_{13}=\theta_{23}=\gamma$= 1.0, β=0.01, δ_{23}=0.0001, CR = 0.00005

Mode m	Mode n	Frequency parameter FPR	System Loss Factor
1	1	0.227×10^{-7}	0.183
2	1	0.801×10^{-7}	0.264
3.	1	0.213×10^{-6}	0.267
4	1	0.463×10^{-6}	0.239
1	2	0.849×10^{-7}	0.249
1	3	0.219×10^{-6}	0.259
1	4	0.470×10^{-6}	0.236
2	2	0.157×10^{-6}	0.268
2	3	0.315×10^{-6}	0.253
3	2	0.312×10^{-6}	0.256

Table (2) FREQUENCY PARAMETER AND ASSOCIATED SYSTEM LOSS FACTOR FOR VARIOUS MODES

$\eta_{13} = \eta_{23} = 1.0$, $\eta_{12} = 0.01$, $\eta_{23} = 0.0001$, CR = 0.0005

Mode m	Mode n	Frequency Parameter FPR	System Loss Factor
1	1	2.2×10^{-7}	0.018
2	1	1.1×10^{-7}	0.187
3	1	2.2×10^{-7}	0.256
4	1	4.6×10^{-7}	0.237
1	2	5.9×10^{-7}	0.0355
1	3	8.6×10^{-7}	0.066
1	4	1.2×10^{-6}	0.094
2	2	3.5×10^{-7}	0.118
2	3	6.9×10^{-7}	0.114
2	4	3.9×10^{-7}	0.205

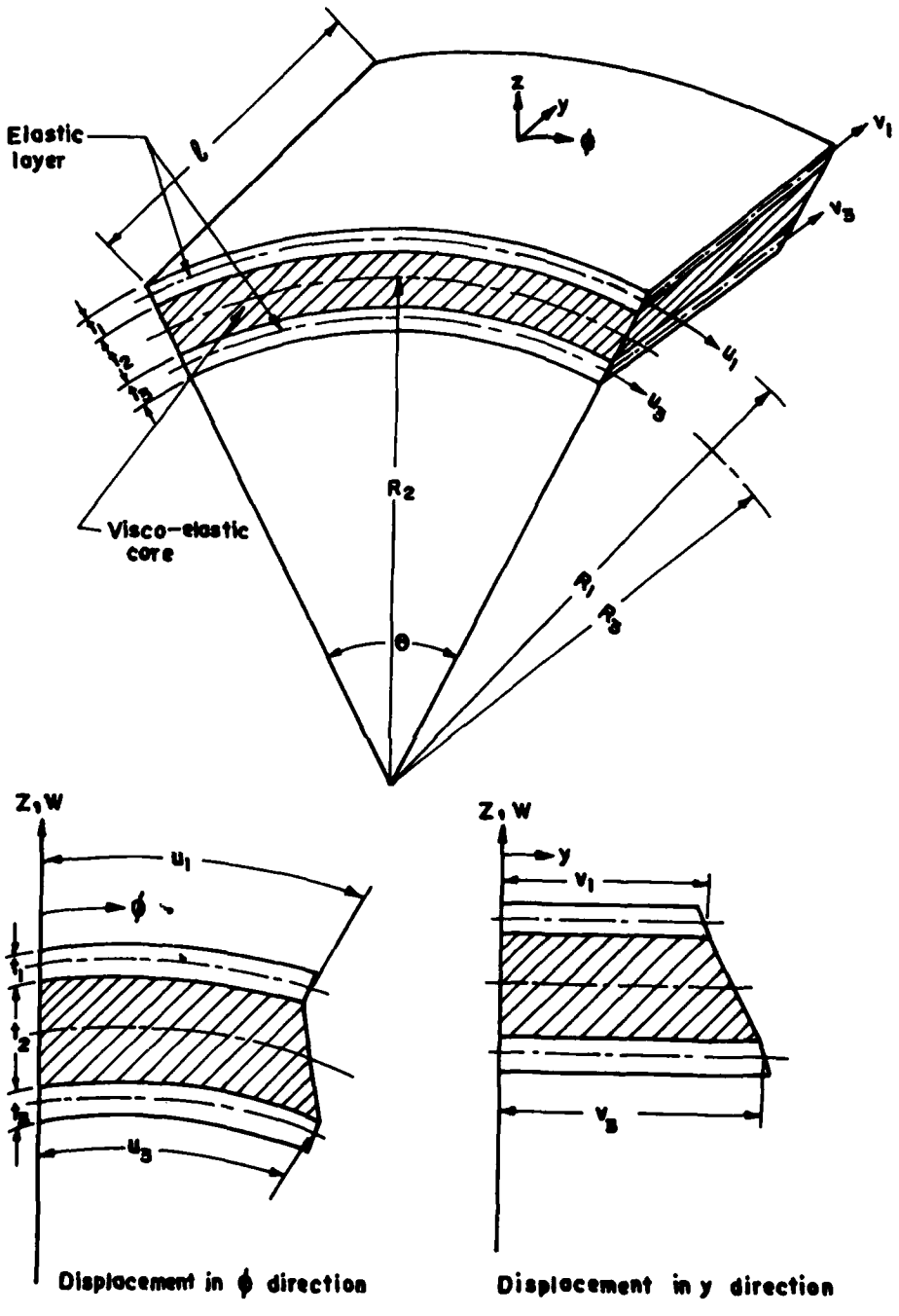

Fig. 1 Curved sandwich panel configuration and displacement pattern.

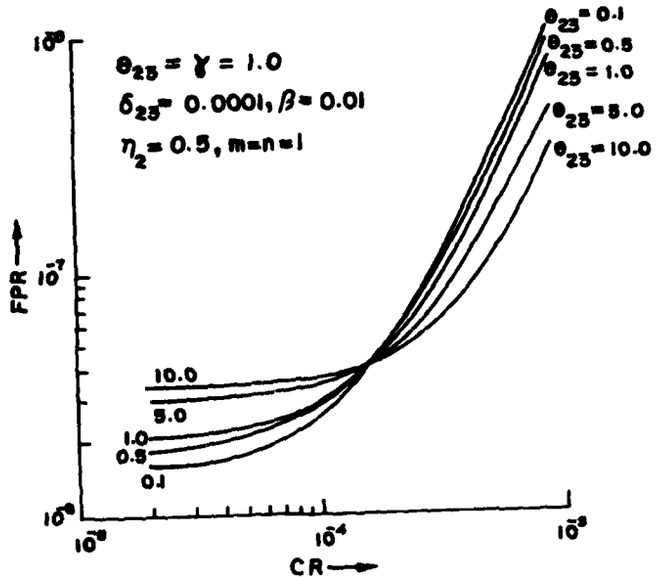

Fig. 2 Variation of FPR with CR at various values θ_{25}

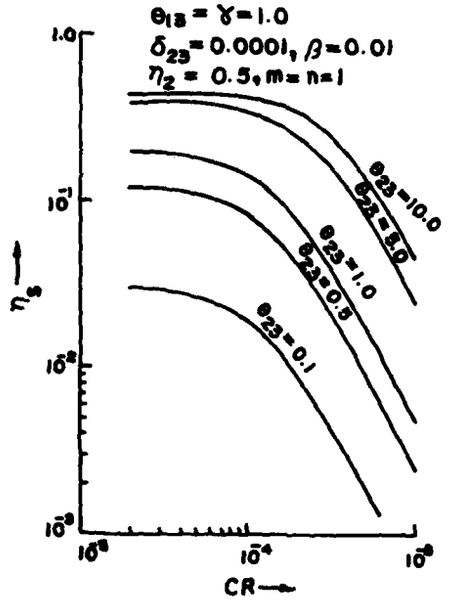

Fig. 3 Variation of η_s with CR at various values θ_{25}

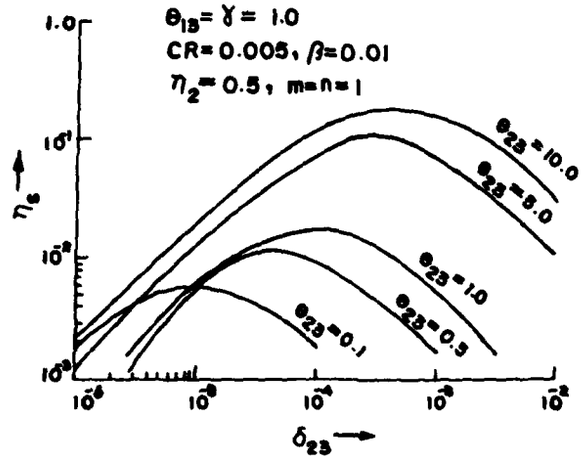

Fig. 4 Variation of η_s with δ_{25} at various values of θ_{25}

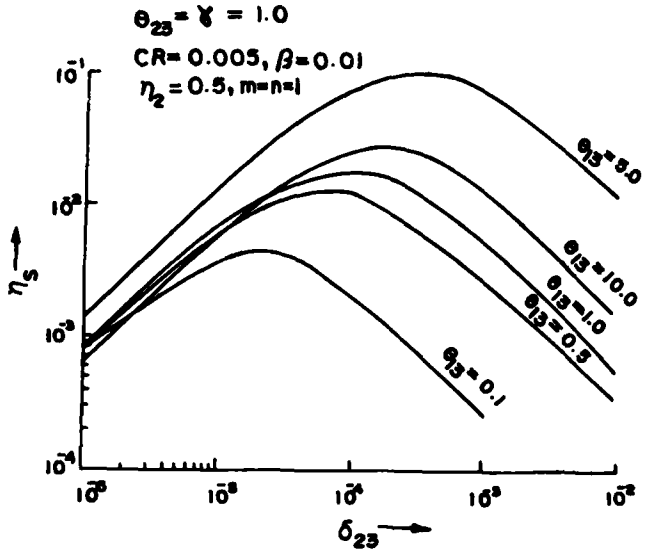

Fig. 5 Variation of η_s with δ_{23} at various values of θ_{13}

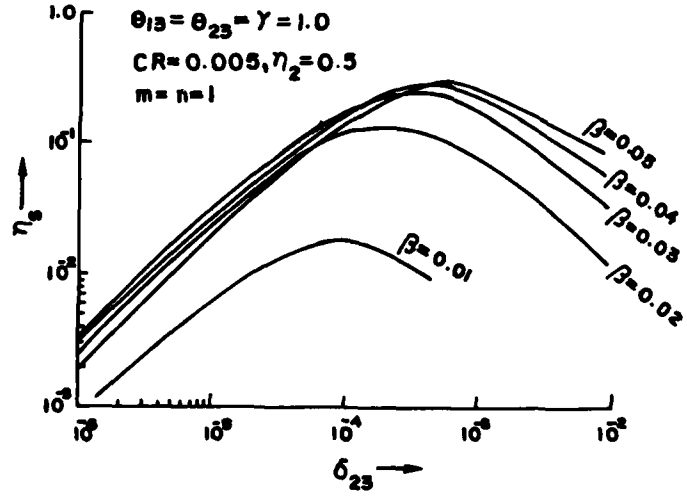

Fig. 6 Variation of η_s with δ_{23} at various values of β

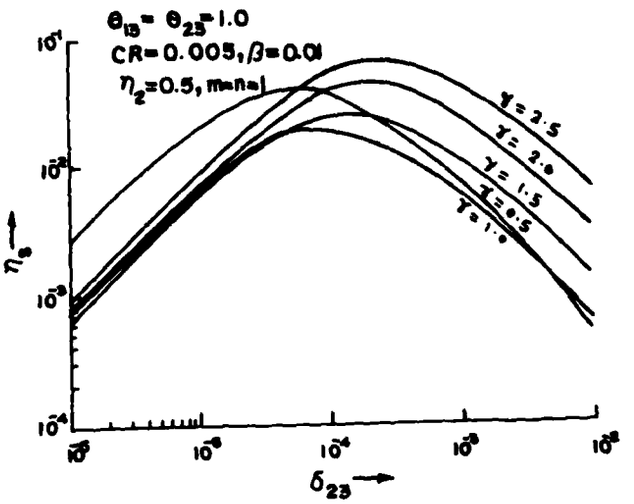

Fig.7 Variation of η_s with δ_{23} at various values γ

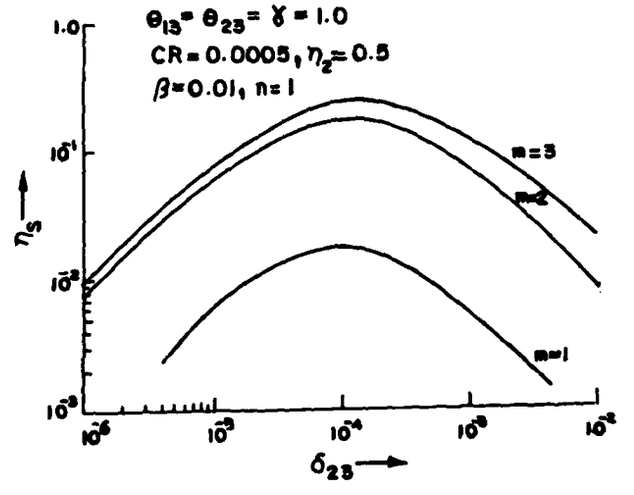

Fig. 8 Variation of η_s with δ_{23} at various values of m

*U.S. GOVERNMENT PRINTING OFFICE: 1985-461-639:20008